Nuclear Science
2014

State-of-the-art Report on Innovative Fuels for Advanced Nuclear Systems

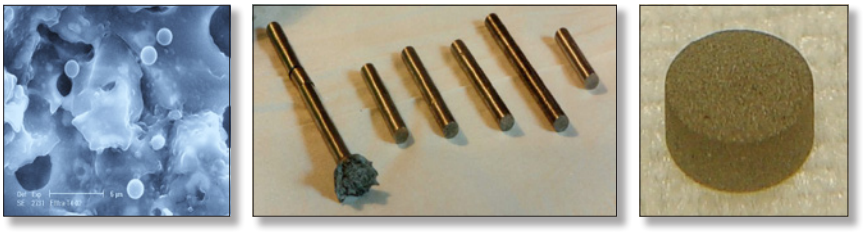

OECD
BETTER POLICIES FOR BETTER LIVES

NEA
NUCLEAR ENERGY AGENCY

Nuclear Science

State-of-the-art Report on Innovative Fuels for Advanced Nuclear Systems

NEA No. 6895

NUCLEAR ENERGY AGENCY
ORGANISATION FOR ECONOMIC CO-OPERATION AND DEVELOPMENT

ORGANISATION FOR ECONOMIC CO-OPERATION AND DEVELOPMENT

The OECD is a unique forum where the governments of 34 democracies work together to address the economic, social and environmental challenges of globalisation. The OECD is also at the forefront of efforts to understand and to help governments respond to new developments and concerns, such as corporate governance, the information economy and the challenges of an ageing population. The Organisation provides a setting where governments can compare policy experiences, seek answers to common problems, identify good practice and work to co-ordinate domestic and international policies.

The OECD member countries are: Australia, Austria, Belgium, Canada, Chile, the Czech Republic, Denmark, Estonia, Finland, France, Germany, Greece, Hungary, Iceland, Ireland, Israel, Italy, Japan, Luxembourg, Mexico, the Netherlands, New Zealand, Norway, Poland, Portugal, the Republic of Korea, the Slovak Republic, Slovenia, Spain, Sweden, Switzerland, Turkey, the United Kingdom and the United States. The European Commission takes part in the work of the OECD.

OECD Publishing disseminates widely the results of the Organisation's statistics gathering and research on economic, social and environmental issues, as well as the conventions, guidelines and standards agreed by its members.

This work is published on the responsibility of the Secretary-General of the OECD.

NUCLEAR ENERGY AGENCY

The OECD Nuclear Energy Agency (NEA) was established on 1 February 1958. Current NEA membership consists of 31 countries: Australia, Austria, Belgium, Canada, the Czech Republic, Denmark, Finland, France, Germany, Greece, Hungary, Iceland, Ireland, Italy, Japan, Luxembourg, Mexico, the Netherlands, Norway, Poland, Portugal, the Republic of Korea, the Russian Federation, the Slovak Republic, Slovenia, Spain, Sweden, Switzerland, Turkey, the United Kingdom and the United States. The European Commission also takes part in the work of the Agency.

The mission of the NEA is:

- to assist its member countries in maintaining and further developing, through international co-operation, the scientific, technological and legal bases required for a safe, environmentally friendly and economical use of nuclear energy for peaceful purposes;
- to provide authoritative assessments and to forge common understandings on key issues, as input to government decisions on nuclear energy policy and to broader OECD policy analyses in areas such as energy and sustainable development.

Specific areas of competence of the NEA include the safety and regulation of nuclear activities, radioactive waste management, radiological protection, nuclear science, economic and technical analyses of the nuclear fuel cycle, nuclear law and liability, and public information.

The NEA Data Bank provides nuclear data and computer program services for participating countries. In these and related tasks, the NEA works in close collaboration with the International Atomic Energy Agency in Vienna, with which it has a Co-operation Agreement, as well as with other international organisations in the nuclear field.

Foreword

Under the guidance of the OECD Nuclear Energy Agency (NEA) Nuclear Science Committee (NSC) and the mandate of the Working Party on Scientific Issues of the Fuel Cycle (WPFC), the Expert Group on Innovative Fuels (EGIF) was established with the objective of conducting joint and comparative studies to support the development of innovative fuels such as homogeneous and heterogeneous fuels, ADS fuels, and oxide, metal, nitride and carbide fuels, all of which can be implemented in advanced nuclear fuel cycles with fast reactors. The scope of the expert group covers innovative fuel fabrication techniques, irradiation performance of innovative fuels, characterisation and post-irradiation examination methods and predictive codes for innovative fuel fabrication and performance.

This report presents the state of the art on the development of various innovative fuels, especially minor actinide-bearing fuels, and the technical issues associated with fabrication, characterisation, irradiation performance, design and safety criteria.

Acknowledgements

The NEA Secretariat would like to express its sincere gratitude to the members of the Expert Group on Innovative Fuels (EGIF) for contributing to this report and for providing consistent assessments on fuel issues. The collaboration of Dr K. O. Pasamehmetoglu (United States) and Ms N. Chauvin (France), the former and current Chair of the EGIF, is gratefully acknowledged. A list of contributors can be found on page 193.

Table of contents

Foreword 3

List of abbreviations and acronyms 13

Executive summary 15

1. Introduction 19

1.1 Fuel types covered in the report 19
1.2 Related activities 20
References 21

2. Metal fuels 23

2.1 Introduction 23
2.2 Characterisation of minor actinide-bearing metal fuels 24
2.3 Fuel fabrication 37
2.4 Irradiation performance 43
2.5 Safety performance 52
2.6 Fuel design criteria 53
2.7 Applicability to reactor systems 55
2.8 Technical issues and future work 55
2.9 Technology readiness levels (TRLs) 56
References 56

3. Oxide fuels 61

3.1 Introduction 61
3.2 Different transmutation oxide fuels and transmutation efficiency 61
3.3 Homogeneous fuels (i.e. minor actinide-bearing fuels, MABF) 67
3.4 Heterogeneous fuels (i.e. minor actinide-bearing blanket, MABB) 83
3.5 Summary 102
References 104

4. Nitride fuels 109

4.1 Introduction 109
4.2 Fabrication techniques 110
4.3 Fresh fuel characterisation 112
4.4 Irradiation experiments and results 118
4.5 Modelling activities for nitride fuels 120
4.6 Safety behaviour of nitride fuels 121
4.7 Technology readiness levels and need of additional research 121
References 122

5. Dispersion fuels 125

5.1 Introduction and generalities 125
5.2 Fuel fabrication 129
5.3 Fuel characterisation 133
5.4 Irradiation tests 141
5.5 Post-irradiation examination (PIE) 147
5.6 Thermomechanical modelling 153
5.7 Safety behaviour 154
5.8 Conclusions and technology readiness levels (TRLs) 159
5.9 Technology readiness levels (TRLs) 160
References 161

6. Special mechanic fuel forms 163

6.1 Introduction 163
6.2 Pellet fuels 163
6.3 Particle fuels 165
References 172

7. Summary and conclusions 177

7.1 Technology readiness levels (TRLs) 179
References 183

Appendix A: Definition of technology readiness levels (TRLs) for transmutation fuel development 185

A.1 Introduction 185
A.2 TRL evaluation elements and attributes 185
A.3 TRL definitions 188
A.4 Summary and conclusions 189

List of contributors 193

Members of the Expert Group on Innovative Fuels 195

List of figures

2.1 Metallography of annealed U-19Pu-10Zr-1.2Np-0.8Am-0.1Y-0.5Ce-1.4Nd alloys (CR11), etched 27
2.2 Metallography of annealed U-19Pu-10Zr-3Np-2Am-0.2Y-1.2Ce-3.6Nd alloys (CR12), etched 27
2.3 Dilatometric curves of U-19Pu-10Zr (CR13), U-19Pu-10Zr-1.2Np-0.8Am-0.1Y-0.5 Ce1.4Nd (CR11) and U-19Pu-10Zr-3Np-2Am-0.2Y-1.2Ce-3.6Nd (CR12) alloys 29
2.4 Measured thermal conductivities of U-19Pu-10Zr (CR13), and U-19Pu-10Zr-3Np-2Am-0.2Y-1.2Ce-3.6Nd (CR12) alloys 29
2.5 Schematic view of diffusion couples for the compatibility test 31
2.6 Reaction layer formed at CR12/15-15Ti interface 34
2.7 Reaction layer formed at REMAAL/15-15Ti interface 34
2.8 Secondary electron image of fuel/cladding interfaces after annealing at 650°C for 125 hours (Fuel: 60U-20Pu-3Am-2Np-15Zr fuel alloy containing 8% rare earth elements (Nd, Pr, Ce, La), cladding: HT9) 35

2.9 (a) Secondary electron image of fuel-cladding interaction zones and (b) an elemental X-ray intensity line scan across the fuel-cladding interface as represented by the yellow line on the image....35
2.10 Estimated thermal conductivity of Pu-40Zr....36
2.11 Specific heats of metallic U-Pu-TRU alloys....36
2.12 MA-bearing fuel alloys for METAPHIX irradiation test....37
2.13 MA-bearing fuel alloys for AFC-2 irradiation test....37
2.14 Fabrication scheme of U-Pu-Zr, U-Pu-Zr-MA, U-Pu-Zr-MA-RE alloy rods for METAPHIX irradiation test....38
2.15 Conceptual diagram of the continuous casting system....39
2.16 Uranium rod is being extracted by rollers from the cooling jacket to air by continuous casting....40
2.17 Preliminary concept of the bench-scale caster, setup for bottom casting tests....41
2.18 SEM image of U-10wt%Zr powder fabricated by centrifugal atomisation....41
2.19 Am and Cm metal production schemes....43
2.20 (a) Post-irradiation optical image of X501 MA-bearing fuel (b) wavelength dispersive spectroscopy line scans showing distribution of actinides and Zr....44
2.21 Schematic diagram of test fuel pins....46
2.22 Gamma-radiography of METAPHIX-1 fuel pins (2.5at% burn-up)....46
2.23 Local axial elongation of METAPHIX-1 fuel stacks (2.5at% burn-up)....47
2.24 Metallography of cross-section of METAPHIX-1 fuel Pin#3 (2.5at% burn-up, U-19Pu-10Zr-5MA-5RE)....48
2.25 AFC-1 irradiation test assembly, capsule assembly and fuel rodlet assembly....49
2.26 Fission gas release from metallic alloy transmutation fuel rodlets irradiated in AFC-1B and AFC-1F capsules....50
2.27 Transverse cross-sectional metallography montages of U-29Pu-4Am-2Np-30Zr samples....51
2.28 Irradiation and modelling maturity levels for metal fuels....56
3.1 Schematic position of MABB in the SFR core....63
3.2 Time dependence of decay heat for irradiated fuel....66
3.3 Time dependence of neutron source for irradiated fuel....66
3.4 Lattice parameter of MOX with or without MA....69
3.5 Evolution of the $\triangle GO_2$ with O/M....69
3.6 Comparison of the $\triangle GO_2$ of $MO_{1.995}$ for several compositions....69
3.7 Variation of solidus and liquidus temperature with Pu and MA contents....70
3.8 Variation of solidus and liquidus temperature with compositions and O/M....70
3.9 Thermal conductivity of MOX with MA....71
3.10 Fabrication flowsheet for the SUPERFACT fuel at ITU....74
3.11 SUPERFACT – micrographs....76
3.12 Fabrication flowsheet of Am-MOX fuel for the AM1 irradiation....77
3.13 AM1 – Ceramographs of Am-MOX fuel pellets....79
3.14 AM1 – Comparison of fuel microstructure between the $(Am,Pu,NpU)O_{2-x}$ fuel (z/L = 0.50, 432W/cm) and the reference MOX fuel (z/L = 0.74, 420W/cm) in the second test (O/M molar ratio 1.98)....79
3.15 AM1 – Comparison of radial distributions of Am and Pu in the $(Am, Pu,Np,U)O_{2-x}$ fuel samples (second test, z/L = 0.5, O/M molar ratio 1.95 and 1.98)....79
3.16 GACID programme organisation: Tri-lateral collaboration in GACID pin-scale test.. 81

3.17 GACID programme: Steps and schedule....82
3.18 Fabrication flowsheet for SUPERFACT pellets (20%Am+20%Np) 84
3.19 Infiltration process for the production of (U,Am)O_{2-x} at JRC-ITU 85
3.20 Fabrication flowsheet for MARIOS-DIAMINO pellets 85
3.21 Macrograph of standard and optimised (tailored open porosity) MABB pellets (∅≈4.5mm)....86
3.22 Heat capacity of NpO_2, together with those of NpO_2, UO_2 and PuO_2, as a function of temperature....87
3.23 Thermal conductivities of NpO_2, AmO_{2-x}, AmO_2, Am_2O_3, UO_2 and PuO_2, as a function of temperature....88
3.24 Oxygen potentials of AmO_{2-x} at 1 333 K, together with those of CeO_{2-x} at 1 353 K and 988 K, as a function of nonstoichiometry, *x* 89
3.25 Oxygen potentials of $(Am_{0.5}Np_{0.5})O_{2-x}$ at 1 333 K, together with those of AmO_{2-x} at 1 333 K and $(Am_{0.5}U_{0.5})O_{2-x}$ at 1 333 K, as a function of the nonstoichiometry, *x* 89
3.26 Thermal conductivity recommended for $(U_{0.5},Am_{0.5})O_x$, $(U_{0.5},Np_{0.5})O_x$ and $(U,Am_{0.25},Np_{0.25})O_x$ 91
3.27 Comparison of ΔG_{O_2} of $(U_{0.5},Np_{0.5})O_x$ as a function of the temperature and O/M ratio and other measurements on $(U_{0.5},Am_{0.5})O_x$, $(U,Am_{0.25},Np_{0.25})O_x$ 91
3.28 Oxygen potentials of $(U,Am_{0.2},Np_{0.2})O_x$ as a function of temperature and O/M ratio....92
3.29 Power history of an MABB pin (case: 20wt%Am)....94
3.30 Helium production for MABB as a function of time 94
3.31 Fuel temperature as a function of time with a subassembly rotation at mid-life 95
3.32 Possible behaviour of MABB material as a function of the irradiation temperature.. 95
3.33 Micrographs of a SUPERFACT fuel fabricated by the sol-gel method indicating: (a) macrostructure and (b) microstructure....98
3.34 Schematic diagram of a mini-pin with 6 MABB discs (in pink) 99
3.35 Irradiation and modelling maturity levels for homogeneous oxide fuel....103
3.36 Irradiation and modelling maturity levels for heterogeneous oxide fuel....104
4.1 Typical CO release curve during carbothermic reduction of oxides-carbon mixture to obtain nitride 110
4.2 Sol-gel and infiltration routes for the production of minor actinide-bearing nitride and carbide fuels 111
4.3 Appearances of the sample in a series of experiments..... 112
4.4 X-ray diffraction pattern of $(Np_{0.279}Pu_{0.307}Am_{0.279}Cm_{0.135})N$....114
4.5 Linear thermal expansions of UN, NpN, PuN and AmN as a function of temperature....114
4.6 Heat capacities of UN, NpN, PuN and AmN as a function of temperature....115
4.7 Thermal conductivities of UN, NpN, PuN and AmN as a function of temperature....116
4.8 Nitride cold press and sinter process....116
4.9 AFCI non-fertile and low-fertile nitride pellets 117
4.10 Structure of U-free nitride fuel pin containing (Pu,Zr)N and PuN+TiN pellets 118
4.11 Structure and dimensions [cm] of rodlet containing MA-bearing mixed nitride fuel irradiated in AFC-1AE and AFC-1F 119
4.12 Variation of mononitride fuel composition with temperature 120
4.13 Irradiation and modelling maturity levels for nitride fuels....122

5.1 Radiation damage around a fissile particle embedded in a matrix....126
5.2 Volume damage of the matrix as a function of diameter and fractional volume of the fissile phase in a composite fuel....126
5.3 Fabrication of the EFTTRA-T4 pellets by pellet infiltration....129
5.4 Fabrication route used for ECRIX fuels....130
5.5 Fabrication route for CAMIX 1....131
5.6 CAMIX 2 and COCHIX 3 fabrication routes....131
5.7 Optical micrograph and α autoradiograph of EFTTRA-T4 pellet....133
5.8 Ceramograph of the EFTTRA-T4 pellets....134
5.9 Visual aspect and microstructure of ECRIX fuel pellets....134
5.10 Thermal conductivity of ECRIX fuels....135
5.11 Visual appearance of CAMIX 1, CAMIX 2 and COCHIX 3 pellets....135
5.12 Ceramographs of CAMIX 1, CAMIX 2 and COCHIX 3 fuels....136
5.13 FUTURIX FTA 5 and 6 CERMET fuels....137
5.14 FUTURIX FTA 7 and 8 CERCER fuels....137
5.15 FUTURIX FTA 5 and 6 CERMET fuels....138
5.16 FUTURIX FTA 7 and 8 CERCER fuels (Jorion 2007)....138
5.17 Thermal conductivity of FUTURIX CERMET fuels....139
5.18 Visual aspect of five different HELIOS fuel pellets....140
5.19 Microstructure of five different HELIOS fuel pellets....143
5.20 Schematic design of ECRIX H pin....144
5.21 ECRIX capsules in Phénix....144
5.22 Location of the ECRIX pin in Phénix core....145
5.23 Power evolution in ECRIX H....145
5.24 ECRIX H element distribution as a function of burn-up....146
5.25 Helium and fission gas generation in the ECRIX H pin....146
5.26 Radial swelling of EFTTRA-T4 and T4bis pins determined by profilometry....147
5.27 Microstructure of the EFFTRA-T4 irradiated sample....149
5.28 EFTTRA-T4 SEM examination following irradiation in the HFR Petten....150
5.29 γ scans of the ECRIX H pin....151
5.30 ECRIX H: Irradiated MgO-$AmO_{1.6}$ pellet....152
5.31 ECRIX H fuel fragments, assembled axially, sectioned and polished....152
5.32 ECRIX H region corresponding to an ex $AmO_{1.6}$ particle....153
5.33 Temperature variation at the core and surface of ECRIX H targets with minimum and maximum radii at the maximum flux plane as a function of the burn-up....154
5.34 Mass spectrometer signals following heat up of an EFTTRA-T4 sample in a Knudsen cell....155
5.35 Fractional release of Xe and He from an EFTTRA-T4 sample....155
5.36 EFTTRA-T4 SEM micrographs taken at different annealing stages....156
5.37 Schematic representation of the vapourisation and structural changes in irradiated EFTTRA-T4 fuel....157
5.38 Mass spectrometer measurements of CERMET FX5 samples....158
5.39 Mass spectrometer measurements of CERMET FX6 samples....158
5.40 Mass spectrometer measurements of CERMET sample FX6....159

5.41 Mass spectrometer measurements of CERMET sample FX6 159
5.42 Irradiation and modelling maturity levels for dispersion fuels 161
6.1 Flowchart of conventional and simplified pellet processes according to JAEA 164
6.2 Comparison of ceramography photos according to the content of Np 171
A.1 Summary of TRL evaluation elements, attributes and bins 186

List of Tables

2.1 Annealing conditions for alloy samples 25
2.2 Compositions (wt%) of phase 0 in the annealed alloy samples, analysed by EPMA 26
2.3 Measured mechanical properties 30
2.4 Transition temperatures (T_{tr}) and enthalpies of transition (ΔH_{tr}) determined from differential scanning calorimetry upon heating and cooling 30
2.5 Conditions and results of the compatibility test 32
2.6 Composition of the phases detected in the reaction zone of CR13-steel couple 33
2.7 Composition of the phases detected in the reaction zone of CR12-steel couple 33
2.8 Composition of the phases detected in the reaction zone of REMAAL-steel couple 33
2.9 Composition of the phases detected in the reaction zone of REAL-steel couple 34
2.10 Irradiation tests of MA-bearing metal fuel 45
2.11 Elemental and isotopic compositions of METAPHIX test fuel alloys in December 2003 47
3.1 Possible isotopic composition at the equilibrium (in%) 63
3.2 Comparison of transmutation performances for MABB and MABF 65
3.3 Decay heat and neutron source level of fresh fuel (reloading) 65
3.4 Pellet and pin design characteristics of the SUPERFACT pellets 75
3.5 SUPERFACT – Irradiation conditions for each pin 75
3.6 AM1 – Irradiation conditions for each pin 78
3.7 AFC-2C and 2D – Irradiation conditions 80
3.8 Fabrication steps and main characteristics of the SUPERFACT fuels 84
3.9 Pellet characteristics – R&D Atalante 86
3.10 O/M determination of $(U,Am,Np)O_{2+x}$ before and after the simulation of a thermal gradient 92
3.11 Results of the sodium compatibility tests 93
3.12 Preliminary pin design as a function of the minor actinide concentration 97
3.13 Experimental grid for MARIOS and DIAMINO analytical experiments 100
4.1 Lattice parameters of actinide mononitrides and candidates for the inert matrix materials 113
5.1 Inert matrix oxide fuel irradiation programmes and their status 128
5.2 HELIOS test matrix 128
5.3 FUTURIX CERMET and CERCER fuels 132
5.4 EFTTRA-T4 fresh fuel characterisation 133
5.5 ECRIX fuel characteristics 134

5.6 CAMIX-COCHIX pellet dimensions 135
5.7 CAMIX-COCHIX chemical composition 136
5.8 XRD analysis of CAMIX COCHIX fuels 136
5.9 FUTURIX FTA pellet dimensions and densities 137
5.10 Compositions of the FUTURIX CERMET fuels 138
5.11 Compositions of the FUTURIX CERCER fuels (Jorion 2007) 139
5.12 HELIOS fuel pellet dimensions and densities 140
5.13 EFTTRA-T4 and T4bis irradiation conditions 142
5.14 Actinide inventory at EOL for EFTTRA T4 143
5.15 Irradiation data EFTTRA T4 and T4bis 148
5.16 ECRIX-H gas analysis 151
7.1 Synthesis of TRL binning for fabrication process and irradiation performance maturity 178
7.2 TRL binning for fabrication process maturity of metal fuels 179
7.3 TRL binning for irradiation performance maturity of metal fuels 179
7.4 TRL binning for fabrication process maturity of homogeneous oxide fuels 180
7.5 TRL binning for irradiation performance maturity of homogeneous oxide fuels 180
7.6 TRL binning for fabrication process maturity of heterogeneous oxide fuels 181
7.7 TRL binning for irradiation performance maturity of heterogeneous oxide fuels 181
7.8 TRL binning for fabrication process maturity of nitride fuels 182
7.9 TRL binning for irradiation performance maturity of nitride fuels 182
7.10 TRL binning for fabrication process maturity of dispersion fuels 183
7.11 TRL binning for irradiation performance maturity of dispersion fuels 183
A.1 TRL completion criteria 188
A.2 TRL binning for fabrication process maturity 189
A.3 TRL binning for irradiation performance maturity 189
A.4 Summary of TRL definition for transmutation fuels 190

List of abbreviations and acronyms

ACS	Advanced casting system
ADS	Accelerator-driven systems
AFCI	Advanced fuel cycle initiative
AGF	Alpha-gamma facility
ATR	Advanced test reactor
BCS	Bench-scale casting system
BOL	Beginning of life
CEA	*Commissariat à l'Énergie atomique et aux Énergies renouvelables*
CER	Ceramic
CERCER	Ceramic-Ceramic
CERMET	Ceramic-metal
CNL	Canadian Nuclear Laboratories (formerly AECL, Atomic Energy of Canada Limited)
CRIEPI	Central Research Institute of Electric Power Industry
DSC	Differential scanning calorimetry
EBR	Experimental breeder reactor
EFPD	Effective full power day
EGIF	Expert Group on Innovative Fuels
EPMA	Electron probe micro analysis
EOL	End of life
EU	European Union
FCCI	Fuel-cladding chemical interaction
FCF	Fuel cycle facility
FCMI	Fuel-cladding mechanical interaction
FFTF	Fast flux test facility
FP	Fission products
IAEA	International Atomic Energy Agency
IFR	Integral fast reactor
IMF	Inert matrix fuel
INL	Idaho National Laboratory
ITU	Institute for Transuranium Elements
JAEA	Japan Atomic Energy Agency

JRC	Joint Research Centre
KAERI	Korean Atomic Energy Research Institute
KIT	Karlsruhe Institute of Technology
LANL	Los Alamos National Laboratory
LBE	Lead-bismuth eutectic
LOF	Loss of coolant flow
LOHS	Loss of heat sink
LWR	Light water reactor
MA	Minor actinide(s)
MABB	Minor actinide-bearing blanket
MABF	Minor actinide-bearing fuel
MOX	Mixed oxide
NSC	Nuclear Science Committee
OECD/NEA	OECD Nuclear Energy Agency
O/M	Oxide to metal ratio
PA	Project arrangement
PIE	Post-irradiation examinations
PSI	Paul Scherrer Institute
PWR	Pressurised water reactor
RE	Rare earth
REAL	Rare earth alloy
REMAAL	Rare earth minor actinide alloy
REPU	Reprocessed uranium
RFEF	Reactor fuel examination facility
RLPD	Relative lattice parameter difference
SFR	Sodium-cooled fast reactor
TD	Theoretical density
TIG	Tungsten inert gas
TOP	Transient of power
TRL	Technology readiness level
TRU	Transuranic
UN	Uranium mononitride
WDS	Wavelength dispersive spectroscopy
WPFC	Working party on scientific issues of the nuclear fuel cycle
XRD	X-ray diffraction
YSZ	Yttrium stabilised zirconia

Executive summary

Spent fuel management continues to be a significant challenge for many countries as they attempt to develop and implement safe and environmentally sound approaches to disposing of spent fuel. An important aspect of this issue is the presence of minor actinides and fission products in spent fuel, which contribute to long-term radiotoxicity. An option that might be considered to address the issues associated with these highly toxic species would be to recycle the fuel using new, innovative technologies in various nuclear fuel cycle schemes. Several member countries have initiated R&D programmes to study a new type of fuel containing minor actinides for burning in fast neutron reactors.

This report reviews the studies of fuels containing minor actinides (MA) to be introduced in advanced nuclear systems, and it gives an overview of the state of the art in the development of innovative fuels, in particular MA-bearing fuels. While the use of MA-bearing fuels has advantages for both final disposition and for radiotoxicity reduction, these fuels must be produced using remote handling technologies due to hazards associated with the presence of transuranic elements.

In this report, different types of fuel were reviewed (metal, oxide, nitride, dispersion fuels and special mechanical fuel forms) for all types of advanced reactors, with a focus on fast neutron spectrum reactors. Different technical issues associated with the fabrication, characterisation, irradiation performance, design and safety criteria of such fuels were also examined, and the technical maturity of each fuel was assessed. Due to their physical properties, metal fuels are considered as ideal candidates for use in fast neutron reactors. A number of irradiation tests have been performed on this kind of fuel through multiple research programmes. Two types of MA-bearing fuel alloys were reviewed: fertile (U-Pu-Zr) based alloys and non-fertile (U-free) or low-fertile alloys.

Although properties of U-Pu-Zr fuel are now well-documented and the physical properties are starting to be understood, non-fertile MA-bearing fuels, on the other hand, are still at an early stage of development. Fuels were characterised through the measurement of their physical properties, such as phase transitions temperatures, thermal conductivity and Young's modulus. These data indicated that the presence of minor actinides and rare earth elements in U-Pu-Zr alloys did not significantly influence the physical properties of the fuels. Fabrication techniques are still being developed for MA-bearing fuels, but the presence of highly radioactive elements requires remote operations in hot cells. Injection casting is one of the most often employed techniques, but other techniques are being examined in an attempt to prevent the evaporation of americium. The effect of the MA and rare earth (RE) on the irradiation performance was assessed at different burn-ups. Post-irradiation examinations (PIE) showed that the presence of minor actinides in fuel (~5wt%) does not affect the irradiation behaviour of fuels.

Oxide fuels are the most widely used fuels worldwide. Two types of MA-bearing fuels were considered and, although mixed oxide fuels with a few percent of MA are under qualification, minor actinide-bearing blankets (MABB) – $(U,MA)O_x$ – are still at an early stage of development. Several international research programmes have investigated two different options: homogeneous (MA-bearing fuels with 1 to 5% MA) and heterogeneous fuels (MABB with 10 to 20% of MA inside a UO_2 support). Some research has focused on studying the effects of the presence of minor actinides on fuel performance. This involves several requirements in the design, fabrication and burn-up. MABF can be

fabricated in only a few facilities and have so far only been produced at laboratory scale. In this report, current fabrication processes were reviewed and fuels were characterised using different analytical techniques, showing that the presence of minor actinides in the fuel composition affects melting point, thermal conductivity, volatility, oxygen potential and helium production. Irradiations of MABF pellets have been conducted through various programmes. Post-irradiation experiments have been performed to observe structural changes, redistribution of Pu and Am, fuel melting and fuel cladding chemical interactions. Heterogeneous fuels are still at an early stage of development, but characterisation and irradiation tests have been carried out. PIE showed that a high concentration of He release causes an increase in the fuel column. The quantity of fission gas release was similar to that of standard fuel. Some pellet cladding interactions were observed, as well as the presence of Cs. Although oxide fuels have shown promising results, the conclusions have demonstrated that more studies will be necessary to gain further insight into the challenges associated with their implementation, in particular in the case of MABB.

Due to their higher fissibility, nitride fuels have numerous advantages for use in accelerator-driven systems (ADS) compared to other types of fuels. Nitride fuel developments were therefore reviewed in this report, although only a few fabrication methods have been developed to date. Fertile and non-fertile fuels have been fabricated, in particular for the FUTURIX-FTA irradiation programme, and low fertile pellets have appeared to be easier to produce than non-fertile ones. However, out-of-pile performance revealed to be poor as some end capping, degradation or cracks were observed. Irradiation tests on U-free nitride fuels have been carried out in Japan, and although they have only been performed at a low burn-up and the fuel did not contain any MA, PIE did not show any detrimental behaviour. Other irradiation tests at the advanced test reactor (ATR) and Phénix have been conducted and PIE is underway. In parallel, some modelling activities are ongoing using the code NITRAF. From a safety point of view, the main concerns about nitride fuels are the limited thermal stability of AmN and the high vapour pressure of Am, which could lead to a redistribution of the americium in the fuel. R&D on nitride fuels remains basic level since more progress on a laboratory scale and more experimental data are needed.

Dispersion fuels are a relatively new concept, which consists of including actinide dioxides in a ceramic phase composed of various materials. Single phase (CER) or ceramic-ceramic (CERCER), ceramic-metal (CERMET) configurations have been examined. The first irradiation tests on inert matrix fuel containing MA was started in the mid-1990s as part of the irradiation programme EFTTRA. Other irradiation programmes (CAMIX, COCHIX, FUTURIX and HELIOS) have been initiated and three types of fuel have now been tested. Some experiments are still ongoing and PIE has been performed only on a few pellets. Fabrication of pellets using infiltration of pellets has proven to be feasible. However, He management remains an issue in the performance of the transmutation target. The ECRIX successfully produced composite CERCER targets via powder metallurgical routes. MgO appeared to have a good capacity to store He during irradiation but can exhibit unfavourable vapourisation behaviour. Pellet swelling was also observed, with transmutation fission rates of 99% and 50% achieved. Although fabrication of fuel pellets were demonstrated, experimental data from irradiation experiments are not available as PIE have yet to be undertaken on numerous samples.

Finally, minor actinides can be integrated in special mechanical fuel forms, which are considered as a new concept to integrate minor actinides in fuels. Innovative processes for pellet fuels are being developed and a new form of fuels (i.e. particle fuels such as *vipac* and *sphere-pac*) are being tested. In the latter case, fuel particle material is compacted into the cladding. The main advantage of the particle fuel process is a reduction in dust production; the pin filling, however, is more difficult than in the pellet process. Different fabrication processes are described in the report but the most widely used remains the external gelation process to produce spherical particles. Producing

nuclear fuel pin from particle fuels is more difficult than from pellet fuels, and it requires additional requirements such as appropriate particle size distribution. Although numerous irradiation programmes have been performed on *vipac* and *spherepac* concepts, only a few have been conducted with MA-bearing fuels, notably in the Russian Federation and Japan. These latter programmes have concluded that the presence of minor actinides (in the case of Np) had minor incidence on the fuel performance.

In summary, transuranic bearing fuels are today being developed only at laboratory scale (gramme quantities of TRU) and irradiation tests have been limited to small samples, rodlets and in some cases one pin. Technology readiness levels were assessed for all fuels and the results ranged from three for nitride and dispersion fuels to four to five for oxide and metal fuels.

1. Introduction

This state-of-the-art report on innovative fuel concepts has been prepared by the NEA Expert Group on Innovative Fuels (EGIF). The scope of the report covers the technical issues associated with the development of innovative fuels and clad materials targeted for use in advanced fuel cycles. The fuel types of interest for EGIF are those that contain minor actinides (MA) as opposed to standard fuels (i.e. uranium or uranium-plutonium fuels that are currently being used in the fuel cycle). The following technical issues associated with innovative fuel development are covered within this report:

- comments on the transmutation performance;
- fuel fabrication techniques and fresh fuel characterisation;
- irradiation performance (including associated clad materials);
- design and safety criteria and safety characteristics;
- system dependency;
- comments on engineering scale modelling when applicable;
- assessment of the technical maturity of the specific fuel types;
- comments on future work.

1.1 Fuel types covered in the report

All fuels containing minor actinides (MA) were considered for any type of reactor and target: homogeneous, heterogeneous and ADS fuels. The following fuel types are covered in this report:

- metallic fuels (Chapter 2);
- oxide fuels (Chapter 3);
- nitride fuels (Chapter 4);
- dispersion fuels (including ceramic-in-ceramic (CERCER) and ceramic-in-metal (CERMET) dispersions) (Chapter 5);
- special mechanical fuel forms (particle fuels, sphere-pac, vibro-pac) (Chapter 6).

Carbide fuels were also considered in the past for fast reactors and they are still the subject of interest of a few international fast reactor programmes. However, the emphasis to date is on U and U-Pu bearing carbides and so far there has been no active programme investigating carbide fuels containing minor actinides. Therefore, carbide fuels will not be reviewed in the report.

Finally, this study also includes, for each fuel type considered, a discussion of the technical maturity assessment methodology in the form of definition of technology readiness levels (TRLs). The definitions of the TRLs as applied to nuclear fuel technology are provided in Appendix A.

1.2 Related activities

Sustainable development of nuclear energy calls for the development of innovative nuclear energy systems with highly efficient utilisation of fissile and fertile resources along with appropriate management of nuclear waste. Hence, development efforts in recycling reprocessed uranium, plutonium and minor actinides in current and future innovative nuclear energy systems are underway. Furthermore, new R&D programmes have also been launched to develop alternative reprocessing techniques and advanced partitioning processes that might support nuclear waste management. Advanced partitioning processes aim to recover minor actinides and other long-lived fission products for the purpose of transmuting them in reactors.

International Atomic Energy Agency

In 2009, the IAEA published a report on minor actinide fuel development [1]. This report reviewed and summarised all available information as well as on-going R&D results on related MA-bearing fuels for transmutation systems and represented the state of the art as of 2009. It covered reactor and fuel cycle options for actinide recycling; MA-bearing fuel types and their performance characteristics; pertinent thermal and physical properties; fabrication processes; and provided an overview of irradiation tests on minor actinide fuels.

The report concluded that a tremendous amount of excellent research had been accomplished. It appeared that the most emphasis had been placed on heterogeneous target fuel concepts with a high content of minor actinides (no plutonium). This trend may have been driven by the desire to set the performance envelope, namely to understand and prove performance characteristics in extreme cases. However, this approach may have overlooked some practical approaches amenable to commercial-scale deployment.

In 2010, the IAEA published a technical document on partitioning processes for transmutation of actinides [2]. The document provides information on the latest results achieved in the area of partitioning of the components present in spent nuclear fuels with emphasis on pyrochemical processes. This publication highlights emerging innovations and R&D needs for the back-end of the fuel cycle, particularly reprocessing of spent uranium and plutonium based ceramic and metallic fuels. The publication was prepared in collaboration with experts from member states and serves as a useful resource for nuclear scientists and engineers involved in reprocessing spent nuclear fuels as well as MA-bearing fuel development.

The IAEA also maintains and regularly updates an electronic database called the minor actinide property database (MAPD). This is a bibliographic database on physico-chemical properties of minor actinide compounds selected based on their importance for the use in advanced nuclear fuel cycle especially for the partitioning and transmutation. The MADB can be accessed through the IAEA's "integrated nuclear fuel cycle information systems" (INFCIS) and is useful for researchers involved in developing innovative nuclear fuels.

OECD Nuclear Energy Agency

The NEA Nuclear Science Committee (NSC) Working Party on Scientific Issues of the Nuclear Fuel Cycle (WPFC) has recently published two reports on the development of technologies to be deployed at an international level in order to minimise wastes. These mainly analyse the impact of recycling the actinides (plutonium and the minor actinides) responsible for the long-term radiotoxicity of waste. The study on the *Potential Benefits of Advanced Fuel Cycles with Partitioning and Transmutation* [3] assessed the effect of P&T on the waste inventory and the impact on different types of repositories.

The report on *Homogeneous versus Heterogeneous Recycling of Minor Actinides in Fast Reactors* (TFHH) [4] compared two recycling modes: the homogeneous mode that implies the multi–recycling of grouped TRU fuels in fast reactor and the heterogeneous recycle that separates out the less radioactive component of the LWR spent fuel transuranics to make driver fuel and use the remaining minor actinides in target fuels/assemblies. The potential impact on both the reactor core and the power plant was demonstrated as well as the potential issues in the implementation of the fuel cycle.

References

[1] IAEA (2010), *Status of Minor Actinide Fuel Development*, Vienna, NF-T-4.6, ISSN 1995-7807.
[2] IAEA (2010), *Assessment of Partitioning Processes for Transmutation of Actinides*, TECDOC-CD-1648.
[3] OECD/NEA (2011), *Potential Benefits and Impacts of Advanced Nuclear Fuel Cycles with Actinide Partitioning and Transmutation,* OECD, Paris.
[4] OECD/NEA (2012), *Homogeneous versus Heterogeneous Recycling of Transuranics in Fast Reactors,* OECD, Paris.

2. Metal fuels

2.1 Introduction

Important factors in selecting a fuel form for a commercial reactor will be performances of fuel itself, reactor core, and fuel cycle (reprocessing and fuel re-fabrication), in addition to safety performance, which will be considered as a combination of fuel and reactor core performances. Metal fuels are ideal for fast reactors because they have higher densities of fissile and fertile materials than any other fuel forms and provide higher reactor core performance such as higher breeding ratio and reduced fissile inventory. Significant amount of metal fuel irradiation tests were conducted in the integral fast reactor (IFR) programme [1,2]. About 2 000 test pins of the U-10wt% Zr binary alloy fuel and about 600 test pins of the U-Pu-10wt% Zr ternary fuel were irradiated in EBR-II and FFTF [3]. Of these test pins, about 300 U-Pu-Zr pins and 1 500 U-Zr pins exceeded 10at% burn-up [3]. The highest burn-up achieved was more than 19at% for the U-19wt%Pu-10wt% Zr fuel pin [4]. All of the driver fuel of EBR-II was converted to Mk-III fuel (U-10wt% Zr) [4]. In-pile transient tests [5] and out-of-pile heating tests [6,7] conducted in the IFR programme revealed metal fuel performance under transient conditions. Reactor transient tests in the EBR-II in 1986 demonstrated the inherent safety performance of metal-fuelled core in the events of loss of coolant flow (LOF) without scram and loss of heat sink (LOHS) without scram.

The reprocessing and fuel re-fabrication of metal fuels have already been demonstrated in the 1960s at Argonne National Laboratory. About 560 fuel subassemblies were processed by the low-decontamination pyro-metallurgical process, called “melt refining”, then fuel slugs were re-fabricated by injection casting from the recovered fuel and additional new alloy [8]. Approximately 34 500 acceptable fuel elements were made remotely in the hot cell at the Fuel Cycle Facility (FCF) adjacent to EBR-II [8]. Current fuel cycle technologies for metal fuel-electrometallurgical process and injection casting were developed in the IFR Programme. These technologies are expected to reduce the fuel cycle cost even for small-scale fuel cycle plants because of the simplicity of the process and the compactness of the equipment [1,2]. In the electrometallurgical process, irradiated metal fuel is anodically dissolved. While uranium is deposited on the solid cathode, plutonium is collected in the liquid cadmium cathode with uranium. Minor actinides (MA: Np, Am, Cm) and part of the lanthanide fission products are also collected in the liquid cadmium cathode, as indicated by the thermo-chemical theory.

From the standpoint of MA transmutation, metal fuels have the following favourable characteristics. Metal-fuelled fast reactors provide the effective transmutation of MA due to the high-energy neutron spectrum [9,10]. Simultaneous recovery of MA with plutonium in the electrometallurgical process facilitates MA recycle for substantial MA transmutation in a fast reactor fuel cycle system. Because of these favourable characteristics of metal-fuelled fast reactor core and metal fuel cycle, there is on-going development in the field of MA-bearing metal fuel in the United States, Japan, the European Commission (EC) and the Republic of Korea.

Two kinds of MA-bearing fuel alloys are being developed at present: U-Pu-Zr-based alloys and non-fertile (U-free) or low-fertile alloys. The former alloys are intended mainly for use as fuel for fast reactor cores loaded with MAs homogeneously. The latter alloys are for use in accelerator-driven transmutation systems or as fuel in transuranium element (TRU) burner reactors. The first irradiation of MA-bearing metal fuel was

conducted in the X501 test assembly in EBR-II [11-13]. Collaboration between the Central Research Institute of Electric Power Industry (CRIEPI) and the European Commission Joint Research Centre – Institute for Transuranium Elements (ITU) started in 1988 for the characterisation and fabrication of U-Pu-Zr alloys containing MAs and rare earth elements (REs) [14,15]. The CRIEPI-ITU collaboration has now been expanded to post-irradiation examinations (PIE) of U-Pu-Zr-MA-RE alloys irradiated at the French fast reactor Phénix, known as METAPHIX [16-20]. A series of irradiation tests on non-fertile and low-fertile alloys, designated as AFC-1 [21-23], has been conducted at the Advanced Testing Reactor (ATR) at the Idaho National Laboratory (INL). Non-fertile and low-fertile alloys similar to the AFC-1 test alloys have been irradiated at Phénix as a part of the FUTURIX-FTA Programme [24,25]. For the more recent AFC-2 irradiation test series [26,27] at INL, MA-bearing U-Pu-Zr-based alloys are to be irradiated. Characterisation of MA-bearing metal fuel alloys has also been performed at INL as has the development of fuel fabrication technology. Research and development activities at the Korea Atomic Energy Research Institute (KAERI) cover the characterisation of U-Zr-Ce alloys, which are used as surrogates for U-Pu-Zr-MA-RE alloys, the fabrication of TRU-bearing metal fuel, and the development of lined cladding for metal fuel.

Carmack et al. [28] summarised the current focus areas of MA-bearing metal fuel research and development as follows:

- Demonstration of MA-bearing feedstock reduction to metal alloy feedstock. It is expected that the MA-bearing feedstock available for fuel fabrication will be in oxide form. This feedstock must be reduced to metal for metal alloy fuel fabrication.
- Due to Am metal volatility, fabrication with high Am retention must be demonstrated using revised casting technology utilising higher pressure systems, shorter heating times, and removing conditions that would promote Am vapour deposition.
- Metal fuel properties must not be seriously degraded as compared to the U-Pu-Zr system performance by the addition of the MAs (Am, Np, and Cm).
- Demonstration of an acceptable level of fuel-cladding-chemical interaction (FCCI) with fuel that includes rare earth impurities and MA fuel constituents over the lifetime of the fuel up to its burn-up limit, ~20at%.
- Assuming that fuel melting and FCCI characteristics are acceptable; behaviour of MA-bearing fuel in over-power transients and run beyond cladding breach should also be acceptable. Performance modelling and perhaps proof testing of these assumptions may be required.
- Burn-up limitation extensions greater than 23at% (at 39 x 10^{22} n/cm^2 or approximately 200 dpa) can be anticipated with current ferritic/martensitic steel cladding and up to 30at% may be achievable with increased high-temperature cladding strength and performance.

From these points of view, this chapter presents a review of work on the characterisation, fabrication, and irradiation performance of MA-bearing metal fuel, followed by speculation on safety performance, fuel design criteria, applicability to reactor systems, technical issues, and future work.

2.2 Characterisation of minor actinide-bearing metal fuels

Phase structures and physical properties of U-Pu-Zr-based alloys and non-fertile or low-fertile alloys are reviewed here. U-Pu-Zr-based fuel alloys usually contain up to 8wt% MAs, and some of them contain mixtures of rare earth (lanthanides) elements (hereinafter abbreviated to REs). Non-fertile (U-free) or low-fertile (low-U) TRU-Zr-based fuel alloys typically studied to date have contained higher fractions of Zr (30-60wt%) than the more traditional U-Pu-Zr alloys that usually contain 10-20wt% Zr. The characterisation

of these alloys is one of the fundamental issues in designing MA-bearing metal fuel. In particular, compatibility with cladding materials is of great importance from the standpoint of fuel lifetime and safety when the alloy contains rare earth elements.

In this chapter, alloy compositions are described in weight percent (wt%), unless otherwise indicated.

2.2.1 U-Pu-Zr based alloys

Phase structures

Kurata et al. [14] examined arc-melted U-20Pu-10Zr-xMA-yRE alloys of various compositions to determine the miscibilities among the alloy constituents. Metallographic observation and electron probe microanalysis (EPMA) of as-fabricated alloys indicated that the solubility of REs in U-Pu-Zr alloy is low. In the RE-containing alloy, a RE-rich phase precipitates and extracts some of the Pu and Am. Homogeneous dispersion of the RE-rich precipitates cannot be attained when the RE content is much higher than 5wt%. In alloys containing no REs but <25wt% MAs, MAs dissolve uniformly in U-Pu-Zr alloy.

Table 2.1: Annealing conditions for alloy samples

Sample	Annealing condition		Cooling
	Temp. (°C)	Time (hr)	
CR11M CR12M	700	3.5	Furnace cool
$CR11M_1$ $CR12M_1$	700	3.5	Quench
$CR11M_2$ $CR12M_2$	600	21	Quench
$CR11M_3$ $CR12M_3$	500	28	Quench
$CR11M_4$ $CR12M_4$	850	25	Quench
$CR11M_5$ $CR12M_5$	600	96	Quench
$CR11M_6$ $CR12M_6$	700	100	Quench
$CR11M_7$ $CR12M_7$	950	18	Quench
$CR11M_8$ $CR12M_8$	500	97	Quench

After annealing at constant temperatures and quenching in water, three kinds of alloys: U-19Pu-10Zr-2MA-2RE (CR11), U-19Pu-10Zr-5MA-5RE (CR12), and U-19Pu-10Zr (CR13) were investigated by Kurata et al. [14]. The annealing conditions are summarised in Table 2.1. Figures 2.1 and 2.2 show the metallography of cross-sections of the CR11 and CR12 alloy samples, respectively, after etching. The dark-coloured precipitates in the figures were rich in REs and Am, which dispersed uniformly in all the samples. The sizes of the RE-rich precipitates were about 3 m and >10 m in the CR11 and CR12 samples,

respectively. The compositions of the phases and precipitates observed in the CR12 samples are summarised in Table 2.2. The matrices of CR12 alloy samples annealed at 500°C and 600°C showed a two-phase structure, presumably + at 500°C and + (or +) at 600°C. In the samples annealed at 700°C and 850°C, the matrix was a single phase, and there were RE-Am-rich precipitates at the grain boundaries. In Table 2.2, the Am content in the precipitate of the sample annealed at 850°C is significantly lower than those annealed at lower temperatures. This may be due to Am evaporation during annealing.

Table 2.2: Compositions (wt%) of phase 0 in the annealed alloy samples, analysed by EPMA

	Alloy samples Annealing temperature (°C)	Elements						
		U	Np	Pu	Am	Zr	Ce	Nd
Precipitate	CR12M furnace cool	0.10	0.06	8.34	28.03	0.12	22.16	41.19
	$CR12M_1$ 700	0.16	0.17	8.78	18.86	0.29	17.74	54.05
	$CR12M_3$ 500	0.33	0.07	8.03	19.61	0.19	18.07	53.77
	$CR12M_4$ 850	0.29	0.08	8.10	4.81	0.28	24.78	61.66
	$CR12M_6$ 700	0.18	0.05	8.09	12.52	0.22	22.75	56.62
	$CR12M_8$ 500	0.49	0.08	8.12	22.52	0.19	19.58	49.03
Matrix	CR12M furnace cool	62.30 76.17	3.23 3.54	20.33 18.76	0.79 0.07	13.17 1.26	0.12 0.06	0.10 0.17
	$CR12M_1$ 700	66.38	3.42	19.86	0.59	9.33	0.28	0.14
	$CR12M_3$ 500	47.06 74.01	3.55 4.26	22.15 18.67	0.99 0.29	25.37 2.57	0.38 0.07	0.50 0.13
	$CR12M_4$ 850	66.24	3.73	20.53	0.39	8.73	0.31	0.07
	$CR12M_6$ 700	66.84	3.65	19.91	0.38	9.13	0.22	0.10
	$CR12M_8$ 500	42.92 75.64	2.52 4.02	22.46 17.64	0.92 0.21	30.76 2 018	0.24 0.13	0.18 0.23

Figure 2.1: Metallography of annealed U-19Pu-10Zr-1.2Np-0.8Am-0.1Y-0.5Ce-1.4Nd alloys (CR11), etched [14]

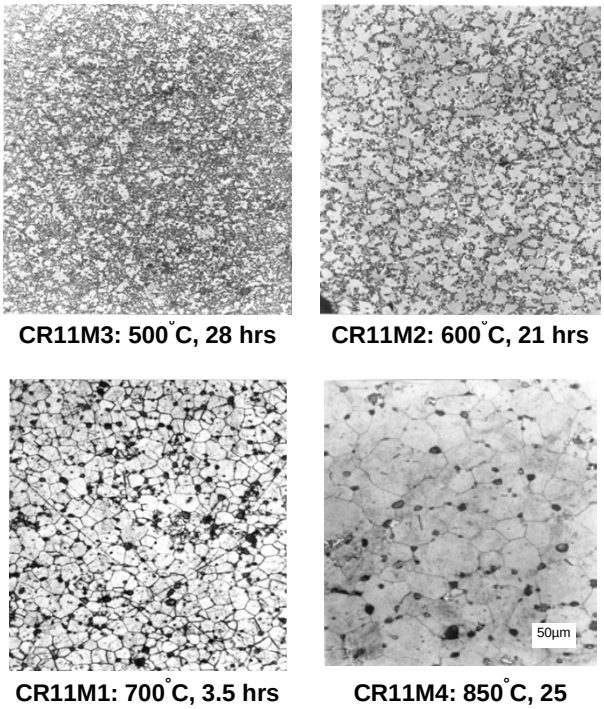

Figure 2.2: Metallography of annealed U-19Pu-10Zr-3Np-2Am-0.2Y-1.2Ce-3.6Nd alloys (CR12), etched [14]

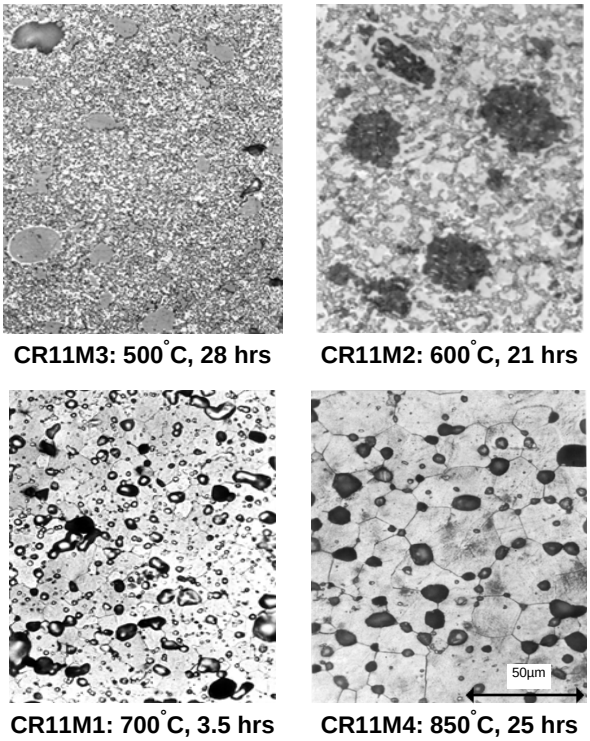

Burkes et al. [29] investigated two fuel alloys, 60U-20Pu-3Am-2Np-15Zr and 58.5U-20Pu-3Am-2Np-15Zr-1.5RE, which were fabricated using an arc-casting process. Right cylindrical fuel slugs were cast into quartz molds upon melting. X-ray diffraction (XRD) for both as-cast alloys showed a significant amount of surface texture generated by the sample preparation method. The major phase observed in both alloys was determined to be δ-(U,Pu)Zr_2 that crystallised from the as-cast state in the hexagonal P6/mmm space group. The δ-UZr_2 phase is an AlB2-type structure and is non-stoichiometric, and exists as a solid solution for all participating elements over a significant compositional range. The addition of rare earths to the 60U-20Pu-3Am-2Np-15Zr alloy appeared to have a minor influence on the as-cast phase structure.

Physical properties

Kurata et al. [14] measured some physical properties of U-19Pu-10Zr-2MA-2RE (CR11), U-19Pu-10Zr-5MA-5RE (CR12), and U-19Pu-10Zr (CR13) alloys. The phase transition temperatures were measured by dilatometry. The dilatometric curves are shown in Figure 2.3. The figure indicates two distinctive phase transition temperatures at approximately 580°C and 630°C in common with these alloys and an insignificant influence upon addition of MAs and REs up to 5wt%. According to the U-Pu-Zr ternary phase diagrams, the U-19Pu-10Zr (in wt%) alloy has phase transitions of ζ+δ to ζ+γ at 580-600°C, and ζ+γ to γ at 660-670°C. The phase transition temperatures observed in the dilatometric curves are in agreement with those for the phase diagrams and are consistent with the phase structures after the annealing described above. The liquidus temperatures of CR12 and CR13 measured by dilatometry were 1 207°C and 1 217°C, respectively. The influence of the addition of MAs and REs of 5wt% on the phase transition temperature and liquidus is minor considering uncertainty in the measurement. The thermal conductivities of CR12 and CR13 were measured by a comparative method with pure iron as a reference material. The alloy sample temperature was restricted to below 650°C to avoid plastic deformation of the sample at a high temperature. The measured data shown in Figure 2.4 indicate an insignificant influence of MA and RE addition on the thermal conductivity. Table 2.3 shows Young's modulus, shear modulus, and Poisson's ratio of CR12 and CR13 measured by an ultrasonic method, and suggest that the influence of MA and RE addition on these properties was not significant.

Burkes et al. [29] obtained heating and cooling curves by differential scanning calorimetry (DSC) for two fuel alloys: 60U-20Pu-3Am-2Np-15Zr and 58.5U-20Pu-3Am-2Np-15Zr-1.5RE. The temperatures and enthalpies of two transitions obtained from the heating and cooling curves are summarised in Table 2.4. Upon cooling, both transitions are reversible based on the transition enthalpies, at least within the reported error. Transition temperatures show a decrease upon cooling, more so for the second transition compared to the first transition, and likely due to super-cooling. Heat capacities for the 60U-20Pu-3Am-2Np-15Zr alloy reported in [29] follow a similar trend to that of uranium up to the first phase transition (873K). This observation is expected since the alloy contains 60wt% uranium. The determined heat capacities and temperature dependencies above the transition temperatures were found to be “peculiar” in both their values and behaviour and further studies are underway.

Figure 2.3: Dilatometric curves of U-19Pu-10Zr (CR13), U-19Pu-10Zr-1.2Np-0.8Am-0.1Y-0.5Ce-1.4Nd (CR11) and U-19Pu-10Zr-3Np-2Am-0.2Y-1.2Ce-3.6Nd (CR12) alloys [14]

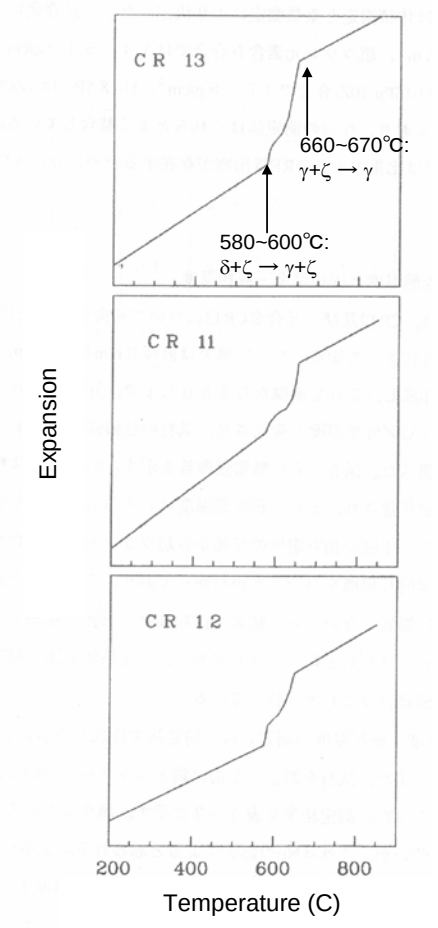

Figure 2.4: Measured thermal conductivities of U-19Pu-10Zr (CR13), and U-19Pu-10Zr-3Np-2Am-0.2Y-1.2Ce-3.6Nd (CR12) alloys [14]

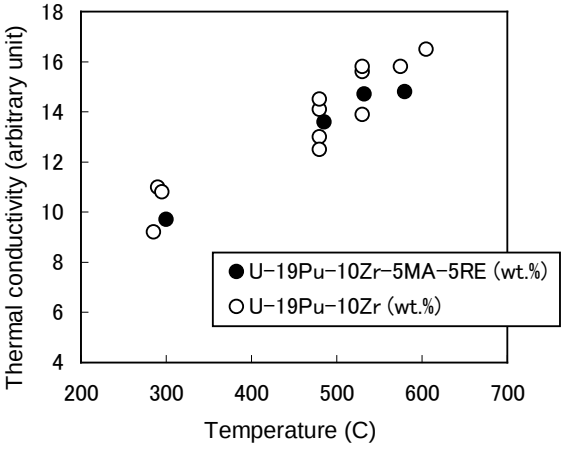

Table 2.3: Measured mechanical properties [14]

	Measured		Reported
	U-19Pu-10Zr	U-19Pu-10Zr 5MA-5RE (CR12)	U-19Pu-10Zr
Density (g/cm^3)	15.501	14.510	15.8
Sample thickness (mm)	4.3	4.33	
Young's modulus (GPa)	93.306	85.215	123
Shear modulus (GPa)	35.391	32.647	
Poisson ratio	0.317	0.305	0.34

Table 2.4: Transition temperatures (T_{tr}) and enthalpies of transition (ΔH_{tr}) determined from differential scanning calorimetry upon heating and cooling [29]

60U-20Pu-3Am-2Np-15Zr alloy				
Transition	Heating		Cooling	
	First	Second	First	Second
T_{tr} (K)	830±0.3	927±0.2	909±0.5	821±1.1
ΔH_{tr} (J/g)	-4.27±0.34	-20.54±2.95	22.58±3.36	4.80±0.41
58.5U-20Pu-3Am-2Np-15Zr-1.5RE alloy				
Transition	Heating		Cooling	
	First	Second	First	Second
T_{tr} (K)	845±0.6	919±0.9	907±0.3	843±0.2
ΔH_{tr} (J/g)	-16.50±2.19	-21.72±2.31	24.01±2.94	14.47±1.95

Cheon et al. [30] measured the thermal diffusivity of U-10Zr-6Ce alloy specimens up to 700°C by using a laser flash technique. The thermal conductivity was evaluated from the measured thermal diffusivity data by using the density determined by an immersion technique and the specific heat estimated in accordance with Kopp-Neumann's law. The evaluated thermal conductivity indicated that Ce addition lowered the conductivity of the U-Zr alloy by less than 5%. This result is consistent with Figure 2.4.

Burkes et al. [31] recently reported the results of X-ray diffraction of six kinds of as-cast MA-bearing fuel alloys including low-fertile alloys: U-20Pu-3Am-2Np-15Zr, U-30Pu-5Am-2Np-20Zr, U-34Pu-4Am-2Np-20Zr, U-29Pu-4Am-2Np-30Zr, U-28Pu-7Am-30Zr, and U-25Pu-3Am-2Np-40Zr. They also measured the transition temperatures and enthalpies of transition extensively by DSC.

Thermo-diffusion of alloy constituents

Kurata et al. [32] reported the results of the thermo-diffusion tests for U-19Pu-10Zr-5MA-5RE and U-19Pu-10Zr alloys. The test results suggest that Am behaves like Nd and Ce, and

Np follows Pu. The U,Pu, and Zr profiles after diffusion annealing were inconsistent with those obtained in the irradiation tests. This may be because the temperature gradients in the thermo-diffusion test (~20K/mm) were too small to attain an equilibrium state within the annealing time of 663 or 1 032 hours. In the case of irradiation tests at EBR-II, the temperature gradients were approximately 70-100 K/mm, and discernible migration was observed after about 1at% burn-up (about 50-60 effective full power days).

Compatibility with stainless steel

The metallurgical reactions of alloys containing MAs and REs with cladding steel were examined by Sari et al. [33] Rods, 3 mm in diameter, of U-19Pu-10Zr-5MA-5RE (CR12), U19Pu-10Zr (CR13), rare earths (REAL), and rare earth-minor actinide (REMAAL) alloys were sandwiched between austenitic steel (15-15Ti) rods, as shown in Figure 2.5. The sandwich (diffusion couple) was loaded in the dilatometer and subjected to heating-cooling cycles. The test conditions are summarised in Table 2.5. The onset temperature of the metallurgical reaction at the alloy-steel interface (or the solidus temperature of the reaction product) was estimated from the dilatometric curve, i.e. the length change of the sandwich detected by the dilatometer, as presented in Table 2.5.

Figure 2.5: Schematic view of diffusion couples for the compatibility test [33]

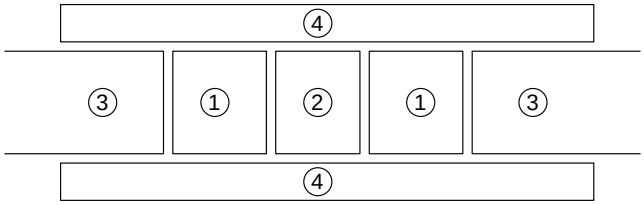

①Phenix Steel ②Sample ③Al_2O_3 pushing bars ④ Al_2O_3 sample holder

The data for the onset temperature for the first cycle may be influenced by the reaction-diffusion in the diffusion couple, while the data for the second or later cycles may correspond to the solidus temperature of the reaction product. The compositions of the phases detected in the reaction zones in the CR13/steel, CR12/steel, REMAAL/steel, and REAL/steel couples are shown in Tables 2.6, 2.7, 2.8, and 2.9, respectively. RE-rich precipitates (see Figure 2.6) formed in the reaction zone in the CR12/steel couple are also rich in Am, Pu, and Ni, as shown in Table 2.9 (Phase 3). The other phases formed in the CR12/steel couple were equivalent to those in the CR13/steel couple. The reaction zone formed in the REMAAL/steel couple is shown in Figure 2.7. The phase compositions for the REMAAL/steel couple (see Table 2.8) indicate that Fe reacts mainly with Pu and Am, while Ni reacts mainly with Am and rare earths (REs). The reaction zone structure in the REAL/steel couple was similar to that in the REMAAL/steel couple. The difference between the reaction onset temperatures for the CR12/steel and CR13/steel couples was not significant, considering the uncertainties arising from the experimental method.

Cole et al. [34] investigated the inter-diffusion between the HT-9 ferritic-martensitic steel and 60U-20Pu-3Am-2Np-15Zr fuel alloy containing 8% rare earth elements (REs: Nd, Pr, Ce, La) after annealing at 650°C for 125 hours. The inter-diffusion zones were composed of several distinct phase regions. A secondary electron image of the fuel-cladding interaction zones (Figure 2.8) revealed significant inter-diffusion between the cladding and the fuel. A higher magnification image of the top interface, as shown in Figure 2.9 (a), reveals more clearly the inter-diffusion structure as well as the formation of several inter-diffusion phases. The result of an X-ray line scan across the interface is shown in Figure 2.9 (b). Zone 1 shows the unreacted HT-9 cladding alloy. In Zone 2, the fuel elements have diffused into the cladding. U,Pu, and Np concentrations in the cladding are appreciable, while Am and REs have apparently not diffused into the cladding. In Zone 3, an inter-diffusion zone within the fuel, there is a matrix phase that

consists primarily of U,Pu, and Fe. Within this matrix phase, there is an inter-dispersion of a secondary phase enriched with Am and REs. Finally, at the interface between the inter-diffusion zone and the unreacted fuel, a highly porous structure is formed. One possible explanation for this structure is the formation of a low-melting-point phase along the interface and subsequent flow of the liquid out of the interconnected cavities.

Table 2.5: Conditions and results of the compatibility test

Couple	Composition	Cycle	Heating rate (K/min)	Temperature (K)	
				Start of reaction	Melting
CR13/3-steel	71U-19Pu-10Zr	1	2	1 090	1093
	15/15Ti$_{CW}$	1a	2	990	1013
		2	7	975	1020
		3	5	975	
CR13/3E2-steel	71U-19Pu-10Zr	1	2	1 095	1 100
	15/15Ti$_{CW}$	2	7	980	1 000
		3	2	970	995
CR12/3-steel	61U-19Pu-10Zr-2Am-3Np-3.6Nd-1.2Ce-0.2Y	1	2	970	1 065
	15/15Ti$_{CW}$	2	2	970	1 000
		3	7	970	1 010
CR12/3E2-steel	61U-19Pu-10Zr-2Am-3Np-3.6Nd-1.2Ce-0.2Y	1	2	998	1 020
	15/15Ti$_{CW}$	1a	2	960	1 000
		2	2	900	970
		3	5	900	985
		4	7	930	990
		5	7	930	1 000
		6	7	920	985
REMAAL-steel	52Nd-16Ce-4Y-8Pu-20Am	1	7	960	970
	15/15Ti$_{CW}$	2	2	870	898
REAL-steel	70Nd-10Ce-10Gd-10Y	1	7	990	1 005
	15/15Ti$_{CW}$	2	1	880	898
		3	2	898	903
		4	2	898	903
		5	2	870	890

Table 2.6: Composition of the phases detected in the reaction zone of CR13-steel couple

Constituent	Concentration (wt%)									
	Region 1			Region 2				Region 3		
	1	2	3	4	5	6	7	8	9	10
Cr	5.5	1.2	9.1	4.1	0.0	11.8	0.0	0.0	13.7	0.1
Fe	24.6	9.1	27.0	25.7	3.9	27.5	15.0	3.9	31.6	11.9
Ni	3.0	0.7	3.0	3.6	0.1	3.2	6.5	0.0	2.0	7.6
Zr	6.4	1.4	17.6	4.0	0.1	20.8	22.3	0.5	38.2	31.7
U	49.9	59.8	39.7	57.0	84.7	33.8	48.1	85.5	13.5	43.5
Pu	10.6	27.8	3.6	5.6	11.2	2.9	8.1	10.1	1.0	5.2

Table 2.7: Composition of the phases detected in the reaction zone of CR12-steel couple

Constituent	Concentration (wt%)					
	Phase 1	Phase 2	Phase 3	Phase 4	Phase 5	Phase 6
Cr	6.4	0.2	0.4	8.4	3.9	0.2
Fe	28.9	3.6	1.8	37.6	28.9	11.8
Ni	2.7	0.2	20.6	1.7	0.6	5.5
Zr	7.1	0.4	0.5	39.7	26.1	27.4
Ce	1.0	0.0	5.6	0.1	0.0	0.1
Nd	0.3	0.0	14.3	0.0	0.0	0.0
U	45.9	78.2	2.8	10.7	38.9	47.9
Np	1.0	3.3	0.4	0.5	0.3	1.3
Pu	6.4	14.1	34.5	1.3	1.3	5.5
Am	0.3	0.0	19.1	0.0	0.0	0.3

Table 2.8: Composition of the phases detected in the reaction zone of REMAAL-steel couple

Constituent	Concentration (wt%)			
	Phase 1	Phase 2	Phase 3	Phase 4
Cr	0.9	0.2	0.1	0.2
Mn	0.7	0.2	0.2	0.0
Fe	29.3	1.0	0.1	0.1
Ni	0.3	10.3	0.2	1.4
Y	2.9	3.6	3.0	0.9
Ce	5.3	19.8	21.5	34.1
Nd	3.9	46.6	56.6	48.9
Pu	35.3	0.9	1.8	0.6
Am	21.4	17.4	16.5	13.8

Table 2.9: Composition of the phases detected in the reaction zone of REAL-steel couple

Constituent	Concentration (wt%)					
	Phase 1	Phase 2	Phase 3	Phase 4	Phase 5	Phase 6
Cr	0.0	0.0	0.0	0.0	0.1	0.6
Mn	0.0	0.1	0.1	0.1	4.5	0.7
Fe	1.5	0.1	0.1	2.5	22.6	45.2
Ni	10.4	0.0	0.0	4.9	2.3	0.7
Y	8.0	3.0	6.2	9.2	7.6	18.4
Ce	10.5	21.4	12.4	10.4	20.8	4.8
Nd	60.6	71.3	71.9	64.3	35.3	17.4
Gd	9.0	4.1	9.3	8.6	6.8	12.2

Figure 2.6: Reaction layer formed at CR12/15-15Ti interface [33]

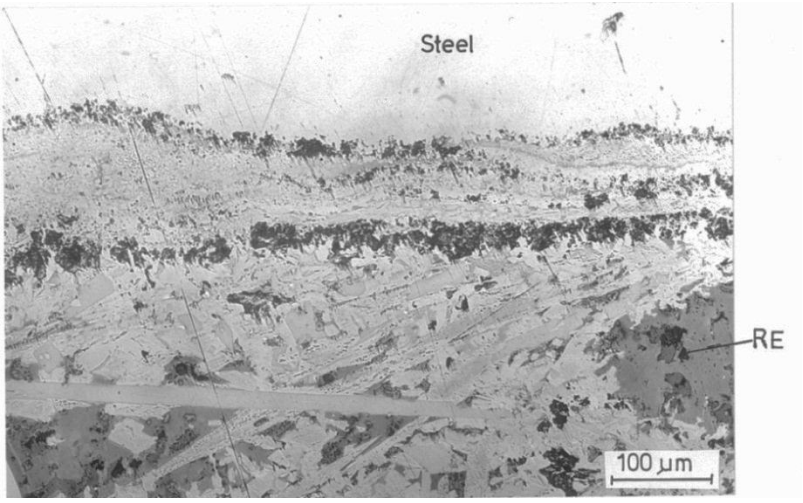

Figure 2.7: Reaction layer formed at REMAAL/15-15Ti interface [33]

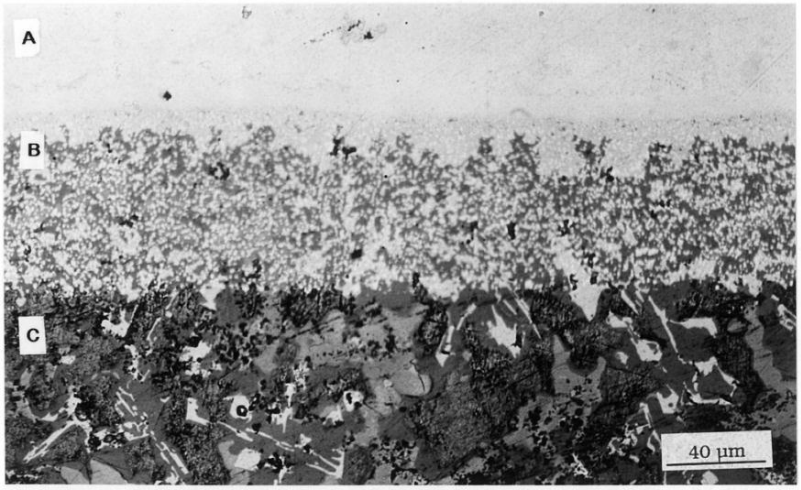

Figure 2.8: Secondary electron image of fuel/cladding interfaces after annealing at 650°C for 125 hours (Fuel: 60U-20Pu-3Am-2Np-15Zr fuel alloy containing 8% rare earth elements (Nd, Pr, Ce, La), cladding: HT9) [34]

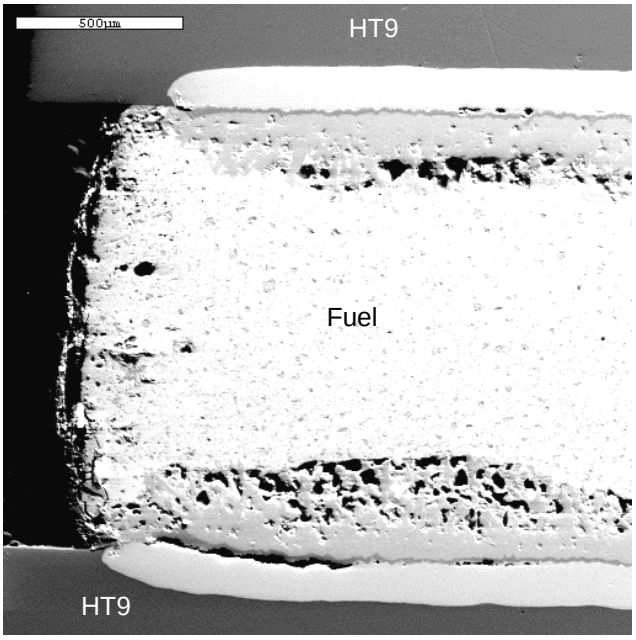

Figure 2.9: (a) Secondary electron image of fuel-cladding interaction zones and (b) an elemental X-ray intensity line scan across the fuel-cladding interface as represented by the yellow line on the image [34]

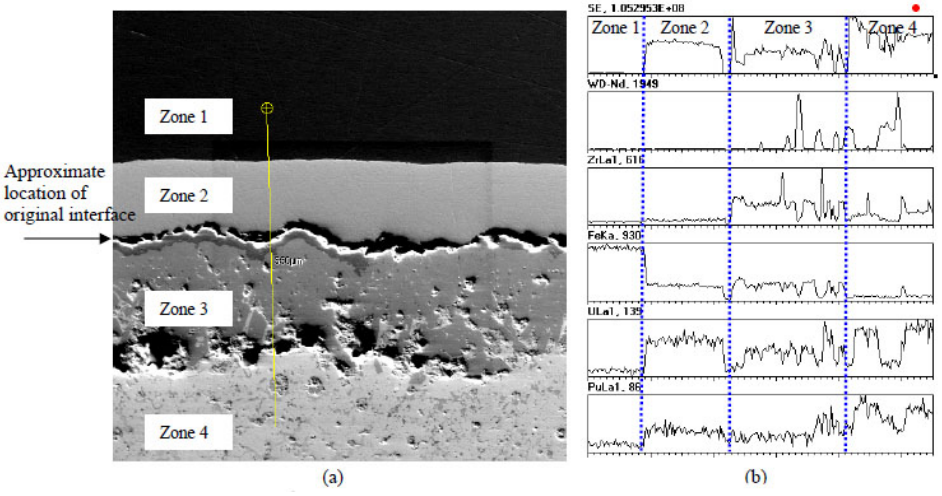

2.2.2 Non-fertile and low-fertile alloys

Cole et al. [35] reported the results of characterisation of non-fertile 48Pu-12Am-40Zr and low-fertile 35U-29Pu-2Np-4Am-30Zr alloys. The alloy specimens were prepared in an argon glovebox by a suction extraction casting method. The feedstock materials were melted in an electric discharge plasma arc melter and thoroughly homogenised. A ZrO_2-coated quartz tube was then dipped into the molten liquid and the liquid was drawn up into the tube using a syringe. The slug dimensions for the fuel alloys were

approximately 5cm in length and 4.9 mm in diameter. X-ray diffraction (XRD) showed that the as-cast non-fertile 48Pu-12Am-40Zr alloy was composed of a single phase having a face-centred cubic structure (FCC, δ-Pu stabilized structure) and the as-cast low-fertile 35U-29Pu-2Np-4Am-30Zr alloy showed only the formation of a hexagonal δ-UZr_2 phase. Thermal studies showed that low-fertile alloy begins to transform to a body-centered cubic phase by 550°C and non-fertile alloy, by 650°C. The general characteristics of low-fertile fuel are similar to non-fertile fuel, having a Zr- and Si-rich outer rind, and an outer perimeter zone containing larger Zr-rich precipitates. This may indicate adherence of constituents from the ZrO_2-coated quartz mold used for the casting of the fuels.

Carmack et al. [28] presented the thermal conductivity of Pu-40Zr estimated from Pu and Zr elemental thermal conductivities, as shown in Figure 2.10. They also presented the specific heat of Pu-Am-Np-Zr alloys estimated using Kopp-Neumann's law, as shown in Figure 2.11.

Figure 2.10: Estimated thermal conductivity of Pu-40Zr [28]

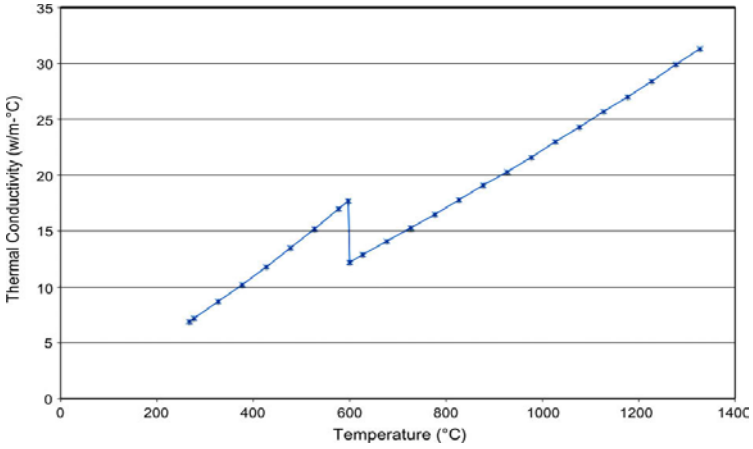

Figure 2.11: Specific heats of metallic U-Pu-TRU alloys [28]

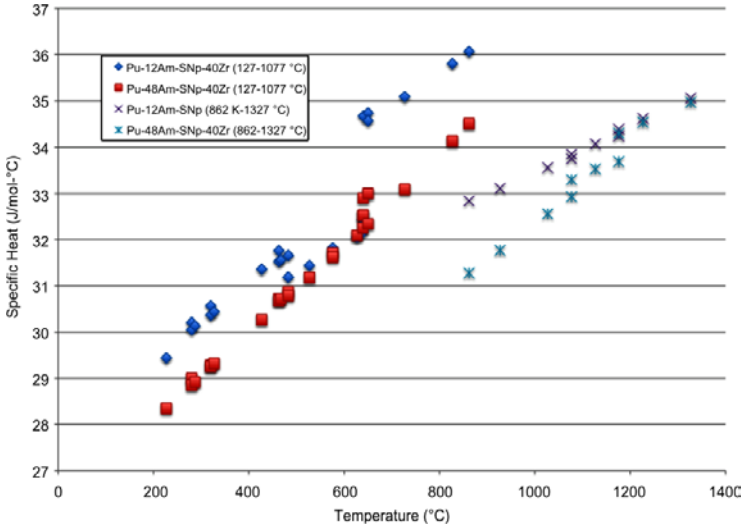

2.2.3 Summary

As for U-Pu-Zr-based fuel alloys, data on the phase structures are accumulating, e.g. dispersion behaviour of RE-rich precipitates and agglomeration behaviour of Am in RE-rich precipitates. Measurements of physical properties such as phase transition temperatures, thermal conductivity, and Young's modulus indicate that the U-Pu-Zr alloy

properties are not significantly influenced by the addition of MAs and REs. Out-of-pile tests on compatibility with steels have also been performed. Further data on alloy characteristics are necessary to better understand the performance of MA-bearing metal fuel. In contrast, characteristics data for non-fertile or low-fertile alloys are still limited.

2.3 Fuel fabrication

The MA-bearing metal fuel alloys for the METAPHIX (Figure 2.12), AFC-1, AFC-2 (Figure 2.13), and FUTURIX-FTA irradiation tests were all manufactured using an arc-melting technique [15,24,26,36]. The fabrication of the METAPHIX test fuel alloys, which have higher rare earth content (2 or 5wt%) than the other test fuel alloys, included pulverising and mechanical mixing steps in the alloying process to improve their homogeneity [15], as shown in Figure 2.14. Although these fuel alloys were successfully manufactured, an arc-melting technique will not be used for larger-scale fuel fabrication. For the X501 irradiation test [11-13], MA-bearing metal fuel slugs were fabricated by injection casting [37], which was a well-established technique for MA-free metal fuel fabrication. However, a significant amount of the initial Am charge was lost in the casting of MA-bearing fuel slugs [37].

Figure 2.12: MA-bearing fuel alloys for METAPHIX irradiation test

Figure 2.13: MA-bearing fuel alloys for AFC-2 irradiation test [36]

A practical process for nuclear fuel fabrication, in general, needs to be safe, cost-efficient, and capable of producing minimal amounts of radioactive waste. These require the MA-bearing fuel fabrication process to be simple as well as capable of mass production and actinide loss minimisation. The existence of MAs, sometimes accompanied by rare earth fission products, needs special attention. The high radioactivity of MAs (and their fission products) requires the process to be suitable for

remote operation in a hot cell. The high volatility of Am requires special measures to suppress Am loss. The chemical activities of the MAs and rare earth fission products raise the issue of their compatibility with such process materials as crucibles, molds, and coatings. Also, MAs and the fission products should be homogenised or uniformly dispersed in the fuel alloy. Recent activities in MA-bearing metal fuel fabrication have been focused on determining the appropriate methods to control the MAs (particularly Am) during the fabrication process [38-42].

Figure 2.14: Fabrication scheme of U-Pu-Zr, U-Pu-Zr-MA, U-Pu-Zr-MA-RE alloy rods for METAPHIX irradiation test

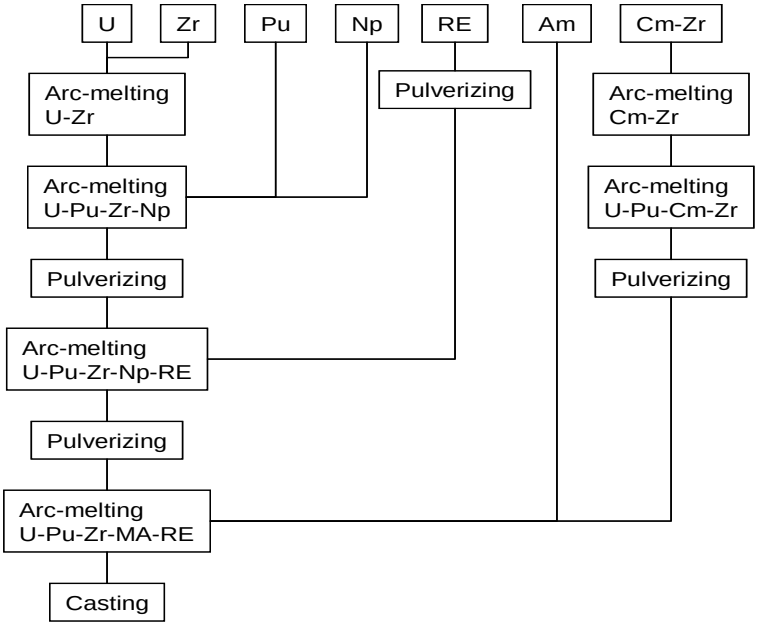

This section reviews possible methods of MA-bearing metal fuel fabrication and related development activities, followed by discussion of a potential issue in MA-bearing metal fuel fabrication, i.e. Am loss. MA alloy preparation methods are also reviewed.

2.3.1 Possible methods of MA-bearing fuel fabrication

Injection casting

One possible method of casting MA-bearing fuel slugs is injection casting with induction heating [37]. The starting materials are melted and homogenised in a crucible at approximately 1 500°C in an Ar gas atmosphere. After evacuating the vessel, the bottom ends of the silica tube molds, the top ends of which are closed, are immersed in the molten alloy. The vessel is then refilled with Ar gas to inject molten fuel alloy into the silica molds. After cooling, the fuel alloy castings are removed from the molds. Fuel slugs are obtained by shearing off both ends of the castings. As the mold must be broken from the cast fuel slug, the glass is not re-usable, and this method is therefore not cost-efficient. The mold shards will be considered as radioactive waste. However, the shards can be used as glass materials for a waste form such as glass-bonded sodalite, so that these may not be additional waste [43].

The injection casting process was used for fabricating a significant amount of metal fuel including driver and test fuel in EBR-II and test fuel in FFTF. Its remote operation was successfully demonstrated in a hot cell [8]. The MA-bearing metal fuel slugs were injection cast for the X501 irradiation test [11-13], where a part of the initial Am charge

was lost during casting due to volatile impurities (Ca and Mg) in the Am-Pu feed stock, [37] as discussed later.

CRIEPI conducted engineering-scale injection casting tests [44] and produced approximately 500 U-10Zr alloy slugs of 6 mm in diameter and 400 mm in length. Although 1.1% Mo, 0.8% Pd, 0.06% Ce, and 0.1% Nd (in wt%) were added to the metal charge, simulating fission product elements that may remain in the pyroprocess products, the precipitation of these elements was not detected in the U-Zr slugs [44]. KAERI has experience of injection casting of U-10Zr-(2,4,6)Ce (in wt%) ternary alloys, where Ce was a surrogate element for MAs or rare earth fission products. Ce particles were found to be dispersed in the U-Zr matrix [41].

Centrifugal casting

In a centrifugal casting process, fuel alloy melt is poured vertically into a rotating plate (distributor), where the melt flow turns to the horizontal direction. The molds are aligned on the edge of the distributor and rotate with it. The melt is injected into the molds by centrifugal force. This process was used to cast U-2Zr alloy fuel slugs for EBR-I, which were significantly larger in diameter than for EBR-II (9.8 mm compared to 3.3-4.4 mm) [38]. Although centrifugal casting could potentially be used to fabricate fuel slugs with dimensions typical of a commercial fast reactor, the process has been considered somewhat complicated and time-consuming [38]. The number and type of manipulations required to assemble and disassemble the furnace and molds are significant, and there are concerns over the relatively low throughput, compared with other fabrication processes [38].

Continuous casting

Continuous casting is widely used in steel plants, and is also a candidate for MA-bearing metal fuel slug fabrication. This process has the advantage that it eliminates the use of molds. KAERI produced a uranium rod with a uniform diameter of 13.7 mm and a length of 2.3 m [41]. The continuous casting of U-Zr alloy slugs with a smaller diameter is under investigation. A conceptual diagram of a continuous casting system is shown in Figure 2.15. Figure 2.16 shows a uranium rod being extracted by rollers from the cooling jacket into the air by continuous casting [41].

Figure 2.15: Conceptual diagram of the continuous casting system [41]

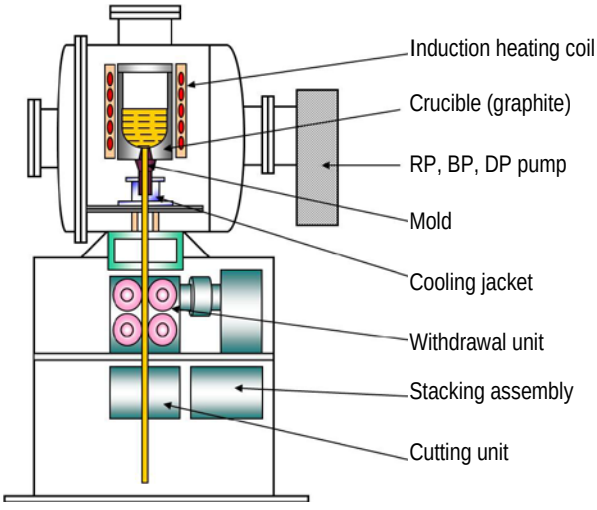

Figure 2.16: Uranium rod is being extracted by rollers from the cooling jacket to air by continuous casting [41]

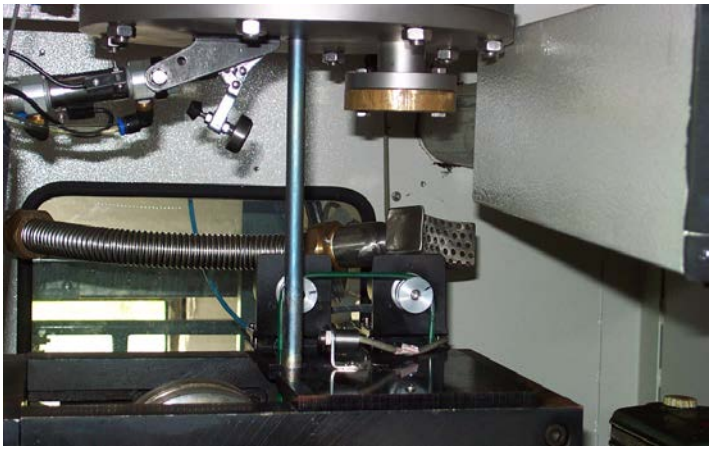

Optimising the casting conditions is difficult when the fuel alloy has a large solidification range [38,41]. For example, the U-19Pu-10Zr alloy liquidus is at 1 300°C, while the solidus is at 1 080°C, which is a 220°C solidification range [38]. The wide solidification range can lead to micro-shrinkage effects and loss of process control during casting [38]. Furthermore, pulling of the cast must be properly aligned to avoid any asymmetric variations in the rod diameter, increasing the complexity of the unit for remote operation [38]. Finally, if continuous casting was to be used, the process would need to be highly automated to minimise the extent of human interaction required for casting a significant number of fuel slugs [38].

Gravity casting

Renewed interest is being taken in gravity casting, where fuel melt is poured into molds by gravity with or without the assistance of a pressure differential. In gravity casting as well as centrifugal casting and continuous casting, the furnace containing the fuel melt is not evacuated, unlike injection casting. This is favourable for suppressing Am evaporation. The gravity casting system is relatively simple.

C. T. Lee et al. [41] fabricated U-10Zr rods by gravity casting with a split graphite mold and a quartz tube mold. A two-piece graphite mold was also used to facilitate the de-molding operation after the casting [41]. Vacuum-assisted gravity casting has also been tested by KAERI, where U-10Zr and U-10Zr-6Ce alloy slugs were successfully fabricated [41].

An advanced casting system (ACS) is being developed at INL (USA) to demonstrate minimal actinide fuel loss by rapid melting and casting under careful atmosphere control in reusable crucibles and molds [39]. The first step in the ACS development activity includes design and construction of a bench-scale casting system (BCS), sized for castings of between 50 g and 300 g, for use with MA-bearing fuel alloys to demonstrate minimal TRU loss [39]. The BCS is based on bottom-pour casting assisted by a pressure differential and has the capability to be configured for injection casting [39]. Figure 2.17 illustrates the preliminary layout of the BCS.

Figure 2.17: Preliminary concept of the bench-scale caster, setup for bottom casting tests [39]

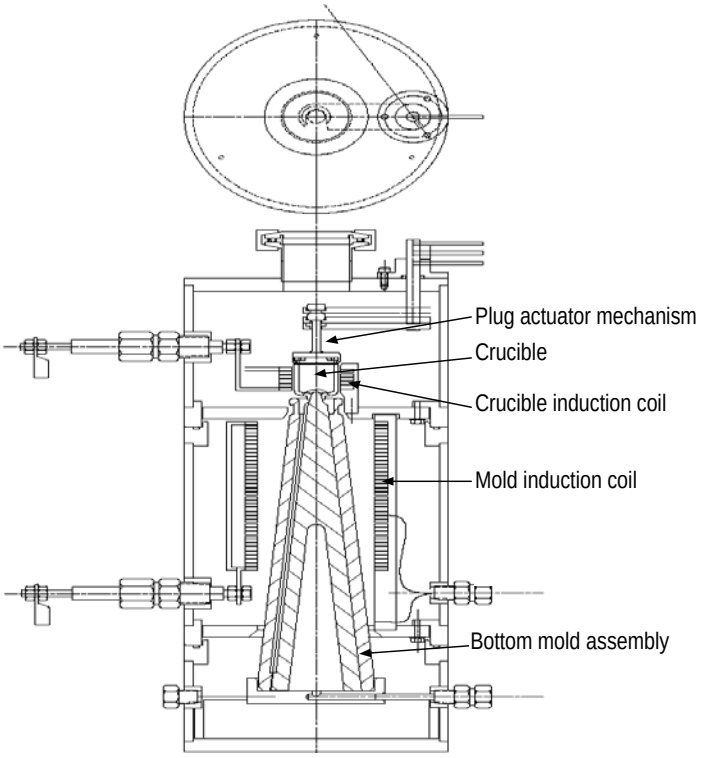

Figure 2.18: SEM image of U-10wt%Zr powder fabricated by centrifugal atomisation [41]

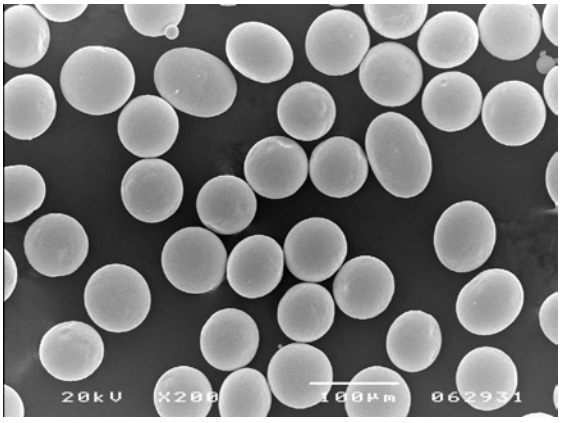

Atomising

In the concept of He-bond particulate metal fuel [45], a cladding tube is filled with fuel alloy particles and the spaces among the particles are filled with He gas, not sodium. A mixture of particles with two different diameters can attain a fuel smear density (filling fraction) of about 75% [45]. The fuel alloy particles can be made by gas atomisation or centrifugal atomisation.

Spherical uranium alloy particles such as U-Mo and U-Zr were successfully fabricated by centrifugal atomisation [41]. Figure 2.18 shows an SEM image of U-10Zr powder fabricated by centrifugal atomisation. The atomisation process does not need molds and is expected to have high throughput.

2.3.2 Loss of Am in the fuel fabrication process

Three full-length fuel slugs (4.3×340mm) of U-20Pu-10Zr-1.2Am-1.3Np alloy were fabricated by injection casting for the X501 irradiation test [11,12,37]. No unusual macro-segregation of the major constituents was observed. About 60% of the initial Am and 100% of the Np charge was present in the as-cast fuel. Am loss was attributed to volatile contaminants in the feedstock and evaporation at the casting temperature (1 465°C). Chemical analysis of sections from the top, centre, and bottom of the fuel slug revealed that the U,Pu,Zr, and Np levels were axially uniform within experimental error, while the Am level was low (1.03wt%) in the bottom section compared to those in the top and centre sections (1.33 and 1.32wt%, respectively) [12].

Trybus [46] performed an injection casting test with U-7.5Zr-1.5Mn alloy, which was the surrogate alloy for U-Pu-Zr-Am-Np alloys. Mn has a similar vapour pressure to Am at the casting temperature. In the surrogate casting test, the alloying temperature was reduced to 1 455°C and the pressure just before injection was increased to ~13.3 kPa compared to the X501 fuel casting (1 495°C and ~670Pa, respectively). The casting was successfully completed and chemical analysis of the samples from the slug centre indicated 1.42wt% Mn, which represents 90% of the initial Mn charge. This means that minimal Mn (and Am) loss is possible by changing the casting parameters [46].

According to the comprehensive discussion on Am evaporation of Burkes et al. [38], Am evaporation can be reduced by decreasing the fuel melt temperature, increasing the cover gas pressure, and/or reducing the Am concentration gradient in the cover gas. The fuel melt temperature can be decreased by adjustment of the fuel alloy composition, e.g. reducing the Zr content in the fuel alloys [45]. From the standpoint of increased cover gas pressure, injection casting may be disadvantageous because the furnace is evacuated before injection. Reduction of the Am concentration gradient can be realised by using a closed system for fuel alloy melting. This is possible for all the above mentioned methods except injection casting.

Nakamura et al. [47] recently used injection-cast U-Pu-Zr metal fuel slugs for an irradiation test in JOYO, where a small amount of Am (~0.3wt%) was included in the fuel alloy. Chemical analysis and gamma-spectrometry of the samples from the yttria coated graphite crucible indicated that Am selectively reacted with the graphite crucible and yttria coating. This suggests that attention needs to be paid not only to Am volatility but also to chemical reactions with the process materials.

2.3.3 MA alloy preparation methods

In the practical fabrication process, a mixture of MAs, in the form of MA alloys, will be charged into the crucible for melting with the other fuel constituents. Depending on the methodology of MA separation from the spent fuel discharged from light water reactors or fast reactors, it may be necessary to prepare MA alloys from the MA oxide stockpile by a reduction process.

A straightforward method of preparing MA metals from MA oxides is direct reduction. In the case of MA metals for METAPHIX fuel fabrication, Am and Cm metals were prepared by the following procedure [48] (see Figure 2.19). The starting materials were procured in the form of dioxides AmO_2 and CmO_2, and then reduced to the sesquioxides Am_2O_3 and Cm_2O_3. The Am and Cm sesquioxide powders were mixed with La and Th metal powders, respectively, ball-milled, and pelletised by pressing. Am_2O_3-La pellets were heated up to about 1 600 K in a closed furnace under vacuum. Reduced Am metal was vapourised, condensed at the colder end of the furnace, and collected by scraping. Cm_2O_3-Th pellets were heated up to about 2 100 K and condensed in the same manner. Collected Am and Cm metals amounted to approximately 8 g and 1 g, respectively, and were used for the fabrication of the MA-bearing metal fuel. These operations were all performed using manipulators in a shielded cell at ITU. Because the

direct reduction process leaves the oxide of the reducing agent, which becomes radioactive waste if not recycled, it will not be deployed in commercial plants.

A potentially applicable method of MA alloy preparation is electrochemical reduction. Kato et al. [49] produced U-60Pu alloy by electrochemical reduction of MOX pellets. Because the product was porous and contained LiCl salt, it was heated up to 850°C for consolidation and salt distillation. Am in the MOX pellets (U/Pu=2/3) was also reduced and entrained in the alloy ingots.

Uozumi et al. [50] successfully partitioned actinide elements including MAs from actual high-level liquid waste as follows. Approximately 440 g of the raffinate from PUREX reprocessing of irradiated MOX fuel was de-nitrated by calcination. The obtained de-nitrated product (~7 g) was then chlorinated in a LiCl-KCl eutectic salt at 650°C with chlorine gas and carbon. The salt containing the actinide chlorides was then brought into contact with a Cd-Li molten alloy at 500°C, where the actinides were reduced by lithium and then extracted in the Cd phase. Actinide metals would be then obtained by distilling the Cd. This pyro-partitioning process can be applicable to the MA oxide stockpile.

Figure 2.19: Am and Cm metal production schemes

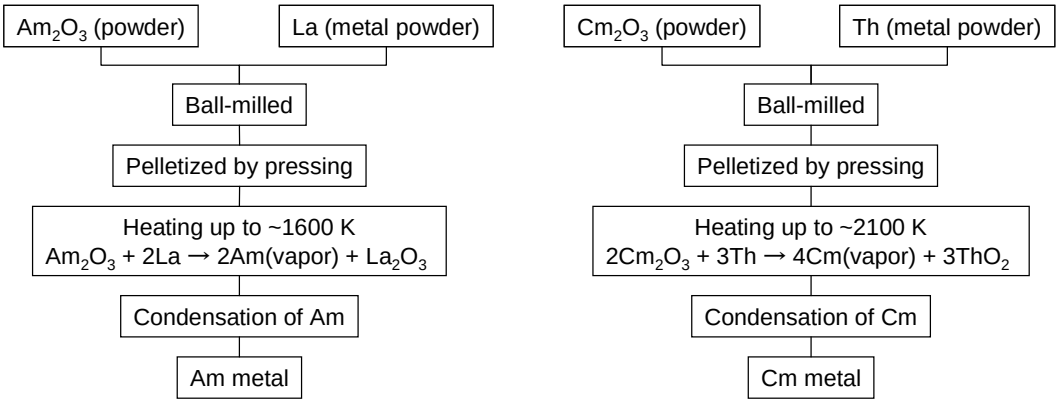

2.3.4 Summary

Fabrication methods for MA-bearing metal fuel are being developed. Although injection casting is well established for MA-free fuel fabrication, other methods such as gravity casting are now being examined from the standpoint of suppression of Am evaporation. Some tests for MA metal preparation methods have been conducted. The test results indicate their feasibility.

2.4 Irradiation performance

As for irradiation tests on MA-bearing metal fuel, the X501 test [11-13] has been completed, and four test series, METAPHIX, [16-20] AFC-1, [21-23] AFC-2, [26,27] and FUTURIX-FTA, [24,25] are now in progress. This subsection summarises the results from the post-irradiation examination of X501, METAPHIX, and AFC-1, and presents irradiation test plans for AFC-2 and FUTURIX-FTA. The main characteristics of these tests are summarised in Table 2.10.

2.4.1 EBR-II X501 test [11-13]

The X501 test was conducted in EBR-II as part of the Integral Fast Reactor (IFR) Programme to demonstrate MA burning through the use of a homogeneous recycling scheme.

The test subassembly contained two metallic fuel elements loaded with relatively small quantities of americium and neptunium. The nominal fuel composition used in the X501 experiment was U-20.3Pu-10.0Zr-2.1Am-1.3Np, based on a concept where the standard IFR fuel is fabricated with Pu extracted from spent LWR fuel that has cooled for 10 years. However, about 40% of the initial Am charge was lost in the as-cast fuel. Am loss was attributed to volatile contaminants in the feedstock and evaporation at the casting temperature (1 465°C). Consequently, as-fabricated fuel slugs for X501 had a composition of U-20.2Pu-9.1Zr-1.2Am-1.3Np. Two MA-bearing fuel elements were inserted into a standard EBR-II subassembly with the remainder of the fuel element locations filled with U-10Zr driver fuel.

The X501 subassembly was irradiated in EBR-II for 339 EFPDs. The calculated burn-up was 7.6at% with a transmutation of 9.1% of ^{241}Am. The peak linear power rate and peak cladding inner temperature were estimated to be 45 kW/m and 540°C, respectively.

Gamma scans for ^{137}Cs showed normal metallic fuel fission product behaviour, with Cs alloying with the bond sodium and migrating to the region near the top of the fuel slug. Optical microscopy of a fuel cross section showed no evidence of fuel-cladding chemical interaction and a microstructure typical of U-20Pu-10Zr, where constituent radial redistribution results in the formation of three microstructural zones within the fuel.

Wavelength dispersive spectroscopy (WDS) line scans indicated fuel constituent radial migration similar to that of U-20Pu-10Zr; the outer zone is enriched in zirconium, the intermediate zone is zirconium depleted, and the central zone is enriched in zirconium and depleted in uranium, and plutonium content remains relatively uniform. WDS line scans also revealed high americium-rich phases, generally depleted in U,Pu, and Zr. Whereas the americium was distributed homogeneously in the as-fabricated fuel slug, the americium-rich phases were present only in the uranium-depleted central and outer zones after irradiation as shown in Figure 2.20. This indicates that americium migration has occurred along with the migration of uranium and zirconium.

Figure 2.20: (a) Post-irradiation optical image of X501 MA-bearing fuel (b) wavelength dispersive spectroscopy line scans showing distribution of actinides and Zr [12]

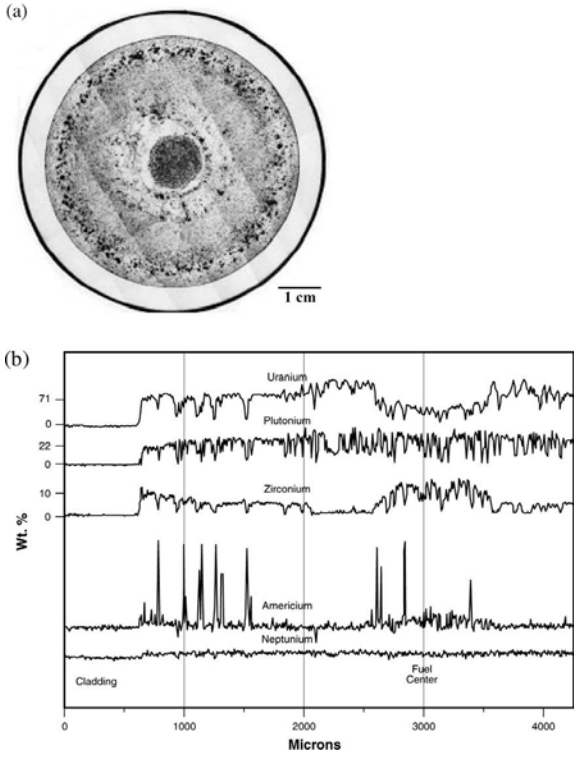

Fission gas and helium gas release from the fuel were estimated based on the results of plenum gas sampling and calculations of fission gas and helium gas production. Helium generation is principally due to a sequence of neutron capture by ^{241}Am and subsequent decay of the ^{242}Cm product to ^{238}Pu by alpha particle emission. The estimation indicated that approximately 90% of the helium gas produced was released into the plenum and fission gas release was 79%, typical of U-Pu-Zr fuel at this burn-up.

Table 2.10: Irradiation tests of MA-bearing metal fuel

	X501	METAPHIX	AFC-1B	AFC-1F, -1H	AFC-2A, -2B	FUTURIX-FTA (Metal)
Reactor for irradiation	EBR-II	Phenix	ATR	ATR	ATR	Phenix
Fuel alloy composition (wt%)	U-20.2Pu-9.1Zr-1.2Am-1.3Np	U-19Pu-10Zr U-19Pu-10Zr-2MA-2RE U-19Pu-10Zr-5MA-5RE U-19Pu-10Zr-5MA (MA : Np, Am, Cm) (RE : Y, Ce, Nd, Gd)	Pu-12Am-40Zr Pu-10Am-10Np-40Zr Pu-60Zr Pu-40Zr	U-29Pu-4Am-2Np-30Zr U-34Pu-4Am-2Np-20Zr U-25Pu-3Am-2Np-40Zr U-28Pu-7Am-30Zr	U-20Pu-3Am-2Np-15Zr U-20Pu-3Am-2Np-1.0RE-15Zr U-20Pu-3Am-2Np-1.5RE-15Zr U-30Pu-5Am-3Np-1.5RE-20Zr U-30Pu-5Am-3Np-1·0RE-20Zr U-30Pu-5Am-3Np-20Zr (RE : La, Pr, Ce, Nd)	U-29Pu-4Am-2Np-30Zr Pu-12Am-40Zr
Fuel slug O.D.* (mm)	4.27	4.9	4.01	4.01	4.24	
Fuel slug length (mm)	343	100 (MA section)	38.1 (25.4 for Pu-60Zr)	38.1	38.1	
Cladding material	HT9	15-15Ti	HT9	HT9	HT9	
Cladding O.D. (mm)	5.84	6.55	5.84	5.84	5.84	
Peak linear power rate (W/cm)	450	350	330 (design limit)	330 (design limit)	350	272 (low-fertile) 320 (non-fertile)
Peak cladding tem. (K)	813	845	823 (design limit)	823 (design limit)	823 (design limit)	
Peak burn-up (at%)	7.6	2.5, 7, 11	4~8	4~8 (1F), 35~40(1H)	>10 (2A), >25 (2B)	7.0 (low-fertile) 11.4 (non-fertile)

(*O.D.: Outer diameter)

2.4.2 METAPHIX [16-20]

The primary objectives of the METAPHIX test are to examine the effects of MA and/or RE addition on the irradiation behaviour of metal fuels, and to confirm the transmutation performance of MAs.

For this test, four types of fuel alloy slugs were prepared: U-19Pu-10Zr, U-19Pu-10Zr-2MA-2RE, U-19Pu-10Zr-5MA, and U-19Pu-10Zr-5MA-5RE. These fuel alloy slugs were cut into lengths of 20-50 mm and inserted into austenitic CW15-15Ti cladding tubes. The fuel-cladding gap was filled with sodium for thermal bonding. As illustrated in Figure 2.21, the MA-bearing slugs were sandwiched by U-19Pu-10Zr slugs stacked to heights of 100 mm and 285 mm. Nine test fuel pins were prepared: three pins of reference U-19Pu-10Zr (Pin #1), three pins containing U-19Pu-10Zr-2MA-2RE (Pin #2), and three pins containing U-19Pu-10Zr-5MA and U-19Pu-10Zr-5MA-5RE (Pin #3).

The test fuel pins had been fabricated by 1994 and stored for about nine years. During storage period, the fuel compositions changed due to the radioactive decay of relatively short-lived actinide isotopes such as ^{241}Pu and ^{244}Cm. The elemental and isotopic compositions of each fuel alloy were evaluated in December 2003 just before the irradiation experiment as shown in Table 2.11. Decay chain analysis did not show any marked change in fuel composition except for a decrease of about 25% in Cm and the generation of helium(He) gas, which mainly resulted from α-decay of ^{244}Cm to ^{240}Pu.

Figure 2.21: Schematic diagram of test fuel pins

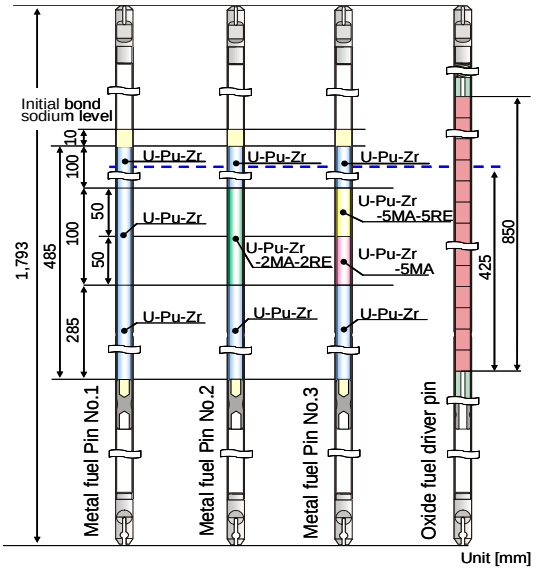

Figure 2.22: Gamma-radiography of METAPHIX-1 fuel pins (2.5at% burn-up)

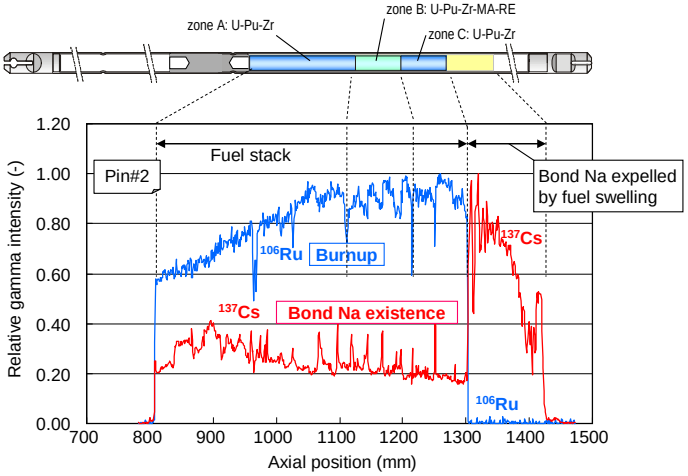

Figure 2.23: Local axial elongation of METAPHIX-1 fuel stacks (2.5at% burn-up)

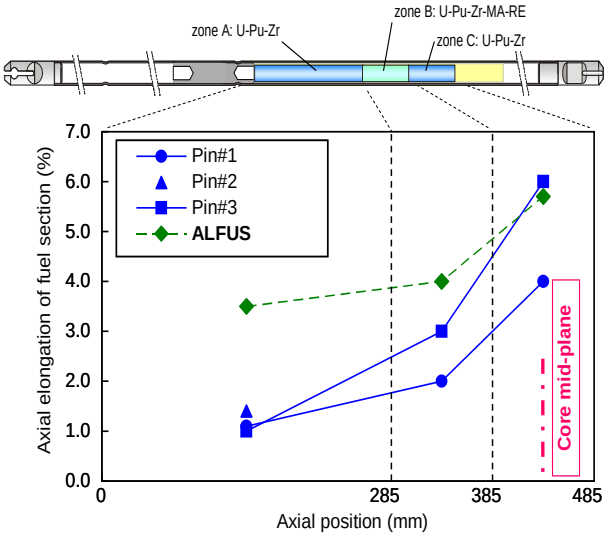

Table 2.11: Elemental and isotopic compositions of METAPHIX test fuel alloys in December 2003 [19]

Component	U-19Pu-10Zr	U-19Pu-10Zr-2MA-2RE	U-19Pu-10Zr-5MA	U-19Pu-10Zr-5MA-5RE
U	71.00	66.86	66.30	63.50
Pu	18.92	19.83	19.41	19.81
Np	-	1.23	2.98	3.05
Am	0.03	0.67	1.45	1.52
Cm	-	0.14	0.24	0.23
Zr	10.19	9.46	8.35	8.19
RE	-	1.73	-	3.38
He*	1.01	9.08	15.63	15.31

(a) Averaged compositions of fuel alloys (wt%) (* : Unit=pp, by weight).

U	%		Pu	%		Am	%		Cm	%
^{234}U	0.001		^{238}Pu	0.006		^{241}Am	41.10		^{244}Cm	80.91
^{235}U	0.407		^{239}Pu	95.313		^{242}Am	0.28		^{245}Cm	10.36
^{236}U	0.003		^{240}Pu	4.619		^{242}Am	58.62		^{246}Cm	8.34
^{238}U	99.589		^{241}Pu	0.055					^{247}Cm	0.39
			^{242}Pu	0.007						

(b) Isotopic compositions (wt%) of U,Pu,Am and Cm in December 2003.

The three test fuel pins, Pin#1, #2, and #3, were distributed to three irradiation capsules of identical configuration to achieve three different burn-ups: ~2.5at% (METAPHIX-1), ~7at% (METAPHIX-2), and ~11at% (METAPHIX-3). Irradiation of METAPHIX-1, -2, and -3 were completed without cladding breach. The peak linear power rate was ~350 W/cm and the peak cladding temperature was ~581°C.

Fuel Zones A (upper U-Pu-Zr fuel), B (MA-containing fuel), and C (lower U-Pu-Zr fuel) were distinguishable in γ-ray autoradiography (see Figure 2.22) because sintering of the loaded fuel slugs is not sufficient at a low burn-up of ~2.5at%. From the γ-ray intensity profile of ^{106}Ru that remains within the fuel matrix, the axial elongations of Zones A, B, and C were estimated as shown in Figure 2.23. The total elongations of the fuel stack were in the range of 1.9-2.5% in METAPHIX-1, which are lower than the existing irradiation data (~6%). This can be explained by the unusual linear power profile of the METAPHIX fuel pins, where the peak linear power appeared near the top of the fuel stack.

Figure 2.22 also indicates that the ^{137}Cs γ-ray intensity is high in the region of 1 200-1 400 mm from the top of the fuel stack. This means that bond sodium dissolving Cs has been extruded to this region. This Cs behaviour in MA-bearing fuels was observed in the X501 test [2] as in the case of the U-Pu-Zr ternary fuel.

Fission gas release was 44.0% for Pin#1, 48.9% for Pin#2, and 45.4% for Pin#3. These data are consistent with the data of U-Pu-Zr fuel pins irradiated in EBR-II up to 1.9-2.7at% burn-up (41-63%). He gas release for the MA-containing fuels was 77.5-80.8% for Pin#2 and 96.3-98.2% for Pin#3.

Figure 2.24: Metallography of cross-section of METAPHIX-1 fuel Pin#3 (2.5at% burn-up, U-19Pu-10Zr-5MA-5RE)

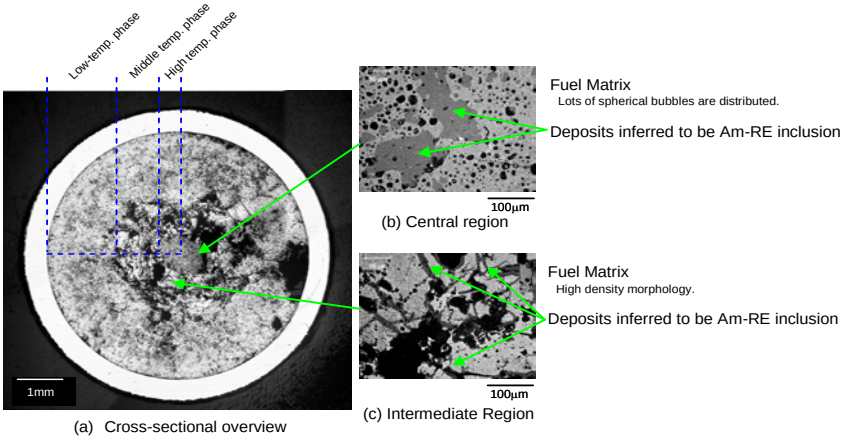

Metallography of the fuel pin cross-sections indicated the following characteristics: the fuel matrix phase structures and textures of Pin#2 and Pin#3 cross-sections were similar to those of Pin#1 and the U-Pu-Zr ternary fuel irradiated in EBR-II. Some large depositions, which are expected to be inclusions of MAs and REs, appear in the high-temperature central γ-phase zone. In the dense matrix zone of (γ+ζ) mixture phases, narrow and dark layered phases, which are expected to be inclusions of MAs and REs, spread along the grain boundaries. In the low-temperature region, the inclusions of MAs and REs are dispersed. Typical examples of the optical metallographs are shown in Figure 2.24.

The mechanical and thermal properties, such as Young's modulus, Poisson's ratio, and thermal conductivity of U-Pu-Zr alloys are practically unchanged after the addition of 5wt% MAs and REs. From the dilatometric analysis of U-19Pu-10Zr, U-19Pu-10Zr-2MA-2RE, and U-19Pu-10Zr-5MA-5RE, two major phase transitions were observed at ~580°C and ~630°C, which correspond to the phase transitions δ+ζ /γ+ζ and γ+ζ /γ, respectively. These phase transitions are consistent with previously reported phase diagrams of U-Pu-Zr ternary systems within the range of experimental error or uncertainty in the phase diagram. Marked anomalies were not observed in the MA-bearing alloy slugs loaded in Zone B in Pins #2 and #3 of the METAPHIX-1 fuel, when compared to the reference U-Pu-Zr alloy fuel. The X501 irradiation test also indicated that the minor addition of MAs did not affect the irradiation behaviour, such as fission gas release and

fuel constituent redistribution, while Am redistribution was observed. These observations lead to the assumption that the irradiation behaviour of U-Pu-Zr alloys containing MAs and REs at 5wt% or less is similar to that of U-Pu-Zr ternary alloys without MAs or REs. This assumption suggests that computer codes developed for irradiation behaviour analysis of U-Pu-Zr ternary fuel may be applicable to the analysis of MA-bearing metal fuel.

2.4.3 AFC-1 series test [21-23]

The AFC-1 irradiation tests were designed under the U.S. Advanced Fuel Cycle Initiative (AFCI) to evaluate the feasibility of the use of actinide-bearing metallic fuel forms in advanced sodium-cooled fast reactors for the transmutation of transuranic elements from spent nuclear fuel. AFC-1B and AFC-1F were the first set of irradiation tests and designed to provide irradiation performance data at intermediate burn-ups of 4-8at% on non-fertile and low-fertile actinide-bearing fuel. The sibling AFC-1D irradiation test is being conducted to reach a final burn-up of up to 40at%.

Figure 2.25: AFC-1 irradiation test assembly, capsule assembly and fuel rodlet assembly [22]

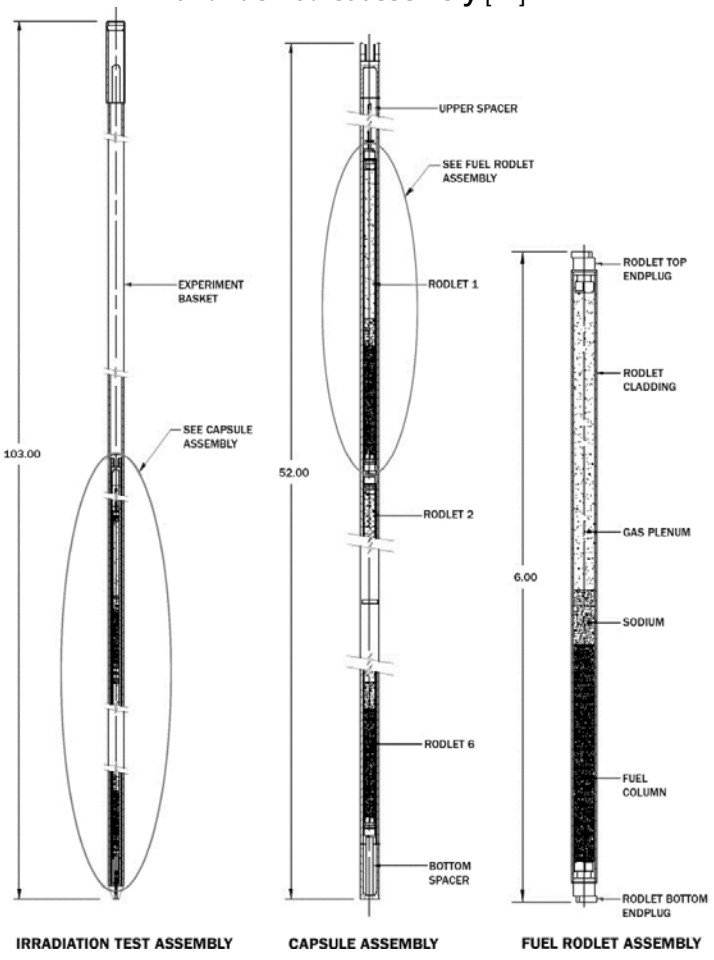

The AFC-1B test examines four non-fertile metallic fuel compositions (Pu-12Am-40Zr, Pu-10Am-10Np-40Zr, Pu-60Zr, and Pu-40Zr). The AFC-1F tests examine four fertile metallic fuel compositions (U-28Pu-4Am-2Np-30Zr, U-27Pu-3Am-2Np-40Zr, U-34Pu-4Am-2Np-20Zr, and U-29Pu-7Am). The irradiation test assembly (see Figure 2.25) consists of an experiment basket and capsule assembly, which contains six rodlet assemblies stacked vertically. The fuel specimens are encapsulated in the rodlet assemblies, which are

designed as miniature fast reactor fuel rods with a prototypical diameter with a reduced length. The rodlet assembly consists of a metallic fuel column, sodium bond, stainless steel Type 421 (HT-9) cladding, and an inert gas plenum. The experiment basket of the test assembly is an aluminum-sheathed cadmium tube designed to interface the capsule assembly with the ATR and to act as a thermal neutron flux filter.

The test assembly was irradiated at INL's Advanced Test Reactor (ATR) to an intermediate burn-up of 4-8at% (3.5-8.9×10^{20}fissions/cm^3). The upper limits for the linear power rate and cladding temperature of the fuel rodlets were 33 kW/m and 550°C, respectively.

No failure has been observed in the rodlet assemblies irradiated to 4-8at%.

It should be noted that non-fertile and low-fertile transmutation fuels have a much lower fission density than traditional U-xPu-10Zr metallic fuels when the irradiation performance of these fuels is discussed. Hilton et al. [22] has pointed out that using fission density (fissions/cm^3) as the burn-up metric eliminates composition dependence in assessing fission damage and provides a standard basis for correcting fuel performance parameters. U-xPu-10Zr metallic fuels exhibit three stages of gas release and swelling:

1) incubation characterised by very low swelling rates up to a threshold burn-up of ~0.35×10^{21}fission/cm^3 (1.0at% for U-xPu-10Zr);
2) transition characterised by rapid fission gas-driven swelling until a network of open pores fully develops whereupon the fuel contacts the cladding and the majority of the fission gas is released at burn-ups of between ~0.35-1.0×10^{21}fission/cm^3 (1.0-3.0at% for U-xPu-10Zr);
3) stable irradiation change characterised by a slowly increasing plateau due to accumulation of solid fission products and retained fission gas at burn-ups of >1.0×10^{21}fission/cm^3 (3.0at% for U-xPu-10Zr).

The fission gas release and swelling of metallic alloy transmutation fuel compositions Pu-TRU-40Zr and U-xPu-TRU-yZr (y = 20-40) are similar to that of U-xPu-10Zr as follows.

Figure 2.26 shows the burn-up dependence of fission gas release for 11 metallic alloy rodlets and includes data from U-xPu-10Zr for comparison. The fission gas release behaviour of the transmutation metallic fuels follows the same trend as the U-xPu-10Zr fuel when correlated with fission density. There is negligible amount of fission gas release until a fission density of ~0.6 x 10^{21} f/cm^3.

Figure 2.26: Fission gas release from metallic alloy transmutation fuel rodlets irradiated in AFC-1B and AFC-1F capsules [23]

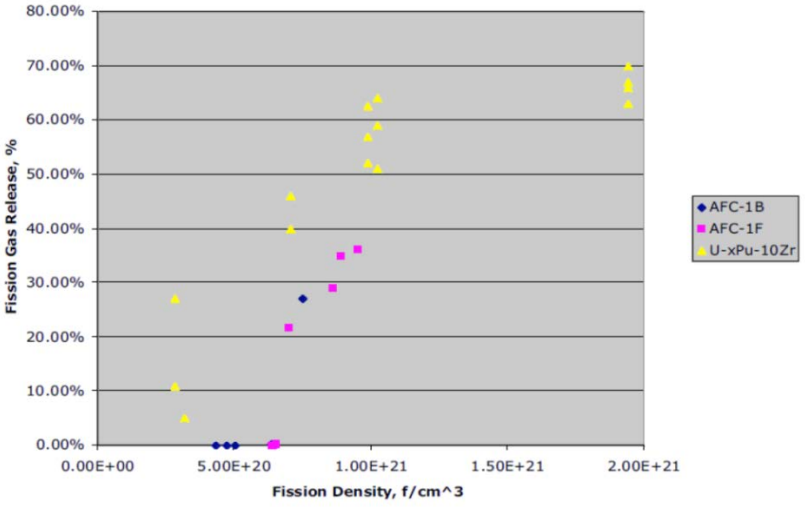

At this threshold burn-up, there is a rapid increase in fission gas release similar to the U-xPu-10Zr behaviour. Figure 2.27 shows a metallographs of the low-fertile metallic alloy composition at two burn-ups, 0.42 and 0.60×10^{21}fission/cm^3, indicating that the metallic transmutation fuel's transition stage occurs at a fission density of around $0.6\text{-}1.2\times10^{21}$fission/cm^3.

In U-xPu-10Zr metallic fuels, porosity developed sufficiently and some of the Cs fission product dissolved into the sodium at 0.35x1 021f/cm3 (1at%) burn-up. By 7.1x1 021f/cm3 (2at%) burn-up, most of the Cs dissolved into the sodium. Gamma scan analyses have indicated that the Cs behaviour in transmutation fuels is also consistent with that observed in the U-xPu-10Zr metallic fuels.

Figure 2.27: Transverse cross-sectional metallography montages of U-29Pu-4Am-2Np-30Zr samples [23]

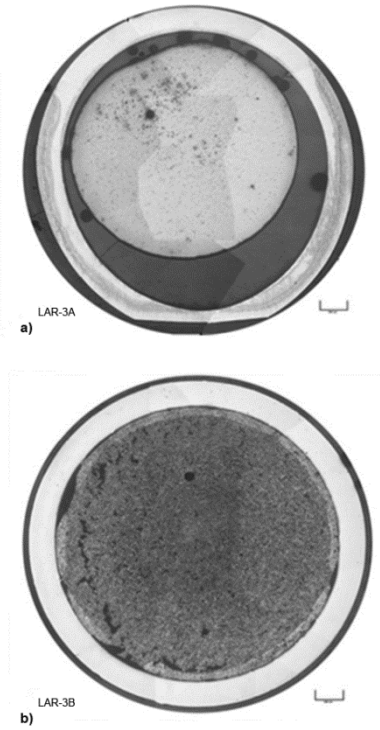

a) Mount LAR-3A irradiated to 0.42×10^{21} fission/cm^3 (6.4at%) bu up showing developing porosity a swelling.

b) Mount LAR-3B irradiated to 6.0×10^{20} fission/cm^3 (8.9at%) burn-up showing fuel fully swollen leading to fuel-cladding contact and initial formation of fuel restructuring with central dense zone and porous annular zone.

2.4.4 AFC-2 series test [26,27]

The AFC-2 test series, which follows the AFC-1 test series, is focused on prototypic fuel compositions for fast reactor transmutation fuel containing recycled transuranics from light water reactor spent nuclear fuel. The AFC-2 test series examines two identical capsules, one in experiment AFC-2A and the other in experiment AFC-2B. Each capsule contains metallic fuel rodlets with various fuel alloy compositions: U-20Pu-3Am-2Np-15Zr, U-20Pu-3Am-2Np-1.0RE-15Zr, U-20Pu-3Am-2Np-1.5RE-15Zr, U-30Pu-5Am-3Np-1.5RE-20Zr, U-20Pu-5Am-3Np-1.0RE-20Zr, and U-30Pu-5Am-3Np-20Zr (in wt%; RE: a rare earth alloy), as shown in Table 2.9. An alloy of rare earth (RE) elements is added to the base compositions to simulate fission product carryover resulting from the pyroprocessing of fast-reactor fuel. The irradiation test assembly for AFC-2 is almost the same as that for AFC-1.

The target burn-up for the AFC-2A test capsule is >10at%, and for the AFC-2B test capsule, it is >25at% (burn-up defined to be the percent depletion of initial ^{235}U and ^{239}Pu). The peak cladding temperature during normal operation is 550°C.

2.4.5 FUTURIX-FTA [24,25]

In the European and American joint irradiation test, FUTURIX-FTA, two metallic fuel pins have been irradiated in the fast reactor Phénix. The fuel alloy compositions are U-29Pu-4Am-2Np-30Zr (low-fertile) and Pu-12Am-40Zr (non-fertile). These compositions are fom the AFC-1 test series. The FUTURIX-FTA metallic fuel pins will provide data for verification of the results from the AFC-1 rodlets irradiated in the thermal neutron reactor ATR.

2.4.6 Summary

The MA-bearing U-Pu-Zr based fuel alloys irradiated in the X501 and METAPHIX tests consistently showed microstructure, constituent migration, fission gas release, and fission product (Cs) behaviour similar to that of MA-free U-Pu-Zr fuel alloys. This means that minor (~5wt%) additions of MAs to the U-Pu-Zr matrix do not significantly affect the irradiation behaviour of the fuel. MA specific irradiation behaviour observed so far is as follows. The Am was migrated along with uranium and zirconium migrations. Am-rich phases were present only in the uranium-depleted central and outer zones after irradiation. He gas release was consistently higher than fission gas release in both the X501 and METAPHIX tests. The fission gas release behaviour of the non-fertile or low-fertile fuel alloys also followed the same trend as that of the U-Pu-Zr based fuel alloys when correlated with fission density.

An issue in MA-bearing fuel performance is fuel-cladding chemical interaction (FCCI) because MAs, particularly Am, are expected to behave like rare earth elements that react with Fe-based cladding materials. However, no FCCI data are available at this point because the inner cladding temperature in the X501 test was too low (<540°C) to observe a sufficient level of FCCI. In METAPHIX-2 or METAPHIX-3, FCCI data may be obtained but the cladding material is austenitic steel, which will not be used for commercial reactor fuel. An irradiation test on MA-bearing fuel clad with ferritic steel at a high cladding temperature is desired in order to obtain prototypic FCCI data in the future.

2.5 Safety performance

Based on the reported results from metal fuel development under the IFR programme in the United States, the safety performance of U-Pu-Zr metal fuel in a sodium-cooled fast reactor can be characterised by seven metal fuel-specific characteristics:

1) The metal fuel pin breached during normal reactor operation behaves benignly and can run in a reactor for days due to the good compatibility between the fuel alloy and sodium [51]. A fuel assembly containing a failed fuel pin can be identified by detecting delayed neutron precursors [51].
2) When the cladding inner temperature is increased beyond a certain level, a liquid phase is formed at the interface between the fuel alloy and cladding, and cladding wastage occurs [6,7] (liquid phase attack).
3) The solidus temperature of the fuel alloy is lower than that of the cladding. When the fuel alloy melts before cladding breach in an overpower transient, the molten fuel alloy expands due to coalescence of fission gas bubbles in the molten fuel alloy [5,52].
4) In the case of a loss-of-flow event lasting for minutes or hours, a part of the peripheral region of the fuel alloy liquefies due to cladding constituent diffusion

to the fuel alloy side. The partially liquefied fuel alloy expands due to coalescence of fission gas bubbles in the liquefied fuel alloy [7].

5) Cladding failure in both transient overpower and loss-of-flow events occurs by the synergic effect of plenum gas pressure rise according to the coolant temperature rise and cladding wastage due to liquid phase attack [5,52].

6) Cladding breach occurs near the top of the fuel alloy slug, where the cladding temperature is highest, the cladding wastage is most significant, and the cladding strength is lowest [5,7].

7) When the molten fuel alloy comes out of the cladding, it fragmentates and disperses as a result of thermal interaction with the coolant sodium [5,53].

These characteristics play important roles in the termination of transient events without scram in the following manner. Even if a transient overpower or loss-of-flow event without scram does not terminate in the early stage in spite of the inherent safety features of a metal-fuelled reactor, characteristics 3) or 4) inputs negative reactivity feedback to the reactor core. Even though the event does not terminate, characteristics 6) and 7) eliminate the fuel materials from the top of the core without core compaction and consequently terminate the transient event.

The metal fuel-specific features described above are attributed to the characteristics of U-Pu-Zr alloys: solidus temperature, reaction with Fe-based cladding materials, compatibility with sodium, and thermal interaction with sodium. The characteristics of U-Pu-Zr alloys containing up to 8wt% MAs and 5wt% REs will be similar to those of MA-free U-Pu-Zr alloys, as shown in Section 2.2, while the solidus temperature and the liquid phase attack onset temperature for MA-bearing alloys may be lower to some extent than those for MA-free alloys. Therefore, we can assume that the safety performance of the MA-bearing U-Pu-Zr based alloys will be similar to that of the MA-free U-Pu-Zr alloys. Verification of this assumption will require more physical property data for MA-bearing alloys, ex-reactor simulative tests for compatibility with Fe-based cladding materials, and/or heating tests with irradiated fuel pins.

Considering the metallurgical similarity of transuranic metals to U-based alloys, the transient behaviour of non-fertile and low-fertile alloy fuel can be assumed to be similar to that of U-Pu-Zr fuel. Physical property measurements and ex-reactor tests with fuel alloys irradiated or unirradiated are necessary to verify this assumption.

2.6 Fuel design criteria

Considering the effects of MA addition on the physical properties and irradiation behaviour of U-Pu-Zr fuel alloys, the main fuel design criteria for MA-bearing U-Pu-Zr based alloy fuel will be determined for the peak linear power rate, peak cladding temperature, peak burn-up, and fuel alloy composition.

2.6.1 Peak linear power rate

The peak linear power rate of a metal fuel pin is determined to ensure a sufficient margin to fuel alloy melting during normal reactor operation and operational transient events. The solidus temperature of MA-bearing U-Pu-Zr-based alloys will decrease with increasing MA content by analogy with the binary phase diagrams of the Np-U and Am-Pu systems [54]. However, the peak linear power rate of MA-bearing U-Pu-Zr-based alloy fuel is assumed to be equivalent to that of MA-free U-Pu-Zr fuel because the thermal conductivity and liquidus temperature of U-19Pu-10Zr alloys containing up to 5wt% MAs and 5wt% REs are not significantly different from those of U-19Pu-10Zr alloys [14].

2.6.2 Peak cladding temperature and peak burn-up

Peak cladding temperature and peak burn-up of a metal fuel pin are determined based on estimations of plenum gas pressure rise, cladding wastage by fuel-cladding chemical interaction (FCCI), in addition to cladding properties such as irradiation swelling and creep.

In estimating the plenum gas pressure of MA-bearing metal fuel, He gas generation due to radioactive decay neutron reaction (transmutation) of MAs and fission gas generation should be considered. He gas release tends to be larger than fission gas release according to the results of the X501 [11,12] and METAPHIX [19] tests.

There are two modes of FCCI: inter-diffusion between cladding and mainly lanthanide fission products, and inter-diffusion between cladding and fuel alloy constituents at an elevated temperature. The former is called "lanthanide attack" here. The latter is accompanied by liquid phase formation in the diffusion zone, which is called "liquid phase attack" here, and occurs above a threshold temperature (the onset temperature of the liquid phase attack). The affinity of Am with the rare earth elements may lead to the promotion of FCCI in MA-bearing metal fuel. Additive rare earth elements like those in the METAPHIX and AFC-2 test fuel may also promote FCCI. These changes in FCCI behaviour in MA-bearing metal fuel should be confirmed by those irradiation tests.

Based on the evaluated U-Pu-Zr-Fe quaternary phase diagram [55-57], ex-reactor diffusion test results, and irradiated fuel heating test data, Nakamura et al. [58] pointed out that the onset temperature of liquefaction at the U-Pu-Zr fuel alloy-cladding interface depends on the atom fraction ratio of Pu/(U+Pu) in the fuel alloy, e.g. the liquefaction starts at a temperature higher than 923 K when Pu/(U+Pu) <0.25. This liquefaction onset temperature, as well as the solidus temperature, may decrease with MA addition. The out-of-pile diffusion tests performed to date are not sufficient for estimating the MA addition effect on the liquefaction onset temperature.

One of the factors controlling the cladding temperature and burn-up of metal fuel is lanthanide attack. The cladding peak temperature is also limited so as to avoid liquid phase attack during normal reactor operation. An idea for eliminating or suppressing FCCI is "lined cladding", which is to place a barrier inside the cladding tube. Successful development of lined cladding will facilitate the use of metal fuel at higher cladding temperatures and higher burn-ups. The development of lined cladding for metal fuel has been conducted in Japan, the United States, and Republic of Korea [59-62]. To date, a wide variety of liner materials, such as W, V, Zr, Ti, Cr, and Zr-N, have been tested. The nitrogen charge on an HT-9 steel surface was also tested to inhibit the reaction with the U-Zr alloy [59]. Most of these tests were ex-reactor isothermal heating tests employing diffusion couples consisting of lined cladding materials and fuel alloys, except for the early irradiation test. Future developments will be necessary for establishing liner reliability, the lining method, and end plug welding technique. It may also be important to assess the influence of such robust cladding on transient events of the reactor core [45].

2.6.3 Fuel alloy composition

Fuel alloy composition will be determined in consideration of the LWR fuel reprocessing scenario, MA transmutation strategy, reactor system design for MA transmutation, required fuel performance, MA separation and recycling technologies, and recycled fuel fabrication technology.

Although up to 25wt% MAs can be dissolved homogeneously in the U-19Pu-10Zr alloy without rare earth elements [14], MA addition may cause a decrease in the solidus temperature, promotion of FCCI, increase in Am evaporation in a fuel recycling process including fuel fabrication, and worsening of the sodium void reactivity coefficient of a reactor core. MA content in the fuel alloy will be determined through considering these factors.

Pu content in the fuel alloy is usually determined in the reactor core design. In the case of MA-bearing metal fuel, reactor core designers may be more concerned about TRU (=Pu+MA) content than Pu content alone.

Most of the metal fuel irradiated in the IFR programme contained 10wt% Zr. When the MA or TRU content is increased for the purpose of efficient MA transmutation, Zr content may be increased, as in the AFC-1 and AFC-2 fuel alloys, to keep the solidus temperature sufficiently high. Increased Zr content, i.e. higher solidus temperature leading to higher melting temperature in the fuel alloy casting, may raise concerns about an increase in Am volatility. From this viewpoint, reducing the Zr content may be one way to decrease Am evaporation [45].

When a pyroprocessing technology is applied to MA recovery from LWR spent fuel or MA recycling, recovered transuranic elements accompany rare earth elements (REs) so that the MA-bearing fuel alloy is contaminated with REs. It is difficult for a high content of REs, particularly above 5wt%, to dissolve or disperse in actinide-based fuel alloys.

2.7 Applicability to reactor systems

Metal fuel alloys such as U-Pu-Zr, U-Pu-Zr-MA, and Pu-Zr-MA alloys show excellent compatibility with sodium, so that "bond sodium" is used in fuel pins containing these alloys. Metal fuel, regardless of the MA content, is suitable for reactor systems with a coolant that is compatible with the fuel alloys and sodium. A typical example is a sodium-cooled fast reactor.

Uranium, plutonium, and sodium form inter-metallic compounds with lead (Pb). When metal fuel is applied to a reactor system with Pb or Pb-Bi coolant, cladding breach may raise concerns about Na-Pb inter-metallic compound precipitation inside the reactor system components and enlargement of the breach due to U-Pb inter-metallic compound formation. However, application of metal fuel to Pb or Pb-Bi coolant systems may not be impossible, depending on future experimentation.

Water-cooled systems will not use metal fuel because of their poor compatibility of bond sodium with water.

2.8 Technical issues and future work

2.8.1 Fuel performance

For fuel performance, technical issues in MA-bearing metal fuel are to understand and quantify the effect(s) of MA addition on the following thermal properties and irradiation phenomena by out-of-pile tests and/or irradiation tests.

- solidus temperature of the fuel alloys;
- fuel-cladding chemical (or metallurgical) interaction (FCCI);
- release of He gas generated by alpha decay and transmutation of MAs.

The solidus temperature can be measured by thermal analysis of fuel alloy samples. Some solidus data have been measured to date, but they are not sufficient. More measured data will be necessary to quantify the solidus temperatures of MA-bearing fuel alloys in a wide compositional range.

FCCI for MA-bearing metal fuel will be understood by out-of-pile tests with the diffusion couples consisting of fuel or MA-RE alloys and Fe-based cladding materials. Irradiation tests on MA-bearing metal fuel with an appropriate cladding material are desired for the quantification of FCCI. Heating tests on the irradiated fuel pin segment are essential to quantify the kinetics of a liquid phase attack. Thermodynamic assessments of relevant alloy systems such as U-Pu-Zr-MA, MA-RE-Fe, and U-Pu-MA-Fe will effectively

assist in understanding the solidus temperature and FCCI. Further development of lined cladding will also be effective in eliminating or suppressing FCCI.

He gas release behaviour in MA-bearing metal fuel is being understood through the X501 and METAPHIX tests: He gas release is much higher than fission gas release. Further progress in post-irradiation examination of the METAPHIX fuel pins will be helpful for a better understanding of He gas behaviour. A nuclear data library of neutron reaction cross-sections of MAs should be established as a basis for estimating He gas generation as well as MA transmutation rates.

2.8.2 Fuel fabrication

As discussed in Section 2.3, a major technical issue in the fabrication of MA-bearing fuel is to suppress Am evaporation in the process. When fuel fabrication technologies other than injection casting are applied, the feasibility of remote and automatic operation should be confirmed.

2.9 Technology readiness levels (TRLs)

Irradiation and modelling maturity are shown in Figure 2.28. The technology readiness levels (TRLs) of metal fuels are described in Chapter 7. Tables for fabrication process maturity and irradiation maturity are shown Tables 7.2 and 7.3.

Figure 2.28: Irradiation and modelling maturity levels for metal fuels

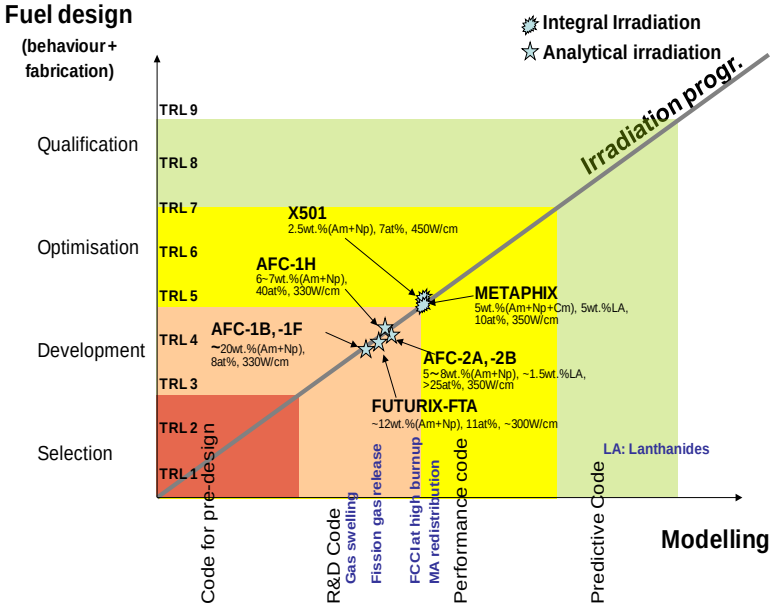

References

[1] Chang, Y.I., (1989), "The integral fast reactor", *Nucl. Technol.*, 88. 129.

[2] Till, C.E., Y.I. Chang (1991), "Progress and status of the integral fast reactor (IFR) fuel cycle development", *Proc. Int. Conf. Fast Reactor and Related Fuel Cycles*, Kyoto, Japan.

[3] Leggett, R.D., L.C. Walters (1993), "Status of LMR fuel development in the United States of America", *J. Nucl. Mater.*, 204. 23.

[4] Crawford, D.C., D.L. Porter, S.L. Hayes (2007), "Fuels for sodium-cooled fast reactors: US perspective", *J. Nucl. Mater.*, 371. 202.

[5] Bauer, T.H., A.E. Wright, W.R. Robinson, J.W. Holland, E.A. Rhodes (1990), "Behavior of modern metallic fuel in TREAT transient overpower Tests", *Nucl. Technol.*, 92. 325.

[6] Cohen, A.B., H. Tsai, L.A. Neimark (1993), "Fuel/cladding compatibility in U-19Pu-10Zr/HT9-clad fuel at elevated temperatures", *J. Nucl. Mater.*, 204. 244.

[7] Liu, Y.Y., H. Tsai, M.C. Billone, J.W. Holland, J.M. Kramer (1993), "Behavior of EBR-II Mk-V-type fuel elements in simulated loss-of-flow tests", *J. Nucl. Mat.*, 204. 194.

[8] Stevenson, C.E., (1987), "The EBR-II fuel cycle story", *American Nuclear Society*, La Grange Park, Illinois, United States.

[9] Inoue, T., et al. (1991), "Development of partitioning and transmutation technology for long-lived nuclides", *Nucl. Technol.*, 93. 206.

[10] Yokoo, T., et al. (1996), "Core performance of fast reactors for actinide recycling using metal, nitride and oxide fuels", *Nucl. Technol.*, 116. 173.

[11] Meyer, M.K., S.L. Hayes, W.J. Carmack, H. Tsai (2008), "The EBR-II X501 minor actinide burning experiment", *INL/EXT-08-13835*, Idaho National Laboratory, United States.

[12] Meyer, M.K., S.L. Hayes, W.J. Carmack, H. Tsai (2009), "The EBR-II X501 minor actinide burning experiment", *J. Nucl. Mater.*, 392. 176.

[13] Kim, Y.S., G.L. Hofman, A.M. Yacout (2009), "Migration of minor actinides in fast reactor metallic fuel", *J. Nucl. Mater.*, 392. 164.

[14] Kurata, M., I. Inoue, L. Koch, J-C. Spirlet, C. Sari, J-F. Babelot (1992), "Development of transmutation technology of long-lived nuclides – properties of the alloy concluding MA and RE –", *CRIEPI Report T92005*, Central Research Institute of Electric Power Industry.

[15] Kurata, M., A. Sasahara, T. Inoue, M. Betti, J.-F. Babelot, J.-C. Spirlet, L. Koch (1997), "Fabrication of U-Pu-Zr metallic fuel containing minor actinides", *Proc. Int. Conf. Future Nuclear Systems, Challenge Towards Second Nuclear Era with Advanced Fuel Cycles* (Global 1997) 2. 1384.

[16] Ohta, H., T. Yokoo, T. Ogata, T. Inoue, M. Ougier, J.P. Glatz, B. Fontaine, L. Breton (2007), "Irradiation experiment on fast reactor metal fuels containing minor actinides up to 7at.% burnup", Global 2007, 9-13 September 2007, Boise, Idaho, United States.

[17] Breton, L., E. Garces, S. Desjardins, B. Fontaine, T. Martella, L. Loubet, H. Ohta, T. Yokoo, M. Ougier, J. P. Glatz (2007), "METAPHIX-1 non-destructive PIE in the irradiated elements cell of PHENIX", Global 2007, 9-13 September 2007, Boise, Idaho, United States.

[18] Ogata, T., K. Nakamura, H. Ohta (2008), "Progress in metal fuel development at CRIEPI", *Trans. ANS*, 98. 977.

[19] Ohta, H., T. Ogata, T. Yokoo, M. Ougier, J.-P. Glatz, B. Fontaine, L. Breton (2009), "Low-burnup irradiation behavior of fast reactor metal fuels containing minor actinides", *Nucl. Technol.* 165. 96.

[20] Ohta, H., T. Ogata, T. Yokoo, T. Koyama, D. Papaioannou, J-P. Glatz, V. Rondinella (2009), "Post-irradiation examinations on fast reactor metal fuels containing minor actinides – fission gas release and metallography of ~2.5at% burnup fuels –", Global 2009, 6-11 September 2009, Paris, France.

[21] Hilton, B.A., S.L. Hayes, M.K. Meyer, D.C. Crawford, G.S. Chang and R. Ambrosek (2003), "The AFC-1AE and AFC-1F irradiation tests of metallic and nitride fuels for actinide

transmutation", Global 2003, 16-20 November 2003, New Orleans, Louisiana, United States.

[22] Hilton, B.A., D.L. Porter, S.L. Hayes (2006), "AFC-1 transmutation fuels post-irradiation hot cell examination 4 to 8at%", *Final Report – Irradiation Experiments AFC-1B, AFC-1F and AFC-1AE, INL/EXT-05-00785 Rev.1*, Idaho National Laboratory, United States.

[23] Hilton, B.A., D.L. Porter, S.L. Hayes (2008), "Postirradiation examination of AFCI metallic transmutation fuels at 8at%", *Trans. ANS*, 98. 773.

[24] Donnet, L., F. Jorion, N. Drin, S.L. Hayes, J.R. Kennedy, K. Pasamehmetoglu, S.L. Voit, D. Haas, A. Fernandez (2005), "The FUTURIX-FTA experiment in Phenix: Status of fuel fabrication", Global 2005, 9-13 October 2005, Tsukuba, Japan.

[25] Jaecki, P., S. Pillon, D. Warrin, S.L. Hayes, J.R. Kennedy, K. Pasamehmetoglu, S.L. Voit, D. Haas, A. Fernandez, Y. Arai (2005), "Update on the FUTURIX-FTA experiment in Phenix", Global 2005, 9-13 October 2005,Tsukuba, Japan.

[26] MacLean, H.J., S.L. Hayes (2007), "Irradiation of metallic and oxide fuels for actinide transmutation in the ATR", Global 2007, 9-13 September 2007, Boise, Idaho, United States.

[27] Hayes S.L., (2007), "Irradiation of metallic fuels with rare earth additions for actinide transmutation in the advanced test reactor – experiment description for AFC-2A and AFC-2B", *INL/EXT-06-11707 Rev. 2,* Idaho National Laboratory, United States.

[28] Carmack, W.J., D.L. Porter, Y.I. Chang, S.L. Hayes, M.K. Meyer, D.E. Burkes, C.B. Lee, T. Mizuno, F. Delarge, J. Somers (2009), "Metallic fuels for advanced reactors", *J. Nucl. Mater.*, 392. 139.

[29] Burkes, D.E., J.R. Kennedy, T. Hartmann, C.A. Papesch (2008), "Characterization of 60U-20Pu-3Am-2Np-15Zr alloys with 1.5wt% rare earth elements", *Trans. ANS*, 98. 1062.

[30] Cheon, J.S., S.J. Oh, B.O. Lee, C.B. Lee (2009), "The effect of RE-rich phase on the thermal conductivity of U-Zr-RE alloys", *J. Nucl. Mater.*, 385. 559.

[31] Burkes, D.E., J.R. Kennedy, T. Hartmann, C.A. Papesch, D.D. Keiser Jr (2010), "Phase characteristics of a number of U-Pu-Am-Np-Zr metallic alloys for use as fast reactor fuels", *J. Nucl. Mater.,* 396. 49.

[32] Kurata, M., T. Inoue, C. Sari (1994), "Redistribution behavior of various constituents in U-Pu-Zr Alloy and U-Pu-Zr alloy containing minor actinides and rare earths in a temperature gradient", *J. Nucl. Mat*er, 208. 144.

[33] Sari, C., C.T. Walker, M. Kurata, T. Inoue (1994), "Interaction of U-Pu-Zr alloys containing minor actinides and rare earths with stainless steel", *J. Nucl. Mater.*, 208. 201.

[34] Cole, J.I., J.R. Kennedy, D.D. Keiser (2008), "An investigation of fuel cladding chemical interaction in metallic transmutation fuels", *Trans. ANS*, 98. 1109.

[35] Cole, J.I., D.D. Keiser, J.R. Kennedy (2007), "Microstructural characterization of cast metallic transmutation fuels", Global 2007, 9-13 September 2007, Boise, Idaho, United States.

[36] Hyde, T.A., (2007), *Fabrication Report for the AFC-2A and AFC-2B Capsule Irradiations in the ATR*, INL/EXT-07-13021, Idaho National Laboratory, United States.

[37] Trybus, C.L., J.E. Sanecki, S.P. Henslee (1993), "Casting of metallic fuel containing minor actinide additions", *J. Nucl. Mater.* 204. 50.

[38] Burkes, D.E., R.S. Fielding, D.L. Porter (2009), "Metallic fast reactor fuel fabrication for the global nuclear energy partnership", *J. Nucl. Mater.,* 392. 158.

[39] Marsden, K., (2007), *Report on Development of Concepts for the Advanced Casting System in Support of the Deployment of a Remotely Operable Research Scale Fuel Fabrication Facility for Metal Fuel*, INL/EXT-07-12469, Idaho National Laboratory, United States.

[40] Lee, C.B., B.O. Lee, C.T. Lee, S.J. Oh, S.H. Kim, G.I. Park, K.C. Song, D.H. Hahn (2009), "Status of metallic fuel development for sodium-cooled fast reactor", Global 2009, 6-11 September 2009, Paris, France.

[41] Lee, C.T., et al. (2009), "Casting technology development for SFR metallic fuel", Global 2009, Paris, France.

[42] Kim, S.K., C.T. Lee, S.J. Oh, Y.M. Ko, Y.M. Woo, H.J. Ryu, C.B. Lee (2009), "Fabrication and characterization of U-Zr alloys for SFR fuel by gravity casting", *Int. Conf. Fast Reactors and Related Fuel Cycles (FR09)*, 7-11 December 2009, Kyoto, Japan.

[43] Sato, K., T. Fujioka, H. Nakabayashi, S. Kitajima, T. Yokoo, T. Inoue (2003), "Conceptual design on an integrated metallic fuel recycle system", Global 2003, 16-20 November 2003, New Orleans, United States.

[44] Ogata, T., T. Tsukada (2007), "Engineering-scale development of injection casting technology for metal fuel cycle", Global 2007, 9-13 September 2007, Boise, Idaho, United States.

[45] Ogata, T., T. Mizuno (2009), "Directions of metal fuel development for fast reactors", Global 2009, 6-11 September 2009, Paris, France.

[46] Trybus, C.L., (1995), "Injection casting of U-Zr-Mn, surrogate alloy for U-Pu-Zr-Am-Np", *J. Nucl. Mater.*, 224. 305.

[47] Nakamura, K., T. Ogata, T. Kato, K. Nakajima, Y. Arai (2009), "Fabrication of metal fuel slug for an irradiation test in JOYO", Global 2009, 6-11 September 2009, Paris, France.

[48] Sasahara, A., et al. (1995), "Development of long-lived radioactive nuclides transmutation technology in metallic fuel FBR – reduction of Am and Cm oxide to metal –", *CRIEPI Report T94024*, Central Research Institute of Electric Power Industry.

[49] Kato, T., et al. (2006), "Development of metal fuel fabrication technology for irradiation test in JOYO – production of uranium-plutonium alloy by electrochemical reduction", *CRIEPI Report L05010*, Central Research Institute of Electric Power Industry.

[50] Uozumi, K., M. Iizuka, M. Kurata, T. Inoue, T. Koyama, M. Ougier, R. Malmbeck, J-P. Glatz, (2009), "Demonstration of pyropartitioning process to recover TRUs from genuine high-level liqiud waste", Global 2009, 6-11 September 2009, Paris, France.

[51] Batte, G.L., G.L. Hofman (1990), "Run-Beyond-Cladding-Breach (RBCB) test results for the Integral Fast Reactor (IFR) metallic fuels program", *Proc. Int. Conf. Fast Reactor Safety*, 12-16 August 1990, Snowbird, Utah, United States.

[52] Carmack, W.J., H.J. MacLean, D.C. Crawford (2007), "Historical review of U.S. transient fast reactor fuel testing", Global 2007, 9-13 September 2007, Boise, Idaho, United States.

[53] Tentner, A.M., Kalimullah, K.J. Miles (1990), "Analysis of metal fuel transient overpower experiments with the SAS4A accident analysis code", *Proc. Int. Conf. Fast Reactor Safety*, 12-16 August 1990, Snowbird, Utah, United States.

[54] Massalski, T.B., (1990), "Binary alloy phase diagrams", ASM International, United States.

[55] Nakamura, K., T. Ogata, M. Kurata (2005), "Analysis of metal fuel/cladding metallurgical interaction during off-normal transient events with phase diagram of the U-Pu-Zr-Fe system", *J. Physics and Chemistry of Solids*, 66. 643.

[56] Kurata, M., K. Nakamura, T. Ogata (2001), "Thermodynamic evaluation of the quaternary U-Pu-Zr-Fe system – assessment of cladding temperature limits of metallic fuel in a fast reactor", *J. Nucl. Mater.*, 294. 123.

[57] Nakamura, K., T. Ogata, M. Kurata, T. Yokoo, M.A. Mignanelli (2002), "Phase relations in the quaternary Fe-Pu-U-Zr system", *J. Nucl. Mater.*, 304. 63.

[58] Nakamura, K., T. Ogata, M. Kurata, M.A. Mignanelli (2001), "Reactions of uranium-plutonium alloys with iron", *J. Nucl. Sci. Technol.*, 38, 2. 112.

[59] Tokiwai, M., R. Yuda, A. Ohuchi, M. Amaya (2002), "Development of eutectic free cladding materials for metallic fuel", *J. Nucl. Sci. Technol.*, Supplement 3. 913.

[60] Keiser, D.D., J.I. Cole (2007), "An evaluation of potential liner materials for eliminating FCCI in irradiated metallic nuclear fuel elements", Global 2007, 9-13 September 2007, Boise, Idaho, United States.

[61] Ryu, H.J., B.O. Lee, S.J. Oh, J.H. Kim, C.B. Lee (2009), "Performance of FCCI barrier foils for U-Zr-X metallic fuel", *J. Nucl. Mater.*, 392. 206.

[62] Yang, S.W., H.J. Ryu, J.H. Kim, B.O. Lee, C.B. Lee (2009), "FCCI barrier performance of electroplated Cr for metallic fuel", *J. Nucl. Mater.*, 392. 206.

3. Oxide fuels

3.1 Introduction

Oxide fuel is contemplated as a reference fuel in several fast reactor systems of Generation-IV, in particular sodium-cooled fast reactors (SFR) and LBE (lead-bismuth eutectic)-cooled reactors.

Despite some disadvantages such as its low density of heavy atoms, its poor thermal conductivity and its chemical reaction with sodium, mixed oxide fuel (U,Pu)O2 is the fuel with the largest experience in fast reactors worldwide. This is due to its high melting point, with no allotropic changes, excellent stability and an excellent behaviour under irradiation, in particular a swelling rate much lower than the other fuels.

The experimental fast reactors built in the 1960s and 1970s were largely using mixed oxide as a reference fuel. This was the case in Rapsodie (France, 1967), BOR 60 (USSR, 1968), KNK II (Germany, 1972), JOYO (Japan, 1978), and FFTF (United States, 1980). As irradiation of oxide fuels in these reactors was highly successful, all the prototype or commercial fast reactors built in the 1970s and later choose oxide as reference fuels for BN350, BN600, Phénix, Superphénix, PFR, Monju and more recently for CEFR, PFBR, BN800. Several hundreds of thousands of oxide fuel pins have been successfully irradiated worldwide in fast reactors (e.g. 180 000 in Phénix, 98 000 in PFR, 63 000 in FFTF). Along with driver fuels, a great number of experimental fuel pins have been irradiated in order either to test new fuel pin designs or new materials, or to test behaviour in off-normal conditions, including accidental situations. These experiments provided a solid background of knowledge on the behaviour of oxide fuel, and a large database for validation of models and fuel performance codes.

The reprocessing of SFR mixed oxide fuels has already been demonstrated at an industrial scale, especially with hydrometallurgy. In addition, their ability to burn minor actinides was proved.

3.2 Different transmutation oxide fuels and transmutation efficiency

3.2.1 Oxide fuel types for transmutation

In the case of oxide fuels, two approaches were identified for MA-bearing fuels: homogeneous fuels with 1 to 5 % MA (also called MA-bearing fuel – MABF) or heterogeneous fuels with 10 to 20% of MA inside an UO_2 support (called also minor actinide-bearing blanket – MABB). In both cases, multi-recycling is assumed with a continuous recycle of the spent fuel. In addition to these fuels, another way for transmutation of minor actinides is target or inert matrix fuels (see Chapter 5) with a once-through cycle management.

Homogeneous fuels

The main challenges for homogeneous fuels are directly linked to its expected performance in terms of (driver) fuel performance and MA transmutation. Acceptance of this particular transmutation method involves two major requirements: core and fuel

performance must not be affected by the presence of minor actinide while transmutation efficiency must be adequate. Specifically, this involves the following points:

- The fuel pin design should be the same as that of standard fuel without minor actinides.
- A loss of less than 0.1% is necessary during the separation step.
- Multi-recycling must be performed in order to reduce radiotoxicity.
- Management of low impurities (lanthanides) resulting from the separation process must be ensured.
- Remote fabrication is performed using several elements (U,Pu, Np, Am, Cm, residual FP and impurities) and several compositions (burn-up of spent fuel, multiple passes in fast reactor, variable conversion ratio) with standard fuel requirements. Clearly, all of the transuranium elements should be incorporated in the homogeneous fuel.
- The MA content will be around 1% at the equilibrium with the objective to burn only its own production. But this content may reach more than 3% to 5% of MA if those coming with Pu from PWR spent fuel are considered. This content is a goal (reduction of the starting phase) and not a requirement. The balance between neutronic limits, scenario objectives and fuel cycle impacts will determine the optimum value of MA content for this starting phase.
- The burn-up and power rate reached must be the same as that of standard fuel.
- There is less impact on fuel element behaviour during normal operation and during a transient or severe accident.
- There is a fuel cycle evolution with higher neutron emission and higher thermal power whose economic impact should be evaluated.

Heterogeneous fuels

In the MABB concept, the minor actinides are diluted in a UO_2 matrix positioned on the peripheral row of a sodium-cooled fast reactor (SFR). Loading these peripheral positions for fuel sub-assemblies with MA offers the advantage of having little impact on the reactor operating parameters and on the core safety and therefore allows rather higher MA content. A disadvantage of periphery loading is that the neutron flux level is relatively low and the flux gradient is steeper. This requires a longer irradiation time than the driver fuel (2 or 3 times). Furthermore, the flux gradient should be managed to ensure that transmutation performance is not degraded.

The composition of transuranium elements may be the mixture coming from reprocessing (Am+Cm+Np) or only Am. A global overview is required to evaluate both solutions with respect to transmutation performances as well as fuel cycle impact (fabrication, reprocessing, storage, transport, decay heat, etc.). At the equilibrium, around 100 MABB subassemblies would be necessary in the case of 20% MA, this number is strongly dependent on core characteristics. The flux level yields a low linear heat generation rate and therefore the pin operates at low temperatures in the MABB concept. The behaviour of such fuel under irradiation and any changes in its physical characteristics are generally unknown. Furthermore, the large quantity of americium results in the generation of large quantities of helium, which will either be released into the pin free volume or may activate matrix swelling, depending on several parameters.

These issues indicate that adapted design changes are needed for the pin and the subassembly and a major experimental programme will be necessary to assess their performance and safety behaviour.

Figure 3.1: Schematic position of MABB in the SFR core [1]

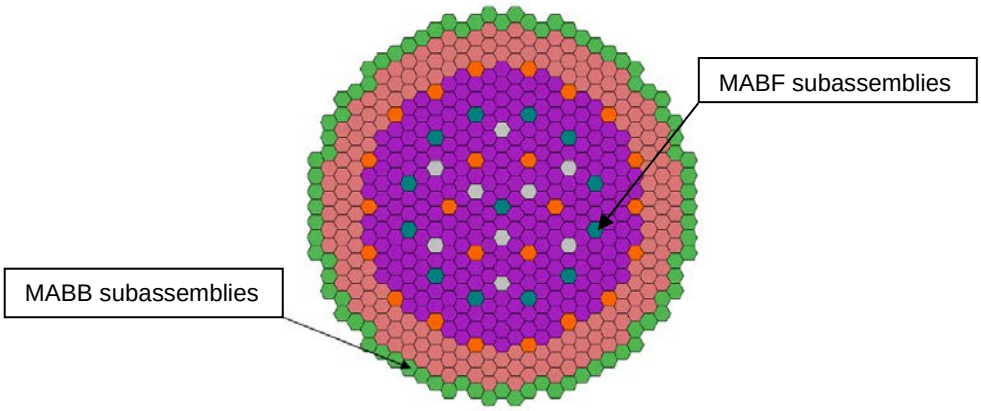

3.2.2 Transmutation efficiency

The homogeneous mode in fast neutron reactors appears to be the easiest solution for transmutation (for neutronic behaviour) given the following performance aspects:

- the homogeneous distribution in the core does not disrupt power distributions;
- the high fluence level and the excess neutrons easily accommodates minor actinide transmutation;
- the overall balance of the reactor, which initially runs on plutonium, is only slightly disrupted;
- the acceptable MA limit is approximately 2.5% by mass and is mainly due to the strong impact of minor actinides on the sodium void coefficient. However, a higher MA loading is possible by using an adapted core design.
- the fission rates reached show that it is necessary to multi- recycle MA.

The isotopic composition of MA for an SFR park at the equilibrium is described in Table 3.1.

Table 3.1: Possible isotopic composition at the equilibrium (in%)

MA Transmutation in homogeneous mode in SFR: Isotopic vectors in 2130									
Elements		Vector U		Vector Pu		Vector Am		Vector Cm	
U	83.5	^{235}U	0.8	^{238}Pu	3.5	^{241}Am	69.4	^{243}Cm	1.6
Pu	15.4	^{236}U	0.7	^{239}Pu	57.8	^{242M}Am	4.0	^{244}Cm	75.0
Tot MA	1.1	^{238}U	98.5	^{240}Pu	31.2	^{243}Am	26.6	^{245}Cm	18.4
Am	0.8			^{241}Pu	2.7			^{246}Cm	5.0
Np	0.2			^{242}Pu	4.8				
Cm	0.2								

This composition depends on the Pu vector and core characteristics but it produces roughly the composition expected for a MABF just when it will have to transmute only self-produced MA, called "equilibrium state" in the next paragraphs. The composition of MABF at the beginning of the SFR park is more dispersed because it is linked to each country's strategy: transition reactor duration, MA coming from previous PWR park.

In [1], the mass balance (kg/TWhe) at EOL (end of life) is more favourable to homogeneous fuel than MABB with a higher MA consumption (7.87 for MABF and 4.79 for MABB, see Table 3.2). It must be noted that the final balance for MABB does not take into account MA production coming from the driver fuel. In such a case, homogeneous fuel is even more effective. Furthermore, the analysis used a 3.2%Am-bearing fuel which is higher than needed for the equilibrium state which is around 1.1% MA with 0.8% of Am. In this case the transmutation efficiency should be higher with lower loading in the fuel.

The MABB concept involves incorporating a large quantity of minor actinides (10 to 40wt%) into radial blankets placed at the periphery of the outer core region. Calculations are first performed to characterise the power levels and the volumetric fractions of the matrix, the structures and the sodium in the assemblies according to fixed values of the minor actinide concentration in the fuel (10, 20 or 40%). For the radial blanket model, the case of Am fuel exhibits relatively good performances with a 28% minor actinide transmutation rate due to a longer irradiation time (twice that of the MABF case). Nevertheless, these encouraging results for MABB must also be considered along with the MA produced in the driver fuel during transmutation. Despite a large curium production (+1.7 kg/TWhe), the americium consumption remains at an acceptable level (close to -7 kg/TWhe). In general, the corresponding mass balance shows lower performance than any of the MABF models.

This study also showed that minor actinides increase the sodium void reactivity effect. However, the maximum discrepancy is only +10% as compared to the reference core. The main impact is observed for the Doppler constant for which the maximum degradation reaches -18.5%.

3.2.3 Impact on fuel cycle

The objective of this section is to give some aspects of the impact of transmutation on fuel cycle operations. These aspects will also be used to optimise the fuel element design if the technological feasibility is difficult or costly for the cycle operations, for example, the maximum level of MA in fuel/target or separation/non-separation of curium.

Front end impact

The large amount of minor actinides leads to some challenges for the front-end of fuel cycles such as manufacturing, storage, and transportation of fresh fuel assemblies. The two main challenges are the decay heat of the fresh fuel assembly, and the neutron source and corresponding dose rate. Table 3.3 shows the values for the tested scenarios.

Table 3.2: Comparison of transmutation performances for MABB and MABF [1]

	MABF			MABB	
	3.2%Am	7.9%Am	18.4%Am	20%Am	20% MA
Charged mass (Kg)					
Np	0	0	0	0	411
Am	2 429	2 430	2 431	2 438	1 866
Cm	0	0	0	0	160
MA	2 429	2 430	2 431	2 438	2 437
Discharged mass (kg)					
Np	43	42	45	20	265
Am	1 435	1 631	1 812	1 493	1 101
Cm	3 90	356	296	242	223
MA	1 867	2 031	2 154	1 589	1 755
Transmutation rate (%) at EOL					
Np	-	-	-	-	-35.5
Am	-40.9	-34.5	-25.4	-38.7	-41
Cm	-	-	-	-	39
MA	-23.1	-18.4	-11.3	-28	-34.8
Mass balance (kg/TWhe) at EOL					
Np	+0.6	+0.62	+0.64	+0.14	-1.02
Am	-13.93	-12.03	-8.64	-6.62	-5.36
Cm	+5.46	+4.99	+4.15	+1.7	+0.44
MA	-7.87	-6.42	-3.85	-4.79	-5.94

Table 3.3: Decay heat and neutron source level of fresh fuel (reloading) [2]

	Reference		Homogeneous		Heterogeneous	
	12% PWR MOX	Driver SFR Fuel	3.2%Am	3.9% MA	20%Am	20% MA
Power per S/A	1	0.4	0.8	1	2	2
Power per tons	1	1.3	2.5	3.1	7	7
Neutron source per S/A	1	0.4	0.7	19	1.2	58
Neutron source per tons	1	1.3	2.2	57	4	198

Once curium is introduced together with other actinides, the impact on decay heat and the neutron source level is much higher than for the case of americium: the decay heat increased by a factor of three (Figure 3.2) and the neutron source by more than one order of magnitude (Figure 3.3). These levels might be problematic for many fields from manufacturing processes to storage and transportation of such assemblies. It is assumed for MABB that a separate plant will be necessary for fabrication, and for MABF the

impacts on the fabrication line may have a strong cost impact if gloveboxes do not provide sufficient protection.

Back-end impact

As shown in the previous section, the heat level is driven by the curium content in the assembly. The same problem arises for the residual heat power (decay heat) on the back-end of the fuel cycle. The ^{241}Am transmutation produces the ^{242}Cm isotope for which the amount remains stable under irradiation (competition between production and disappearance by alpha decay). This contribution has a large impact on the decay heat behaviour. If we make the assumption that subassemblies can be handled below 40 kW using dedicated devices, 20 days are needed before handling for both 20% MA and 20%Am. To give an order of magnitude, the equivalent time for the standard fuel (without MAs) is around 2 or 3 days.

Concerning the irradiated fuel neutron source level, the main contributors remain ^{244}Cm, ^{246}Cm and ^{248}Cm. The neutron source level is 20 to 40 times higher than that of reference (U,Pu)O_2 fuel or even homogeneous fuel.

Figure 3.2: Time dependence of decay heat for irradiated fuel [1]

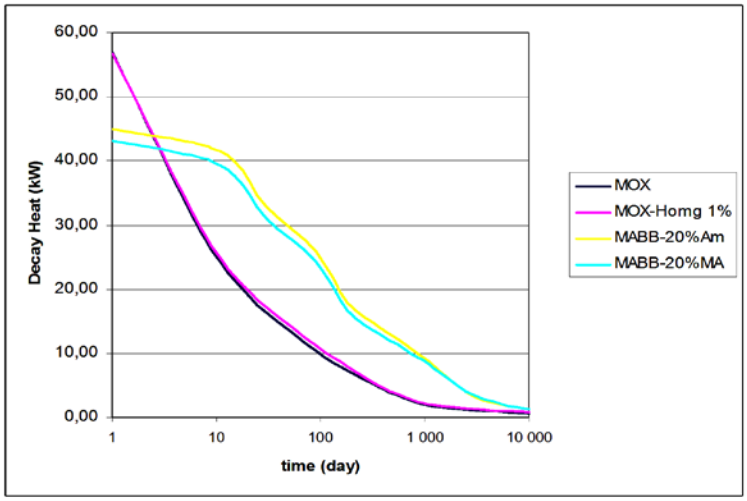

Figure 3.3: Time dependence of neutron source for irradiated fuel [1]

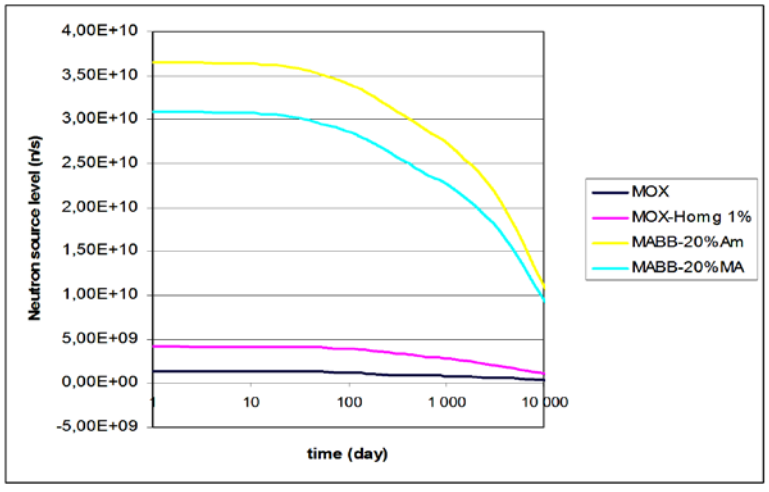

The impact on the reprocessing chains (radioprotection) and transportation (criticality) of such options are currently under investigation and will have consequences on several parameters.

3.3 Homogeneous fuels (i.e. minor actinide-bearing fuels, MABF)

3.3.1 Fabrication

MA fuels can be fabricated at Atalante & LEFCA Facilities (CEA, France), MA-Lab (ITU Karlsruhe, Joint Research Center, UE), RIAR Institute (Russian Federation), AFCF Facility (INL, USA), PF-4 Lab (LANL, USA), Plutonium Fuel Development Facility (JAEA, Japan). Several fabrications of homogeneous fuels have been performed at a laboratory scale at ITU, CEA, JAEA and INL/LANL. The SUPERFACT pellets were fabricated at ITU using the sol-gel process, and more recently, JAEA started a wide campaign of MA-MOX fabrication for both irradiation in JOYO (see Section 3.3.4 irradiation AM1) and a properties measurement programme. All these samples and pellets were fabricated using a powder mixing process, described in the section devoted to the irradiation. In addition, pellets for the AFC-2C and -2D irradiations in the Advanced Test Reactor (ATR) at INL were fabricated at LANL.

All results are linked to fabrication at a laboratory scale (see Section 3.3.4) and any on-going R&D supports necessary process improvement; the main fabrication development needs are linked to its ability to be industrialised.

Fabrication requirement

In order to minimise the impact of an introduction of minor actinides on fast-reactor safety parameters, the minor actinide content in the fuel is kept relatively low (less than 5% of heavy atoms). At this level, the impact of MA content is much higher for fuel fabrication plants than for fuel behaviour aspects. The powerful neutron emission and high thermal power resulting from americium and more crucially from curium, generate additional constraints, in terms of workforce exposure-, criticality- or new heat-related risks.

Fabrication process development

The use of powder metallurgy to produce oxide fuel is the initial reference process because it is the most mastered process and can be readily implemented. However, the huge difficulty in managing dust at all steps where powder form is expected (dosage, grinding, granulation, sieving, loading the presses) must be taken into consideration. Contamination of all the equipment resulting from an accumulation in some areas increases a radiological risk when considering the characteristics of each isotope listed.

It is clear that the first impact of MA introduction into MOX fuel is greater during the fabrication step than in any other steps (behaviour, reprocessing, etc). Neutron emission and thermal power of americium and curium primarily increase the risk in manufacturer exposure or in criticality risk (see Table 3.3). Therefore, a dedicated study is now necessary to evaluate if fabrication facilities should move towards manufacturing in shielded cells instead of using traditional gloveboxes.

Another interesting approach should be to determine the MA content limit and composition (MA or Am alone) in gloveboxes. Once fixed, it will lead to the definition of the transmutation scenario within this limit in order to keep the fabrication facilities using traditional equipment (glovebox). If shielding cells are necessary, the resulting increase in fabrication cost and its subsequent impact on electricity production costs should be determined.

In the future, it seems that in order to enhance the industrialisation of MABF fabrication, the fabrication process that directly yields the right isotopic mixture should have two main objectives:

- the simplest fabrication processes scheme;
- a risk reduction for each step.

Considering these two objectives, the following processes are being developed: the co-conversion process, the sol-gel process and the weak acid resin process [3,4]. These processes also have the advantage of guaranteeing a high homogeneity of the pellet.

The next step in the development of the fabrication process involves:

- demonstration of MA pellet fabrication on a significant scale prior to industrialisation (1 full subassembly);
- qualification of remote handling fabrication equipment;
- demonstration of co-precipitation on a significant scale;
- demonstration of MABF fabrication with actinides (MA, U,Pu) coming from reprocessed fuel including fission products residue and impurities.

3.3.2 Characterisation and properties

During the SUPERFACT programme, properties measurements were devoted to MA bearing UO_2 because it was important for safety reason to evaluate differences between this new fuel and the well-known standard MOX fuel. The results of these measurements will be detailed in the chapter on MABB (see section 3.4). No measurements were conducted to evaluate the properties on SUPERFACT homogeneous fuel.

Recent measurements have been performed in Japan on MABF [5-9], the results of which are summarised in this section. The samples were fabricated with the same processes as those used for the AM1 irradiation pellets (see Section 3.2.4). Details for sample fabrication are given in references [5,11].

Lattice parameter

The solid solutions of $(U_{1-z-y'-y''}Pu_zAm_{y'}Np_{y''})O_{2-x}$ were investigated by X-ray diffraction measurements. A database of the lattice parameters of $(U,Pu, Np, Am)O_{2-x}$ was updated over a wide range of compositions. The ionic radii were estimated from lattice parameters, and a model to calculate the lattice parameters was derived as a function of Pu content, MA content and O/M ratio. The derived model represented the experimental data with a precision of r= ±0.025%. It was considered that Np^{4+} and Am^{4+} were stable in stoichiometric MOX having a low MA content as the samples evaluated in this work. The difference of theoretical density was 0.01-0.02g/cm^3.

This model expressing *a* for $(U_{1-z-y'-y''}Pu_zAm_{y'}Np_{y''})O_{2-x}$

where the range is $z = 0–1$, $y' = 0–0.07$ and $y'' = 0–0.12$

$$a = \frac{4}{\sqrt{3}.(r_c(1+0.112x)+r_a)}$$

where $r_c = r_u(1–z–y'–y'') + r_{Pu}z + r_{Am}y'+r_{Np}y''$ and r_a is the ionic radius of anion, r_c is the ionic radius of cation.

The lattice parameter slightly decreases with MA content, and increases with decreasing O/M, as shown in Figure 3.4.

Figure 3.4: Lattice parameter of MOX with or without MA [7]

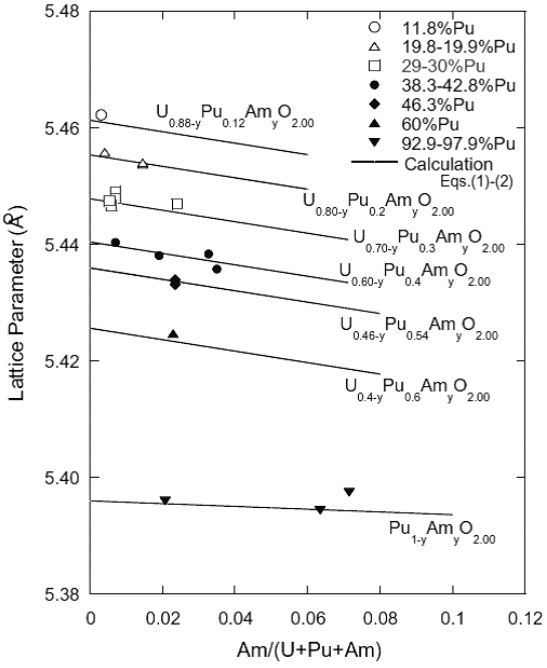

Oxygen potential

The ΔGO_2 of $(U,Pu,Am,Np)O_{2-X}$ is slightly higher than those of MOX without MA. The experimental values are given in Figures 3.5 and 3.6.

Figure 3.5: Evolution of the ΔGO_2 with O/M [6]

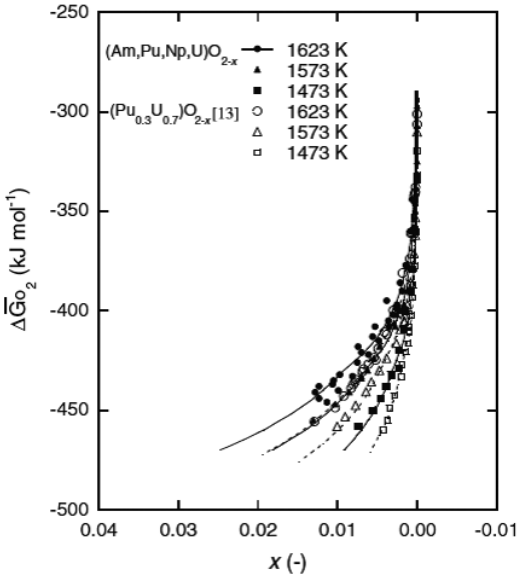

Figure 3.6: Comparison of the ΔGO_2 of $MO_{1.995}$ for several compositions [10]

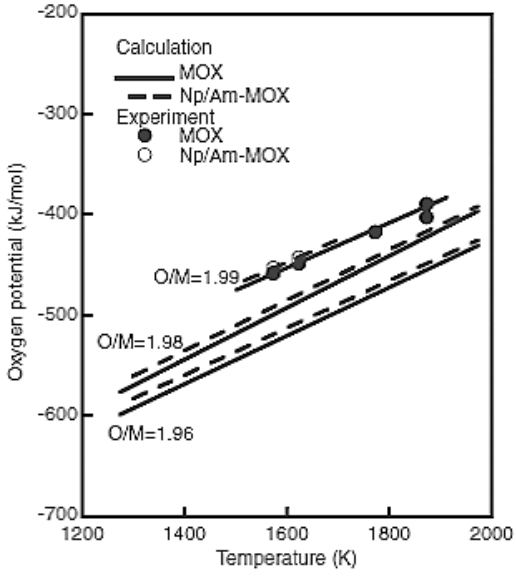

Melting temperatures

The data were measured and analysed by the ideal solid solution model. The solidus and liquidus temperatures decreased with increasing Pu content, increased with decreasing O/M ratio, and the Np and Am addition caused a decrease of 2-4 K (Figures 3.7 and 3.8). MA content caused a decrease of 2-3K/%MA in the melting temperature. However, the solidus temperature of MABF was over 3 000 K.

Figure 3.7: Variation of solidus and liquidus temperature with Pu and MA contents [8]

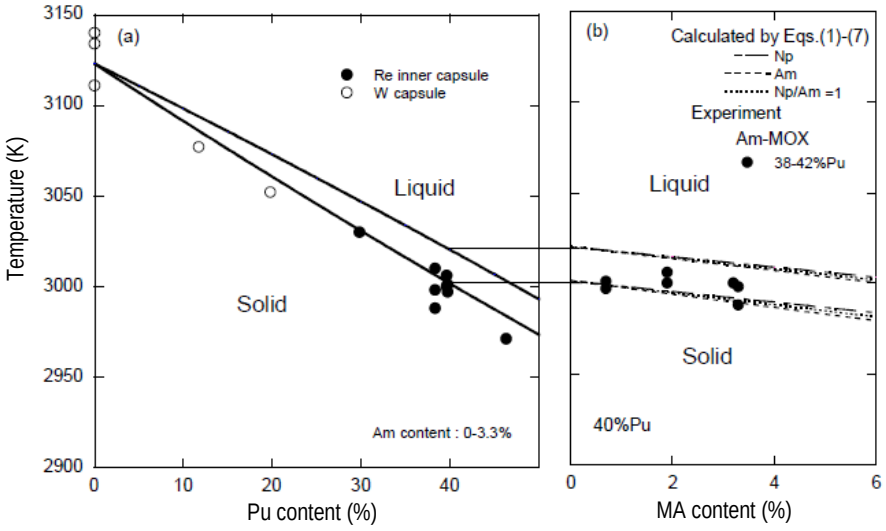

Figure 3.8: Variation of solidus and liquidus temperature with compositions and O/M [8]

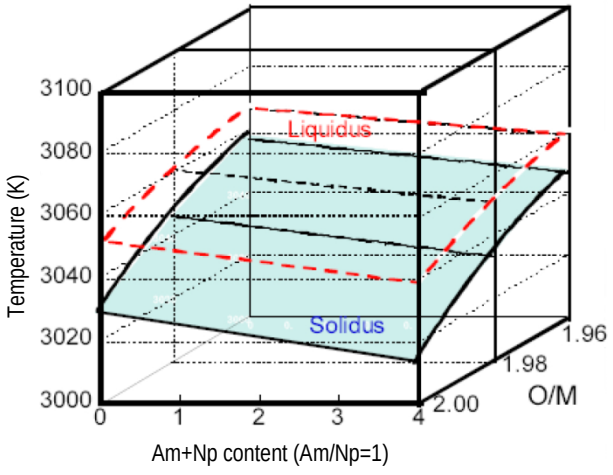

Thermal conductivities

- Influence of Am-content

Thermal diffusivity and specific heat measurements were performed to evaluate the influence of MA content on thermal conductivity. The data were measured as a function of MA content, density, O/M and temperature (Figure 3.9). The addition of MA slightly decreased the thermal conductivities in the temperature range of less than 1 000 K.

Figure 3.9: Thermal conductivity of MOX with MA [10]

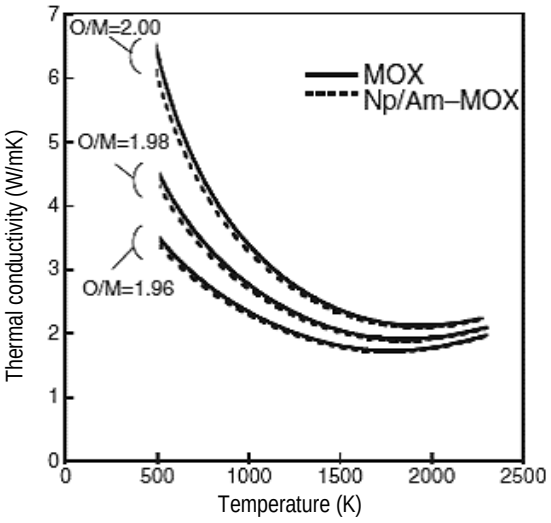

The thermal conductivity of Am-MOX could be expressed by the following equation, based on the classical phonon transport model- ($\lambda = (A + BT)^{-1}$) for low-and intermediate-temperature (<1 600°C) with an electron conduction term ($\lambda = A/T^2EXP(-B/T)$) for higher temperature.

The values of coefficients in both thermal conductivity components were determined by fitting the thermal conductivity data to the above equation. Finally, an expression of thermal conductivity with MA content is proposed [10]:

$$\lambda = \frac{(1-p)}{(1+0.5p)}\left[\frac{1}{2.713x + 3.583\times10^{-1}\times z_1 + 6.317\times10^{-2}\times z_2 + 1.595\times10^{-2}) + (-2.625x + 2.493)\times10^{-4}T} + \frac{1.541\times10^{11}}{T^{5/2}}\exp\left(-\frac{1.522\times10^{4}}{T}\right)\right]$$

where p is porosity, z_1 is Am content, z_2 is Np content and x is deviation x in MO_{2-x}.

The correlation of this equation was made with thermal conductivity measurements at temperatures of less than 1 873 K for the Am and Np contents dependence [11,12], and investigated the O/M dependence at temperatures of less than 2 273 K [13]. This model would be modified with results at very high temperature. Nevertheless, it was estimated that the addition of 1.6%Am and 1.6%Np caused the thermal conductivity to decrease by 2.0–2.5%.

- Influence of density

The dependence of thermal conductivities on the effective porosity can be represented by the Maxwell–Eucken equation:

$$F = (1 - p)/(1 + \beta \times p),$$

with the correction coefficient β of 0.5 (F: factor for thermal conductivity correction, p: porosity). Given the predominant effect of porosity on thermal conductivity, this factor β should be established and controlled experimentally on samples manufactured. For example, a porosity of 10% can lead to a reduction in thermal conductivity of 15% if the factor β is equal to 2 or 25% if this factor is 0.5. Beyond the effect on the conductivity of the content of minor actinides, the influence of the manufacturing process on the microstructure is the

dominant phenomenon. In addition, during irradiation, the production and distribution of helium will increase the porosity ratio (relative to standard MOX irradiated under the same conditions) and thus amplify this effect of the porosity on thermal properties.

Conclusion on characterisations

As a summary of the JAEA characterisation programme, the following can be concluded:

- The physical properties, lattice parameters, phase diagram, oxygen potentials, melting temperatures and thermal conductivities, of Am and Np-bearing MOX were measured. Data or even laws with MA parameter are proposed.
- The effects of MA addition on the physical properties are small. MA addition does not significantly affect fuel properties.
- Basic data for conducting the irradiation tests of MABF are given.

3.3.3 MA-bearing fuel behaviour and safety performances

Minor actinide-bearing mixed oxide fuels should behave as standard $(U,Pu)O_x$ MOX. Previous experimental results have proven to be in agreement with this assessment as described in Section 3.3.4. However, specific properties must be determined and performance must be checked to justify that a small content of MA addition will not "degrade" standard fuel for fast reactors.

The specifics of MA bearing MOX fuels

The thermal and physicochemical properties of MABF compared to the standard $(U,Pu)O_2$ are:

- a lower melting point;
- a low thermal conductivity;
- a higher volatility;
- a higher oxygen potential;
- a higher helium production;
- the MA effect on mechanical properties is not known.

The expected consequences of small decreases of thermal conductivity and melting temperature on MA-MOX behaviour are:

- maximum temperature and thermal gradient increase slightly in the pellet;
- decrease in melting margin;
- faster and larger restructuring;
- higher migration of O, Pu,Am and volatile FPs.

However, taking into account the small effects seen on thermal properties, the changes are expected to be reasonable but have to be specifically determined. These changes combined with higher helium production and a higher oxygen potential will affect fuel performances such as:

- helium production and release;
- gaseous and solid swelling (if He retention);
- microstructure evolution: restructuring, gas precipitation inside grains or at grain boundaries;

- risk of fuel clad mechanical interaction (FCMI) by gaseous swelling and internal pressure due to He;
- risk of fuel clad chemical interaction (FCCI) by internal corrosion due to volatile FPs and enhanced by higher oxygen potential and temperature;
- fuel clad gap conductance improved by high gas pressure mainly filled with He;
- oxide clad joint may be modified.

As a consequence, the risk of fuel melting and the risk of pin failure may be enhanced with the presence of MAs. The irradiation programme will have to determine the actual impact on both of these effects. Although low MA content could have a very small effect, this must be proven. For higher MA content, all this phenomena will have to be checked. So far, all tests have been made on contents of less than 3% MA and a burn-up less than 7at%. For higher concentrations in MA all the phenomena above mentioned have to be studied.

Behaviour at low burn-up (<0.5at%)

The lower thermal conductivity of MABF leads to an increase in the maximum center line temperature at the beginning of life (BOL) when the fuel is the hottest. At the centre of the pellet, the temperature is expected to be higher than in standard MOX mainly due to the loss of density combined with the increase of Pu and MA with a lower O/M ratio. Meanwhile, the Pu and high MA level reduce the melting point. Therefore, the main concern about MABF is its thermal behaviour at BOL when temperature is the highest because the gap is open and thermal properties are degraded due to restructuration and the MA effect. A BOL programme [14] was carried out in Japan at the JOYO fast reactor and no fuel melting was found even for 5%Am. Pu and Am redistribution were shown to occur with a depletion of oxygen near the central hole which had already been formed. All the details of this experimental programme are given in Section 3.2.4. However, without a thermocouple inside of fuel pellet during irradiation, it was difficult to evaluate the temperature increase in MABF compared to MOX standard fuel.

Behaviour at intermediate burn-up (7-10at%)

At an intermediate burn-up, worries arise mainly concerning helium and fission gas production. Consequences are expected on pin internal pressure increase and on gaseous swelling. Consequences of higher oxygen potential, higher internal pressure and higher fuel swelling on clad behaviour must be determined. SUPERFACT [15] was the first experiment on homogeneous (and heterogeneous) MA recycling in the fast spectrum reactor, Phénix. Fuels reached 7at% with no significant differences with MOX fuels irradiated at the time. The quite low power rate (360 W/cm) has to be considered in these results which are detailed in Section 3.2.4.

Behaviour at very high burn-up (15-20at%)

At a very high burn-up, all phenomena resulting from helium and fission gases are intensified. Clad strain due to swelling (damage) and irradiation creep (internal pressure) may be the most important consequence of MA presence. Inner pressure will be increased by 15 to 30% in the case of 2-4%Am. An increase in clad corrosion (wastage) is also expected due to the chemical reaction with volatile fission products (Cs, Te) combined with a higher oxygen potential with MA MOX. The burn-up limit should be reduced or the fuel pin should have a new design for increasing free volume in order to reduce gas pressure on the clad. So at very high burn-up, FCMI and FCCI may be directly affected by the MA presence.

For these reasons, INL has launched a programme aimed at understanding MABF behaviour [16] through irradiation at the ATR reactor with an objective of burn-ups higher

than 10at%. This programme is on-going and detailed in Section 3.2.4. To complete these results, the effect of high neutron dose on clad behaviour will need to be determined at a high burn-up which may be reached only in a fast neutron spectrum. This is the objective of the irradiations of Steps 1 and 2 of GACID programme (see Section 3.2.4).

Safety criteria

For safety performances, both the margin to melt and margin to clad failure must be examined. In the case of pin failure, the MA effect on sodium compatibility is also of concern. All the Na compatibility tests on SUPERFACT samples were performed for MABB and not on MABF samples. All these phenomena must be evaluated at a high burn-up for representative conditions (linear power, temperature). There has been no transient testing of homogeneous fuels, but this should be checked especially at high burn-up when a lot of gas is inside the fuel.

3.3.4 Irradiation performance

Technical feasibility of transmutation in a homogeneous approach has been demonstrated in fast reactors due to the SUPERFACT irradiation performed at the Phénix fast reactor. Several years after, irradiation was completed with the TRABANT irradiations in HFR, AM1 at the JOYO fast reactor and the AFC-2C and -2D irradiations were carried out at the ATR (material testing reactor). Most of these irradiations are still in progress.

SUPERFACT irradiation at Phénix, 1986 to 1988 [17-19]

This programme was carried out by ITU and the CEA in the 1980s.

The experimental capsule contained:

- 4 MOX pins with pellets containing 2% ^{241}Am or 2% ^{237}Np (homogeneous concept);
- 4 pins UOX with 45% ^{237}Np or 20% ^{241}Am + 20% ^{237}Np (heterogeneous concept);

The fabrication was performed at ITU using the sol-gel process (Figure 3.10).

Figure 3.10: Fabrication flowsheet for the SUPERFACT fuel at ITU [18]

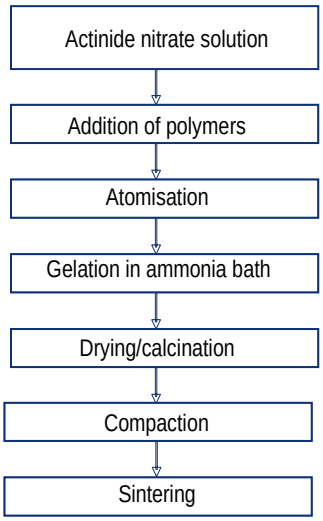

The process requires the addition of polymers in the initial mixture to increase viscosity. After atomisation, the beads are recovered as a solid in a bath of ammonia. They are then washed and dried before being pressed into pellets and sintered at 1 600°C under Ar-5% H_2 for 6 hours. The characteristics obtained on the fuel pellets are detailed in Table 3.4 and the irradiation conditions are presented in Table 3.5.

Table 3.4: Pellet and pin design characteristics of the SUPERFACT pellets [19]

Fuel composition	$(U_{0.74}Pu_{0.24}Np_{0.02})O_2$	$(U_{0.74}Pu_{0.24}Am_{0.02})O_2$
Thermal treatment of the SOLGEL beads	400°C/2h argon	400°C/2h argon
	400°C/2h air	400°C/2h air
	850°C/2h air	900°C/4h air
	850°C/2h Ar 5% H_2	1 050°C/2h Ar 5% H_2
Pressing	5.1-6.4t/cm^2	4.4-5.6t/cm^2
Green density	58.6% TD	58.0% TD
Sintering	1 620°C/6h Ar 5% H_2	1 620°C/6h Ar 5% H_2
Pellet diameter	5.363±0.052mm	5.417±0.029mm
Pellet density (%T.D.)	97.5±0.8%	96.8±0.7%
O/M	1.973	1.957
Lattice parameter (X-ray diffraction)	5.4578±5Å	5.4570±5Å

Table 3.5: SUPERFACT – Irradiation conditions for each pin [18]

Fuel	N of pins	Fissile Column Length (cm)	Linear Power (W/cm)		BU_{max}(at%)
			BOL	EOL	EOL
$(U,Pu_{0.24},Np_{0.02})O_{1.97}$	2	85	385	350	6.6
$(U,Pu_{0.24},Am_{0.02})O_{1.96}$	2	85	379	346	6.48
$(U,Np_{0.20},Am_{0.20})O_{1.93}$	2	40	174	286	4.1
$(U,Np_{0.45})O_{1.99}$	2	40	197	302	4.56
$(U,Pu_{0.20})O_2$	11	85	402	353	7.38

The irradiation conditions of the homogeneous pins (No 7 and 13 with 2%Np – No 4 and 16 with 2%Am) are:

- 382 EFPD;
- Max. linear power = 380 to 345 W/cm;
- Burn-up = 6.7at%.

Main results:

Good in-pile performance of fuels fabricated using the sol-gel technique was demonstrated in the SUPERFACT experiment. Non-destructive examinations of the four pins did not show any anomaly in their behaviour. In particular, no accelerated corrosion was observed.

Figure 3.11: SUPERFACT – micrographs [18]

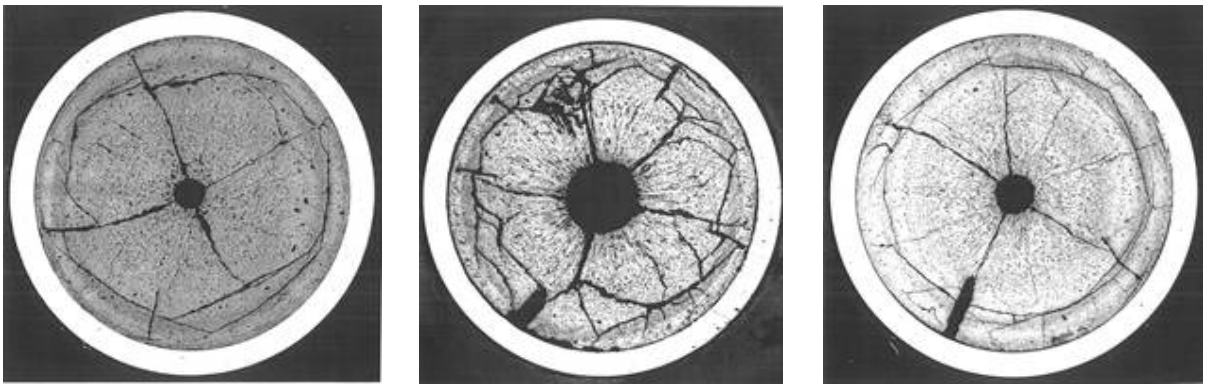

MOX + 2%Am : 380-350 W/cm | Std MOX : 400-350 W/cm | MOX + 2%Np : 385-350 W /cm

The interpretation of the physicochemical and ceramographic (Figure 3.11) examinations of the fuels led to the following conclusions:

- The fuel temperature was probably higher for the americium-containing fuel.
- The fission gas production and release were as predicted for the operating power.
- The Am pins had a higher helium production, mainly due to the daughter products with high specific alpha activity (e.g. ^{242}Cm and ^{238}Pu). The released helium contributed to an increase in the internal pressure of the pin. In addition, higher porosities and swelling were found, probably due to the helium still confined in the fuel. A volume of 40 cm^3 of He was released for a fissile column of 85 cm. This can be compared with 10 cm^3 of He released into the standard MOX pins irradiated simultaneously (mass of fuel equivalent to about 210 g).
- Fuel restructuring is similar to $(U,Pu)O_2$ at the same linear power.
- U,Pu,Am and Np radial distributions are very flat: no specific actinide redistributions were observed.
- The corrosion depth was as expected.
- Cesium was found at the end plugs. Its accumulation is probably due to the particularity of the pins with high Am and Np contents (short fuel column).
- The cesium-profiles for the neptunium-containing fuels showed anomalous behaviour of this fission product when compared to the other pins.
- The clad diametric deformation was slightly higher (+ 0.4 to 0.5%) than for standard pins (+0.3%).

Analyses of the samples of fresh and irradiated SUPERFACT fuels performed at ITU are in excellent agreement with the observations made at the CEA. The neptunium measurement is difficult (not available at the CEA) and has a higher uncertainty than the measurement of the usual nuclides. The measured extent of transmutation (CEA and ITU) of americium at the maximal flux level is 28% for fuels with low minor actinide content. From neptunium analyses an average extent of transmutation of 30% was determined for the three samples. Comparison of the measured values with calculations is satisfactory in the case of americium. In the case of neptunium, comparison with calculations showed less agreement for the fuels with low minor actinide content. At an intermediate burn-up and for low linear power, there is no real influence of the low MA amount in the fuel behaviour except for the He production and release.

Irradiation AM1 in JOYO, 2007 [14,20,21]

Two short-term irradiation tests were carried out within the AM1 programme. They were scheduled to be completed with a steady state (5 and 10at%) irradiation that was delayed when JOYO was shut down for repair in June 2007.

The first AM1 experimental capsules contained:

- 3 pins Am-MOX with pellets containing 3% ^{241}Am or 5% ^{241}Am with 2 different O/M;
- 3 pins Am-Np MOX with pellets containing 2% ^{241}Am+2% ^{237}Np with 2 different O/M.

The fuel pellets containing 3% or 5%Am were fabricated using the remote handling system in the AGF. The AGF was originally constructed as the PIE facility for irradiated fuels. It was later equipped with a small-scale fuel fabrication unit in the hot cell for the purpose of developing a remote handling fuel fabrication technology for MA-MOX fuel. The conventional powder metallurgy method was adopted for the fabrication of Am-MOX fuel pellets.

Figure 3.12 shows a flowsheet of the fuel pin fabrication process. UO_2 powders and two kinds of Am-containing PuO_2 powders were used as raw materials. Before the sintering step, these three powders were annealed in a furnace to remove their absorbed moisture. After heat treatment, the powders were weighed using an electronic balance in the correct ratios for the target compositions. This was followed by mixing in a ball mill for 5 h. Zinc stearate was added as binder and the powder was further mixed for 30 min before cold-pressing to green pellets under a pressure of 3.84 t/cm^2. The green pellets were pre-sintered at 1 073 K for 2.5 h in the furnace to remove the binder and were sintered at 1 973 K for 3 h in a furnace with a tungsten mesh heater. The pellets were then heat treated to adjust O/M ratio to 1.98. The O/M ratio of the pellets was confirmed gravimetrically at room temperature. All of the heat treatments and sintering processes were carried out under the flowing gas atmosphere of Ar-5% H_2 or Ar-0.05% H_2 by adding an appropriate amount of moisture.

Figure 3.12: Fabrication flowsheet of Am-MOX fuel for the AM1 irradiation [21]

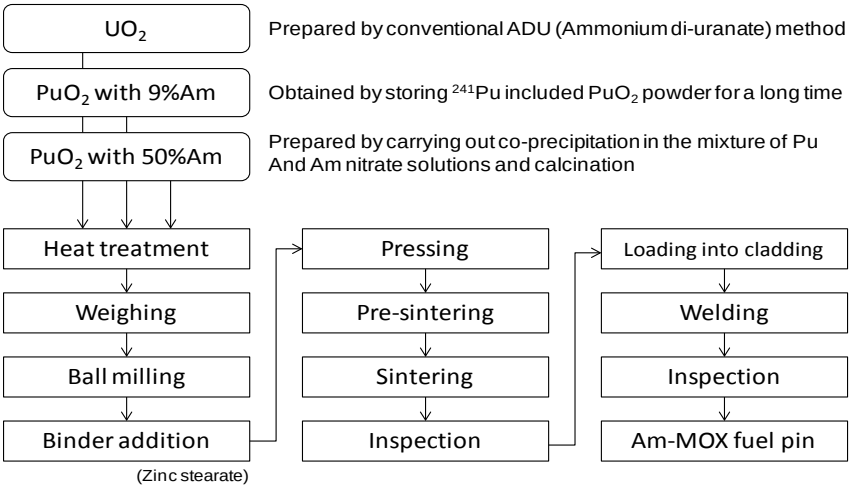

The Am-MOX fuel pellets were inserted into austenitic stainless steel cladding tubes together with thermal insulator pellets of UO_2 and reflector components. The Am-MOX fuel pellets containing 5%Am were loaded in the middle of the fuel column and 3%Am-containing MOX fuel pellets were placed in the lower and upper ends of the fuel column (see Figure 3.13). The fuel pins were sealed by TIG welding and then inspected using a He-leak detection system for confirmation of their air-tightness/soundness.

The irradiation conditions, as shown in Table 3.6, are the following:

- 10 minutes : irradiation B11(1) and 24hours: irradiation B11(2);
- Max. linear power = 430 W/cm;
- Burn-up = 6.7at%.

Table 3.6: AM1 – Irradiation conditions for each pin [21]

Fuel	Number of pins	Fissile column (cm)	LHR (W/cm)	Irradiation length
$(U,Pu_{0.30},Am_{0.05})O_{1.95}$ $(U,Pu_{0.30},Am_{0.05})O_{1.98}$ $(U,Pu_{0.30},Am_{0.03})O_{1.95}$ $(U,Pu_{0.30},Am_{0.03})O_{1.98}$	3	20	430	10 mins and 24h
$(U,Pu_{0.30},Am_{0.02},Np_{0.02})O_{1.95}$ $(U,Pu_{0.30},Am_{0.02},Np_{0.02})O_{1.98}$	3	20	430	10 mins and 24h
$(U,Pu_{0.20})O_{1.95}$ $(U,Pu_{0.20})O_{1.98}$	3	20	430	10 mins and 24h

Main results:

The main objective of these short-term irradiations was to demonstrate that there is no fuel melting, although the fuel is the hottest during the beginning of the life phase.

Post-irradiation examinations of both fuels led to the following conclusions:

- Structural changes occurred such as the formation of lenticular pores and a central hole formed before a 10-minute irradiation B11(1) was completed (Figures 3.13 and 3.14).
- Quick redistribution of Pu and Am increased, whereas U depletion was observed near the central hole. The maximum Pu concentration was 34% compared to 29% in the fresh fuel. The maximum Am concentration was 6.2% for 4.7% in the fresh fuel (Figure 3.15).
- There was no apparent sign of fuel melting.
- There was no significant difference in the restructuring between the 5%Am-MOX fuel and the 3%Am-MOX.
- No FCCI was observed.
- There was a smaller redistribution of Pu and Am for O/M = 1.95 than that with O/M= 1.98.

These results indicate that careful consideration must be given to the redistribution of Pu and Am in evaluating the impact on the thermal performances since it decreases the melting margin by increasing temperature through thermal conductivity reduction and decreasing melting temperature.

Figure 3.13: AM1 – Ceramographs of Am-MOX fuel pellets [21]

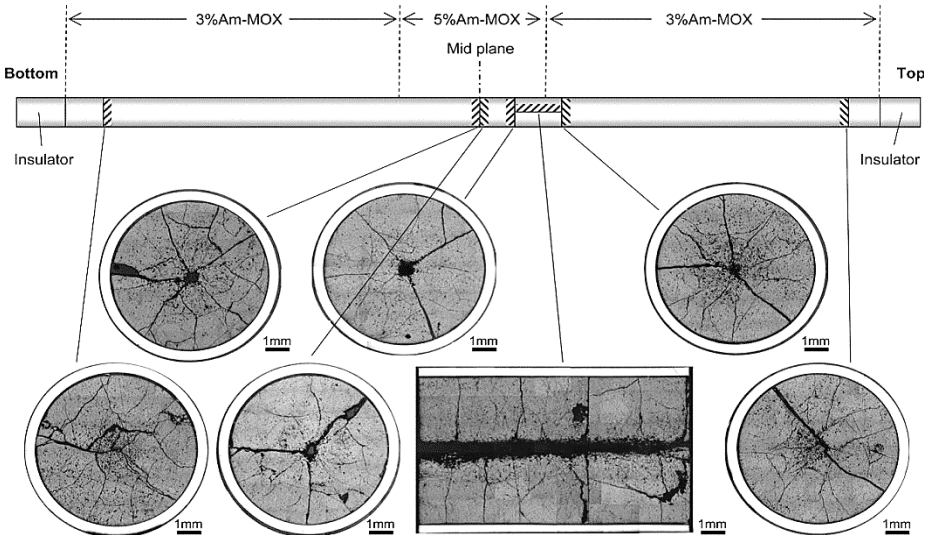

Figure 3.14: AM1 – Comparison of fuel microstructure between the (Am,Pu,Np,U)O_2-x fuel (z/L = 0.50, 432W/cm) and the reference MOX fuel (z/L = 0.74, 420W/cm) in the second test (O/M molar ratio 1.98) [14]

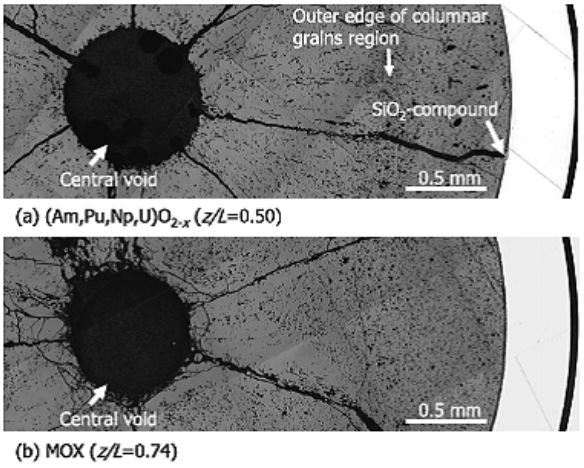

Figure 3.15: AM1 – Comparison of radial distributions of Am and Pu in the (Am,Pu,Np,U)O_{2-x} fuel samples (second test, z/L = 0.5, O/M molar ratio 1.95 and 1.98) [14]

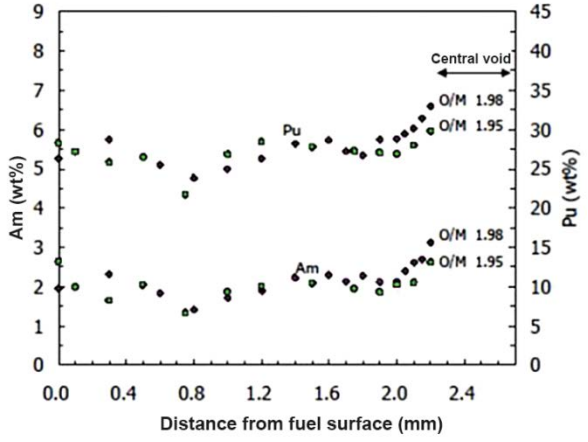

AFC-2C and 2D irradiations in ATR (2008) [22]

The AFC-2C and 2D tests consist of MOX fuels loaded with minor actinides for fast reactor-based transmutation. The experimental capsules containing the AFC-2 fuel rodlets were inserted into ATR inside cadmium baskets that filter the thermal flux, producing a somewhat hardened neutron spectrum in the test region.

The capsule contained:

- 4 MA-MOX rodlets with pellets containing 3% ^{241}Am and 2% ^{237}Np with 2 different O/M under 2 different linear heat rates.
- 2 reference rodlets with reference MOX pellets.

The irradiation conditions, as shown in Table 3.7, are the following:

- 262 EFPDs (AFC-2C), 685 EFPDs (AFC-2D);
- Max. linear power = 350 W/cm;
- Burn-up = ~15at% (AFC-2C) and ~30at% (AFC-2D).

The AFC-2C test was discharged in March 2010 and the AFC-2D in December 2011.

Main results: under PIE for AFC-2C

The objective of both irradiations was to measure the impact of MA at high burn-up. All the PIE will be devoted to evaluating MABF performances, in particular FCCI, the restructuring and thermal behaviour of the pellets. No anomalous differences have been observed between the MA-MOX and MOX rodlets during initial PIE of AFC-2C.

Table 3.7: AFC-2C and 2D – Irradiation conditions [22]

Rodlet	AFC-2C (262 EFPD)	Burn-up calculations (at%): Heavy Metal	Burn-up calculations (at%): ^{239}Pu+^{235}U	Average linear heat rate (W/cm)
1	$(U_{0.75},Pu_{0.2},Am_{0.03},Np_{0.02})O_{1.95}$	5.8%	10.4%	219
2	$(U_{0.8},Pu_{0.2})O_{1.98}$	7.1%	13.8%	296
3	$(U_{0.75},Pu_{0.2},Am_{0.03},Np_{0.02})O_{1.98}$	8.4%	15.0%	321
4	$(U_{0.8},Pu_{0.2})O_{1.98}$	7.9%	15.4%	335
5	$(U_{0.75},Pu_{0.2},Am_{0.03},Np_{0.02})O_{1.95}$	7.9%	14.1%	299
6	$(U_{0.75},Pu_{0.2},Am_{0.03},Np_{0.02})O_{1.99}$	6.4%	11.5%	241
Rodlet	AFC-2D (633 EFPD)	Burnup calculations (at%): Heavy Metal	Burnup calculations (at%): ^{239}Pu+^{235}U	Average linear heat rate (W/cm)
1	$(U_{0.75},Pu_{0.2},Am_{0.03},Np_{0.02})O_{1.95}$	13.3%	24.5%	217
2	$(U_{0.8},Pu_{0.2})O_{1.98}$	16.9%	32.1%	291
3	$(U_{0.75},Pu_{0.2},Am_{0.03},Np_{0.02})O_{1.98}$	19.1%	34.9%	315
4	Dummy Rodlet	–	–	–
5	$(U_{0.75},Pu_{0.2},Am_{0.03},Np_{0.02})O_{1.95}$	17.9%	32.8%	295
6	$(U_{0.75},Pu_{0.2},Am_{0.03},Np_{0.02})O_{1.99}$	14.8%	27.2%	240

3.3.5 Need of additional results

While AM1, AFC2C and 2D were analytical irradiations, SUPERFACT was an integral irradiation with representative conditions of spectrum but did not reach sufficient burn-up and had a reduced linear power. Thus, some data on the effects of MA on fuel performance (linear power, burn-up, etc) and safety aspects (margin to melt, clad failure risk) are still needed. This will be made possible through an irradiation programme devoted to fuel qualification (representative fuel element and representative conditions) with a parallel analytical programme to learn the MA effect on FCCI, FCMI, fission gas release, swelling and fuel temperature (mainly in ATR and JOYO).

The necessity of irradiation tests is placed within a particular context for SFR. It should be noted that a few fast reactors are available for irradiation. There is also international co-operation on SFR through the GIF sodium-cooled fast reactors (SFR) system arrangement.

In this context, a project management board was set up within the SFR arrangement in order to carry out the irradiation programme for homogeneous fuel qualification, namely, GACID (Global Actinide Cycle International Demonstration) [23]. The GACID collaboration framework between the United States, France and Japan is currently defined using the JOYO and MONJU fast reactors in order to implement a common irradiation programme, particularly on SFR fuels, pins and subassemblies, with Np, Am and Cm. The programme is planned to span the 2007-2025 period with a first step from 2007 to 2012 consisting of the project arrangement.

Figure 3.16 shows an overview of the whole GACID Project conceptual scheme.

Figure 3.16: GACID programme organisation: Tri-lateral collaboration in GACID pin-scale test [23]

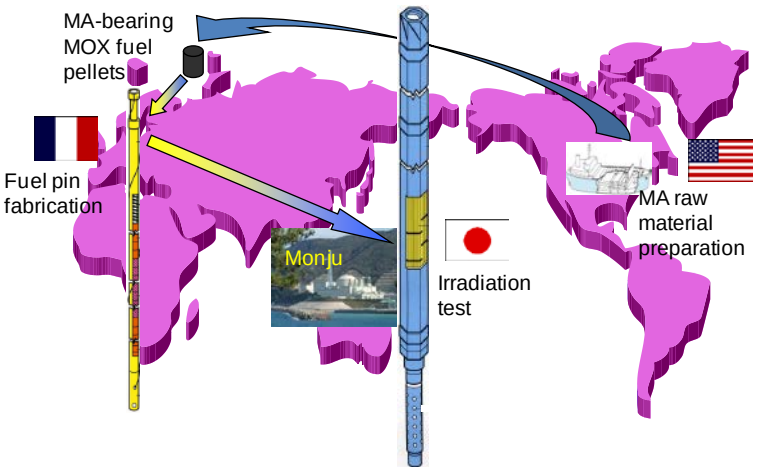

A programme of irradiation tests in JOYO and Monju in three steps was proposed by JAEA and the Project Plan was determined to conduct the following irradiations.

- Step-1: Precedent limited MA-bearing fuel preparatory irradiation test

This test assumes ^{237}Np and ^{241}Am only for the MAs. The radiation and heat source intensities of these isotopes are relatively moderate. Moreover, only a single pin-scale irradiation test in Monju is planned, while the precedent JOYO irradiation tests are already underway. Therefore, this test is expected to be implemented at an early stage of the Project because the test fuel can be prepared with minimum effort by using only a small amount of MA raw materials with minimal additional radiation protection for assembly of the test bundle. Although the MA isotopes are limited, the fundamental framework for the subsequent future MA-bearing fuel irradiation tests is expected to be

established by this precedent test, as a model case of the irradiation tests carried out at Monju.

- Step-2: Pin-scale Cm-bearing fuel irradiation test

A full-range of MA composition is assumed for this test. Not only Np and Am but also Cm will be contained in the test fuel, although the test will be conducted on a pin scale. Gamma-ray and neutron radiation from ^{232}Am (resulting from the daughter nuclide: ^{239}Np) and ^{244}Cm will no longer be ignored in this test. However, being only a single pin fabrication and irradiation will allow for easier management of raw material preparation, radiation protection and heat removal issues. A precedent irradiation test at JOYO is being planned for the Monju irradiation licensing. Fabrication and irradiation of Cm-bearing MOX fuel will be the world's first trial.

- Step-3: Bundle-scale MA-bearing fuel irradiation demonstration

After completing the above mentioned two steps of the precedent irradiation tests, the final goal, bundle-scale full-range-MA-bearing fuel irradiation demonstration, will be performed at Monju. Engineering-scale pilot plants for MA raw material preparation, MA-bearing fuel fabrication and assembly will be needed for this demonstration. Therefore, the technical demonstration will be performed in a reasonable time frame and the whole project is to be conducted over a period of 20 years.

Figure 3.17 shows the schedule and different steps of the programme.

Figure 3.17: GACID programme: Steps and schedule [23]

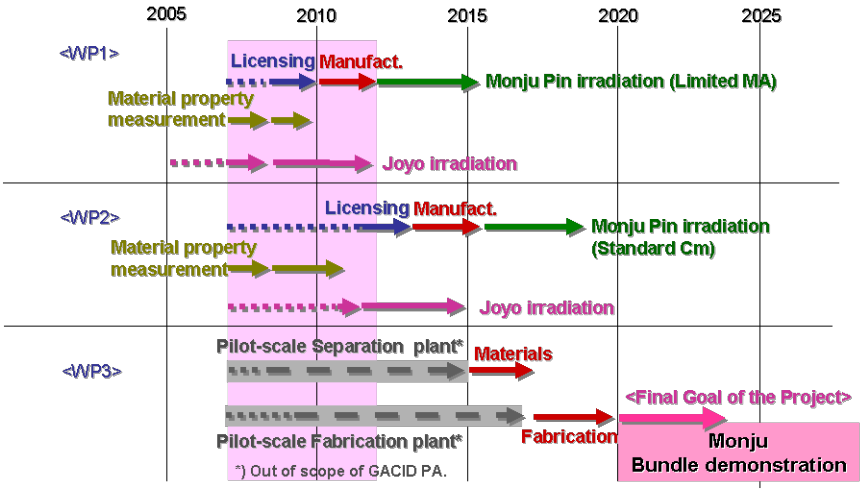

Work Package 1 STEP 1: Preparatory limited MA composition test
Work Package 2 STEP 2: Pin-scale Cm bearing fuel test
Work Package 3 STEP 3: bundle-scale demonstration

The effective period of time of the current project arrangement (PA) is 5 years, with a first milestone two years after the PA signature to decide on the feasibility of pursuing the remaining tasks included in the original five-year project. Therefore, the purpose of the current PA is to conduct collaborative R&D with a view to demonstrating the MA incineration capability of fast reactors at an engineering scale with a MA-bearing MOX fuel.

The current status of the project can be summarised as follows:

- *MA raw material preparation and shipping*: In mid-2008, the United States provided France (CEA/ATALANTE) with AmO_2 and NpO_2 feedstocks for the Step-1 fuel material property measurement. Additional AmO_2 and CmO_2

feedstocks for the Step-2 fuel material property measurement are under preparation at the United States national laboratories.

- *MA-bearing MOX fuel pellet sintering*: Am and Am/Np-bearing MOX fuel pellets have already been sintered and irradiated at JOYO by Japan (JAEA). Preliminary Am/Np-bearing MOX fuel sintering for material property measurement is underway in France and in the United States.
- *Material property measurement*: Material property measurement for Step-1 Am/Np-bearing MOX fuel is underway based on the planned measurement matrices of each organisation. A Np content of up to 3wt% HM, Am content of up to 4wt% HM and Cm content of up to 0.6wt% HM is being assumed as the envelope MA composition of once-through LWR, recycled LWR (MOX) and recycled FBR spent fuel with MA doping. Preliminary measurements carried out in Japan showed a tendency of slight decrease in melting point and deterioration in thermal conductivity, at the lower temperature region, by Am doping for low-Am-bearing MOX fuel having an Am content of up to 3wt% HM.
- *Licensing in Monju and JOYO*: Fuel specifications and licensing strategy for the Step-1 Monju irradiation test are being discussed. Discussions on the material-property and irradiation-behaviour data-base preparation, linear heat rate, correlations, models and design methods for licensing, fabrication tolerances, etc. are underway. Similar discussions for the Step-2 JOYO irradiation test are also on-going.
- *Preliminary programme planning for bundle-scale irradiation demonstration:* A national overall schedule, procedures and steps to achieve the bundle-scale MA-bearing fuel irradiation demonstration at Monju are under preparation.

3.3.6 Technology readiness level (TRL)

A tentative application of the TRL approach to the homogeneous fuel led to determining how each irradiation contributes to qualification of this fuel. A common evaluation of the existing results contributes to a TRL level of 5 on a full scale of 9 (see Chapter 7).

3.4 Heterogeneous fuels (i.e. minor actinide-bearing blanket, MABB)

3.4.1 Fabrication

Fabrication requirements

MABB can be fabricated at Atalante (CEA, France), MA-Lab (ITU-Karlsruhe, EU) and RIAR facilities (Russian Federation). Several fabrications of MABB have been performed at a laboratory scale at ITU and Atalante. Fabrication requirements are strongly linked to fuel design. A preliminary design of the MABB pin exists based on some assumptions but the whole pin and sub-assembly design have not been achieved. The MABB specifications are focused on density, porosity and homogeneity in MA distribution.

Fabrication process development [24-26]

Results to date come from three different fabrication studies which are based on a variety of processes:

- $(U,Am_{0.2}, Np_{0.2})O_2$ for SUPERFACT irradiation using a sol-gel method;
- $(U,Am_{0.2})O_2$ for local structure determination using an infiltration method;
- $(U,Am_{0.3})O_2$ or $(U,Am_{0.1})O_2$ for MARIOS and DIAMINO irradiations.

For SUPERFACT, the fuel was fabricated at the JRC-ITU using a sol-gel external gelation route, shown schematically in Figure 3.18. The process requires the addition of polymers to the feed solution to increase its viscosity. Following dispersion of the

solution into droplets a conversion to solid is obtained when they are collected in an ammonia bath. The resulting beads are washed, dried and calcined before being pressed into pellets and sintered at 1 600°C under Ar-5%H_2 for 6 hours. This programme was realised in the ITU laboratory, as presented in the following flowsheet (see Table 3.8).

Figure 3.18: Fabrication flowsheet for SUPERFACT pellets (20%Am+20%Np) [19]

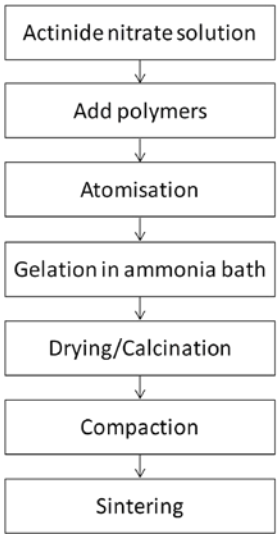

The main characteristics of the pellets are described in Table 3.8 below.

Table 3.8: Fabrication steps and main characteristics of the SUPERFACT fuels [19]

Fuel composition	$(U_{0.55}Np_{0.45})O_2$	$(U_{0.6}Np_{0.2}Am_{0.2})O_2$
Thermal treatment of the SOLGEL beads	400°C/1h argon	400°C/1h argon
	400°C/4h air	400°C/4h air
	865°C/3h air	900°C/5h air
	865°C/4h Ar 5% H_2	900°C/3h Ar 5% H_2
Pressing	6.1t/cm^2	6.1t/cm^2
Green density	55.6% TD	56.4 TD
Sintering	1 620°C/6h Ar 5% H_2	1 620°C/6h Ar 5% H_2
Pellet diameter	5.418±0.037mm	5.434±0.013mm
Pellet density	95.1±0.6%d*	95.9±10%d*
O/M	1.996	1.926
Lattice parameter (X-ray diffraction)	5.4545±5Å	5.4735±5Å 5.4696±5Å

The JRC-ITU has recently tested a new variation of this sol-gel approach to the production of MABB, as shown in Figure 3.19. The sol-gel method is used to produce porous UO_2 beads which are then calcined at about 800°C, and then subsequently infiltrated by an Am nitrate solution. Simple heating converts the Am nitrate to the oxide, permitting the resulting powder to be compacted into pellets for sintering at 1 600°C under Ar/H_2. Pellet densities around 90%T.D. were achieved and XRD analysis showed a single fluorite phase material [27].

Figure 3.19: Infiltration process for the production of $(U,Am)O_{2-x}$ at JRC-ITU [27]

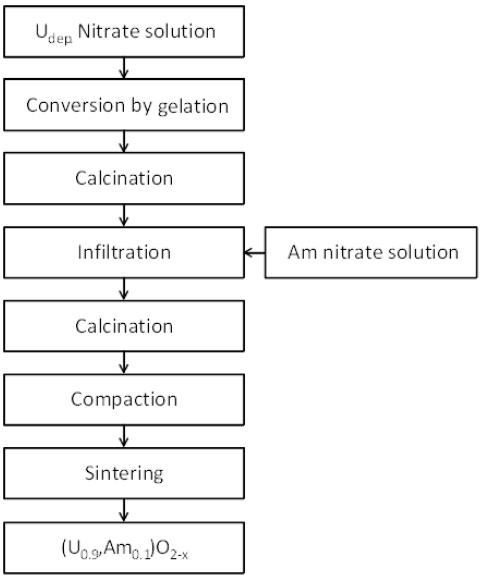

During the R&D fabrication, precursor to MARIOS and DIAMINO fabrication samples, UO_2 pellets containing 10% and 30%Am were fabricated at the Atalante Facility (CEA, Marcoule centre). Pellets were fabricated by conventional powder metallurgy processes in a hot cell at laboratory scale for small batches. The fabrication process used is described in Figure 3.20.

Figure 3.20: Fabrication flowsheet for MARIOS-DIAMINO pellets [25]

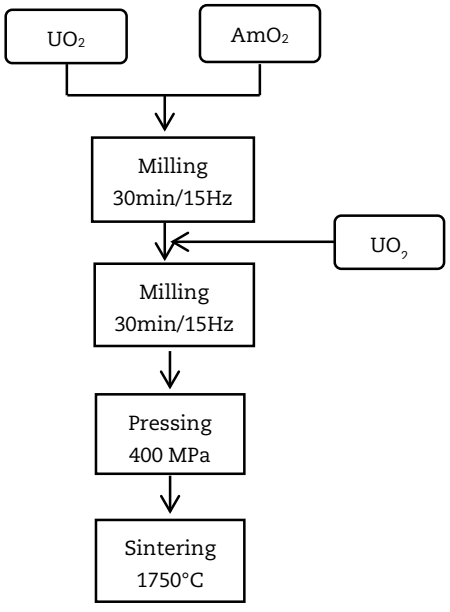

Sintering under reducing atmosphere results in an excessive reduction of the oxide even at low temperatures. If this reduction is not properly controlled, volatilisation of a significant amount of Am may occur. This Am volatilisation leads to lower Am content than expected and a heterogeneity in the target and perhaps metallic phase inside the pellet.

Another issue is the very high activity level that can lead to damage in the material with changes in its properties as well as macroscopic swelling. Controls are needed to evaluate these effects after different periods of storage. A second campaign of fabrication at CEA was devoted to the optimisation of two different microstructures: one with and one without tailored porosity, and for 10 and 15%Am. For the tailored porosity compounds, a pore former was used in order to favour the creation of an interconnected porosity. The pellet characteristics are given in Table 3.9.

Table 3.9: Pellet characteristics – R&D Atalante [25]

Composition	$U_{0.90}Am_{0.10}O_{2-x}$	$U_{0.90}Am_{0.10}O_{2-x}$	$U_{0.85}Am_{0.15}O_{2-x}$	$U_{0.85}Am_{0.15}O_{2-x}$
Microstructure	Dense	Tailored porosity	Dense	Tailored porosity
Sintered density (%TD)	95	85	92	87
Open porosity (%)	n.m.	n.m.	2.4	9.1

XRD analysis confirms that the materials achieved good homogeneity with only one phase. The lattice parameters were also determined for all samples and presented in reference [26]. The $(U,Am)O_2$ discs for the mini-pins in the MARIOS experiment were manufactured with a powder metallurgy process at the ATALANTE facility in Marcoule and then delivered to Petten in the first six months of 2010. As mentioned above, two different microstructures were manufactured:

- a standard microstructure with a high density (~ 92%T.D.);
- an optimised microstructure with open, interconnected porosity (~88%T.D.).

A major R&D phase was required to develop the manufacturing processes, especially to elaborate a pore-forming material for optimised microstructures capable of resisting radiolysis and thermolysis phenomena owing to the high americium content. The microstructures developed during this R&D phase are shown below (Figure 3.21).

Figure 3.21: Macrograph of standard and optimised (tailored open porosity) MABB pellets (∅≈4.5mm) [25]

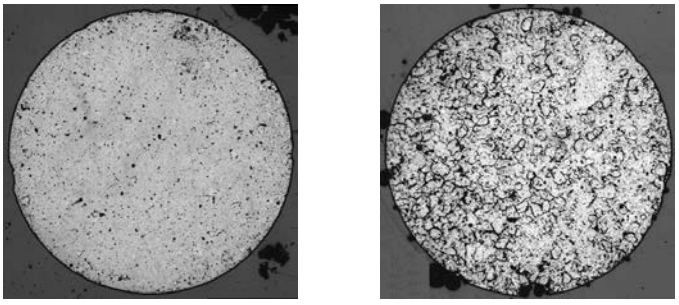

The manufacturing process involved the successive dosing and mixing of UO_2 and AmO_2 powders, followed by dry grinding, press shaping and sintering at 1 750°C in a reducing atmosphere. The pore-forming material for the optimised microstructure was added to the powder mixture before pressing. X-ray diffraction analysis showed that the material had a single fluorite-type phase after sintering for both microstructures. The sintered pellets were then cut and polished to produce 1.5 mm thick discs (sample geometry for analytical irradiation).

The physical characteristics of several MABB compositions (different Am contents and O/M ratios) will soon be measured in order to optimise the design of the fuel pins to undergo reactor irradiation in the future. The main characteristics to be measured are: thermal conductivity, thermal expansion, melting point and vapour pressure.

3.4.2 Characterisation and properties

In order to develop the MA-bearing oxide fuels, it is important to study the fundamental properties of minor actinide oxides. Thermal expansion, heat capacity, thermal conductivity and oxygen potentials of minor actinide oxides have been studied for AmO_x and NpO_x. These studies were followed by measurements performed on materials synthesised for the MA bearing blanket, mainly $(U,Am)O_x$.

AmO_x, NpO_x

- Thermal expansion

Thermal expansions of NpO_2, AmO_2, Am_2O_3 and CmO_2 were determined from the temperature dependence of the lattice parameters measured by high-temperature X-ray diffractometry [28-30]. The measurements were performed in flowing air for NpO_2, AmO_2 and CmO_2, and in flowing N_2-4%H_2 mixed gas for Am_2O_3. All the actinide dioxides have a face-centered cubic crystal structure. The crystal structure of Am_2O_3 is a hexagonal close-packed structure. The thermal expansion of Am_2O_3 was not isotropic, where the thermal expansion along c-axis was larger than that along the a-axis. The volume expansion of Am_2O_3 was larger than that of AmO_2. The oxygen non-stoichiometry affects the thermal expansion and the control of the oxygen/metal ratio of the sample during measurement is important.

- Heat capacity

The heat capacities of NpO_2, AmO_2 and Am_2O_3 were determined by the drop calorimetry [31,32] technique. A disk shaped sample was loaded in a platinum container. The container was evacuated and sealed under an argon gas atmosphere. The enthalpy increment was measured with a twin-type drop calorimeter kept at a given temperature, in which the container was at room temperature when dropped. The heat capacity of NpO_2 [31], together with those of the reported values for NpO_2 [33,34], UO_2 [35] and PuO_2 [35], are shown in Figure 3.22. The heat capacity of NpO_2 was slightly larger than that of UO_2 and smaller than that of PuO_2. The heat capacity of AmO_2 [32] was smaller than that of NpO_2.

Figure 3.22: Heat capacity of NpO_2 [31], together with those of NpO_2 [33, 34], UO_2 [35] and PuO_2 [35], as a function of temperature

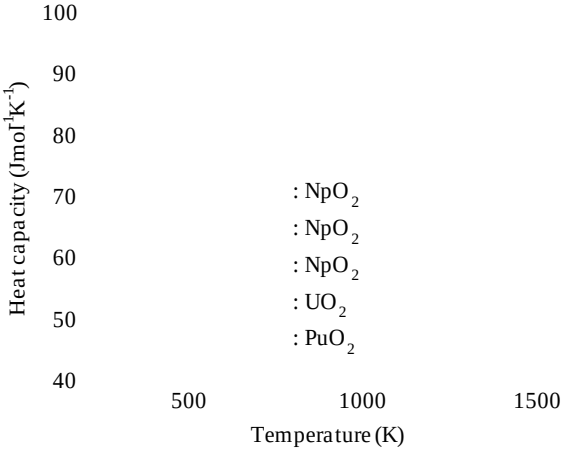

- Thermal conductivity

The thermal diffusivities of NpO_2, AmO_{2-x}, AmO_2 and Am_2O_3 were measured by the laser flash method [31,32,36]. Disk samples of NpO_2, AmO_{2-x}, AmO_2 and Am_2O_3 were prepared by pressing and sintering the respective oxides. The O/Am ratio of the AmO_{2-x} disk sample

was about 1.9 at the beginning of the measurement. The thermal diffusivity measurements were performed during both the heating and cooling processes. The thermal diffusivity of AmO_{2-x} from 573 to 773 K obtained in the first run was found to be larger than that in the second run, while the thermal diffusivity from 873 to 1 273 K obtained in the first run was in good agreement with that in the second run. The data obtained in the third run were in good agreement with those in the second run. After the thermal diffusivity measurement, the O/Am ratio was found to be 1.73. In the case of a hypo-stoichiometric oxide, MO_{2-x}, it is known that the decrease in the O/M ratio lead to the decrease in the thermal diffusivity. The thermal diffusivity of AmO_2 was reproduced in the temperature range 473 to 773 K in the heating and cooling measurements, and that of Am_2O_3 in the temperature range 473 to 1 373 K. In these temperature ranges the composition of samples remained unchanged during measurements. The thermal diffusivity of NpO_2 obtained in the heating and cooling measurements showed good reproducibility. The thermal conductivity of AmO_{2-x} of theoretical density was calculated from the measured thermal diffusivity, and bulk density and specific heat capacity from the literature [37], while the thermal conductivities of NpO_2, AmO_2 and Am_2O_3 were calculated with the measured thermal diffusivity , bulk density and specific heat capacity [31,32].

The thermal conductivities of NpO_2, AmO_{2-x}, AmO_2 and Am_2O_3, together with those of UO_2 [38] and PuO_2 [39] are shown in Figure 3.23, for comparison. The thermal conductivities of NpO_2, AmO_{2-x}, AmO_2 and Am_2O_3 decreased with increasing temperature in the temperature range investigated. This temperature dependence was similar to that of UO_2 and PuO_2. The thermal conductivity of AmO_{2-x} was smaller than those of the literature values of UO_2 and PuO_2. The thermal conductivity of NpO_2 from 873 to 1 473 K lies between those of UO_2 and PuO_2. The thermal conductivity of AmO_2 was much larger than that of Am_2O_3.

Figure 3.23: Thermal conductivities of NpO_2 [31], AmO_{2-x} [36], AmO_2 [32], Am_2O_3 [32], UO_2 [38] and PuO_2 [39], as a function of temperature

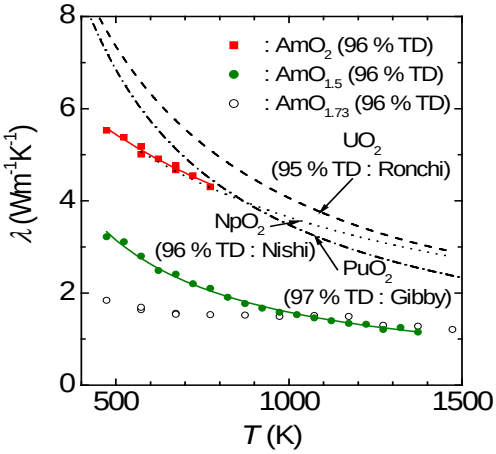

- Oxygen potential

The oxygen potentials of AmO_{2-x} [40], $(Am_{0.5}Np_{0.5})O_{2-x}$ [41], $(Am_{0.5}Pu_{0.5})O_{2-x}$ [42] and $(Cm_{0.09}Pu_{0.91})O_{2-x}$ [43] were measured as a function of the oxygen non-stoichiometry, *x*, and temperature by the electromotive force method with a zirconia solid-electrolyte. For the measurements, disks of the oxides 3 mm in diameter and 1 mm in thickness were prepared. The galvanic cell type used was expressed by:

(Pt-electrode) sample / $Zr(Ca)O_{2-x}$ / air (Pt-electrode).

Figure 3.24 shows the oxygen potentials of AmO_{2-x} as a function of *x* at 1 333K, together with those of CeO_{2-x} at 988 and 1 353 K [44]. The relation between the oxygen potential and *x* of AmO_{2-x} is similar to those of CeO_{2-x}. The oxygen potential of AmO_{2-x}

changed from -20 to -360kJ/mol with increasing x from 0.01 to 0.5 at 1 333 K, which was higher than that of CeO_{2-x} at the corresponding x value by approximately 200 kJ/mol. The oxygen potentials obtained were generally consistent with the published phase diagram of the Am-O system. However, the measured potentials suggested the presence of the intermediate stable phases of Am_9O_{16} and Am_7O_{12} [40].

Figure 3.24: Oxygen potentials of AmO_{2-x} at 1 333 K [40], together with those of CeO_{2-x} at 1 353 K and 988 K [44], as a function of nonstoichiometry, x

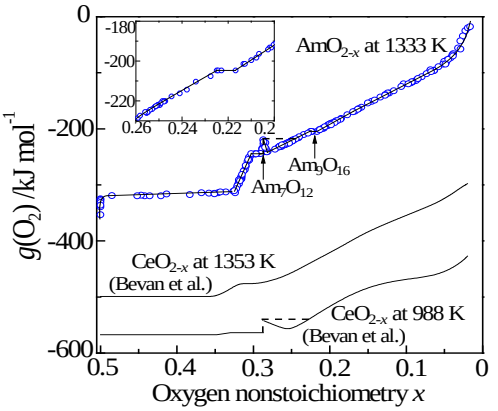

Figure 3.25 shows the oxygen potentials of $(Am_{0.5}Np_{0.5})O_{2-x}$ and AmO_{2-x} obtained as a function of non-stoichiometry at 1 333 K, together with those of $(Am_{0.5}U_{0.5})O_{2-x}$ at 1 333 K from the literature [44]. The oxygen potentials of $(Am_{0.5}Np_{0.5})O_{2-x}$ suddenly dropped around -440kJ/mol with increasing x. This could be attributed to the reduction of Am^{3+} to Am^{2+} or Np^{4+} to Np^{3+} at $x = 0.25$, where the chemical composition is $(Am^{3+}_{0.5}Np^{4+}_{0.5})O_{1.75}$. The oxygen potentials of $(Am_{0.5}Np_{0.5})O_{2-x}$ decreased smoothly from -93.63 to -440.1 kJ/mol with increasing x from 0.021 to 0.25. This result suggested that the $(Am_{0.5}Np_{0.5})O_{2-x}$ sample should be composed of the single oxygen-deficient fluorite-type phase in this x range at 1 333 K. The oxygen potentials of $(Am_{0.5}Np_{0.5})O_{2-x}$ were higher than those of $(Am_{0.5}U_{0.5})O_{2-x}$ by approximately 200 kJ/mol at the corresponding x value.

Figure 3.25: Oxygen potentials of $(Am_{0.5}Np_{0.5})O_{2-x}$ at 1 333 K [41], together with those of AmO_{2-x} at 1 333 K and $(Am_{0.5}U_{0.5})O_{2-x}$ at 1 333 K [45], as a function of the nonstoichiometry, x

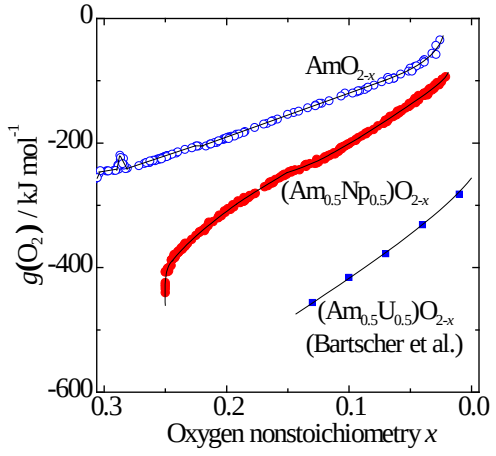

For the oxygen potential measurements of $(Am_{0.5}Pu_{0.5})O_{2-x}$, x was controlled at 1 333 K over the range $0.02<x\leq0.25$ by the coulometric titration method. It was found that the

oxygen potentials decreased smoothly with increasing *x* from 0.02 to 0.22 and that the oxygen potentials remained almost constant around *x*=0.23. The tendency of the change in oxygen potential with increasing *x* from 0.02 to 0.22 at 1 333K for $(Am_{0.5}Pu_{0.5})O_{2-x}$ was similar to that for AmO_{2-x}. This suggested that the phase relations of $(Am_{0.5}Pu_{0.5})O_{2-x}$ should be similar to those of AmO_{2-x} at 1 333 K over $0.02<x\leq0.25$ [42].

(U,Am) O_x

Measurements of $(U,Am)O_x$ were performed during the R&D phase of the SUPERFACT irradiation and are underway on MARIOS and DIAMINO samples (ESFR European project).

- Characteristics after fabrication

The main characteristics of pellets made in ITU for SUPERFACT are:

- pellet density : 96.4%T.D;
- stoichiometry : O/M=1.926.

Samples made at Atalante for the MARIOS irradiation (see Section 3.3.3) were characterised with the following observations:

- neither cracking nor strain was detected for the 10%Am composition;
- 30%Am pellets (sintered at high temperatures) clearly exhibit significant swelling and cracking;
- pellets densities are quite low: 83-89%T.D. for 10%Am and 85%T.D. for 30%Am;
- XRD measurements of 30%Am targets give peaks that are located between UO_2 and Am_2O_3 peaks, which indicate that a biphasic compound was obtained. In addition to UO_{2+x} phase, a major fluorite type is present in the sample. It is quite homogeneous and does not correspond to AmO_2 or Am_2O_3.

On the second campaign of fabrication made at Atalante, the study of α-decay showed that MABB undergo a significant macroscopic swelling: for the 10%Am type, the diameter increase for dense fuel is twice those of tailored porosity compounds. For 15%Am, the diameter increase is very close between both microstructures.

- Thermal conductivity

In order to complete the safety report for the irradiation of $(U,Am)O_2$ in the SUPERFACT irradiation, it was necessary to determine certain thermal properties, so that the fuel behaviour under irradiation can be predicted.

To determine the thermal conductivity, two different approaches were used:

1. Indirect determination via measurements of thermal diffusivity. The thermal diffusivity of $(U,Am)O_2$ and $(U,Np)O_2$ respectively, was determined between 1 100 and 1 800 K by an electron bombardment technique. The results of diffusivity measurements were completed with the evaluation of Cp values, i.e. calculation from $(U,Pu)O_2$, in order to evaluate thermal conductivity.
2. The average thermal conductivities at high temperatures (from about 1 700 K to melting temperature) were evaluated from measurements of the electric power necessary to cause melting by direct electric heating. By interpolation from the melting temperatures of UO_2 and Am_2O_3, the melting temperature of $(U,Am)O_2$ was estimated to be 2 750±100 K. The conductivity values were thus calculated.

Based on the above results, the recommended values of the thermal conductivity between 1 000 K and the melting temperature are given in Figure 3.26. The thermal conductivity of the mixed oxides with 50%Americium is significantly lower than that of $(U,Pu)O_2$. The data obtained for the $(U,Am,Np)O_2$ sample with 25%Am and 25%Np are coincident with the values for $(U,Pu)O_2$.

Figure 3.26: Thermal conductivity recommended for $(U_{0.5}, Am_{0.5})O_x$, $(U_{0.5},Np_{0.5})O_x$ and $(U,Am_{0.25}, Np_{0.25})O_x$ [19]

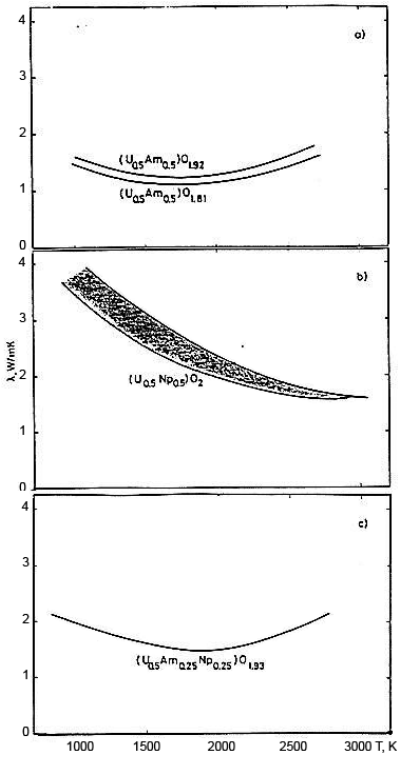

- Oxygen potentials

During the SUPERFACT programme, oxygen potential measurements were performed. It was observed that AmO_2 forms a solid solution with UO_2. The oxygen potentials of the uranium and neptunium-containing mixed oxides, measured by thermogravimetry in the hyper-stoichiometric region, are presented in Figure 3.27.

Figure 3.27: Comparison of $\Delta G O_2$ of $(U_{0.5},Np_{0.5})O_x$ as a function of the temperature and O/M ratio and other measurements on $(U_{0.5}, Am_{0.5})O_x$, $(U,Am_{0.25}, Np_{0.25})O_x$ [19]

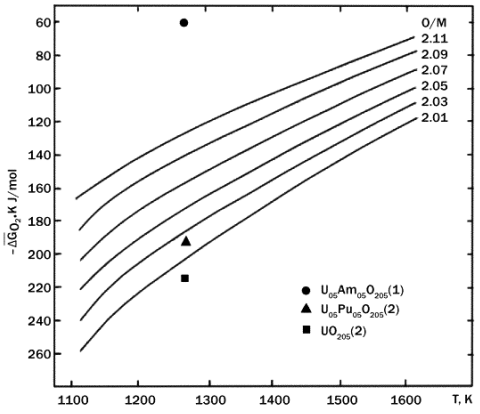

Figure 3.27 shows clearly that the addition of Pu or Np, and especially of Am, decreases the stability of these hyper-stoichiometric dioxides. The oxygen potentials of the mixed oxides of (U,Np)Ox and (U,Pu)Ox are comparable, while that of the oxide of (U,Am) is much higher. Figure 3.28 gives the oxygen potentials of $(U_{0.6}Np_{0.2}Am_{0.2})$ O_2-x.

Figure 3.28: Oxygen potentials of $(U,Am_{0.2},Np_{0.2})O_x$ as a function of temperature and O/M ratio [19]

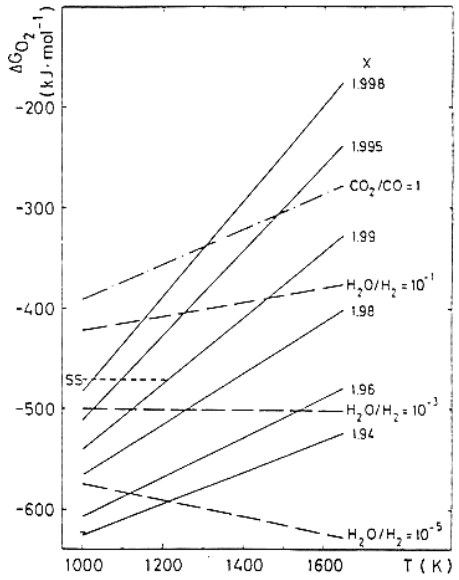

It can be concluded that higher uranium-content and/or the presence of neptunium leads to a decrease in the partial molar enthalpy of the AmO_2 built-up by the decay, although the partial molar entropy remains constant.

Since the O/M ratio of the pellet under irradiation varies as a function of the radial temperature profile, these experiments were repeated with a $(U_{0.6}Np_{0.2}Am_{0.2})\ O_{1.93}$ pellet, where the surface temperature reached 900°C and the central temperature was estimated to be 1 800°c. The results are given in Table 3.10.

Table 3.10: O/M determination of $(U,Am,Np)O_{2+x}$ before and after the simulation of a thermal gradient

Condition	ΔGO_2, 1 273 K, Kcal/mol	O/M
after fabrication after fabrication	-133 -129	1.919 1.925
after the thermal gradient test : - in the centre - on the external part	 -141.5 -109	 1.908 1.951

- Compatibility between actinide-containing fuel and sodium

In the case of americium, a decomposition of sodium americiate occurs at 800°C:

$$Na_3AmO_4 \xrightarrow{800^\circ C} Na_2AmO_3 + Na + O$$

The reaction of sodium with americium (or neptunium) containing mixed oxides was studied under physico-chemical conditions representative of a cladding rupture in the reactor. The capsules, ensuring contact between the pellet and the sodium, were heated to different temperatures (see Table 3.11). The $(U_{0.5}Am_{0.5})\ O_{2-x}$ pellets react with the sodium and completely lose their integrity if the O/M ratio passes a threshold level near 1.84. Low O/M ratio cannot be used since the thermal conductivity would be too low. The mixed oxide $(U,Am)O_2$ with 50% americium was therefore abandoned in favour of $(U_{0.6}Np_{0.2}Am_{0.2})\ O_2$.

Sodium compatibility tests, carried out on the latter compound show that the pellets keep their integrity at an O/M ratio of 1.93, but react with the sodium at an O/M ratio of 1.99.

Table 3.11: Results of the sodium compatibility tests [24]

Capsule	1st thermal treatment		2nd thermal treatment	
	K/h	Reaction*	K/h	Reaction
C5 : $(U_{0.5}Am_{0.5})O_{1.88}$	870/6	Yes	-	
C6 : $(U_{0.5}Am_{0.5})O_{1.64}$	1 170/120	No	-	
D1 : $(U_{0.5}Np_{0.5})O_{2.0}$	770/6	No	1 070/120	No
D0 : $(U_{0.6}Am_{0.2}Np_{0.2})O_{1.93}$	770/6	No	1 070/120	No
C2 : $(U_{0.6}Am_{0.2}Np_{0.2})O_{1.99}$	1 020/6	Yes	-	
C8 : $(U_{0.6}Am_{0.2}Np_{0.2})O_{1.93}$	1 020/6	No	1 070/120	No
D2 : $(U_{0.8}Pu_{0.2})O_{2.00}$	770/6	No	1 070/120	No
*Reaction means a change in the physical aspect of the sample, indicating that a chemical reaction has occurred.				

3.4.3 MABB behaviour and safety performance

Characteristics of MABB

The major advantages of this minor actinides management approach, decoupled from the driver fuel subassembly, are the following:

- this option only has a small impact on safety coefficients;
- it has almost no impact on the core management;
- it enables optimisation of a specific S/A with a specific management in order to reach high transmutation rates;
- it degrades plutonium quality as compared to traditional UO_2 blankets;
- it separates the fuel cycle heavy nuclides streams (especially the fabrication) between electricity production and transmutation goals: the MOX fuel for the SFR fissile cores is not disturbed by MAs and they are concentrated in a reduced stream of heavy nuclides. In the case of fresh fuel fabrication for the heterogeneous transmutation solution, a dedicated facility is necessary in addition to the standard facility for the MOX driver fuel. The additional cost of this new facility and the development of a new process will have to be compared to other solutions (mainly homogeneous recycling).

Despite all these advantages, this very innovative concept presents several R&D challenges in many fields that have to be carefully considered for the fuel assembly design such as helium production, fuel behaviour under irradiation, decay heat level, neutron source, fresh fuel thermal power, reactor operation, etc.

The MABB behaviour [46]

Assuming a standard fuel element with (U, MA)O_x pellets inside of a standard pin, the fuel design consists in the optimisation of pellet characteristics (diameter, density, porosity) and pin constituents. Results for this standard design are described below. Some very innovative fuel element designs should be considered in the future in order to enhance the performance of MABB and to minimise its main drawbacks (i.e. He product).

The principle aim of the standard design was to define pin geometry and its integration into a fuel bundle for an assembly with a given inner cross-flat distance. Since the feasibility of an assembly bearing 40% MA has not been established due to manufacturing and handling problems (excessively high thermal power); the thermohydraulic calculation should focus on the assembly bearing 20% MA, which covers the 10% MA case study. As the neutron flux gradient is especially steep in the outer region of the core, an assembly rotation would be necessary to homogenise damage on each pin of a given sub-assembly. Based on this scenario (assembly rotation), the total irradiation time is divided between two cycles, i.e. C1 (before rotation) and C2 (after rotation). Therefore, the thermo-hydraulic calculations focus on the beginning-of-life and end-of-life for each of these two cycles. The typical power history for a MABB pin is very different from that of a standard fuel and is given in Figure 3.29 in a case without subassembly rotation.

Figure 3.29: Power history of an MABB pin (case: 20wt%Am) [46]

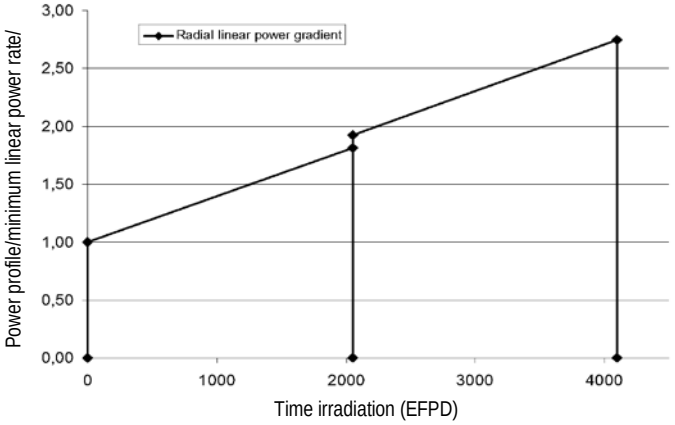

Another particularity of MABB standard $(U,Pu)O_2$ fuel is the helium production. A comparison with a MOX standard fuel is given in Figure 3.30.

Figure 3.30: Helium production for MABB as a function of time [46]

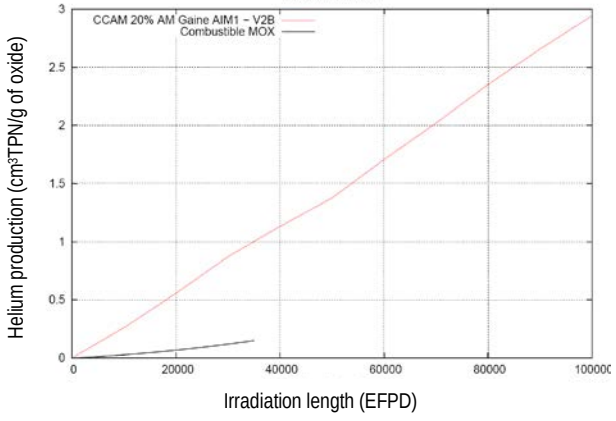

A preliminary evaluation of thermal behaviour of a MABB pin is given in Figure 3.31. The pellet centre temperature at the maximum flux plane is very low (600-700°C) and then higher (1 300-1 500°C) when the subassembly is rotated.

Figure 3.31: Fuel temperature as a function of time with a subassembly rotation at mid-life [46]

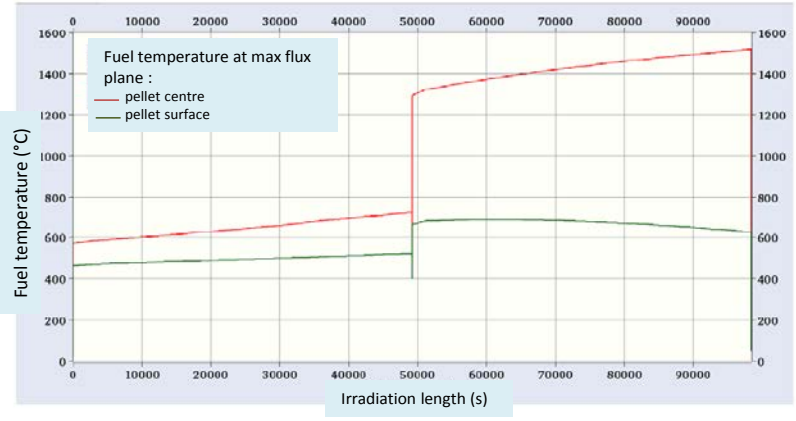

This temperature profile corresponds to a pellet diameter of 8.64 mm. The pin is in the outer part of the subassembly for the two first cycles and then the subassembly is rotated and the pin is found at the position in the subassembly closest to the centre core, which explains the step observed in temperature level at mid-life.

For a smaller pin diameter of 6.44 mm, the maximum temperature decreases to under 1 200°C at the pellet centre.

MABB pellet design

This unusual behaviour (low temperature, high gas production) may lead to safety issues through FCMI. As shown in Figure 3.32, significant MABB pellet swelling may occur due to helium bubble coalescence in the grain boundaries between the 500-700°C (T1) and 1 100-1 400°C (T2) temperature ranges. It should be pointed out that temperature levels T1 and T2 are likely to change in relation to the burn-up rate.

Figure 3.32: Possible behaviour of MABB material as a function of the irradiation temperature [48]

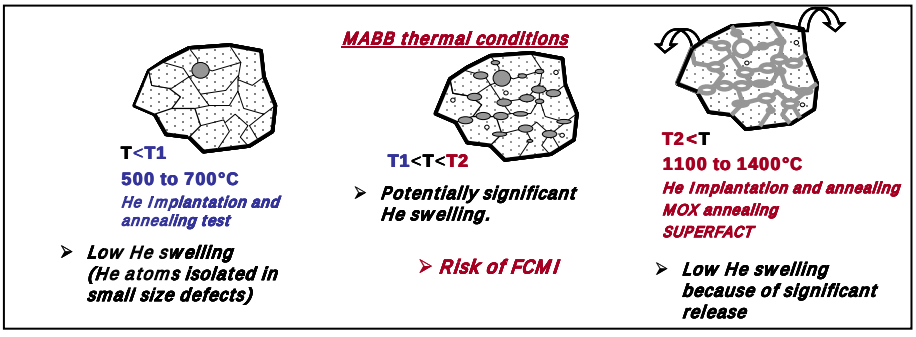

This swelling phenomenon will be studied and quantified during the MARIOS analytical experiments at the HFR in JRC/Petten, as well as during the DIAMINO experiments at the OSIRIS reactor in CEA/Saclay. The main objective of these experiments is to control and homogenise the fuel thermal conditions to correlate helium swelling with the fuel temperature. This explains why small, thin $(U,^{241}Am)O_{2-x}$ fuel discs will be used in these experiments rather than pellets.

Two types of microstructures will be assessed during these experiments. There will be a "standard" microstructure with a high density (~92%T.D.) achieved with a

manufacturing process comparable to that used for SFR standard $(U,Pu)O_2$ fuels. The other "optimised" microstructure will have a lower density with interconnected open porosity stable under irradiation which should promote the release of helium into the pin free volumes in order to limit swelling.

MABB pin design

The fuel pin design, particularly the radial dimensions of the fuel pellet and clad radius, are anticipated to be the same as for the standard fuel without minor actinide (but may change during optimisation phase). It should be noted that the larger production of helium can be accommodated by just increasing the length of the gas expansion volumes.

Therefore, the preliminary design studies for MABB pins are based on several key assumptions:

- The fuel pellets release all of the helium produced. This assumption is conservative as regards the internal pin pressure, but not in terms of fuel swelling.
- Only swelling due to fission product (solid and gaseous) is taken into account. Some analytical irradiation will evaluate the swelling due to helium. Without this analysis, no swelling law may be used.
- Swelling due to these fission products is considered identical to that of standard UO_2 fuel.
- The fuel-cladding mechanical interaction is not modelled for the preliminary design because of the lack of experimental data especially in the case of contact.
- The thermal conductivity of MABB fuel and its behaviour under irradiation are considered identical to the UO_2 mixed oxide reference laws. The lack of measurements on very porous fuels with high Am content does not permit a better modelling of thermal behaviour.

These assumptions on the MABB behaviour make it difficult to reliably assess the transmutation capacity and thus the technical feasibility of such a concept. The type of cladding material also has an impact on performance, though it is not yet possible to choose the most suitable steel grade for the concept.

MABB subassembly design

MABB subassemblies are characterised by:

- Long irradiation times currently defined around 4 100 EFPD (10 cycles each lasting 410 EFPD, i.e. twice that of standard fuel), though limitation may arise by the behaviour of MABBs (internal pressure or pellet-cladding gap, see below).
- 180° subassembly rotation at mid-life to homogenise the cladding damage and the transmutation performance of the pins in the subassembly because of the drastic radial flux profile in this region. This rotation limits the maximum power and makes it possible to reduce the internal pin pressure at the end of life. As the temperature ramp transients, this rotation will be considered as a normal operating transient which will have to be treated carefully when defining the experimental irradiation programme. High-gas retention (helium + fission gases) in the fuel can result in additional gas swelling during the transient temperature rise, which will have to be quantified and modelled.
- Pre- and post-irradiation radiological characteristics (neutron emissions and thermal power) outside the qualification range of standard MA-free fuels whose

consequences need to be assessed in terms of manufacturing, transport and handling.

- All the pins in the fuel bundle initially contain the same MA concentration.

The subassembly design is performed with the objectives of defining the coolant flow that is required to meet the nominal cladding temperature criterion, the coolant pressure losses, and the cladding and coolant temperature ranges. The main geometric characteristics of the pin and the assembly are given in Table 3.12.

These results show that the MA concentrations in the MABB fuel concept require changing the design criterion:

- for a fuel containing 10% MA, the limiting design criterion is the pellet-cladding gap closure at the end-of-life;
- for a fuel containing 20 or 40% MA the cladding resistance to internal pressure limits the fuel pellet diameter and therefore the fuel fraction in the assembly.

Results show that the flow rate and pressure losses are acceptable in terms of meeting the cladding nominal temperature criterion. However, the effect of the strong power variation (50 to 150 W/cm) in the core outlet temperature between the beginning and the end of the irradiation should be addressed. These issues indicate that a major experimental programme will be necessary to correctly design these pins and assess their performance.

Table 3.12: Preliminary pin design as a function of the minor actinide concentration (%) [46]

Variable	10%	20%	40%
Initial pellet diameter (mm)	11.28	8.64	6.76
Helium volume TPN (cm^3)	1 991	2 448	2 477
Gap at end-of-life (μm)	36	21	83
Pellet central temperature (°C)	1 472	1 519	1 348
Hot pressure (bar)	69	99	156
R1 criterion	1.57	1.06	1.01
Creep usage fraction	<0.01	1.9×10^{-6}	<0.001
Plenum height (m)	0.170	0.470	0.470
Pin diameter in cold conditions (mm)	13.08	10.44	8.56
Number of pin rows	7	9	11
Fuel volume fraction	41%	37.8%	33.8%

Safety criteria

Behaviour of MABB during transient of power (TOP) is of concern for its viability, for example. A fuel with a great amount of helium inside should have a quick and large swelling leading to a strong pellet-clad mechanical interaction with a possible pin failure after that kind of transient. This may be managed with an adapted microstructure but a TOP with a long cold stop beforehand should be the worse case for the cladding. Furthermore, thermal properties at high burn-up may be strongly degraded and then decrease the margin to melt. A wide experimental programme linked with dedicated modelling should improve current knowledge on MABB safety issues.

3.4.4 Irradiation performance

SUPERFACT irradiation in Phénix, 1986-1988 [27,28,29]

The experimental capsule contained:

- 4 MOX pins with pellets containing 2% ^{241}Am or 2% ^{237}Np (homogeneous concept);
- 4 UOX pins with 45% ^{237}Np or 20% ^{241}Am + 20% ^{237}Np (heterogeneous concept).

- Main results:

The photographs depicting the macro and microstructure of a SUPERFACT fuel are shown in Figure 3.33.

Figure 3.33: Micrographs of a SUPERFACT fuel fabricated by the sol-gel method indicating: (a) macrostructure and (b) microstructure

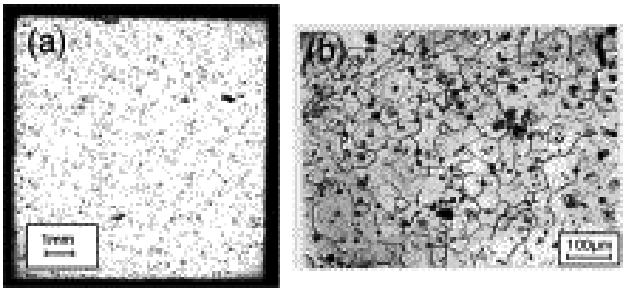

The high concentration of americium in the $(U_{0.60}Np_{0.20}Am_{0.20})O_2$ fuel led to an substantial increase in the fuel column length and to a more significant diametrical deformation of the cladding. This is probably due to the beginning of a mechanical interaction between the oxide fuel and the cladding. The fission gas release rates were in good agreement with those of standard fuels, even for fuels with a high concentration of minor actinides. The interpretation of the physico-chemical and ceramographic examinations of the fuels led to the following conclusions:

- A beginning of a pellet-cladding mechanical interaction was observed for the $(U_{0.60}Np_{0.20}Am_{0.20})O_2$ pins.
- Cesium was found at the end plugs. Its accumulation is probably due to the particularity of the pins with high Am and Np contents (short fuel column).
- The cesium-profiles for the neptunium-containing fuels showed anomalous behaviour of this fission product when compared to the other pins.
- The corrosion depth was as expected.
- No central hole was observed due to the low power during irradiation.
- The expansion of the fuel column is higher than those of the other pins (homogeneous ones and standard ones), typical values are between 2.2% and 3%.
- The fuel temperature was probably higher for the americium-containing fuel because the porosity and the columnar grain diameter are larger than those of the pins with neptunium only. The restructuring of the 20%Am-20%Np pins seems to be higher than those of the 45%Np ones, whereas the gap conductance is better because of its lower thickness filled with a very high He pressure.
- The fission gas production and release were as predicted for the operating power.

- The Am pins had a higher helium production, mainly due to the daughter products with high specific alpha activity (e.g. ^{242}Cm and ^{238}Pu). The He production was around 10 times those of the standard $(U,Pu)O_2$ fuel. The released helium contributed to an increase in the internal pressure of the pin because the entire He produced during the irradiation was released and that produced during the cooling was partially released. In addition, higher porosities and swelling were found, probably due to the helium still confined in the fuel.
- Fission gas release rate is around 61% for pins with Am and Np and around 54% for pins containing 45%Np.
- U,Pu,Am and Np radial distributions are very flat: no specific actinide redistributions were observed.

Analyses of the samples of fresh and irradiated SUPERFACT fuels performed by ITU are in good agreement with the observations made at the CEA. The neptunium measurement is difficult (not available at the CEA) and has a higher uncertainty than the measurement of the usual nuclides. The measured extent of transmutation (CEA and ITU) of americium at the maximal flux level is 31.5% for fuels with high minor actinide content. From neptunium analyses, an average extent of transmutation of 30% was determined for the three samples. Comparison of the measured values with calculations is satisfactory in the case of americium. In the case of neptunium, comparison with calculations showed less agreement for the fuels with low minor actinide content.

MARIOS experiment in the HFR and DIAMINO in the OSIRIS reactor [1]

The design principle applicable to the MARIOS experiment at the HFR and the DIAMINO experiment at the OSIRIS reactor is illustrated in Figure 3.34.

Figure 3.34: Schematic diagram of a mini-pin with 6 MABB discs (in pink) [47]

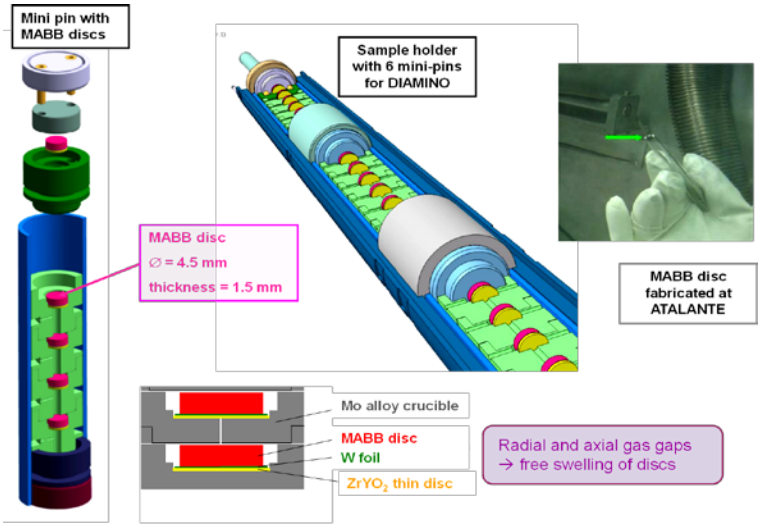

Small MABB discs (∅≈5mm, h=1.5 mm) will be placed in molybdenum alloy crucibles. Molybdenum will provide a source of heat by gamma heating and will make it possible to axially remove the heat produced by the sample during irradiation (fission and gamma heating) so as to limit the thermal gradients of the latter. Top axial and radial gaps will be incorporated to allow for free swelling of the sample. An insulating ceramic disc will be added under the MABB sample to balance thermal resistance created by the top axial gap. This measure will limit the thermal gradients inside the MABB discs.

Several mini-pins will be placed inside an irradiation capsule which will then be inserted into the core for irradiation (4 mini-pins for MARIOS and 6 for DIAMINO). Each

mini-pin will be used to study an experimental configuration, e.g. 1 target temperature × 1 microstructure × 1 helium production rate for DIAMINO. The conditions tested for each experiment are listed in Table 3.13 below.

Table 3.13: Experimental grid for MARIOS and DIAMINO analytical experiments [48]

Composition		Targeted temperature (°C)			
		600	800	1 000	1 200
MABB (15%Am)	Standard microstructure	DIAMINO	DIAMINO	MARIOS	MARIOS
	Optimised microstructure	DIAMINO	DIAMINO	MARIOS	MARIOS
MABB (7.5%Am)	Standard microstructure		DIAMINO	← *Low He production* ← *rate*	
	Optimised microstructure		DIAMINO		

Two irradiation temperatures (~1 000°C and 1 200°C) were defined for the two microstructures in the MARIOS experiment (started in 2011 at HFR). The target neutron flux must be able to generate a quantity of helium similar to that which will be produced in MABBs containing 20% minor actinides loaded in an SFR. This leads to an irradiation time of 310 EFPD for a MABB loaded in position C3 of the HFR core (compared with 4 100 EFPD planned for future SFRs). The irradiation was started in early 2011 and the results on MABB behaviour are not yet available.

The DIAMINO experiment (started in 2012 at the OSIRIS Reactor) is currently testing two irradiation temperatures (600 and 800°C) on the two types of microstructures to supplement and readjust results in relation to the MARIOS experiment. The impact of the helium production kinetics will also be studied at 800°C by irradiating samples with different compositions in order to produce the same quantity of helium over a period twice as long, i.e. about 400 instead of 200 EFPD. These conditions will be used to examine whether the irradiation tests under a thermal flux (which notably accelerates the helium production rate) are well suited to MABBs when studying the problem of helium swelling. The irradiation device will be equipped with several insulating gas-filling bonds whose composition will be adjusted during irradiation. It will also be equipped with a heater element to precisely adjust the temperature of the MABB discs during the irradiation experiment.

3.4.5 Need of additional results [48]

Additional results are needed in order to demonstrate the feasibility of the MABB pin concept, i.e. to achieve the predicted transmutation performance while ensuring safe and reliable operation under all circumstances. At the end of this step, this should reinforce the technological choices for the MABB fuel element concept and the reference manufacturing process for the MABB fuel will be defined.

Irradiation programme

A first series of analytical experiments (separate-effect tests) are planned on several fuel samples in available experimental reactors such as OSIRIS, HFR or JHR (soon to be commissioned). These experiments aim to study the behaviour of the MA-bearing fuel material under irradiation (helium swelling, gas releases) within the temperature range covering all normal conditions in MABB subassembly pins. Furthermore, these experiments will allow the correlations of the irradiation behaviour with the MABB manufacturing process in order to optimise the microstructure of future MABB fuel pellets for improved performance.

A second series of "semi-integral" experiments with the fuel and cladding are planned; the geometry will not necessarily be representative of the final fuel pins. These

experiments will help gain better understanding of the phenomena preventing high transmutation rates, e.g. mechanical and/or chemical interactions between the cladding and the MABB, neutron damage to the cladding, internal pin pressurisation, gas swelling during normal or incident transients, the migration of volatile and gaseous species and any oxide-cladding bond restructuring and/or formation with respect to standard Am-free fuel etc. The partial or total representativeness of the future Gen-IV SFR technology irradiation conditions is important as the phenomena coming into play depend on the fuel thermo-chemical conditions (temperature and thermal gradient profile in the fuel and the cladding). Where possible, these irradiation experiments will be performed in a fast reactor. Otherwise, they will be performed in the MTR with a device capable of screening the thermal component of the flux without overly reducing it. These types of experiments are currently being assessed for reactors such as the ATR (USA), OSIRIS and the HFR in the short term and for the future JHR in the long term.

Fuel design and modelling

The detailed pin specifications resulting from the MABB subassembly design studies and a proven, reproducible manufacturing process should both be available around 2025. To assess the thermo-mechanical behaviour of the pins (needed to design the subassemblies), a reliable modelling tool needs to be developed and validated by 2025 on the basis of feedback from the analytical and semi-integral irradiation experiments. The code reliability will be directly conditioned by the amount of knowledge collected on MABB behaviour during the irradiation experiments.

A new version of the code used to simulate the MABB fuel element behaviour under normal operating conditions will also be available. This goal requires an extensive property measurement programme, which is foreseen in the project ESFR (European project) and improvement in understanding of behaviour through irradiation results.

Normal operating conditions

Integral experiments will first be performed on full pins representing the final concept. These experiments will be conducted in the fast flux of the ASTRID prototype reactor. The pins required for the irradiation programme will be manufactured at the ALFA facility which should be commissioned in 2025.

The first tests will be performed under normal operating conditions up to an actinide fission rate, which will be very close to the nominal rate targeted in SFRs (around 15at%). The pins will be subjected to intermediate examinations, which require twice as much pins for each irradiation condition under investigation. The MABB subassembly 180° rotation at mid-life will also be reproduced for the pins which will be maintained up to a maximum burn-up. The main goal in this case will be to control the potential factors limiting the lifespan of the MABB pins. The most conservative conditions in terms of behaviour (particularly the irradiation temperature) will have to be modelled and applied during these tests.

If the transmutation of all of the MA (Am + Np + Cm) is still relevant at this time, several pellets containing Np and Cm may be inserted into the fissile columns of several pins for irradiation in this type of integral experiment. Several full MABB pins may also be loaded into a MABB bundle.

The impact of manufacturing variations in the fuel element characteristics (pellets and cladding) upon behaviour during irradiation should be quantified during this optimisation phase. The goal is to achieve the target operational values by determining all the possible margins of variation in the manufactured objects.

Incident conditions

The second tests will assess the safety and the impact of the different incident and accident transients in the core upon the MABB fuel elements. These tests may be

performed on either whole irradiated pins or pin sections reconditioned into instrumented mini-pins to be irradiated in an experimental reactor.

Fuel cycle

In the long term, studies on the manufacture, reprocessing and handling of MABB fuel pins should also make it possible to validate the technical specifications and determine any uncertainties on specific parameters.

Qualification

The qualification stage will have to:

- demonstrate the manufacturing process at an industrial scale from the fuel material through to the subassembly;
- qualify the production line to be set up;
- confirm the correct behaviour of the subassemblies under incident and accident conditions;
- demonstrate core safety;
- validate modelling up to the scale of the subassembly.

As the ASTRID prototype will be available during this phase, the subassembly qualification tests could be performed in this reactor. A fabrication facility with a greater capacity than that of the ALFA project will have to be commissioned to manufacture the whole subassemblies. An irradiation test on a whole subassembly could be performed up to operating levels exceeding the nominal conditions targeted for this technology. This would guarantee its correct operation in the specified operating range. A specific monitoring programme will have to be set up for this subassembly qualification operation.

3.4.6 Technology readiness level (TRL)

An initial assessment of the TRL on MABB led to determining how each irradiation contributes to this fuel qualification. A common evaluation of the existing results yields a TRL level of 3 on a full scale of 9 (Chapter 7).

3.5 Summary

Based on the R&D results detailed in this report, the challenge for homogeneous fuel is to perform a representative (burn-up, linear power) irradiation of a full pin and then a full subassembly. The impact on a fabrication facility (glovebox or shielding cell) should be evaluated for technological feasibility and cost evaluation. The challenges for MABB are clearly the behaviour under irradiation with the necessity to address issues identified that can affect performance. Furthermore, the impact of the high decay heat and neutron emission must be addressed for all the steps of the life in the reactor and in the fuel cycle.

3.5.1 Homogeneous fuels

The homogeneous approach is a promising route, consolidated by recent complementary programmes at SUPERFACT (Japanese and very soon, American ones as well). This transmutation mode gathers a shared interest on the international scale: because of its sufficient maturity it is easier to define future steps needed until MABF qualification. Mainly, it lacks a demonstration on the scale of a fuel pin bundle (in capsules) or on the scale of an assembly. The objective of demonstration is to prove that MA does not affect safety and economic performance.

No experiment exists yet that can allow researchers to assert that the presence of minor actinides in the fuel does not reduce the operational life time of the fuel. Furthermore, limited access of fast reactors in the world will not allow such a demonstration to be carried out for at least another ten years. In this context, Idaho National Laboratory (USA) is currently conducting a complementary programme to SUPERFACT and AM1 at the ATR thermal reactor. Its objective is to reach a higher burn-up of 15 to 20at%. The irradiation is designed to approach the conditions of an irradiation in fast flux. This experiment should provide lacking elements pertaining to clad resistance to internal corrosion and the behaviour of transmutation fuel with high burn-up.

Furthermore, the international GACID Project (Global Actinide Cycle International Demonstration) carried out within the framework of the Gen-IV International Forum aims to demonstrate transmutation in the homogeneous mode on the scale of a whole fuel pin under representative conditions followed by a complete subassembly.

Technology readiness level (TRL)

Irradiation and modelling maturity levels of the homogeneous oxide fuel are shown in Figure 3.35. Tables 7.4 and 7.5 show the fabrication process maturity and the irradiation maturity.

Figure 3.35: Irradiation and modelling maturity levels for homogeneous oxide fuel

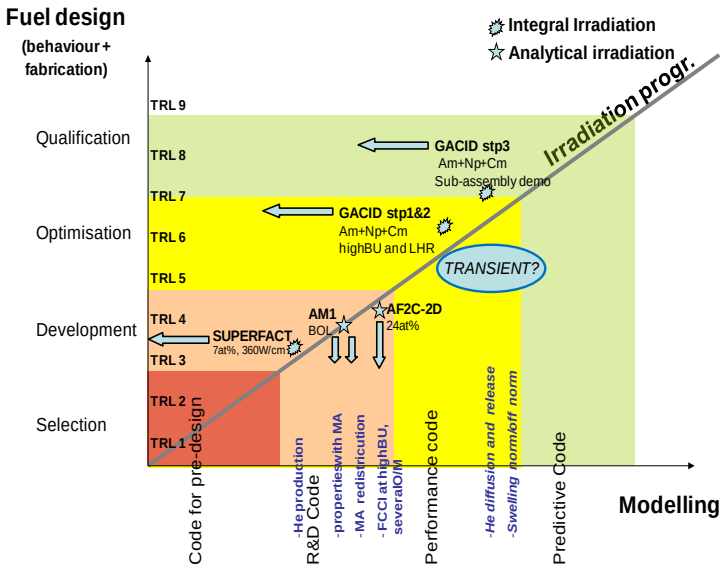

3.5.2 Heterogeneous fuels

The minor actinide-bearing blanket is at the earlier stage of design and preliminary tests. This heterogeneous fuel is expected to be a complex system, substantially different from driver fuel behaviour (He production, operating temperature) with a fuel cycle to be adapted to its very special characteristics (very high decay heat and neutron source).

An important experimental programme is needed to improve its design in the area of composition, fuel element dimensions, fabrication, properties and behaviour laws and to validate its performance. Some analytical irradiations are being prepared to give data for feasibility.

All the steps of development and optimisation are necessary to obtain some details on performances and safety impact of this transmutation approach. This R&D should

provide results to assess the design of a MABB subassembly and its management in the core and in the fuel cycle plants. In particular, it is important to examine several fuel cycle issues out of scope this report.

Technology readiness level (TRL)

Figure 3.36 shows the TRL of the heterogeneous oxide fuel. Tables 7.6 and 7.7 show the fabrication process maturity and irradiation maturity.

Figure 3.36: Irradiation and modelling maturity levels for heterogeneous oxide fuel

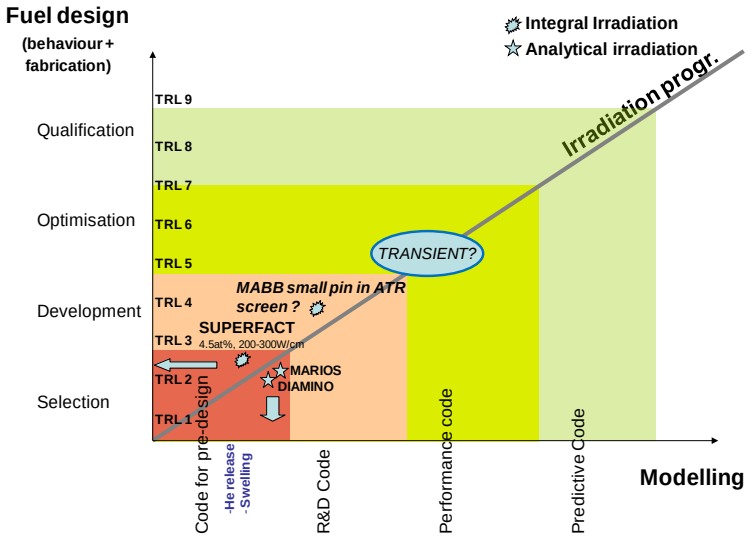

References

[1] Buiron, L., F. Varaine, D. Verrier, D. Ruah, D. Massara, D. Garzenne (2009), "Heterogeneous minor actinide transmutation on a UO_2 blanket and on (U,Pu)O_2 fuel in a sodium-cooled fast reactor – assessment of core performances", Global 2009, 6-11 September 2009, Paris, France.

[2] Varaine, F., L. Buiron, L. Boucher, D. Verrier (2010), "Overview on homogeneous and heterogeneous transmutation in a French new SFR: Reactor and fuel cycle impact". *11th International Exchange Meeting On P&T*, 7 November 2010, San Francisco, United States.

[3] Boidron, M., D. Ochem, V. Royet, L. Jerrige, P. Dehaudt, M. Puyou, F. Jorion (2009), "ALFA: Atalante Laboratory for actinides bearing fuel manufacturing" Global 2009, 6-11 September 2009, Paris, France.

[4] Grandjean, S. et al. (2009), "TRU recycling: Recent experiments and results for the conversion of minor actinides into oxide", Global 2009, 6-11 September 2009, Paris, France.

[5] Morimoto, K., M. Kato, M. Ogasawara, M. Kashimura, T. Abe (2008), "Thermal conductivities of (U,Pu,Am)O_2 solid solutions", *J. Alloys. Comp.*, 452. 54.

[6] Kato, M., T. Tamura, K. Konashi (2009), "Oxygen potentials of mixed oxide fuels for fast reactors", *J. Nucl. Mater.*, 385. 419.

[7] Kato, M. K. Konashi (2009), "Lattice parameters of (U,Pu,Am, Np)O_{2-x}", *J. Nucl. Mater.*, 385. 117.

[8] Kato, M., K. Morimoto, A. Komeno, S. Nakamichi, M. Kashimura (2009), "Experimental evaluation of Am and Np bearing mixed oxide fuel properties", *Proc. Int. Conf. International Conference on Fast Reactors and Related Fuel Cycles: Challenges and Opportunities (FR09)*, 7-11 December 2009, Kyoto, Japan.

[9] Kato, M. (2009), "Development of Np and Am bearing MOX fuels for Japan sodium cooled fast reactors", *Proc. Int. Conf. International Conference on Fast Reactors and Related Fuel Cycles: Challenges And Opportunities (FR09)*, 7-11 December 2009, Kyoto, Japan.

[10] Kato, M., K. Maeda, T. Ozawa, M. Kashimura, Y. Kihara (2011), "Physical properties and irradiation behavior analysis of Np- And Am-bearing MOX fuels", *J. Nucl. Sc. Tech.*, 484.646.

[11] Morimoto, K., M. Kato, M. Ogasawara, M. Kashimura (2009), "Thermal conductivity Of (U,Pu,Np)O_2 solid solutions", *J. Nucl. Mater.*, 389. 179.

[12] Morimoto, K., M. Kato, M. Ogasawara, M. Kashimura (2008), "Thermal conductivities of hypostoichiometric (U,Pu,Am)O_{2-X} oxide", *J. Nucl. Mater.*, 374. 378.

[13] Morimoto, K., M. Kato, A. Komeno, M. Kashimura (2007), "Evaluation of thermal conductivity of (U,Pu,Am)O_2_X", *Trans. ANS*, 97. 618.

[14] Maeda, K. et al. (2009), "Short-term irradiation behavior of minor Actinides Doped Uranium Plutonium Mixed Oxide Fuels Irradiated in an Experimental Fast Reactor", *J. Nucl. Mater.*, 385. 413.

[15] Prunier, C. et al. (1991), "Transmutation of minor actinides: Behaviour of Am and Np based fuels under irradiation", *International Conference On Fast Reactors And Related Fuel Cycles,* 28 October-1 November 1991, Kyoto, Japan.

[16] Hilton, B.A. et al. (2007), "US Plans for the next fast reactor transmutation fuels irradiation test", Global 2007, 9-13 September 2007, Boise, Idaho, United States.

[17] Prunier, C. et al. (1993), "Some specific aspects of homogeneous Am and Np based fuel transmutation through the outcomes of the SUPERFACT Experiment in Phénix", Global 1993, 12-17 September 1993, Seattle, United States.

[18] Walker, C.T., G. Nicolaou (1995), "Transmutation of neptunium and americium in a fast neutron flux: EPMA results and KORIGEN predictions for the SUPERFACT fuels", *J. Nucl. Mat.,* 218. 2.

[19] Nicolaou, G., K. Richter, L. Koch, C. Prunier (1993), "Experience with fast reactor fuels containing minor actinides: Transmutation rates and radiation doses", Global 1993, 12-17 September 1993, Seattle, United States.

[20] Tanaka, K. et al. (2009), "Microstructure and elemental distribution of americium-containing uranium plutonium mixed oxide fuel under a short term irradiation test in a fast reactor", *J. Nucl. Mater.,* 385. 407.

[21] Tanaka, K., S. Miwa, I. Sato, M. Osaka, T. Hirosawa, H. Obayashi, S. Koyama, H. Yoshimochi, K. Tanaka (2008), "Microstructural evolution and Am migration behaviour in Am-containing fuels at the initial stage of irradiation", *Proc. Int. Conf. Actinide And Fission Product Partitioning And Transmutation*, 10th Information Exchange Meeting, 6-10 October 2008, Mito-Japan.

[22] Maclean, H.J., S. L. Hayes (2007), "Irradiation of metallic and oxide fuels for actinide transmutation in the ATR", Global 2007, 9-13 September 2007, Boise, Idaho, United States.

[23] Nakashima, F., T. Mizuno, H. Nishi, L. Brunel, S. Pillon, K. Pasamehmetoglu, J. Carmack (2009), "Current status of global actinide cycle international demonstration project", *Proc. Int. Conf. Gif Symposium 2009*, 9-10 September 2009, Paris, France.

[24] Prunier, C., F. Boussard, L. Koch, M. Coquerelle (1993), "Some specific aspects of homogeneous Am and Np based fuels transmutation through the outcomes of the SUPERFACT Experiment in Phenix fast reactor", Global 1993, 12-17 September 1993, Seattle, Washington, United States.

[25] Prieur, D., A. Jankowiak, C. Leorier, N. Herlet, L. Donnet, P. Dehaudt, Jean Paul Laval, P. Blanchart (2009), "Fabrication and characterization of minor actinides bearing materials by conventional powder metallurgy process", Global 2009, 6-11 September 2009, Paris, France.

[26] Prieur, D., A. Jankowiak, C. Leorier, N. Herlet, L. Donnet, Ph. Dehaudt, J.Lechelle, Jp. Laval, Ph. Blanchart (2010), "Influence of the microstructure on the $U_{1-Y}Am_YO_{2-X}$ (Y= 0.1; 0.15) pellet macroscopic swelling", *Advances in Science and Technology*, 73.104.

[27] Vespa, M., M. Rini, J. Spino, T. Vitova, J. Somers (2012), "Fabrication and characterisation of $(U,Am)O_{2-X}$ targets", *J. Nucl. Mater.,* 421. 80.

[28] Yamashita, T., N. Nitani, T. Tsuji, H. Inagaki (1997), "Thermal expansions of NpO_2 and some other actinide dioxides", *J. Nucl. Mater.,* 245. 72.

[29] Fahey, J.A., R. P. Turcotte, T. D. Chikalla (1974), "Thermal expansion of the actinide dioxides", *Inorg. Nucl. Chem. Lett.*, 10. 459.

[30] Noe, M., J. R. Peterson (1972), "Thermal expansion coefficient of curium-248 dioxide", *Inorg. Nucl. Chem. Lett.,* 8. 897.

[31] Nishi, T., M. Takano, A. Itoh, M. Akabori, Y. Arai, K. Minato, M. Numata (2008), "Thermal conductivity of neptunium dioxide", *J. Nucl. Mater.*, 376. 78.

[32] Nishi, T., A. Itoh, K. Ichise, Y. Arai (2011), "Heat capacities and thermal conductivities of AmO_2 and $AmO_{1.5}$", *J. Nucl. Mater.*, 414. 109.

[33] Barin, I., O. Knacke (1973), *Thermochemical Properties of Inorganic Substances*, Springer, Berlin, Heidelberg, New York, United States.

[34] Yamashita, T., N. Nitani, T. Tsuji, T. Kato (1997), "Thermal expansion of neptunium-uranium mixed oxides", *J. Nucl. Mater.*, 247. 90.

[35] Carbajo, J.J., G.L. Yoder, S.G. Popov, V.K. Ivanov (2001), "A review of the thermophysical properties of MOX and UO_2 fuels", *J. Nucl. Mater.*, 299. 181.

[36] Nishi, T., M. Takano, A. Itoh, M. Akabori, Y. Arai, K. Minato, M. Numata (2008), "Thermal conductivity of AmO_{2-x}", *J. Nucl. Mater.*, 373. 295.

[37] Silva, R.J., G. Bidoglio, M. H. Rand, P. B. Robouch, H. Wanner, I. Puigdomenech (1995), *Chemical Thermodynamics*, Vol. 2, Chemical Thermodynamics of Americium, OECD/NEA, Elsevier, Amsterdam, North-Holland.

[38] Ronchi, C., M. Sheindlin, M. Musella, G.J. Hyland, (1999), "Thermal conductivity of uranium dioxide up to 2900 K from simultaneous measurement of the heat capacity and thermal diffusivity ", *J. Appl. Phys.*, 85. 776.

[39] Gibby, R.L. (1971), "The effect of plutonium content on the thermal conductivity of $(U,Pu)O_2$ solid solutions", *J. Nucl. Mater.*, 38. 163.

[40] Otobe, H., M. Akabori, K. Minato (2008), "Oxygen potential measurement of americium oxide by electromotive force method", *J. Am. Ceram. Soc.,* 91. 1981.

[41] Otobe, H., M. Akabori, Y. Arai, K. Minato (2009), "Oxygen potentials of $(Am_{0.5}Np_{0.5})O_{2x}$", *J. Am. Ceram. Soc.*, 92. 174.

[42] Otobe, H., M. Akabori, Y. Arai (2009), "Oxygen potential measurements of $Am_{0.5}Pu_{0.5}O_{2-x}$ by EMF method", *J. Nucl. Mater.*, 389. 68.

[43] Otobe, H., M. Akabori, Y. Arai (2010), "Oxygen potential measurements of $Cm_{0.09}Pu_{0.91}O_{2-x}$ by EMF method", *IOP Conf. Series: Mater. Sci. Eng.* 9. 012015.

[44] Bevan, D.J.M., J. Kordis (1964), "Mixed oxides of the type MO_2 (fluorite)-M_2O_3-I oxygen dissociation pressures and phase relationships in the system CeO_2•Ce_2O_3 at high temperatures", *J. Inorg. Nucl. Chem.*, 26. 1509.

[45] Bartscher, W., C. Sari (1983), "A thermodynamic study of the uranium-americium oxide $U_{0.5}Am_{0.5}O_{2\pm x}$", *J. Nucl. Mater.,* 118. 220.

[46] Valentin, B., H. Palancher, C. Yver, V. Garat, S. Massara (2009), "Heterogeneous minor actinide transmutation on a UO_2 blanket and on $(U,Pu)O_2$ fuel in a sodium fast reactor – preliminary design of pin and subassembly", Global 2009, 6-11 September 2009, Paris, France.

[47] Bejaoui, S., E. D'Agata, R. Hania, T. Lambert, S. Bendotti, C. Neyroud, N. Herlet, J. M. Bonnerot (2011), "Americium-bearing blanket separate-effect experiments: MARIOS and DIAMINO irradiations", Global 2011, Paper No. 503621, 11-16 December 2011, Makuhari, Japan.

[48] Bonnerot, J.M. et al. (2010), "Development program on minor actinides bearing blankets at CEA", 11th Information Exchange Meeting, 1-4 November 2010, San Francisco, United States.

4. Nitride fuels

4.1 Introduction

Nitride fuels contain numerous advantages when compared to the more familiar oxide fuels and other forms possessing a high fissile density such as carbides. The form most consistently investigated historically is uranium mononitride (UN), but plutonium nitride and mixed variants continue to be explored. The principle advantages of these systems include a high melting point comparable to the oxide and significantly enhanced thermal conductivity nearing the range of metallic fuels. Historically UN has received attention due to its high fissile density and relief from swelling problems encountered by carbide fuels, but recent interest has been dominated by its potential as a transmutation matrix fuel. Foremost, nitrides support a hard spectrum as required for efficient actinide fission. Both UN and PuN offer the additional advantage of nearly complete miscibility with the actinide nitrides, greatly relaxing a number of fabrication and operational concerns that exist in oxide and metallic fuel forms.

In Japan, progress is underway in the study of the nitride fuel forms with a high content of minor actinides (e.g. Np, Am, and Cm) as well as exploration of the physical properties of the various individual actinide nitride forms and their solid solutions. The aim of this work is to develop a fuel form suitable for an accelerator driven system (ADS) for efficient transmutation of minor actinides (MA). This concept focuses on use of a pyrochemical process to treat spent fuel. One of the major advantages in this process is that ^{15}N can be readily recovered and recycled. Nitrogen enrichment is a necessary and significant consideration in design of a fuel cycle incorporating nitrides. Neutron capture in ^{14}N produces ^{14}C; the neutron capture will result in deterioration of the neutron economy in a reactor and the presence of ^{14}C will be detrimental to reprocessing given its radioactivity. The cost of supplying fresh ^{15}N will be prohibitive when fabricating pellets in large scales and thus recycling efforts will be required.

Interest in the United States has been along a similar vein. Research has been devoted to mixed nitrides with an emphasis on developing fabrication routes as well as conducting test irradiations to establish property-burn-up correlations. In addition to recent examination of both transmutation fuels and targets for accelerator driven systems (ADS) or fast reactors, the high fissile density of UN and reasonable stability during burnup prompted its selection as the reference fuel for a number of space reactor studies in 1980s and 2000s. Most US programmes focus on fabrication studies performed to facilitate inclusion of Pu in conjunction with MA to construct a mixed nitride form. Experience has revealed that plutonium significantly complicates nitride fuels fabrication compared to uranium alone. Inclusion of Am has been found to dictate the sintering temperature ceiling as volatilisation becomes a important concern. A number of current and recently concluded reactor irradiations of both fertile and non-fertile matrix nitride forms containing MA will be analysed in the coming years and will substantially increase the existing mixed nitride property database.

Much of the early work on the development and production of nitride fuels took place at the Institute for Transuranium Elements (ITU) and at Los Alamos National Laboratory (LANL). More recently, the Japan Atomic Energy Agency (JAEA) has done extensive studies of nitride compositions for transmutation. Much of the work done at ITU on the

development of fabrication routes is described in this chapter, including the refinement of the carbothermic reduction process, in particular.

4.2 Fabrication techniques

Two primary fabrication routes for MA bearing nitride fuels are available. Their comparative attractiveness must be weighed with respect to their position within a larger fuel cycle, specifically the reprocessing method in use. The first is carbothermic reduction of oxides partitioned by an aqueous process. The second is nitridation-distillation of actinide metals recovered in a liquid cadmium cathode through a pyrochemical process. Two process variants exist in the former: carbothermic reduction and cold press/sinter methods, and sol-gel and infiltration methods.

4.2.1. Carbothermic reduction and cold press/sinter methods

Production of nitride fuels through carbothermic reduction is the most common method of fabrication. In the carbothermic reduction method, the base oxides are mixed with graphite and then compacted and heated in flowing nitrogen to obtain nitrides. The initial carbon-to-metal ratio is usually chosen to be 20-30% above the stoichiometric quantity to ensure complete absence of oxides in the final form. The carbothermic reduction heating is done at 1 573-1 773 K. During sintering, carbon monoxide is released as a product of the free carbon and the oxygen in the source material. Once the reaction has gone to practical completion (monitored either through a spectrometer during bench-top work or through process time controls in industrial fabrication), the gas flow is switched to a reducing atmosphere (i.e. N_2-H_2) and the temperature elevated to eliminate remaining free carbon. Figure 4.1 shows an example carbon monoxide release curve during the carbothermic reduction of oxides to obtain the nitride.

The resulting pellets are generally of good quality but obtaining good density can be problematic given the thermodynamic complexity of the process. Past and ongoing research efforts have favoured carbothermic reduction to produce material both for direct characterisation and irradiation studies. JAEA has supported synthesis of a wide range of individual actinide nitrides (UN, NpN, PuN, and AmN) [2-5], binary forms ((U,Pu)N, (U,Np)N, (Np,Pu)N, (Np,Am)N, (Pu,Am)N, and (Cm,Pu)N) [6-9], and ternary and quaternary ((Pu,Am,Cm)N and (Np,Pu,Am,Cm)N [10] nitride forms for various studies. Several kinds of minor actinide nitrides with inert matrix materials such as ZrN and TiN have also been produced through carbothermic reduction in Japan. Similar studies have been performed in the U.S. at LANL using similar methods [11,12].

Figure 4.1: Typical CO release curve during carbothermic reduction of oxides-carbon mixture to obtain nitride [1]

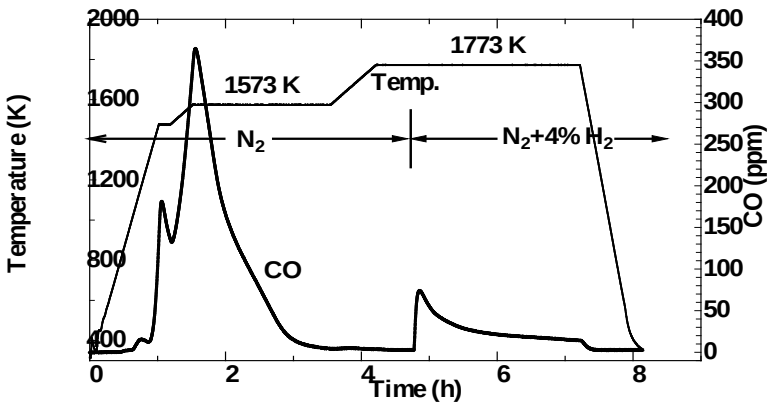

4.2.2. Sol-gel and infiltration methods

ITU has proposed and tested the combined use of sol-gel and infiltration methods for the production of MA bearing nitride fuels [13]. The process is shown schematically in Figure 4.2.

Figure 4.2: Sol-gel and infiltration routes for the production of minor actinide-bearing nitride and carbide fuels [13]

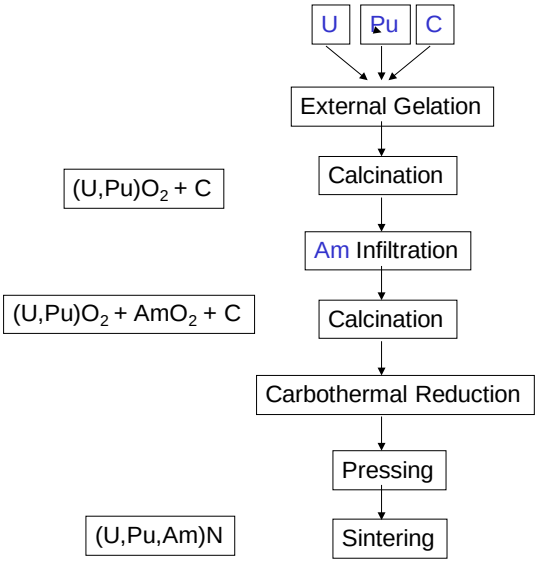

This technique originated from the actinide nitrate solution emanating from the reprocessing steps for the preparation of a feed solution containing the required stoichiometric quantity of carbon. The feed solution could be composed of uranyl nitrate or uranyl/Pu nitrate in the required quantities according to the fuel specifications. The specific composition of the solution is tailored to the fuel form; if an inert matrix fuel based on zirconium nitride is required, the solution should contain zirconyl nitrate.

This feed solution is converted to solid by means of a gelation process. External gelation requires polymer addition to the uranyl, uranyl/Pu, or zirconyl nitrate feed solution. The solution is then atomised into small droplets that are collected in an ammonia bath where a precipitation occurs to yield solid particles. The type of atomiser determines the size distribution of the particles. Following washing and drying steps, the particles are heated under argon, which causes sublimation of the polymer, leaving highly porous particles consisting of the metal oxide and the stoichiometrically equivalent ratio of carbon.

The MA nitrate solution is prepared at a concentration required to match the porosity of the beads so that the addition of the required actinide solution is equivalent in volume to that required to reach the incipient wetness point, i.e. the point at which the solid particles become fluid. A further heating step is required to transform the MA from the nitrate into the oxide. At this point in the process, the particles are constituted predominantly by the oxide of the initial metal, carbon, and the MA oxide. The latter is present in the form of small particles of the order of 1 µm in size. Ideally, subsequent carbothermic reduction causes diffusion of the MA oxide into the major oxide component to form a solid solution prior to reaction of the oxide with carbon under vacuum to give the carbide or under nitrogen gas to give the nitride.

So far, this process has been used to produce pellets of $(U_{0.8}Pu_{0.18}Am_{0.02})N$ and (Zr,Am)N. Further process optimisation is required to minimise the residual impurity

oxide, but promising results have been obtained. Translation of the product to a pellet form can prove difficult as the power character is generally poor and results in low densities (65-70% theoretically). A post-carbothermic step performed to produce better quality powder could improve the sintering response. If SPHEREPAC or VIPAC fuel pins are required, the situation is far more favourable, as particles are produced directly by sintering and no compaction step is required.

4.2.3. Nitridation-distillation method

When the pyrochemical process is applied to the nitride fuel, actinides are recovered in the liquid metal cathode. It was observed that actinides beyond their solubility limit form intermetallic cadmium compounds. This finding encouraged the research for a process to obtain actinide nitrides from the recovered actinide-Cd compounds.

The nitridation-distillation combined reaction has been developed at JAEA using Pu-Cd, U-Pu-Cd, and Am-Cd alloys. The nitridation of actinides and the distillation of Cd occurred simultaneously by heating the alloy in a nitrogen gas stream at 973K [14-16]. After the nitridation-distillation combined reaction, the formation of single phases of PuN, (U,Pu)N and AmN were confirmed. The product was then milled, pressed, and sintered to obtain a typical pellet form.

Figure 4.3: Appearances of the sample in a series of experiments: (a) (U,Pu) pellet before electrolysis, (b) liquid Cd cathode after electrolysis, (c) powder formed by the nitridation-distillation combined reaction, (d) sintered (U,Pu)N pellet prepared from the recovered powder [16]

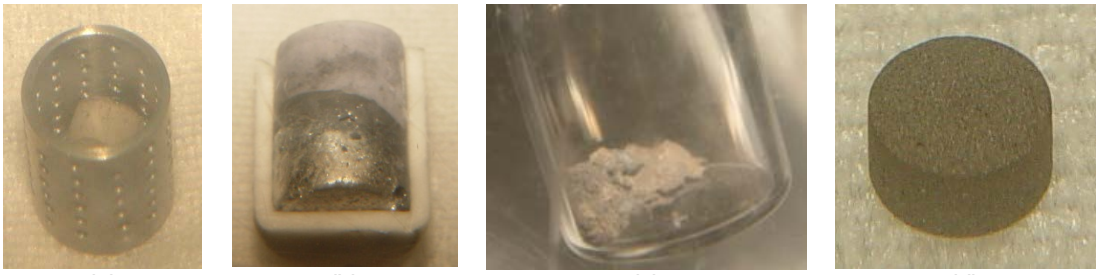

Figure 4.3 shows the appearances of (U,Pu)N at different steps of the fabrication process. According to preliminary characterisation results, the sintered pellet had an almost single phase of (U,Pu)N and density of about 84%TD. The oxygen impurity contents ranged from 0.1 to 0.2wt%. While this technique is promising, the levels of oxygen impurities in particular must be reduced for irradiation in a reactor.

4.3 Fresh fuel characterisation

Significant attention has been given in recent years to the development of novel synthesis routes for nitrides and the characterisation of the resulting product. Identification and implementation of a specific processing technique for fabrication is a critical part of programme development. Furthermore, processing may have important implications to the properties obtained in a particular fuel and it is therefore vital to catalogue fuel properties not only as a function of composition but also processing parameters. So far most efforts have been devoted to understanding fundamental thermophysical properties of nitrides as a function of their composition. Other studies are ongoing in parallel to examine more complex responses in preparation for irradiation tests of both fertile and non-fertile compositions.

4.3.1. Fundamental properties of minor actinide nitrides

To develop the MA-bearing nitride fuels, it is important to study the fundamental properties of minor actinides. The lattice parameter, thermal expansion, heat capacity, thermal conductivity, and vaporisation behaviour of minor actinide nitrides have been studied for a number of compositions.

Lattice parameter

Actinide mononitrides have the NaCl(B1)-type structure. Table 4.1 compares the lattice parameters of the actinide mononitrides, together with candidates for the inert matrix materials (ZrN and TiN).

Table 4.1: Lattice parameters of actinide mononitrides and candidates for the inert matrix materials

Nitride	Lattice parameter a_{MeN} (nm)	RLPD $(a_{MeN}-a_{PuN})/a_{PuN}$ (%)
UN	0.4888	-0.35
NpN	0.4897	-0.16
PuN	0.4905	–
AmN	0.4991	+1.8
CmN	0.5027	+2.5
ZrN	0.4576	-6.7
TiN	0.4242	-13.5

The experimental data on fission product solubilities in nitride fuel have been reviewed in [17]. The Relative Lattice Parameter Difference (RLPD) is defined by:

$$RLPD = (a_{MeN} - a_{MN}) / a_{MN},$$

where a_{MeN} and a_{MN} are the lattice parameters of solute and solvent nitrides, respectively. Complete solubility is observed for -7.5% < RLPD < +8.5%, limited solubility for -16% < RLPD < -7.5%, and solubility is negligible for RLPD < -16%.

Based on the results shown in Table 4.1, the actinide mononitrides are predicted to have complete solid solubility. X-ray diffraction (XRD) analyses of numerous mixed nitrides confirmed these predictions, revealing a single phase of NaCl-type structure to form the solid solution, as shown in Figure 4.4 [10].

Further study has emphasised work integrating possible matrix materials. Using ZrN as the inert matrix, the solid solutions of (Pu,Zr)N were obtained experimentally and examined for structure [18]. For the AmN-ZrN system, where the relative lattice parameter difference between AmN and ZrN is -8.3%, syntheses and XRD analyses of mixtures were reported [19]. The experimental results show that a single phased solid solution was obtained when the molar ratio Am/(Am+Zr) was 10%, while two solid solutions developed when the molar ratio exceeded 30%. In the case of TiN, the solubility between PuN and TiN was very small (RLPD -13.5%). The study of this system confirmed immiscibility as a composite was formed [18].

Figure 4.4: X-ray diffraction pattern of $(Np_{0.279}Pu_{0.307}Am_{0.279}Cm_{0.135})N$ [10]

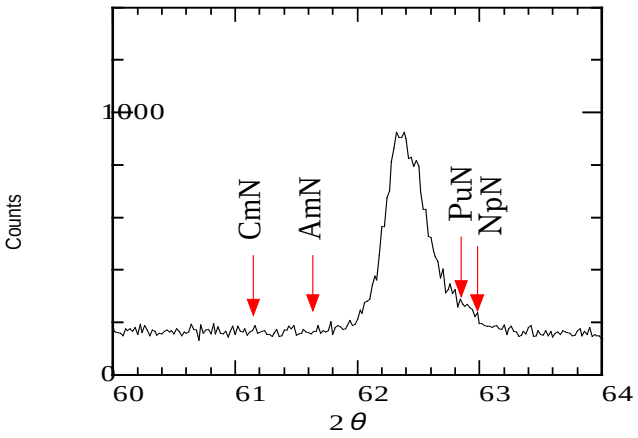

Thermal expansion

The thermal expansion of NpN, PuN and AmN [20] and the solid solutions of $(Np_{0.55}Am_{0.45})N$, $(Pu_{0.59}Am_{0.41})N$, $(Np_{0.21}Pu_{0.52}Am_{0.22}Cm_{0.05})N$, and $(Zr_{0.61}Pu_{0.21}Am_{0.18})N$ [21] were determined from the temperature dependence of the lattice parameters measured by the high-temperature XRD. The diffractometer installed in a glovebox with a purified argon gas atmosphere was used to prevent the samples from hydrolysis and/or oxidation during handling and measurements. About 20 mg of the nitride powder prepared by the carbothermic reduction of the oxide was loaded on a platinum or tungsten holder. The measurements were carried out at room temperatures up to 1 478 K.

The thermal expansions of NpN, PuN and AmN, together with that of the reported values for UN [22], are shown in Figure 4.5. The thermal expansions of AmN and PuN were found to be close to each other and larger than that of UN, whereas the thermal expansion of NpN was nearly the same as UN. For the solid solutions, the average thermal expansion coefficient for each solid solution was approximated from the values for the constituent nitrides by the linear mixture rule.

Figure 4.5: Linear thermal expansions of UN, NpN, PuN and AmN as a function of temperature [20]

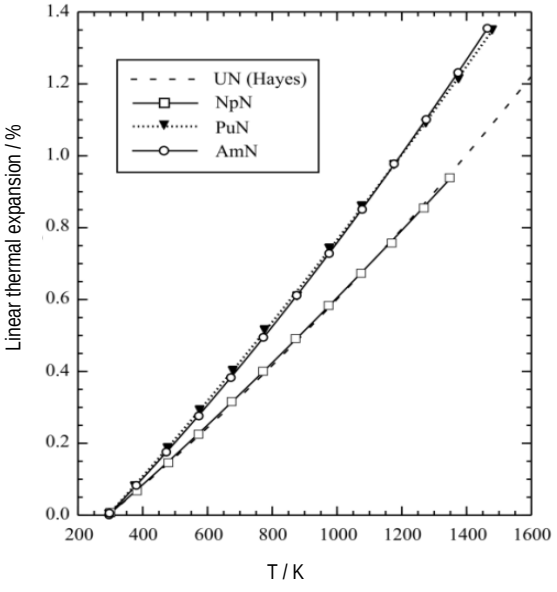

Heat capacity

The heat capacities of UN, PuN, NpN, and AmN were determined by drop calorimetry [23-26], and those of UN, PuN and NpN by differential scanning calorimetry [27]. The heat capacities of UN [24], NpN [26], PuN [25] and AmN [26] are shown in Figure 4.6. The heat capacity of AmN was found to be slightly lower than those of UN, NpN and PuN.

The heat capacities of mixed actinide nitrides of $(Np_{0.75}Am_{0.25})N$, $(Np_{0.50}Am_{0.50})N$, $(Pu_{0.75}Am_{0.25})N$ and $(Pu_{0.50}Am_{0.50})N$ were also studied by the drop calorimetry to test the validity of the Neumann-Kopp rule [8].

Figure 4.6: Heat capacities of UN, NpN, PuN and AmN as a function of temperature [26]

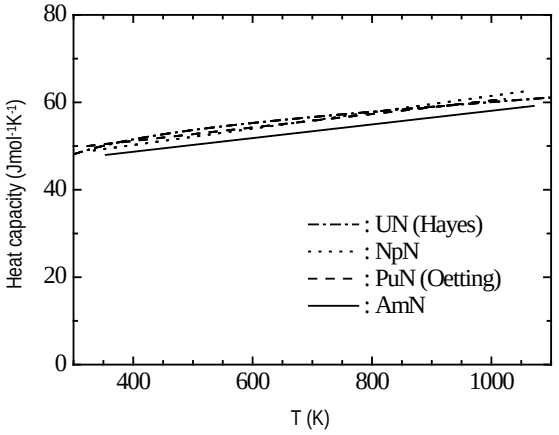

The heat capacities of mixed actinide nitrides of $(Np_{0.75}Am_{0.25})N$, $(Np_{0.50}Am_{0.50})N$, $(Pu_{0.75}Am_{0.25})N$ and $(Pu_{0.50}Am_{0.50})N$ were also studied by the drop calorimetry to test the validity of the Neumann-Kopp rule [8].

Thermal conductivity

The thermal diffusivities of UN, NpN, PuN, AmN and the solid solutions of (U,Pu)N, (U,Np)N, (Np, Pu)N, (Np, Am)N and (Pu,Am)N were measured by the laser flash method, and the thermal conductivity was calculated from the measured thermal diffusivities, bulk densities and specific heat capacities as a function of temperature [8] [28-31].

Figure 4.7 shows the thermal conductivities of UN, NpN, PuN and AmN as a function of temperature [28-30]. The thermal conductivities of the actinide nitrides gradually increase with temperature over the temperature range investigated. This behaviour is significantly different form that of oxide fuel, which shows "1/T" temperature dependence. For these nitrides, the electronic component contributes dominantly to the total thermal conductivity, and the increase in the thermal conductivity is due to the increase in the electronic component. Figure 4.7 shows that the thermal conductivities decrease with increasing atomic number from UN to AmN. This is probably due to the decrease in the electronic component contributing to the thermal conductivity. The electrical resistivity of actinide mononitride tends to increase with atomic number [31].

Vapourisation behaviour

Vapourisation behaviours of UN, NpN, PuN and the solid solutions of (U,Pu)N, (Np, Pu)N, and (Pu,Am)N were studied with Knudsen-effusion high-temperature mass-spectrometry [32-35]. It is well-known that UN vapourises incongruently precipitating liquid uranium while PuN vapourises congruently. For the vapourisation behaviour of NpN, it was found that the vapour pressure of Np(g) was similar to that of Np(g) over liquid Np metal, which

means that liquid neptunium was precipitated during the measurements from 1 630 to 2 090 K [33]. The vapour pressures of UN, NpN, and PuN increase in this order at an identical temperature [32,33].

The vapourisation behaviours of AmN and (Am, Zr)N in flowing helium gas were studied by measurement of nitrogen gas release by gas chromatography [36]. For AmN, a N_2 gas release was detected and a large weight loss was found above 1 570 K. For (Am, Zr)N, a mole fraction of Am/(Am+Zr) decreased from 0.1 to 0.03 was observed after heating, which means that selective vapourisation of AmN from (Am,Zr)N occurred. Although some experimental data are available, the vapourisation behaviour of AmN and AmN-containing nitrides still need to be clarified.

Figure 4.7: Thermal conductivities of UN, NpN, PuN and AmN as a function of temperature [30]

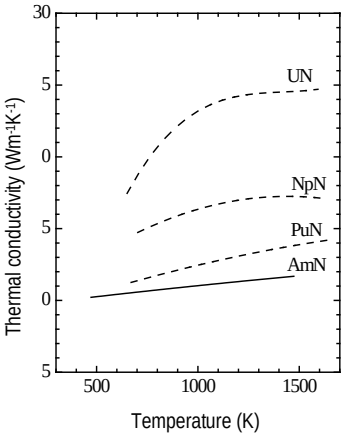

4.3.2. *Fabrication of minor actinide containing fissile nitrides*

FUTURIX-FTA irradiation

Fertile and non-fertile nitride fuel pellets for the FUTURIX-FTA irradiation were fabricated at LANL using standard cold press/sinter methods beginning with feedstock powder in oxide form [11,12]. As described in Figure 4.8, the source powders were first blended, milled, and thermally treated to produce a solid solution before undergoing carbothermic reduction. These processing steps were taken in an attempt to bind the Am in solution to minimise boil volatilisation at the final sintering temperature.

Figure 4.8: Nitride cold press and sinter process [11]

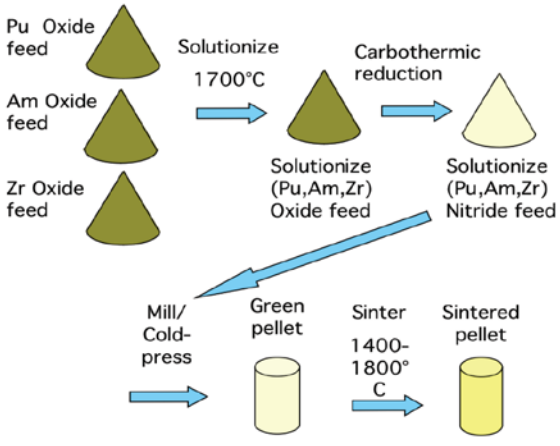

Previous actinide nitride fuel fabrication materials for the Advanced Fuel Cycle Initiative programme were used to acquire low burn-up irradiation data in the Advanced Test Reactor (ATR) and establish process parameters for the fuel designated for insertion in the FUTURIX-FTA experiment. Results show that the target porosity of 15% was a challenge for the non-fertile composition $(Pu_{0.50}Am_{0.50})N$-36ZrN, which averaged 80% theoretical. The difficulty in achieving the desired density in the non-fertile material is most likely attributed to the RLPD between ZrN and the actinide nitrides. XRD data corroborate this hypothesis, showing at least two distinct phases in the non-fertile FUTURIX-FTA composition.

The low fertile composition $(U_{0.50}Pu_{0.25}Am_{0.15}Np_{0.10})N$, was easier to fabricate. A density of 90% theoretical was readily achievable. XRD results for the low fertile material displayed a solid solution with the actinide constituents miscible in a single phase. Development work optimising the carbothermic reduction process reduced residual carbon and oxygen levels, which in both the low fertile and non-fertile compositions were below 5 000 ppm, the specified limit in the nitride fuel for the FUTURIX-FTA experiment.

One recurring problem with the fabrication of mixed nitride fuel pellets using the process described earlier was a poor out-of-pile pellet performance. End capping or degradation at the corners of the pressed pellets, in particular was observed repeatedly. Cracking of the pellets was also observed in many cases, appearing as numerous laminations, giving the pellet a layered appearance. These issues were attributed to the lack of optimisation of the feedstock powder characteristics but refinements in the powder sieving process and pressure applied during cold pressing were able to result in an acceptable product for reactor insertion. Figure 4.9 displays examples of low-fertile and non-fertile fuel pellets fabricated for AFC-1G irradiation at the ATR. Figure 4.9 shows that these pellets do not suffer from cracks and end capping evident in previous actinide nitride fabrications at LANL.

Figure 4.9: AFCI non-fertile and low-fertile nitride pellets [11]

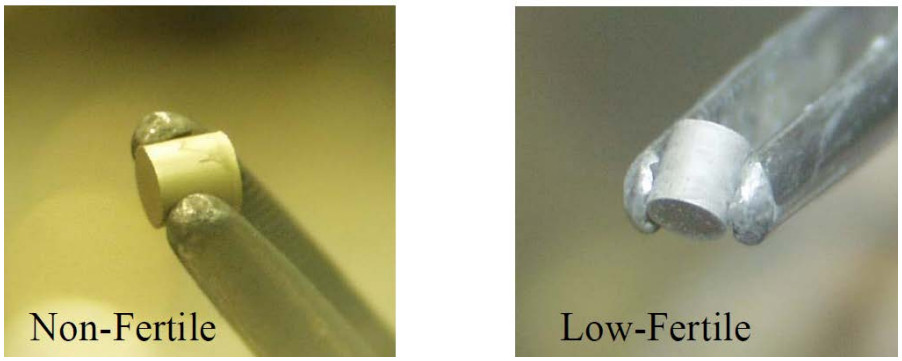

These processes are capable of producing pellets for the required irradiation programmes. However, numerous opportunities exist for increased understanding. First, the attempts to minimise Am volatilisation were only partially successful. A reduction in carbothermic reduction temperature would offer a remedy, but this must be balanced with observed effects on the pellet density and structure. Residual oxygen and carbon contents have also been greatly improved over initial efforts for the mixed nitride compositions, but increased study of the practical thermodynamic aspects of this process could push these even lower.

Adaptation of this fabrication process beyond the laboratory also presents unique challenges. The standard form for pellet irradiation is sodium bonding. This meets safety and instrumentation needs, but is problematic to apply on a large scale. Exploration and implementation of helium bonding would likely be necessary for transition to an

industrial process. Finally, exploration of the properties of fuel forms as a function of composition is a vital requirement not only for reactor operation but also to define a feedstock specification for a separation facility.

4.4 Irradiation experiments and results

The number of irradiation experiments on MA-bearing nitride fuels is limited. This situation is not unique for the nitride fuels but also for other types of fuels, such as MA-bearing oxide and metal fuels.

4.4.1. Irradiation experiment of U-free nitride fuels in JMTR

In order to understand the irradiation behaviour of U-free nitride fuel, irradiation testing of (Pu,Zr)N and PuN+TiN fuels was carried out by JAEA. One short fuel pin containing (Pu,Zr)N and PuN+TiN pellets was fabricated and irradiated at the Japan Materials Testing Reactor (JMTR). In this case, Pu content in each pellet was adjusted at 20wt%. A structure of fuel pin is shown in Figure 4.10 [37].

Figure 4.10: Structure of U-free nitride fuel pin containing (Pu,Zr)N and PuN+TiN pellets [37]

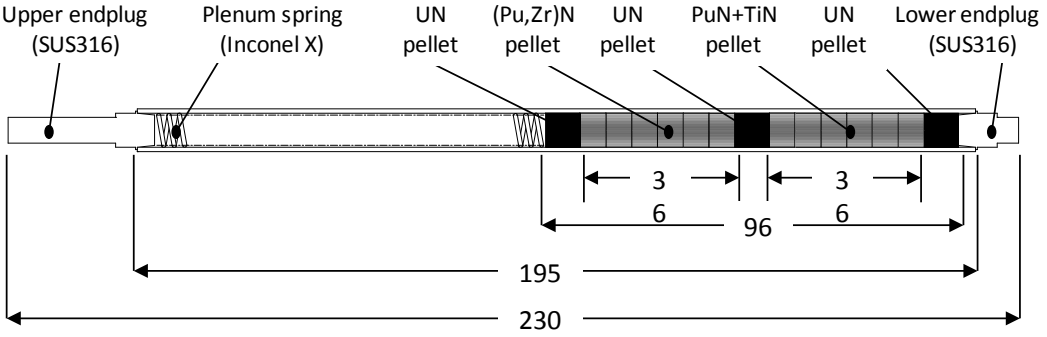

The average linear power was about 408 and 355W/cm for (Pu,Zr)N and PuN+TiN fuel. The attained burn-up of (Pu,Zr)N and PuN+TiN fuel was evaluated at 132 000MWd/t(Pu) and 153 000MWd/t(Pu), or 14.7at%(Pu) and 17.0at%(Pu), respectively. Because of a relatively low linear power and a high thermal conductivity of the fuel derived from the addition of ZrN or TiN, the maximum fuel temperature was estimated at lower than 1 273 K. So the "cold fuel" concept would be attained in the present irradiation test.

Post-irradiation examination (PIE) was carried out in the hot cells of the Reactor Fuel Examination Facility (RFEF) at JAEA. As for non-destructive PIE, appearance examination, weight and dimension measurements, X-ray radiography, profilometry, and gamma scanning of the fuel pin were carried out. As for destructive PIE, density and porosity measurements, metallography, micro-gamma scanning, alpha- and beta/gamma-autoradiography, X-ray diffraction and electron probe microanalyses of the pellets were carried out in addition to pin puncture test.

Although the attained burn-up was low and MA elements were not included in the present U-free nitride fuel, no detrimental behaviour has been observed by the addition of ZrN and TiN under the irradiation condition.

4.4.2. Irradiation experiment AFC

Two nitride irradiation experiments have been completed at the Advanced Test Reactor in the United States. The first, designated AFC-1AE, contained a total of six compositions: three non-fertile and three fertile MA-bearing mixed nitride compositions are described in Section 4.3.2. The second, AFC-1F, is an identical experiment designated to remain in

the reactor longer to obtain higher burn-ups with a maximum of 30%. The densities obtained in fabrication of these pellets were lower than desired, ranging from 78-88% theoretical. The AFC-1AE experiment contained three burn-up positions, allowing for three data points with a peak of 6-8at%. The rodlet linear power density was 330 W/cm and the calculated nominal fuel temperature during irradiation was 1 673 K. The rodlet dimensions are shown in Figure 4.11 below.

Upon removal from the reactor, each capsule will be evaluated through visual inspection and neutron radiography. The capsules will be punctured to measure the internal gas pressure and collect gas samples for radiochemistry analysis. After unloading, the rodlets will be visually inspected and measured to quantify any dimensional changes experienced during irradiation. The rodlets will then be subjected to neutron radiography and gamma spectroscopy. Finally, the pellets will be sectioned and examined using optical and SEM techniques to evaluated microstructural or chemical evolutions under irradiation. PIE is ongoing in the case of AFC-1AE and AFC-1F (as planned in 2011).

Figure 4.11: Structure and dimensions [cm] of rodlet containing MA-bearing mixed nitride fuel irradiated in AFC-1AE and AFC-1F

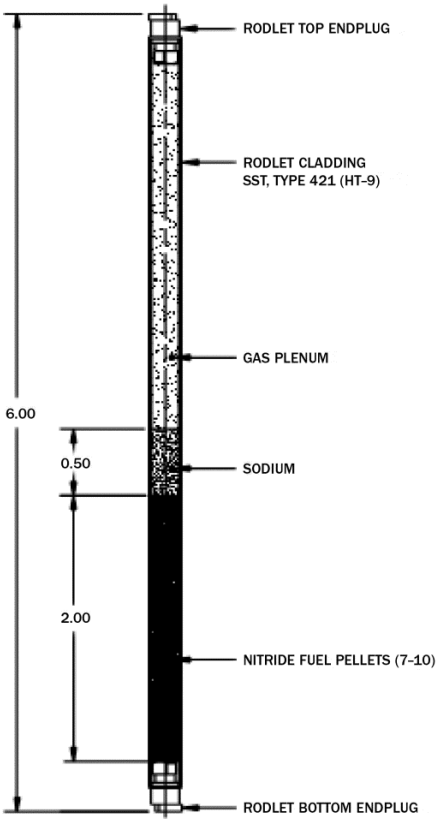

4.4.3. Irradiation experiment FUTURIX-FTA

Production of MA-bearing mixed nitride fuel pellets using the same techniques described above has also been performed at LANL for inclusion in the FUTRIX-FTA irradiation in the Phénix reactor in France. The aim of this programme is to explore the performance of the same fuel composition explored in AFC-1F, but under a fast spectrum. The irradiation has concluded and fuel rods are awaiting transport back to the United States for PIE. The parameters of study will match those described above.

4.5 Modelling activities for nitride fuels

An equilibrium chemistry model has been written for the nitride fuel pin with modelling code NITRAF [38]. The initial fuel composition was one mole of the U,Pu mononitride comprising small amounts of the minor actinides, $(U_{0.45}Pu_{0.45}Np_{0.04}Am_{0.04}Cm_{0.02})N$, and the chemical state was calculated after 20at% burn-up and for a range of temperatures. Clad components Fe, Cr and Ni were also included as input species in the ratio appropriate to 316 stainless-steel and the fill gas of the pin was assumed to be inert.

Figure 4.12: Variation of mononitride fuel composition with temperature [38]

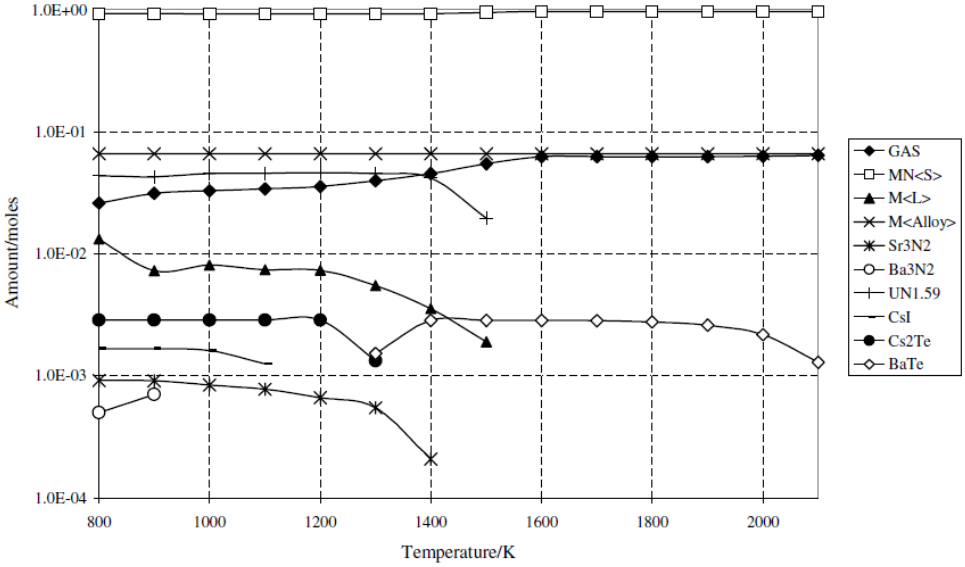

The results of the equilibrium chemistry calculations for temperatures between 800 and 2 100 K are shown in Figure 4.12 [38]. The main condensed phase formed is the fuel solid solution MN that comprises U,Pu, and the minor actinides, and the dissolved fission products Ce, La and Zr. The concentration of uranium in the MN phase changes due to the formation of $UN_{1.59}$ (i.e. the uranium sesquinitride) at lower temperatures. The sesquinitride is stable up to ~1 673 K. Above this temperature only the mononitride is stable. The formation of other nitride compounds of the fission products is limited for the reducing conditions of the nitride fuel; both Sr_3N_2 and Ba_3N_2 are stable only at low temperatures (<1 473 and <1 073 K, respectively). Strontium nitride dissociates to form the metal phase which is stable up to ~1 800 K and at higher temperatures gaseous species of Sr are formed (e.g. Sr(g) and SrI(g)). Similar behaviour occurs in the case of the barium nitride phase, although the calculations predict the formation of the BaTe phase at high temperatures. Molybdenum and ruthenium remain as the metal phase under these conditions. The more volatile fission products Cs, I and Te occur as stable condensed phase species, Cs_2Te and CsI, up to ~1 400 K and form gaseous species at higher temperatures. The gas phase is dominated by N_2, Xe, Cs, Te, I, Sr and Ba species. These results are consistent with the observations of the chemical state of irradiated and simulant nitride fuel [39] and the calculations performed by Schram and Konings [40]. No clad nitrides are predicted to form.

Similar calculations performed on fuel without UN initially present have also been performed (U-free fuel). In this case, the excess nitrogen formed during irradiation is not consumed by the formation of the sesquinitride at low temperatures and clad nitrides are predicted to form (e.g. CrN). At high temperatures (>1 200 K), these phases are unstable and the excess nitrogen is released to the pin plenum.

4.6 Safety behaviour of nitride fuels

The advantage of improved thermal conductivity couple with nitride fuel's high melting point is to offer first a lower centerline temperature that retains an excellent margin of safety during operation. In addition, this capacity could be directed towards higher fissile actinide contents in the fuel. Safety behaviours concerning the fuel specific matters, such as the limited thermal stability of AmN and the core performance of ADS with minor actinide-based fuel have been discussed in detail in [41].

The main concern is the limited thermal stability of AmN and the high vapour pressure of Am. Americium redistribution in the fuel can be expected during irradiation, especially in the case of high linear power and high radial or axial thermal gradient. ZrN was early suggested as the best adjuvant to improve the nitride stability, considering neutronics and thermophysical properties. In addition, it crystallises in a cubic lattice, which corresponds with the lattice of plutonium nitride so that solid solution is formed with MA nitrides. Heating AmN and (Am,Zr)N in helium atmosphere revealed that the dissociation of AmN starts at ~1 573 K, and selective vapourisation of Am in (Am,Zr)N occurred at higher temperatures [36]. The use of sodium bonding in the pin could be an interesting design solution to limit the fuel operation temperature and therefore the volatilisation and redistribution risk, but this solution complicates the fabrication and reprocessing processes.

As the core physics of the ADS with minor actinide-based fuel is different from that of traditional fast reactors, different performance and safety criteria will apply. When designing the ADS, a special concern is that a source transient will lead to a similar increase in core power. Since temperature feedback has a very small effect in deeply subcritical systems, the fuel must be able to cope with larger overpowered insertions than is the case for critical reactors. In the design studies made in the CONFIRM and FUTURE projects, it was required that the fuel should be able to survive a 50% transient overpower at the beginning of life (BOL), roughly corresponding to a ratio between operational and maximum allowable linear power equal to 2/3 [41].

It should be noted that in a closed fuel pin, possible dissociation of AmN is suppressed by the build-up of nitrogen gas pressure. The pressure of americium vapour in an intact pin should be negligible up to temperatures of 2 200 K [42]. This allows the design of the ADS core with He-bonded fuel and an average linear power of 35 kW/m. The maximum temperature in the hottest pellet during normal operation then does not exceed 1 600 K.

In the CONFIRM and FUTURE projects, ~800 MW(thermal) cores have been studied, the total power being limited by the heat possible to be deposited in the spallation target at the minimum reactivity level (k ~0.95). Simulations of unprotected 50% overpower transient showed that the nitride fuel temperature for the adopted geometry remained below 2 000 K, ensuring that no fuel damage occurs even under the worst possible conditions [42]. In the case of clad rupture, a more detailed study would be required.

4.7 Technology readiness levels and need of additional research

R&D on MA nitride fuel was still classified at the basic level though a significant progress was recognised. More progress and experimental studies are needed on the laboratory scale. Development of economical Nitrogen-15 enrichment as well as recycling processes and measures against heavy decay heat are also essential. On the other hand, the fundamental study on He behaviour in MA-bearing fuel is important not only for MA nitride fuel but also for the other fuel concepts for transmutation of MA.

Irradiation and modelling maturity level for nitrides fuels are shown in Table 4.13 below. The Technological Readiness Level (TRL) of nitride fuels is described in Chapter 7. Tables 7.8 and 7.9 show the fabrication process maturity and irradiation maturity.

Figure 4.13: Irradiation and modelling maturity levels for nitride fuels

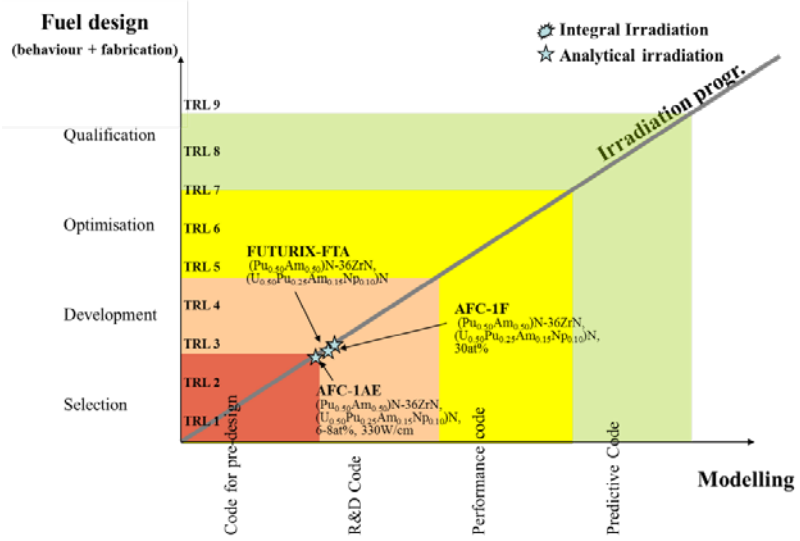

References

[1] Akabori, M., M. Takano, T. Nishi, A. Itoh, K. Minato (2005), "Development of nitride fuels for transmutation of minor actinides", Global 2005, 9-13 October 2005, Tsukuba, Japan.

[2] Arai, Y., S. Fukushima, K. Shiozawa, M. Handa (1989), "Fabrication of (U,Pu)N fuel pellets", *J. Nucl. Mater.*, 168. 280.

[3] Suzuki, Y., Y. Arai, Y. Okamoto, T. Ohmichi (1994), "Preparation of neptunium mononitride by carbothermic reduction", *J. Nucl. Sci. Technol.*, 31. 677.

[4] Arai, Y., Y. Suzuki and M. Handa (1995), "Research on actinide mononitride fuel", *Proc.* Global 1995, 11-14 September 1995, Versailles, France, 1. 538.

[5] Takano, M., A. Itoh, M. Akabori, T. Ogawa, S. Kikkawa and H. Okamoto (1999), "Synthesis of americium mononitride by carbothermic reduction method", Global 1999, Jackson Hole, Wyoming, 29 August-3 September, 1999, CD-ROM.

[6] Arai, Y., T. Iwai, K. Nakajima, Y. Suzuki (1997), "Recent progress of nitride fuel development in JAERI: Fuel property, irradiation behavior and application to dry reprocessing", Global 1997, 5-10 October 1997, Yokohama, Japan, 1. 664.

[7] Suzuki, Y., T. Ogawa, Y. Arai, T. Mukaiyama (1999), "Recent progress of research on nitride fuel cycle in JAERI", *Proc. 5th Information Exchange Meeting on Actinide and Fission Product P&T*, Mol, 25-27 November 1998, 213.

[8] Nishi, T., M. Takano, A. Itoh, S. Miyata, M. Akabori, Y. Arai, K. Minato (2010), "Thermal conductivities of (Np,Am)N and (Pu,Am)N solid solutions", *IOP Conf. Series: Materials Science and Engineering*, 9.012017.

[9] Takano, M., A. Itoh, M. Akabori, T. Ogawa, M. Numata, H. Okamoto (2001), "Carbothermic synthesis of (Cm,Pu)N", *J. Nucl. Mater.*, 294. 24.

[10] Minato, K., M. Takano, H. Otobe, T. Nishi, M. Akabori, Y. Arai (2009), "Thermochemical and thermophysical properties of minor actinide compounds", *J. Nucl. Mater.*, 389. 23.

[11] Voit, S.L., K. J. Mcclellan, C.R. Stanek, J.T. Dunwoody, T. Hartmann, S.A. Maloy, S.P. Willson, G.E. Egeland, R.W. Margevicius, H.T. Hawkins (2005), "The design and production of nitride fuels for the AFCI Program", Global 2005, 9-13 October 2005, Tsukuba, Japan, Paper No. 489.

[12] Donnet, L., F. Jorion, N. Drin, S. L. Hayes, J.R. Kennedy, K. Pasamehmetoglu, S.L. Voit, D. Haas, A. Fernandez (2005), "The FUTURIX-FTA Experiment in Phenix: Status of fuel fabrication", Global 2005, 9-13 October 2005, Tsukuba, Japan, Paper No. 258.

[13] Somers, J., private communication.

[14] Arai, Y., T. Iwai, M. Akabori, K. Minato (2008), "Synthesis of actinide nitrides in molten cadmium", *Nucl. Technol.*, 162. 244.

[15] Hayashi, H., H. Shibata, M. Akabori, Y. Arai, K. Minato (2009), "Electrolysis of AmN in LiCl-KCl eutectic melts and renitridation of Am recovered in liquid Cd cathode", *Electrochemistry*, 77. 673.

[16] Arai, Y., M. Akabori, K. Minato (2010), "Development of nitride fuel and pyrochemical process for transmutation of minor actinides", *Proc. of 10th Information Exchange Meeting on Actinide and Fission Product Partitioning and Transmutation*, 6-10 October 2008, Mito, Japan, 189-197.

[17] Benedict, U. (1980), "Solid solubility of fission product and other transition elements in carbides and nitrides of uranium and plutonium", *Thermodynamics of Nuclear Materials* (IAEA, 1980), 453-470.

[18] Arai, Y., K. Nakajima (2000), "Preparation and characterization of PuN pellets containing ZrN and TiN", *J. Nucl. Mater.*, 281. 244.

[19] Itoh, A., M. Akabori, M. Takano, T. Ogawa, M. Numata, F. Itonaga (2002), "Fabrication of americium-based nitrides by carbothermic reduction method", *J. Nucl. Sci.Technol.*, Suppl. 3.737.

[20] Takano, M., M. Akabori, Y. Arai, K. Minato (2008), "Lattice thermal expansions of NpN, PuN and AmN", *J. Nucl. Mater.*, 376. 114.

[21] Takano, M., M. Akabori, Y. Arai, K. Minato (2009), "Thermal expansion of TRU nitride solid solutions as fuel materials for transmutation of minor actinides", *J. Nucl. Mater.,* 389. 89.

[22] Hayes, S.L., J. K. Thomas, K. L. Peddicord (1990), "Material property correlations for uranium mononitride I. Physical Properties", *J. Nucl. Mater.*, 171. 262.

[23] Oetting, F.L., J. M. Leitnaker (1972), "The Chemical Thermodynamic Properties of Nuclear Materials I: Uranium Mononitride", *J. Chem. Thermodynam.*, 4. 199.

[24] Hayes, S.L., J. K. Thomas, K. L. Peddicord (1990), "Material Property Correlations for Uranium Mononitride IV: Thermodynamic Properties", *J. Nucl. Mater.*, 171. 300.

[25] Oetting F.L. (1978), "The Chemical Thermodynamic Properties of Nuclear Materials III: Plutonium Mononitride", *J. Chem. Thermodynamics*, 10. 941.

[26] Nishi, T., A. Itoh, M. Takano, M. Numata, M. Akabori, Y. Arai, K. Minato (2008), "Heat capacities of NpN and AmN", *J. Nucl. Mater.*, 377. 467.

[27] Nakajima, K., Y. Arai (2002), "Heat capacity of neptunium mononitride", *J. Nucl. Sci. Technol.,* Suppl. 3. 620.

[28] Arai, Y., Y. Suzuki, T. Iwai, T. Ohmichi (1992), "Dependence of the thermal conductivity of (U,Pu) N on porosity and plutonium content", *J. Nucl. Mater.*, 195. 37-42.

[29] Arai, Y., Y. Okamoto, Y. Suzuki (1994) "Thermal conductivity of neptunium mononitride from 740 to 1 600 K", *J. Nucl. Mater.*, 211. 248.

[30] Nishi, T., M. Takano, A. Itoh, M. Akabori, K. Minato, M. Kizaki (2006), "Thermal diffusivity of americium mononitride from 373 to 1 473 K", *J. Nucl. Mater.*, 355. 114.

[31] Arai, Y., K. Nakajima, Y. Suzuki (1998), "Thermal conductivity of actinide mononitride solid solutions", *J. Alloys Comp.*, 271-273. 602.

[32] Suzuki, Y., A. Maeda, Y. Arai, T. Ohmichi (1992), "Vaporization behavior of uranium-plutonium mixed nitride", *J. Nucl. Mater.*, 188. 239.

[33] Nakajima, K., Y. Arai, Y. Suzuki (1997), "Vaporization behavior of neptunium mononitride" *J. Nucl. Mater.*, 247. 33.

[34] Nakajima, K., Y. Arai, Y. Suzuki (1998), "Vaporization behavior of (Np, Pu)N", *J. Alloys Comp.,* 271-273. 666.

[35] Ogawa, T., T. Ohmichi, A. Maeda, Y. Arai, Y. Suzuki (1995), "Vaporization behaviour of (Pu,Am)N", *J. Alloys Comp.*, 224. 55.

[36] Takano, M., A. Itoh, M. Akabori, K. Minato, M. Numata (2003), "Study on the stability of AmN and (Am,Zr)N", Global 2003, New Orleans, Louisiana, 16-20 November 2003, CD-ROM, 2285.

[37] Arai, Y., M. Akabori,K. Minato (2007), "Progress of nitride fuel cycle research for transmutation of minor actinides", Global 2007, 9-13 September 2007, Boise, Idaho, CD-ROM, 980.

[38] Thetford, R., M. Mignanelli (2003), "The chemistry and physics of modelling nitride fuels for transmutation", *J. Nucl. Mater.*, 320. 44.

[39] Matzke, Hj. (1986), *Science of Advanced LMFBR Fuels*, Amsterdam, North Holland.

[40] Schram, R.P.C., R.J.M. Konings (1996), "Chemical form of fission products in high burnup fuels", *Proc. Technical Committee Meeting on Advances in Pellet Technology for Improved Performance at High Burn-up,* Tokyo, IAEA-TECDOC-1036. 245.

[41] Pillon, S., J. Wallenius (2006), "Oxide and nitride TRU fuels: Lessons drawn from the CONFIRM and FUTURE Projects of the 5th European Framework Program", *Nucl. Sci. Eng.*, 153. 245.

[42] Eriksson, M., J. Wallenius, M. Jolkkonen, J. E. Cahalan (2005), "Inherent safety of fuels for accelerator-driven systems", *Nucl. Technol.*, 151. 314.

5. Dispersion fuels

5.1 Introduction and generalities

With the focus on Pu and minor actinide stockpile reduction strategies, prevalent in the mid 1990s, a concept was developed to increase their transmutation rate. Namely, the fertile component (^{238}U), normally used as a fuel matrix, was removed from the fuel and replaced by a neutrononically inert matrix, and thus were named inert matrix fuels (IMF). The matrix itself serves to dilute the transuranium material, so that acceptable power levels and fuel operating temperatures can be reached. A number of materials were proposed. Most were oxides (e.g. magnesium aluminate spinel ($MgAl_2O_4$), yttrium stabilised zirconia ($(Zr,Y)O_2$)). Other materials considered were zirconium and titanium nitrides (see Chapter 4), SiC and various metals (Mo, Cr, V). Apart from their neutronic inertness, these materials should possess specific properties, consistent with in-pile reactor performance. The swelling being due to neutron, irradiation should be low and their thermal conductivities should be at least as high as UO_2. In addition, their mechanical properties should not induce unacceptable strains when in contact with cladding materials. Furthermore, the inert matrix materials should neither react with the fuel, the cladding material nor the reactor coolant (e.g. Na, Pb, or Pb/Bi). They should be readily available and pose no economic penalty.

Concerning their interaction with the fissile phase, the inert matrix should not form a low-temperature eutectic compound with a low melting point, or a non-cubic crystallographic structure. Indeed, their interaction with the actinide phase is a design criterion. Yttrium stabilised zirconia (YSZ) has the same crystallographic structure as actinide dioxides, enabling their incorporation into the crystal lattice to form a solid solution, i.e. a single ceramic (CER) phase is obtained. In contrast, the fuel or target can be designed as a composite in order to tailor its properties. Dispersion of the (mixed) actinide oxide in a second material with a higher thermal conductivity is a convenient means to increase the overall thermal conductivity of the sample. Ceramic-ceramic (CERCER) and Ceramic-metal (CERMET) configurations have been studied.

For composite fuels, the size of the fissile bearing particles can be chosen to optimise the material behaviour during irradiation. While the fissile component will be subjected to significant neutron, fission product and α-recoil damage, the matrix itself will only be affected by neutron irradiation. A thin shell (~12 μm) around the fissile particle will be subjected to damage due to fission (see Figure 5.1). For a given volume fraction (%vol), the proportion of the matrix represented by this shell varies dramatically with the particle size (see Figure 5.2). For large particle sizes (e.g. macrodispersion), the majority of the matrix is only affected by the less harmful neutron damage. In contrast, composites with small particles (i.e. microdispersions) result in near complete matrix damage approaching that of the most extreme microdispersion, i.e. that of the solid solution.

For minor actinide transmutation, only the compositions shown in Table 5.1 have been irradiated. These will be discussed in the following sections, along with the few other compounds that have been prepared for characterisation purposes.

Figure 5.1: Radiation damage around a fissile particle (1) embedded in a matrix

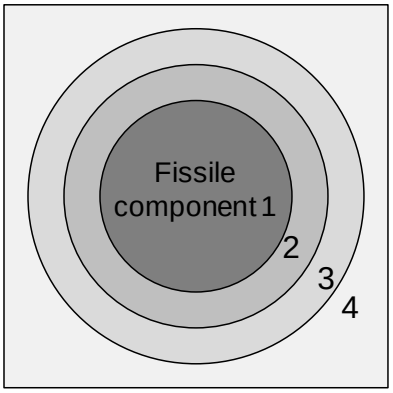

Shells (2) and (3) are at 5 µm (recoil of fission products and energetic alpha particles) and 13 µm (alpha particles with the matrix, while region (4) subject to neutron damage only.

Figure 5.2: Volume damage of the matrix as a function of diameter and fractional volume of the fissile phase in a composite fuel

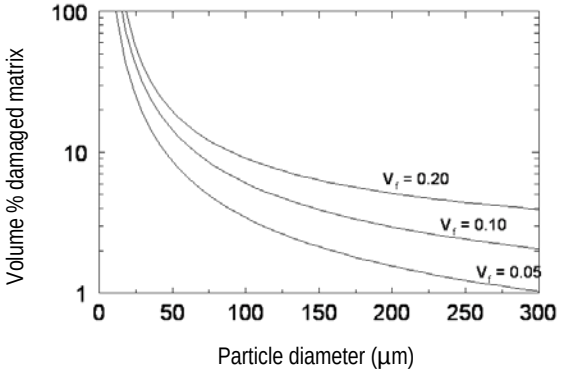

5.1.1 *The EFTTRA-T4 irradiation programme*

The EFTTRA-T4 experiment was launched by the EFTTRA (Experimental Feasibility of Targets for TRAnsmutation) partners (CEA, JRC, NRG, FzK (now KIT), EdF) in the mid-1990s. It was the first irradiation test on an inert matrix material bearing Am oxide as a target. The selected matrix was magnesium aluminate spinel ($MgAl_2O_4$), which was selected on the basis of its low neutron cross-section, its acceptable thermal conductivity, moderate melting point, and the lack of interaction with cladding and coolant (Na). In all, two pins were irradiated at the HFR Petten at different burn-ups, and PIE was made at JRC-ITU and NRG. A full account of these experiments is provided in [11,12,19,20,22].

5.1.2 *The ECRIX irradiation programme*

Within the inert matrix fuel (IMF) concept, the choice of fuel matrix is not only dependent on the irradiation feasibility, but also on the transmutation strategy. Highly insoluble matrices, such as magnesium aluminate spinel or zirconia, are ideally suited to "Once Through and Then Out (OTTO)" strategies, whereby a single irradiation to ultra-high burn-up is followed by direct geological disposal. Achievement of such high burn-ups is problematic due to the long-irradiation times, and concomitant irradiation damage of fuel and its cladding material. Thus multi-recycling of the fuel must also be

considered, for which soluble matrices are required. In general, aqueous routes based on the PUREX process are advantageous. MgO is a good candidate as it is readily soluble under such conditions. It also has a higher thermal conductivity than UO_2, and a reasonably high melting point (2 850°C).

For the ECRIX irradiation tests, MgO-AmO_{2-x} fuels were fabricated and irradiated at the Phénix reactor in France. For this experiment, the fast neutrons were moderated by CaH_2 or B_4C to take advantage of higher fission cross-sections at thermal energies combined with the higher neutron flux available in the fast neutron reactor.

5.1.3 The CAMIX-COCHIX irradiation programme

Following the EFTTRA-T4 and ECRIX irradiation experiments, focus has been given to yttria stabilised zirconia, $(Zr,Y)O_2$, (or YSZ) as a matrix for transmutation. Americium dioxide readily forms a solid solution with this material, and it has also been tested in other programmes as a support matrix for Pu incineration in LWRs, a subject that has been reviewed extensively recently (see for example IAEA TECDOC 1 516). YSZ has one main disadvantage, namely its thermal conductivity, which at about 1.5 $W.m^{-1}K^{-1}$ restricts the quantity of Am that can be loaded in the fuel, without risk of excessive fuel centre line temperatures. Within this irradiation programme, tailoring of the fuel thermal conductivity by using a dispersion fuel concept was tested. The CAMIX 1 fuel pin was a solid solution of $(Zr,Y,Am)O_2$, while CAMIX 2 used a composite MgO-$(Zr,Y,Am)O_2$. In this case, the fuel particles were small enough so that the majority of the MgO matrix would be "damaged" by fission products. A final pin, COCHIX 3 had the same chemical composition as CAMIX 2, but the fissile component was embedded in large particles, so that the majority of the MgO matrix was subjected solely to damage by neutron irradiation. These materials were irradiated at the Phénix reactor in France.

5.1.4 The FUTURIX irradiation programme

The FUTURIX FTA irradiation experiment was performed in a collaborative project, with US-DOE, CEA and JRC-ITU as participants. Metal and nitride fuel experiments are described in Chapters 2 and 3. The CEA and JRC-ITU produced four fuels based on CERCER and CERMET composites (see Table 5.1). The FUTURIX FTA experiment marked a departure from earlier concepts, in which Am was the sole actinide in the target. The FUTURIX FTA CERCER and CERMET fuels contained a fissile phase (Pu) and were considered as conceptual fuels for the ADS. The MgO and Mo matrices were chosen to increase the thermal conductivity of the fuel. MgO is readily compatible with the PUREX process as it is soluble in nitric acid. Tests on Mo dissolution under the same conditions show that it can be reprocessed using known technology. As Mo has a wide range of isotopes, it should be enriched in ^{92}Mo to ensure low neutron absorption. The recovery of this material is crucial for an industrial application. The fuel fissile phase was chosen with various Pu/Am ratios in a search for the most appropriate composition to optimise Am transmutation. The irradiation test was performed at the Phénix reactor, France.

Table 5.1: Inert matrix oxide fuel irradiation programmes and their status

Fuel Form	Composition	Reactor	Programme	Status
CER	$(Zr,Y,Am)O_2$	Phénix	CAMIX	Irradiated
	$(Zr,Y,Am)O_2$	HFR Petten	HELIOS 2	Irradiated
	$(Zr,Y,Pu,Am)O_2$	HFR Petten	HELIOS 3	Irradiated
CERCER	$MgAl_2O_4 – AmAlO_3$	HFR Petten	EFTTRA T4	PIE complete
	$MgO –AmO_2$	Phénix	ECRIX- B	Irradiated
	$MgO –AmO_2$	Phénix	ECRIX- H	Irradiated
	$MgO - (Zr,Y,Am)O_2$	Phénix	COCHIX	Irradiated
	$MgO – (Pu,Am)O_2$	Phénix	FUTURIX 7	Irradiated
	$MgO – (Pu,Am)O_2$	Phénix	FUTURIX 8	Irradiated
	$MgO – Zr_2Am_2O_7$	HFR Petten	HELIOS 1	Irradiated
CERMET	$Mo – (Pu,Am)O_2$	Phénix	FUTURIX 5	Irradiated
	$Mo – (Zr,Y,Pu,Am)O_2$	Phénix	FUTURIX 6	Irradiated
	$Mo – (Pu,Am)O_2$	HFR Petten	HELIOS	Irradiated
	$Mo – (Zr,Y,Pu,Am)O_2$	HFR Petten	HELIOS	Irradiated

5.1.5 *The HELIOS irradiation programme*

The HELIOS irradiation test was performed at the HFR Petten, with distinct goals centred on the study of the behaviour of He in the fuels and the performance of various fuel forms (see test grid in Table 5.2). Zirconia based fuels (HELIOS 1, 2 and 3) were specifically designed to investigate composition and operating power variants. HELIOS 1 is a CERCER based fuel with MgO as matrix. The fissile phase is based on a pyrochlore compound ($Zr_2Am_2O_7$) atomically ordered cubic structures, with unit cell double that of the non-ordered phase. HELIOS 2 and 3 are based on conventional yttria stabilised zirconia, an atomically disordered system. The linear power of HELIOS 3 was increased by the addition of Pu to $(Zr,Y,Am)O_2$ to give $(Zr,Y,Pu,Am)O_2$. The concomitant higher operating temperature of the fuel will lead to higher He release and likely less swelling of the fuel pellets. A novel aspect of these two fuel pins is a central thermocouple inserted in annular pellets at the top of the fuel column, providing on line operational fuel temperature data. HELIOS 4 and 5 also investigate He behaviour in CERMET fuels. Mo was the selected matrix, and the chosen ceramics were low operating power $(Zr,Y,Am)O_2$ and higher operating power $(Pu,Am)O_2$ phases.

Table 5.2: HELIOS test matrix

HELIOS	Material	Am	Pu	Particle Size
		$g.cm^{-3}$	$g.cm^{-3}$	µm
1	Zr_2,Am_2O_7 - MgO	0.76		
2	Zr,Y,AmO_2	0.76		
3	Zr,Y,Pu,AmO_2	0.76	0,42	
4	Zr,Y,AmO_2 - Mo	0.76		80-100
5	Pu,AmO_2 - Mo	0.32	1.28	20-150

5.2 Fuel fabrication

5.2.1 *EFTTRA-T4*

The EFTTRA-T4 fuel was fabricated at JRC-ITU, in a predecessor laboratory of the current MA-LAB, whereby all liquid (solution) handling steps of Am were made in shielded cells, while pellet handling was made in conventional glove boxes shielded with Pb glass. The fabrication route was based on the infiltration of pellets [16], as shown in Figure 5.3. The porous pellets were prepared from a commercial powder (Baikalose S33CR, Baikowski Chemie), that had been granulated and then compacted at 390 MPa in a bi-direction press. Following a thermal (650°C) treatment step (to remove Zn stearate lubricant), the pellets had a density of 49% of the theoretical density (TD), a diameter of 6.5 mm and heights between 8 and 9 mm.

For the infiltration step, AmO_2 powder was dissolved in nitric acid and concentrated to 400g/l. Up to 12 pellets were placed batch wise on a perforated teflon tray and lowered slowly into the Am nitrate solution, where they were maintained for at least 10 minutes. Following their withdrawal from solution, they were allowed dry in the ambient atmosphere, before they were calcined at 700°C for 4 hours in Ar/H_2 and sintered at 1 650°C under the same atmosphere.

Figure 5.3: Fabrication of the EFTTRA-T4 pellets by pellet infiltration [15,19]

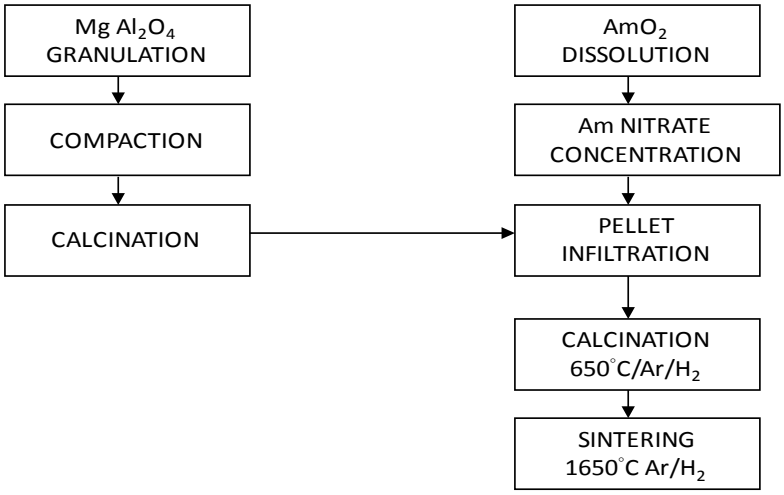

5.2.2 *ECRIX*

The ECRIX fuel was fabricated by powder metallurgical methods at the CEA's ATALANTE laboratories at Marcoule in France [6]. The flowsheet is shown in Figure 5.4. The AmO_2 source material was purified by aqueous methods and converted to solid in an oxalate precipitation step. The MgO was dried and granulated before being blended with the AmO_2 powder. This powder mixture was granulated by light compaction and sieving, before being pressed again and sintered to give the product pellets.

Figure 5.4: Fabrication route used for ECRIX fuels

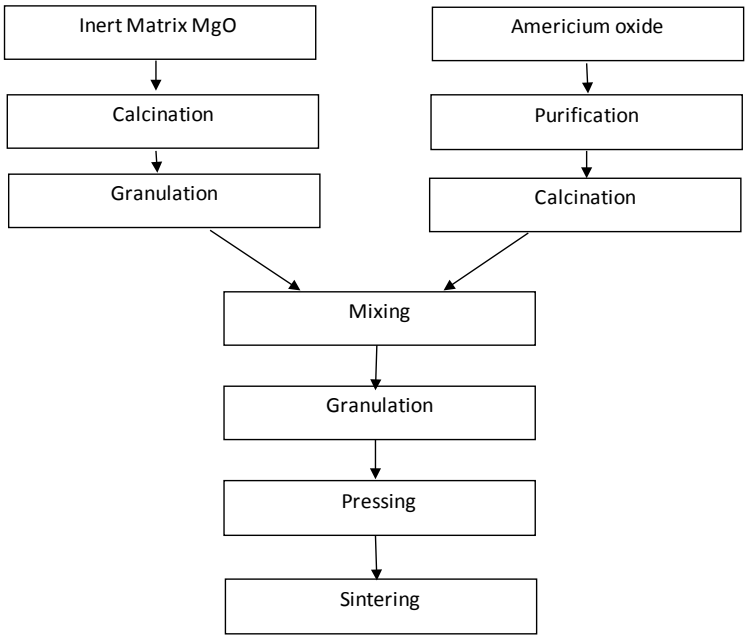

5.2.3 *CAMIX-COCHIX*

The CAMIX-COCHIX fuels were manufactured in JRC-ITU's minor actinide laboratory [6]. The process deployed for CAMIX 1 is shown schematically in Figure 5.5. The zirconyl and yttrium nitrate salts were dissolved in water at room temperatures to give saturated solutions. These solutions were then analysed, and the Zr, Y nitrate solution was prepared and analysed before being converted to solid via a droplet to particle conversion step, based on sol-gel external gelation [6]. These particles were calcined at 800°C. Americium oxide was dissolved in nitric acid, analysed, its concentration adjusted, and added to the $(Zr,Y)O_2$ beads, until the incipient wetness point was reached. The infiltrated beads were then calcined at 800°C to convert the Am nitrate to oxide. The powder was compacted and sintered to give the CAMIX 1 fuel pellets.

The fabrication of CAMIX 2 and COCHIX 3 fuel pellets differed from CAMIX 1 (see Figure 5.6) in that the primary $(Zr,Y)O_2$ beads were size fractioned after production. This was achieved by selecting 40-60 µm and 100-125 µm particles by sieving, which were needed for the micro and macro CERCER dispersion fuels, respectively. Am nitrate solution was infiltrated into these beads using the same procedure as for CAMIX 1, but due to the higher quantity of Am needed in the fissile fraction, a solution with higher Am concentration and two infiltration steps were needed. In both cases the fuels were blended with MgO at the required mass fraction to provide the blend for compaction and sintering.

Figure 5.5: Fabrication route for CAMIX 1

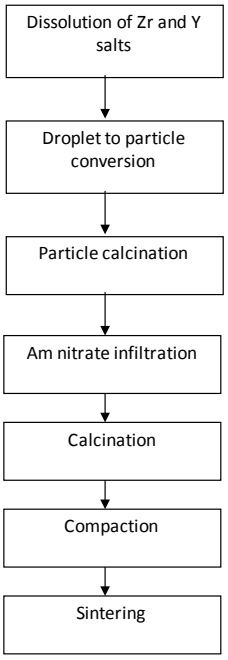

Figure 5.6: CAMIX 2 and COCHIX 3 fabrication routes

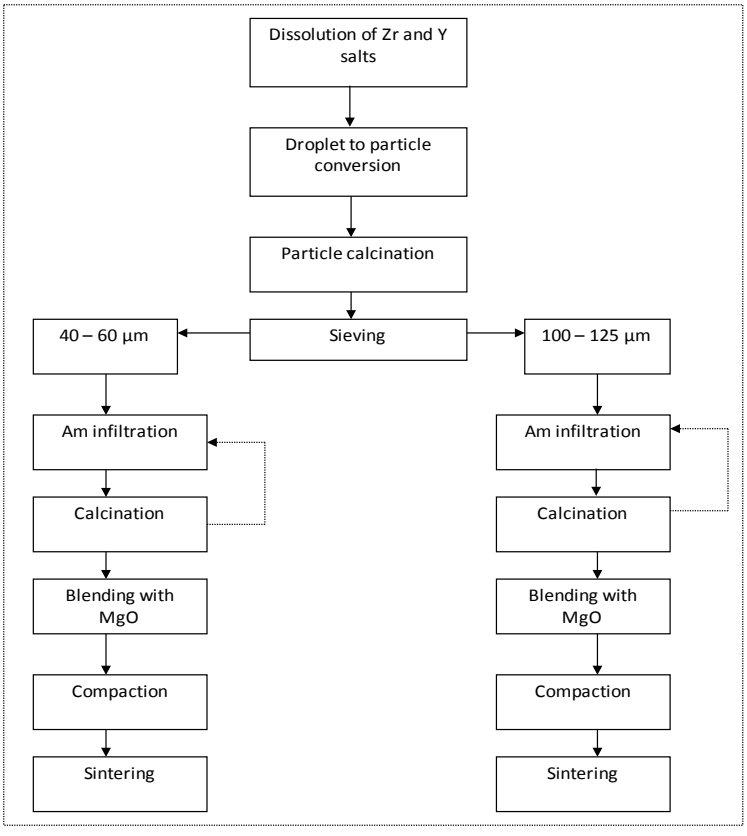

5.2.4 *FUTURIX FTA*

The CERMET fuels (FX5 and FX6) for the FUTURIX FTA experiment (see Table 5.3) were manufactured at JRC-ITU's minor actinide laboratory. The process is very similar to that shown in Figure 5.6 for CAMIX 2 and COCHIX 3 fuels, except that no size selection of the beads to be infiltrated was performed. The zirconyl nitrate and plutonium nitrate salts were dissolved in water to give saturated solutions. These solutions were then analysed, and the Zr Pu nitrate solution was prepared and analysed, before being converted to solid via a droplet to particle conversion step, which is based on sol-gel external gelation. The Pu nitrate solution was converted to solid directly, after concentration adjustment. These particles were then calcined at 800°C. Americium dioxide was dissolved in nitric acid analysed, its concentration adjusted, and added to the PuO_2 or $(Zr,Pu)O_2$ beads until the incipient wetness point was reached.

Due to the high quantity of Am needed in the fissile fraction, two infiltration steps were needed. In both cases the fuels were mixed with Mo at the required mass fraction to provide the blend for compaction and sintering.

Table 5.3: FUTURIX CERMET and CERCER fuels

	Fuel	Fabrication route	Fabrication facility
Fx 5 Fx 6	Mo – $(Pu_{0.797}Am_{0.198}Np_{0.005})O_{2-x}$ Mo – $(Zr_{0.532}Pu_{0.228}Am_{0.124}Np_{0.006})O_{2-x}$	Sol-gel infiltration Powder blending	MA Lab
Fx 7 Fx 8	MgO – $(Pu_{0.5}Am_{0.5})O_2$ MgO – $(Pu_{0.2}Am_{0.8})O_2$	Oxalate precipitate Powder Blending	Atalante

The CERCER fuels (FX 7and FX8) for the FUTURIX FTA experiment were fabricated at CEA Atalante laboratories in Marcoule, France. MgO was the fuel matrix. Both of the $(Pu,Am)O_{2-x}$ fissile phases were produced by an oxalate precipitation from solution of Pu and Am nitrate salts. The oxalate product was calcined for conversion to the oxide. The resulting $(Pu,Am)O_2$ powder was milled, blended with MgO, compacted and sintered to give the product pellets. The Pu vs. Am ratios tested were 50:50 and 20:80, as might be considered for ADS fuels.

5.2.5 *HELIOS*

HELIOS 1 is a CERCER fuel based on MgO manufactured at CEA Atalante facility. The Am phase is a pyrochlore compound $Zr_2Am_2O_7$ [2,3,13]. The fuel was produced in two steps. In the first step ZrO_2 and AmO_2 were mixed in the desired quantities, and heated at 900°C under Ar/H_2 before being fired a 1 600°C under Ar. The resulting product was crushed and sieved for the second step of the process, in which it was blended with MgO. After a compaction-sieving granulation step, pellets were pressed and sintered under Ar.

The fuels for HELIOS 2 and HELIOS 3 were produced at the JRC-ITU in the same manner as CAMIX 1 (see Figure 5.5). A process innovation was used to improve the microstructure of the fuel, namely carbon powder was added to the sol-gel broth used to prepare the porous $(Zr,Y)O_2$ and $(Zr,Y,Pu)O_2$ beads for HELIOS 2 and 3, respectively. This carbon was pyrolysed at 800°C in air to give softer beads, which improved their tendency to sinter between each other during the pellet sintering step. Am was incorporated using the infiltration method following carbon pyrolysis. First tests showed a severe anomaly and the pellets produced exhibited irregular shape and spalling of the outer layers, immediately indicative of gas release (possibly CH_4) at temperatures high enough that pore closure had occurred. Residual carbon was the main suspect for the cause of this feature. An additional process step was introduced, with the pressed pellets being heated in air at 1 000°C before being sintered in Ar/H_2 at 1 600°C. High-quality pellets were obtained. To accommodate the thermocouples, several pellets were pressed with an annual die.

The HELIOS 4 and 5 CERMET pellets were prepared according to the same procedure used for FUTURIX (FX5 and FX6).

5.3 Fuel characterisation

5.3.1 EFTTRA-T4

Visual inspection and physical measurements

The various measurements on the EFTTRA-T4 as fabricated materials are provided in Table 5.4. The pellet densities were 96.5% TD and their diameter was 5.39 mm.

Table 5.4: EFTTRA-T4 fresh fuel characterisation

Density (%TD)	Pellet diameter (mm)	Am content (wt%)	Am content ($g.cm^{-3}$)
96.5 ± 0.5	5.39 ± 0.03	11.1 ± 0.7	0.4

EFTTRA-T4 chemical composition

X-ray diffraction showed evidence of an additional phase in the CERCER composite, which had a perovskite structure, and could not be correlated with the expected diffraction pattern for Am dioxide or its sesquioxide. Subsequently, it was determined in an EXAFS/XRD investigation [17] that this extra phase is formed due to the following reaction [22], which is facilitated by the H_2 in the sintering gas stream.

$MgAl_2O_4 + ½\ Am_2O_3 \rightarrow MgO + AmAlO_3$ [21]

As $MgAl_2O_4$ is difficult to dissolve, γ-spectometry was used to determine the average Am content in each pellet, which varied between 9.7 and 11.9wt% (i.e. 11.1 ± 0.7wt%). In addition, an unfortunate (or perhaps fortunate) Am inhomogeneity was found within the pellet. Electron probe microanalysis (EPMA) and α-auto-radiography (see Figure 5.7) reveal a roughly cylindrically symmetric shell (200 µm thick) throughout the pellet. Within this shell, the Am content was 14wt% while in the surrounding inner and outer regions, it was 9wt%, as determined by EPMA. This shell is also observed in the ceramograph of the pellet, which might indicate that it is due to an inhomogeneity of the porosity in the original green pellet used for the infiltration of americium nitrate solution. Ceramographic examination at higher magnification reveals that the $AmAlO_3$ particles are less than 3µm in diameter (see Figure. 5.8).

Figure 5.7: Optical micrograph and α autoradiograph of EFTTRA-T4 pellet

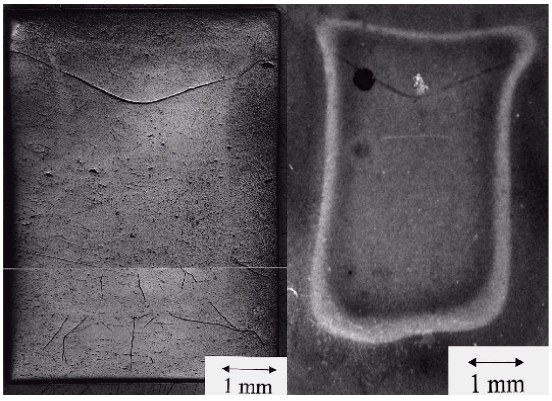

Figure 5.8: Ceramograph of the EFTTRA-T4 pellets

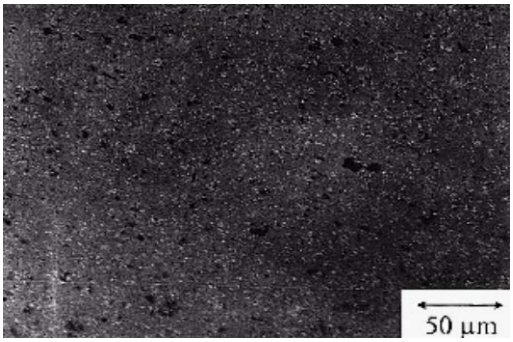

5.3.2 ECRIX

ECRIX fuel physical characteristics

Visual aspect and microstructure of ECRIX fuel pellets (5.14 mm in diameter) are shown in Figure 5.9 [6]. The pellets were of good quality. The $AmO_{1.61}$ particles were distributed evenly throughout the MgO matrix. Their density was around 97% of the theoretical value.

Figure 5.9: Visual aspect and microstructure of ECRIX fuel pellets

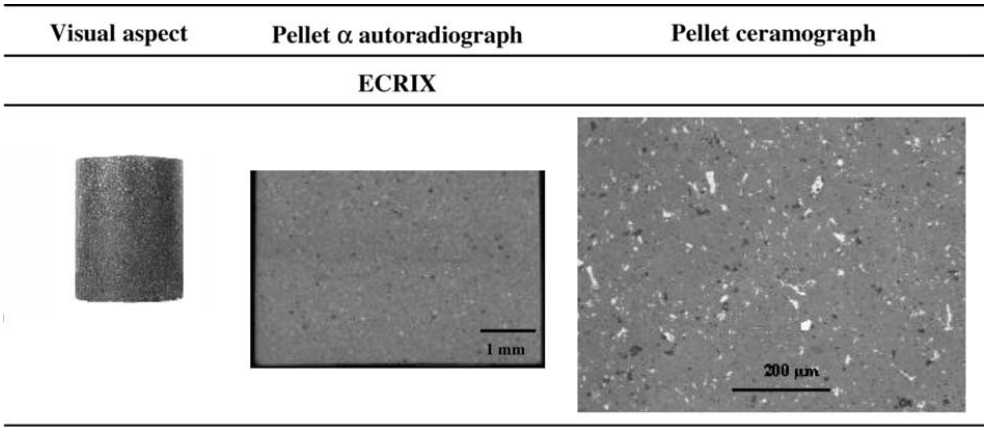

ECRIX chemical characterisation

The chemical composition of the ECRIX fuel is given in Table 5.5 [6].

Table 5.5: ECRIX fuel characteristics

Am density ($g.cm^{-3}$)	Am (wt%)	O/Am	%TD*	$Am^{243}/\Sigma Am$	Open porosity	Particle sizes
6.6	16.6±1	1.62±0.04	97±0.5	5%	0.15%	50-74% < 2 µm 24-48% 2-50 µm 1-2% 50-100 µm

*The theoretical density (TD) was $3.98/g.cm^{-3}$

ECRIX thermal properties

The thermal conductivity of the ECRIX fuels has been reported [1,16], and is provided here in Figure 5.10. It is a factor of 3-4 higher than UO_2 and marginally less than pure MgO [16]. Given the relatively low content of the $AmO_{1.6}$ phase in the fuel, the O/Am ratio of this phase does not significantly affect the thermal conductivity of the composite. The heat capacity, Cp, of the ECRIX fuels has also been reported [16].

Figure 5.10: Thermal conductivity of ECRIX fuels

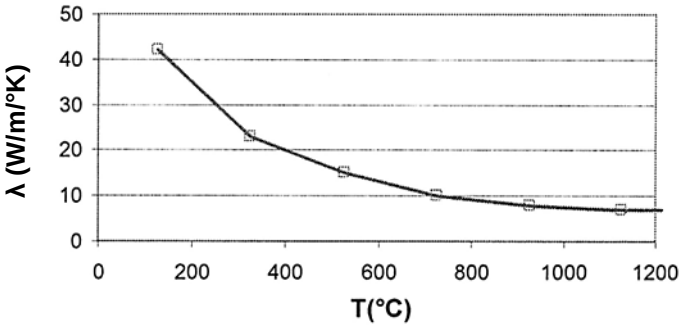

5.3.3 CAMIX COCHIX

CAMIX COCHIX fresh fuel visual examination

Visual appearance of the CAMIX-COCHIX fuels is presented in Figure 5.11. The average pellet diameters are given in Table 5.6. Ceramographic analysis of the fuels was also made, and typical examples are shown in Figure 5.12. The open porosity in all fuels was about 1%.

Figure 5.11: Visual appearance (from left) **of CAMIX 1, CAMIX 2 and COCHIX 3 pellets**

Table 5.6: CAMIX-COCHIX pellet dimensions

Fuel	Ave. diameter (mm)	Stack length (mm)	Ave. density (% TD)	TD ($g.cm^{-3}$)
CAMIX 1	5.42	102	91.2	
CAMIX 2	5.22	90	91.2	4.68
COCHIX 3	5.20		89.2	4.66

Figure 5.12: Ceramographs (from left) **of CAMIX 1, CAMIX 2 and COCHIX 3 fuels (scale bars are 100, 100 and 500 µm respectively)**

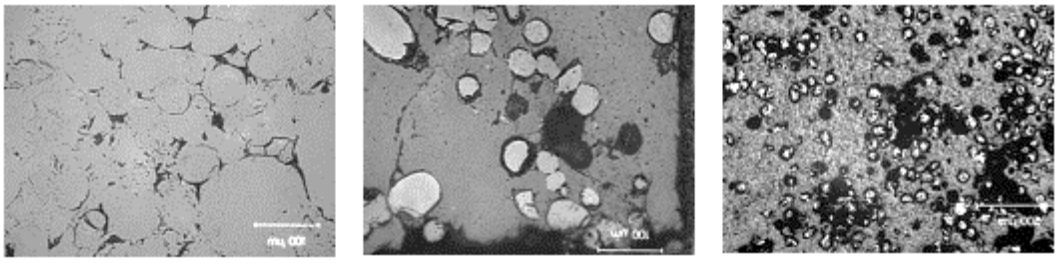

Chemical characterisation

The chemical composition of the CAMIX COCHIX fuels is given in Table 5.7. The phase composition was determined by X-ray diffraction (XRD). Only cubic zirconia-americia and MgO phases were detected. The lattice parameters are also given in Table 5.8.

Table 5.7: CAMIX-COCHIX chemical composition

Fuel	(Zr, Y, Am)O_2 phase	MgO	Am density (g.cm^{-3})
CAMIX1	$(Am_{0,057}\ Y_{0,159}\ Zr_{0,784})O_{1.63}$		0,67
CAMIX2	$(Am_{0,195}\ Y_{0,135}\ Zr_{0,670})O_{1.60}$		0,63
COCHIX3	$(Am_{0,189}\ Y_{0,136}\ Zr_{0,674})O_{1.55}$		0,61

Table 5.8: XRD analysis of CAMIX COCHIX fuels

Fuel	Structure	Lattice parameter	
		Am phase (nm)	MgO (nm)
CAMIX1	cubic	0,5167	
CAMIX2	cubic	0,521	0,421
COCHIX3	cubic	0,521	0,421

5.3.4 *FUTURIX FTA*

Visual aspect and dimensions

The visual aspect of FUTURIX FTA CERMET and CERCER fuel pellets are shown in Figures 5.13 and 5.14, respectively. An excellent appearance was found for all four fuels. The dimensions of the pellets are given in Table 5.9. Figures 5.15 and 5.16 show the ceramographic analysis of sectioned and polished fuel surfaces.

Figure 5.13: FUTURIX FTA 5 (left) **and 6 CERMET fuels** (right)

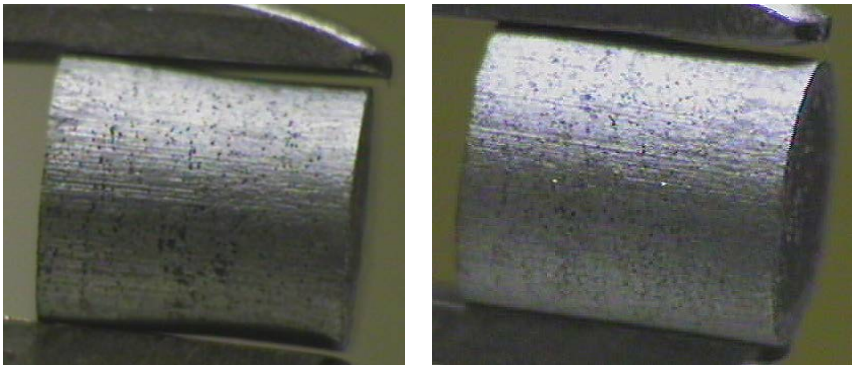

Figure 5.14: FUTURIX FTA 7 (left) **and 8 CERCER fuels** (right)

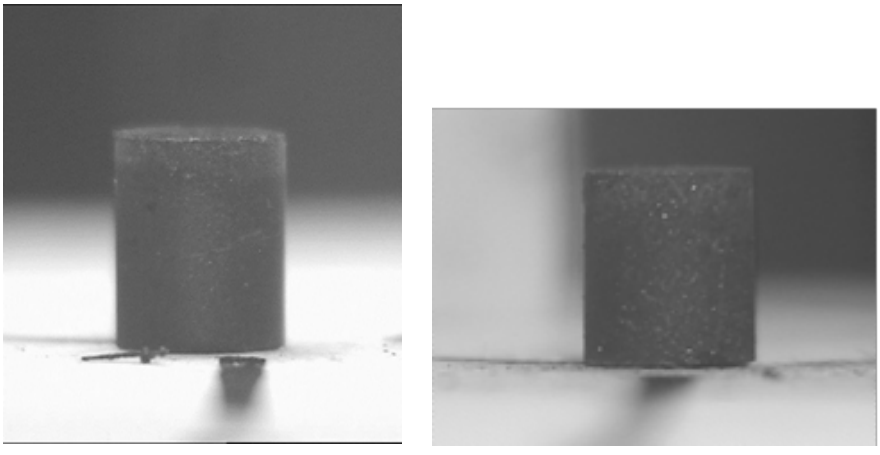

Table 5.9: FUTURIX FTA pellet dimensions and densities

Fuel	Diameter (mm)	Density (%TD)
FX5	5.15-5.24	95-97%
FX6	5.15-5.27	95-97%
FX7	5.19	95%
FX8	5.14	92%

Figure 5.15: FUTURIX FTA 5 (left) **and 6 CERMET fuels** (right)

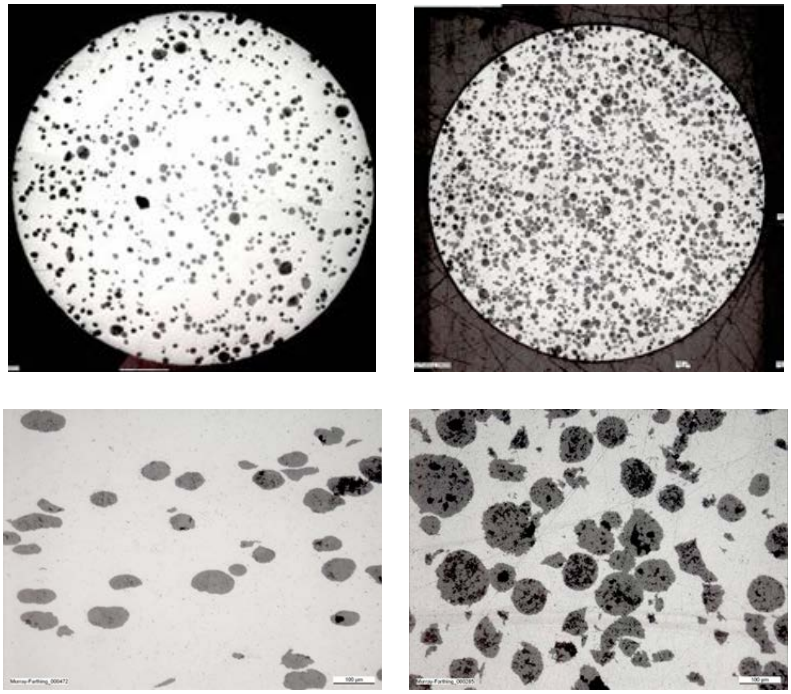

Figure 5.16: FUTURIX FTA 7 (left) **and 8 CERCER fuels (Jorion 2007)** (right)

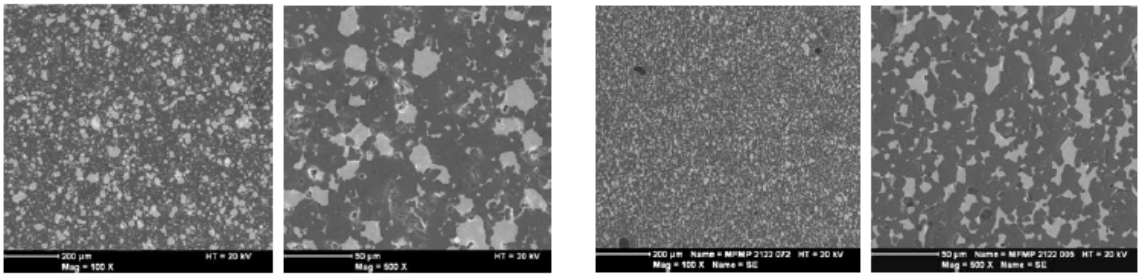

Chemical composition

The FUTURIX FTA CERMET and CERCER fuel compositions are given in Tables 5.10 and 5.11, respectively.

Table 5.10: Compositions of the FUTURIX CERMET fuels

Fuel	Pu (wt%)	Am (wt%)	Mo + ZrO_2 (wt%)
FX5	10.2	2.7	87.1
FX6	9.4	10.3	80.3

Table 5.11: Compositions of the FUTURIX CERCER fuels (Jorion 2007)

Fuel	Pu (wt%)	Am (wt%)	MgO (wt%)
FX7	19.9	19.6	32.8
FX8	9.12	35.6	28.8

The XRD determination of the phases in the CERMET pellets showed that no interaction between the Mo and the actinide ceramic phase occurred. For FX5 a single cubic ceramic phase was found. For FX 6, a single cubic pyrochlore phase was found.

The XRD measurements on the CERCER fuels showed evidence for a number of phases apart from MgO. No interaction product between MgO and the actinide phase was found. For FX 7 three actinide phases were found, namely a body-centred cubic structure consistent with a $(Pu_{0.5}Am_{0.5})_2O_3$ phase and a face centred cubic phase consistent with the dioxide. For FX8, a single actinide phase with a monoclinic structure consistent with $(Pu_{0.2}Am_{0.8})_2O_3$ was found.

FUTURIX thermal properties

The thermal conductivity of the FUTURIX CERMET fuels is provided in Figure 5.17.

Figure 5.17: Thermal conductivity of FUTURIX CERMET fuels

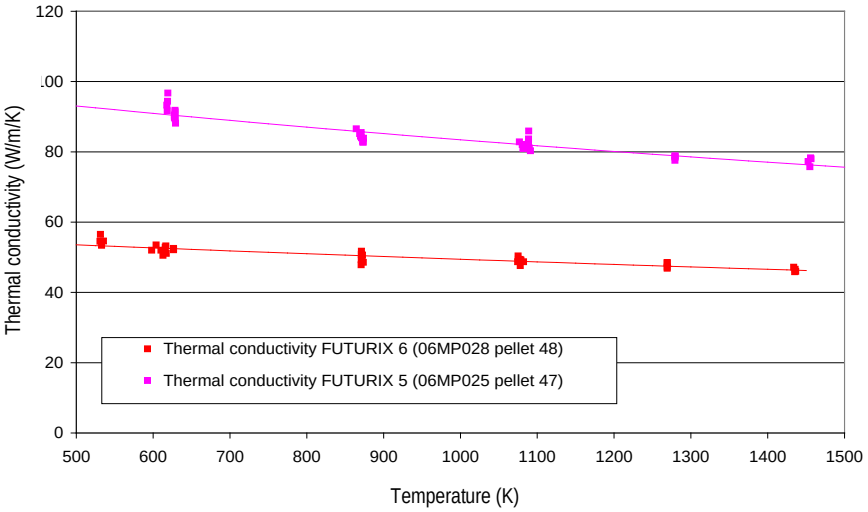

FUTURIX Sodium compatibility

The FUTURIX FTA CERMET fuels passed the sodium compatibility. No structural deterioration was observed. The CERCER fuel pellets tended to collapse, but XRD measurements provided no indication of a reaction. The mechanical instability could have been due to minor impurities in the sample.

5.3.5 *HELIOS*

Visual aspect and physical properties

The pellets were of good quality on visual inspection. The mean diameter of the HELIOS fuel pellets is given in Table 5.12. Images of polished sections of the pellets are shown in Figure 5.18.

Figure 5.18: Visual aspect of five different HELIOS fuel pellets (from top 1-5)

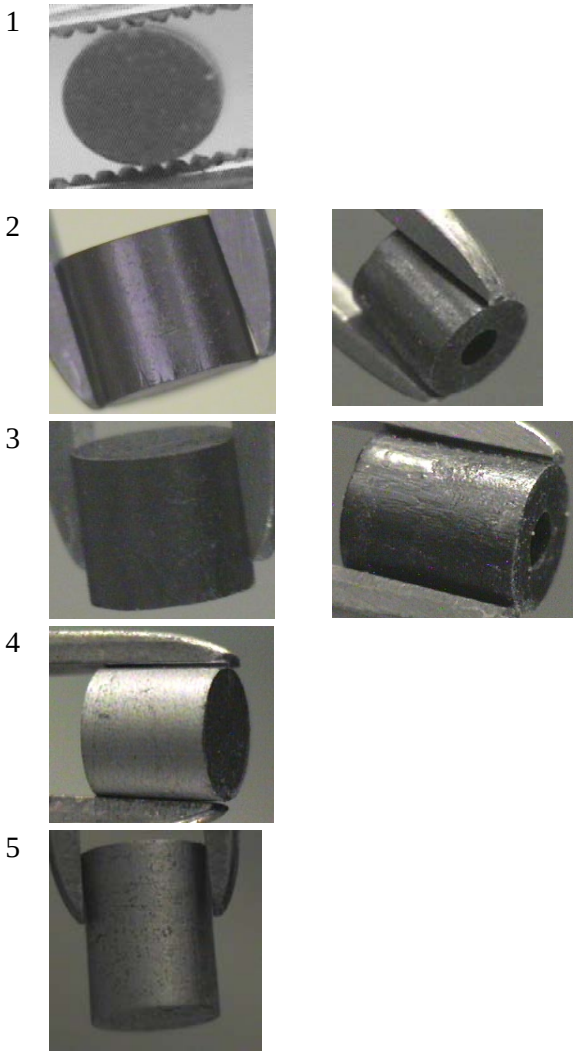

Table 5.12: HELIOS fuel pellet dimensions and densities
(brackets indicate density of the annular pellets)

HELIOS fuel type	D (Full pellet)	D (Annular pellet)	Hole diameter	Density
	(mm)	(mm)	(mm)	%TD
1	5.46	–	–	94.2
2	5.43	5.29	1.94	92.6 (90.9)
3	5.42	5.35	1.94	89.7 (89.1)
4	5.44	–	–	94.2
5	5.40	–	–	95.9

Chemical composition

Following their fabrication, the chemical form and theoretical densities of the ceramic Am bearing component of the five different HELIOS fuels are given as:

HELIOS 1: $\mathbf{Zr_2Am_2O_7}$

HELIOS 2: $\mathbf{Zr_{0.800}Y_{0.134}Am_{0.066}O_{2-x}}$

HELIOS 3: $\mathbf{Zr_{0.767}Y_{0.127}Pu_{0.038}Am_{0.068}O_{2-x}}$

HELIOS 4: $\mathbf{Zr_{0.666}Y_{0.111}Am_{0.223}O_{2-x}}$

HELIOS 5: $\mathbf{Pu_{0.801}Am_{0.199}O_{2-x}}$

The final composition of the MgO and Mo composite fuels were:

HELIOS 1: $\mathbf{Zr_2Am_2O_7}$ **(15%vol)+ MgO (85%vol)**

density 4.33 g·cm^{-3}

HELIOS 4: $\mathbf{Zr_{0.666}Y_{0.111}Am_{0.223}O_{2-x}}$ **(28.65 % vol) + Mo (71.35 %vol)**

density 9.396 g·cm^{-3}

HELIOS 5: $\mathbf{Pu_{0.801}Am_{0.199}O_{2-x}}$ **(15.77 % vol)** + **Mo (84.23 %vol)**

density 10.405 g·cm^{-3}

5.4 Irradiation tests

5.4.1 *EFTTRA-T4*

EFTTRA-T4 pin fabrication

Two target pins were produced, with 10 pellets in each. The stack lengths were 70 mm and were terminated at each end by a spinel pellet (l = 4.9 mm), a Hf pellet (l = 6.0 mm) and a stainless steel slug (l = 17.0 mm). The cladding tube was Aim1 15:15 Ti stainless steel with inner and outer diameters of 5.65 and 6.55 mm, respectively (Phénix standard). The capsules were closed using stainless steel end caps welded by the tungsten inert gas (TIG) method.

EFTTRA T4 and T4bis irradiation conditions and burn-up calculations

The EFTTRA-T4 irradiation tests were performed in central core positions of the HFR-Petten [11,12]. The T4 sample was loaded in a channel of a TRIO rig, fitted with a series of 24 thermocouples and 4 neutron detector sets and 4 gamma scanning wires (GSW). A series of gas gaps were used to set the temperature of the cladding surface (400°C). The irradiation lasted 358.42 equivalent full power days (EFPD). The EFTTRA-T4bis pin was loaded in a similar configuration and was irradiated for 652.55 EFPD. For both experiments, the neutron flux was determined and is summarised in Table 5.13.

Table 5.13: EFTTRA-T4 and T4bis irradiation conditions

	T4	T4bis
Irr. time, EFPD	358.4	652.55
Irr. duration, HFR cycles	14	26
Energy	Neutron fluence, $\times 10^{25}$ (m^{-2})	
E > 1.353 MeV	6.515	8.02
67.4 keV < E < 1.353 MeV	11.15	14.3
0.683 eV < E < 67.4 keV	12.125	19.77
E < 0.683 eV	5.21	9.72
Total	35	51.81
E > 0.1 MeV	16.8	21.3
E > 1 MeV	8.04	
Actinide depletion*	28	~ 57
Instrumentations	12 thermocouples 4 fluence detector sets 4 gamma scan wires	12 thermocouples 4 fluence detector sets 4 gamma scan wires
^{241}Am EOI/BOI, %	3.7	< 1
Temperature, K	~ 670 – (< 1 050)	~ 670
Fission power, W cm-3	30 / 272	28 / 104 (max 300)
^{241}Am transmutation	96%	99-87
Actinide destruction	28%	50%

* The depletion is defined as (actinides(BOI) – actinides(EOI))/ actinides(BOI) x 100%.

Detailed burn-up calculations were performed using the MCNP-4B [5] and FISPACT-4 codes [8]. For the T4 pin, the ^{241}Am transmutation was 96%, while about 28% actinide destruction was achieved. Due to a longer irradiation, the T4bis targets reached a higher burn-up i.e. an ^{241}Am transmutation of 99.8% and an actinide destruction of 50% (see Table 5.13). It should also be noted that the power generated in the targets rises from about 30W/cm^3 at the beginning of life (BOL) and peaks at about 300 W/cm^3 before decreasing again. This complex burn-up history differs from conventional fuels and is caused by the generation of ^{242}Cm by neutron capture, its decay to^{238}Pu with subsequent neutron capture to form, and eventually fission, ^{239}Pu. The actinide inventories for the T4 test at end of life (EOL) are given in Table 5.14.

Table 5.14: Actinide inventory at EOL for EFTTRA-T4

	Initial (%)	Final (%)
		End-of-irradiation
^{241}Am	100	3.7 ± 0.2
^{243}Am		5.1 ± 0.2
^{238}Pu		24.1 ± 0.1
^{239}Pu		6.5 ± 0.1
^{242}Pu		7.4 ± 0.5
^{242}Cm		15.6 ± 0.1
Total actinides	100	72.1 ± 0.2

5.4.2 ECRIX irradiation in Phénix

For the ECRIX irradiation test, two pins (see Figure 5.19) were fabricated and were placed in two very specific carrier subassemblies [14]. The fuel column length was ~ 200 mm [18], with three UO_2 pellets (^{235}U=4%) or either side of the MgO-$AmO_{1.61}$ stack. These enriched UO_2 pellets were included as a safety feature to detect possible pin failure, by a delayed neutron detection system at the Phénix reactor. The fuel pins were of the standard Phénix type (AIM1 grade 15:15Ti austenitic steel) with inner and outer diameters of 5.65 and 6.55 mm, respectively. The upper and lower plenum volumes were 9.76 and 11.25 cm^3, respectively [18] and the filling gas was He (0.1MPa at 20°C).

Figure 5.19: Microstructure of five different HELIOS fuel pellets

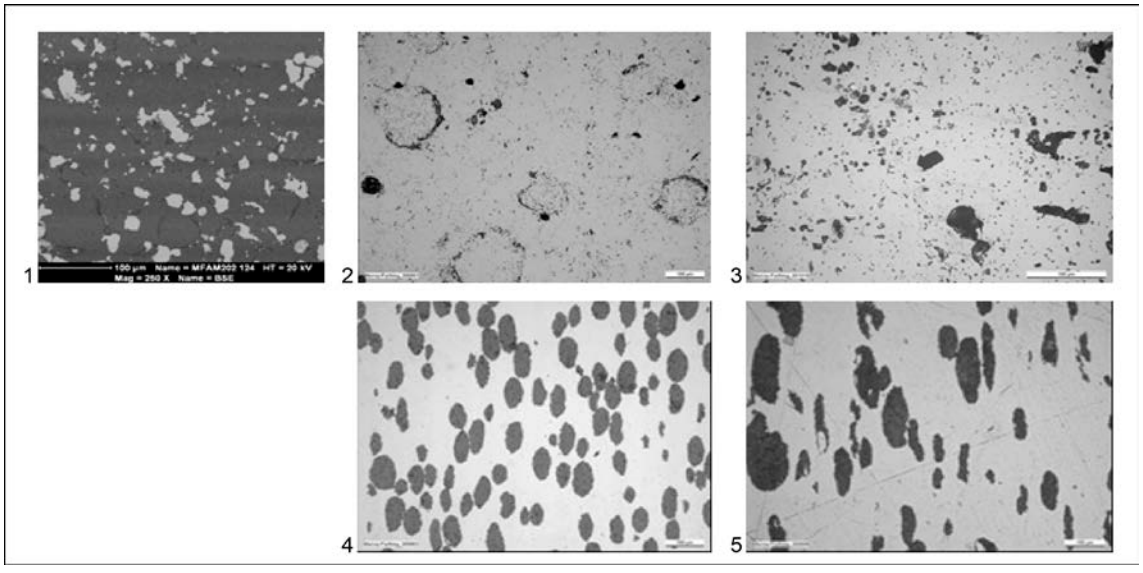

Figure 5.20: Schematic design of ECRIX H pin

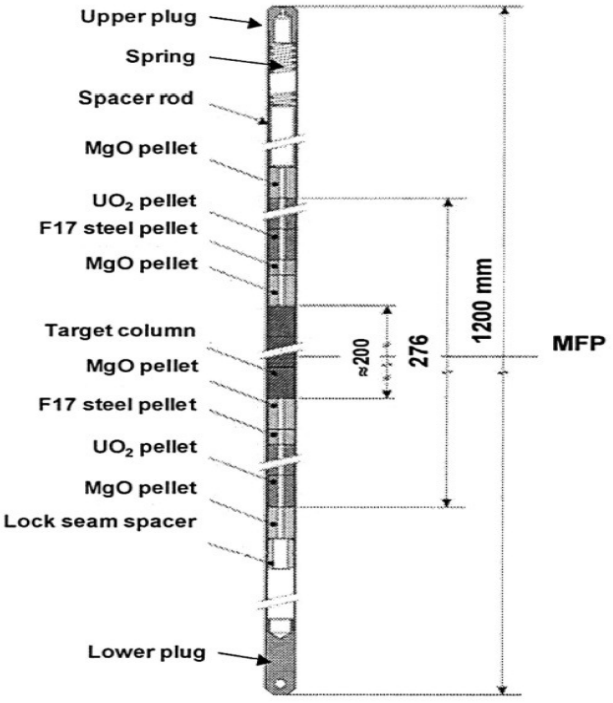

Figure 5.21: ECRIX capsules in Phénix [18]

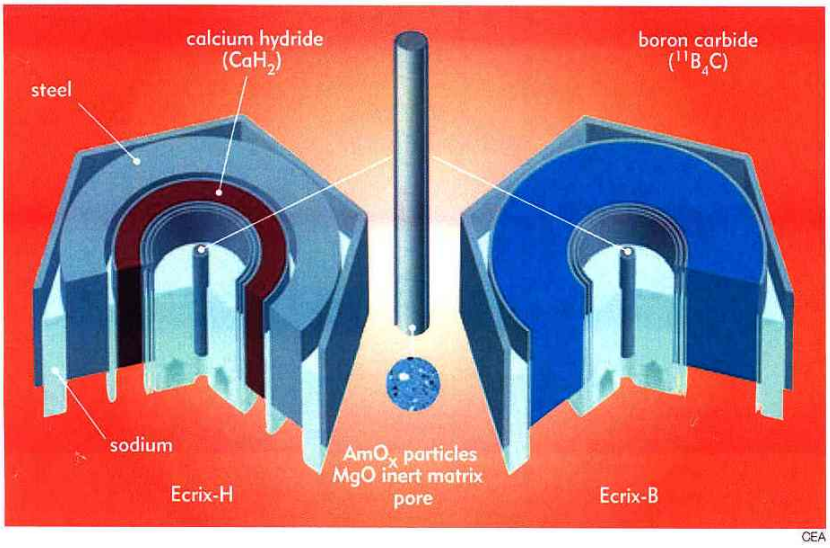

The pins were fitted with moderation blocks (see Figure 5.21) of CaH_2 (ECRIX H) and B_4C (ECRIX B) [18]. In this way, the neutron energy spectrum is shifted to lower energies to avail of the higher Am cross-sections so that an accelerated transmutation is achieved. The moderator efficiency is higher for CaH_2 which resulted in a planned irradiation of 500 EFPD (ECRIX H), while the B_4C capsule was planned for an irradiation of 700 EFPD [9]. The position of the pins ECRIX B and H in the Phénix core are shown schematically in Figure 5.22 [18]. The ECRIX B fuel pin was placed in the 4th ring from the core, while ECRIX H was placed in the first radial breeding blanket. Neutron induced damage of the clad should not be severe (56 dpa and 12 dpa for ECRIX B and H respectively) [18].

Figure 5.22: Location of the ECRIX pin in Phénix core [18]

The pins were irradiated successfully in the Phénix reactor, with the ECRIX H pin being withdrawn following an irradiation period of 318 EFPD. Its integrated neutron fluence was 6.12×10^{26}n/m^2. About 29% thereof corresponded to fast neutron fluence (E> 0.1 MeV). The integrated neutron dose was 8.78 dpa. The irradiation data have been used to simulate the transmutation and fission yields, which give 92.6 and 33.9%, respectively and correspond to a burn-up of 210 GWd/m^3.

The expected power evolution at the maximum flux plane in the ECRIX H pin is shown in Figure 5.23 [1]. The rise at the beginning of life (BOL) is due to thermal neutron capture reactions, resulting in ^{242}Am, which undergoes β-decay to ^{242}Cm, which by α-decay produces ^{238}Pu, in turn, producing fissile ^{239}Pu by neutron capture. Within the slightly harder neutron spectrum of the sample with B_4C, this maximum at BOL is not expected [9].

Figure 5.23: Power evolution in ECRIX H [1]

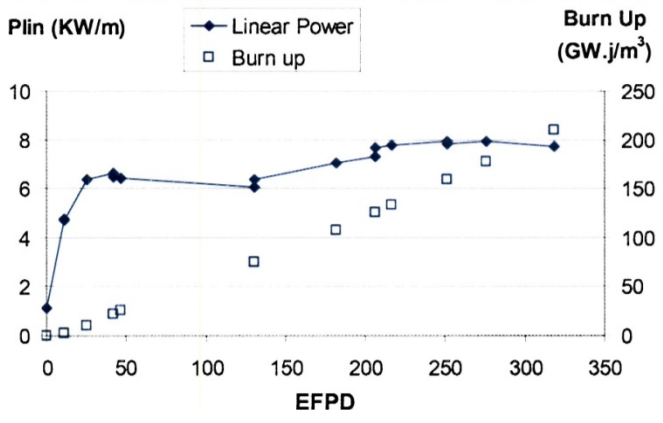

The expected evolution of the heavy metal element content in the fuel during irradiation is shown in Figure 5.24 [1]. The Am content decreases continuously from 2.75 to 0.4 g but the Pu and Cm contents, at the end of life (EOL), increase to 1.2 and 0.45 g. After 135 EFPD there is a discontinuity in the Pu and Cm contents, which is due to a reactor outage, during which ^{242}Cm decays to ^{238}Pu. The α-decays also result in a significant build-up of He (see Figure 5.25), which is about 20 times larger than the fission gas generation.

Figure 5.24: ECRIX H element distribution as a function of burn-up [1]

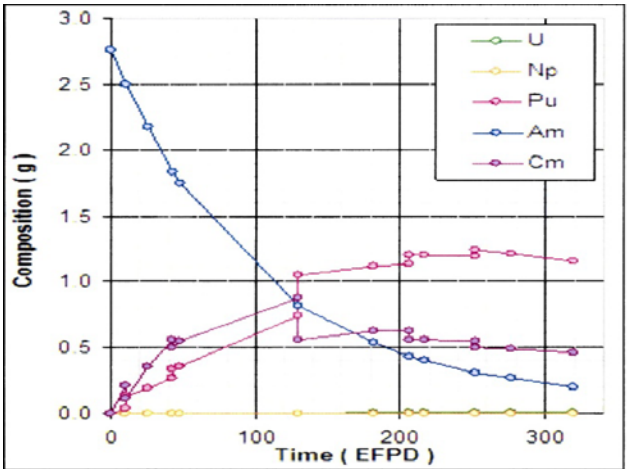

Figure 5.25: Helium and fission gas generation in the ECRIX H pin [1]

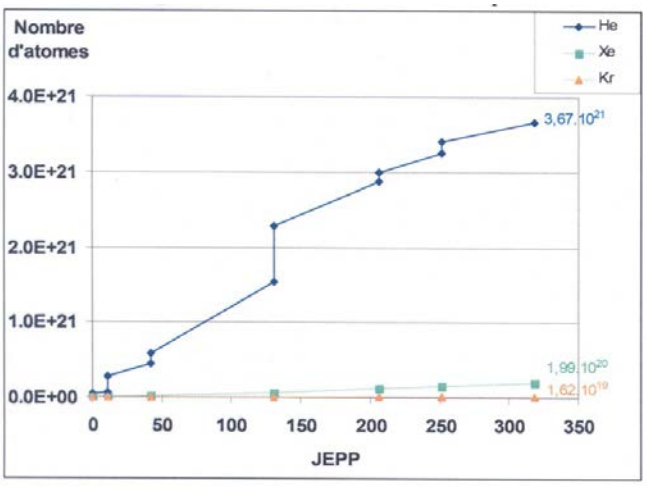

5.4.3 *CAMIX-COCHIX*

The CAMIX-COCHIX fuel pellets were loaded in standard Phénix AIM1 15:15Ti steel rods and were welded under 1 atmosphere He. The fuel pins included several enriched UO_2 pellets, as a security measure for the reactor operation. The CAMIX 1, CAMIX 2 and COCHIX 3 fuel pins were loaded in the Phénix core in the first row of the radial blanket [7] and were irradiated for 234, 178 and 178 EFPD, respectively. Maximum linear powers of 70 W/cm were expected.

5.4.4 *FUTURIX FTA*

The CERCER and CERMET fuel pellets were loaded in standard Phénix cladding (AIM1 15:15 Ti stainless steel) with internal and external diameters of 5.65 and 6.55 mm,

respectively. The fuel column lengths were 100 mm. The fuel pins were loaded pair wise in dedicated capsules. The CERMET fuel pins were loaded in the 1st row of the reactor. Due to their high thermal conductivity, highest linear power operation could be envisaged. The CERCER fuel pins were located in a lower flux position in the 5th row. All four fuel pins were irradiated for 235 (of the planned 240) EFPD at the Phénix reactor, with the irradiation completed in March 2009. Currently the pins are awaiting PIE, and no further information is available other than no pin failure occurred.

5.4.5 *HELIOS irradiation in HFR Petten*

All fuel pins were manufactured at the JRC-ITU. Standard Phénix cladding (AIM1 15:15 Ti steel) with internal and external diameters of 5.65 and 6.55 mm, respectively, was used to encapsulate the fuel. The capsule was constructed and loaded at JRC-IE and NRG laboratories in Petten. Two capsules were used to accommodate HELIOS 1 and 3 and HELIOS 2.4 and 5 fuel pins. Heat removal, predominantly in the radial direction, was achieved through a stagnant Na bath, while the surface temperature of the cladding could be adjusted by modifying the He/Ne ratio in gas caps in the outer region of the capsule. The HELIOS capsules were loaded at the HFR in April 2009 and the irradiation was completed following 10 cycles in February 2010. At the time of writing this review, no further information is available, but all fuels and fuel thermocouples performed satisfactory.

5.5 Post-irradiation examination (PIE)

5.5.1 *EFTTRA-T4 and T4bis PIE*

Non-destructive examination

Neither visual inspection nor X-ray radiographic examination of the T4 and T4bis pins revealed any irregularities. Profilometry of the pins (see Figure 5.26) revealed that an appreciable radial swelling of the pellets had occurred, and is more marked in the higher burn-up T4bis irradiation test. Furthermore, the measured profiles of the outer cladding exhibit a structure which can be correlated with the pellet heights, and also with the ends of the Am rich cylindrical shells present in the fresh fuel pellets. The average volumetric swelling for the T4 and T4bis irradiation tests has been determined as 17 and 28%, respectively [11,12]. The axial swelling was 4-5% and 6-7%, respectively.

Both pins were examined by γ-spectrometry [11,12]. It was noted that the Cs remained within the pellet stack, and that the axial distribution of the measured fission products (^{141}Cs, ^{131}I, ^{137}Cs) closely followed the Am content in the fresh fuel pellets [12].

Figure 5.26: Radial swelling of EFTTRA-T4 (top) **and T4bis** (bottom) **pins determined by profilometry**

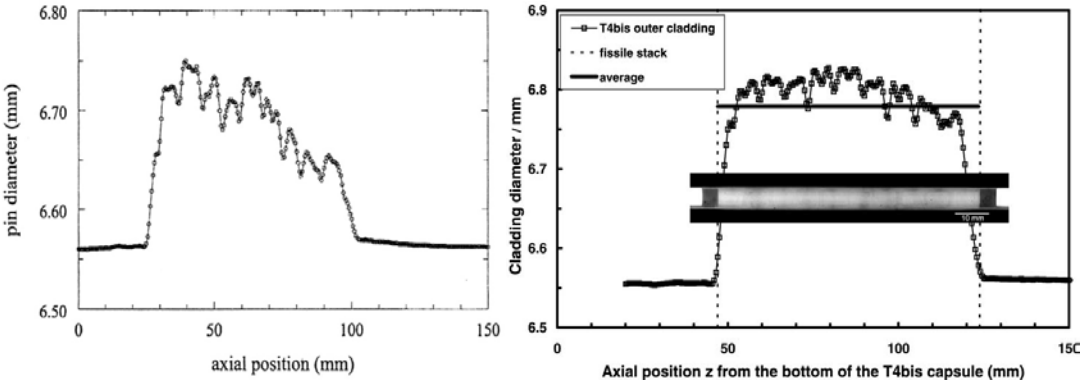

Table 5.15: Irradiation data EFTTRA T4 and T4bis

Irradiation	EFTTRA T4			EFTTRA T4bis		
Irradiation time	358.4 full power days			652.6 full power days		
^{241}Am burn-up	96%			99.8%		
Swelling	18 vol.% (max., 17 vol.% average)			27 vol.% (average)		
Pressure	0.5 MPa			1.74 MPa		
Gas contents	Produced amount (mol)	Released amount (mol)	Fractional release (%)	Produced amount (mol)	Released amount (mol)	Fractional release (%)
He	1.37×10^{-3}	2.66×10^{-4}	19.5	1.84×10^{-3}	8.88×10^{-4}	48
Xe + Kr	2.29×10^{-4}	1.19×10^{-5}	5.2	4.21×10^{-4}	6.85×10^{-5}	16
Total	1.60×10^{-3}	2.78×10^{-4}	17.4	2.27×10^{-3}	9.56×10^{-4}	42

The T4-data are taken from Konings et al. (Konings 2000) and the T4bis data from Klaassen et al. [11].

Puncturing and gas analysis of the pin were also performed. The results of experiment and MCNP/FISPACT calculations are collected in Table 5.15. The most important gas produced is helium, due to α-decay during irradiation, and in the cooling period. In the T4 experiment, He release was about 20% of that produced, whereas for the T4bis experiment, the released fraction rose to 50%. The release of Xe+Kr was also higher in the T4bis experiment (16% vs. 5%). Both experiments were performed in conditions such that the fuel operating temperature was similar. Thus, the higher swelling and gas release of the T4bis experiment might suggest that the gas is mostly occupied in isolated bubbles but as the irradiation proceeds, the total gas volume increases and eventually the bubbles start to link to form an open porosity, enabling a higher gas release.

Destructive examination of the EFTTRA-T4 pin

No destructive examination of the T4bis pin has been reported in the open literature. However, an extensive set of investigations has been reported for the T4 pin [12,19,20]. A sample was cut at the highest activity position as determined by γ-spectroscopy, and was then polished for ceramographic examination. The results (see Figure 5.27) indicate that the pellet-cladding gap is closed (as expected), and that crack healing has occurred. Furthermore, a band at $r/r_0 \approx 0.7$ is observed, within which the porosity (mean 4.5 µm) is higher than the surrounding areas. Konings has also reported [12] that the porosity changes as a function of the radial position. At the periphery ($r/r_0 \approx 1$) mainly spherical pores (~1.4 µm) are observed and they are uniformly distributed in the matrix. At the highly porous band, correlated to the original Am rich shell, the porosity towards the cladding consists of smaller pores than on the side towards the pellet centre. Finally, at the centre larger pores (4.5 µm) with greater inter pore separation are observed. The area fraction of the pores was about 16% at the periphery and the centre, while at the highly porous zone, it reaches 40%. Overall, the porosity is about 18% (c.f. 3.5% of the fresh material).

Figure 5.27: Microstructure of the EFFTRA-T4 irradiated sample

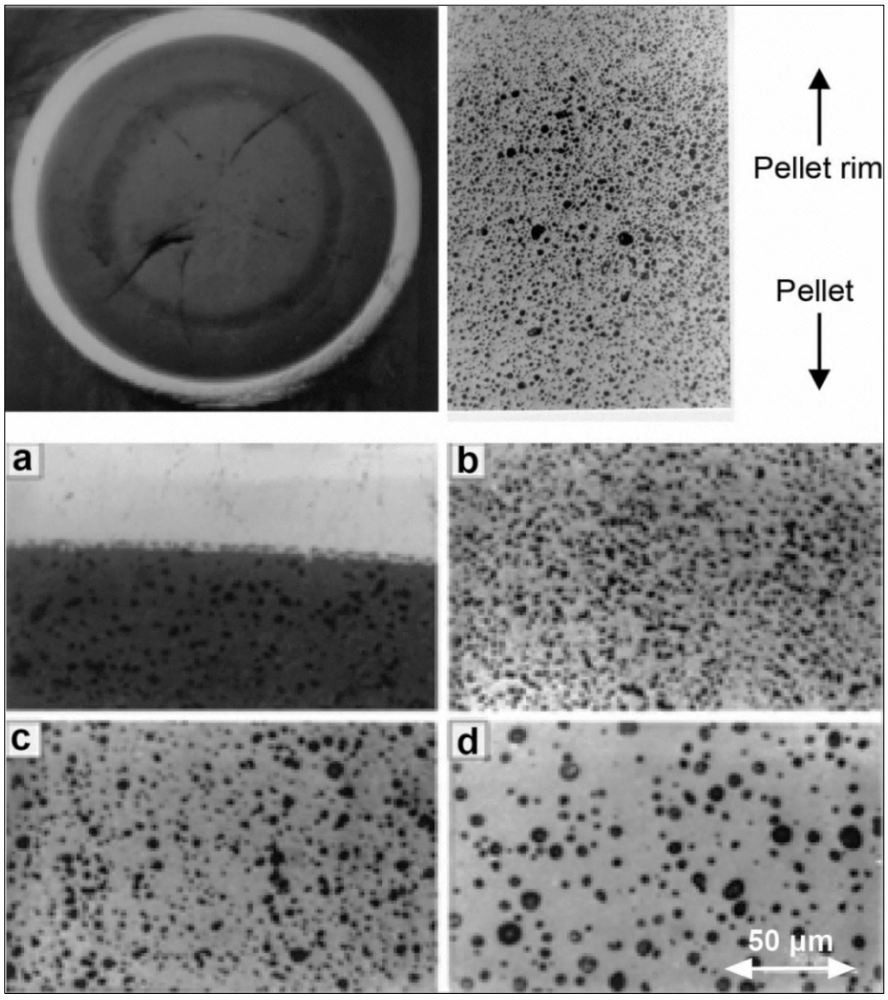

Wiss et al. [20] have reported SEM-EDX and EPMA measurements on the EFTTRA-T4 irradiated targets. SEM studies show high porosity in fractured surfaces (see Figure 5.28). Metallic fission product precipitates (2 µm in size) containing Mo, Tc, Ru, Rh and Pd were also observed. The transmutation product, Pu, is found in a Mg deficient phase close to the pores (see Figure 5.28). Indeed, there is a sharp boundary between the Pu/Al rich phase and the surrounding $MgAl_2O_4$ matrix, which had recrystallised in nanometre sized grains, possibly during interim storage [20].

EPMA investigations [21] reveal a relatively flat distribution for Xe and Nd. In contrast, the Pu profiles exhibit a distinct maximum concentration at the fuel centre, not observed in the Xe or Nd profile. The reason lies in the Pu isotopic composition, which is dominated by ^{238}Pu, so that extra fission products are not detectable. EPMA also finds evidence for Pu as a second phase or phases, whose composition relative to Mg and Al varies across the fuel diameter.

Figure 5.28: EFTTRA-T4 SEM examination following irradiation in the HFR Petten

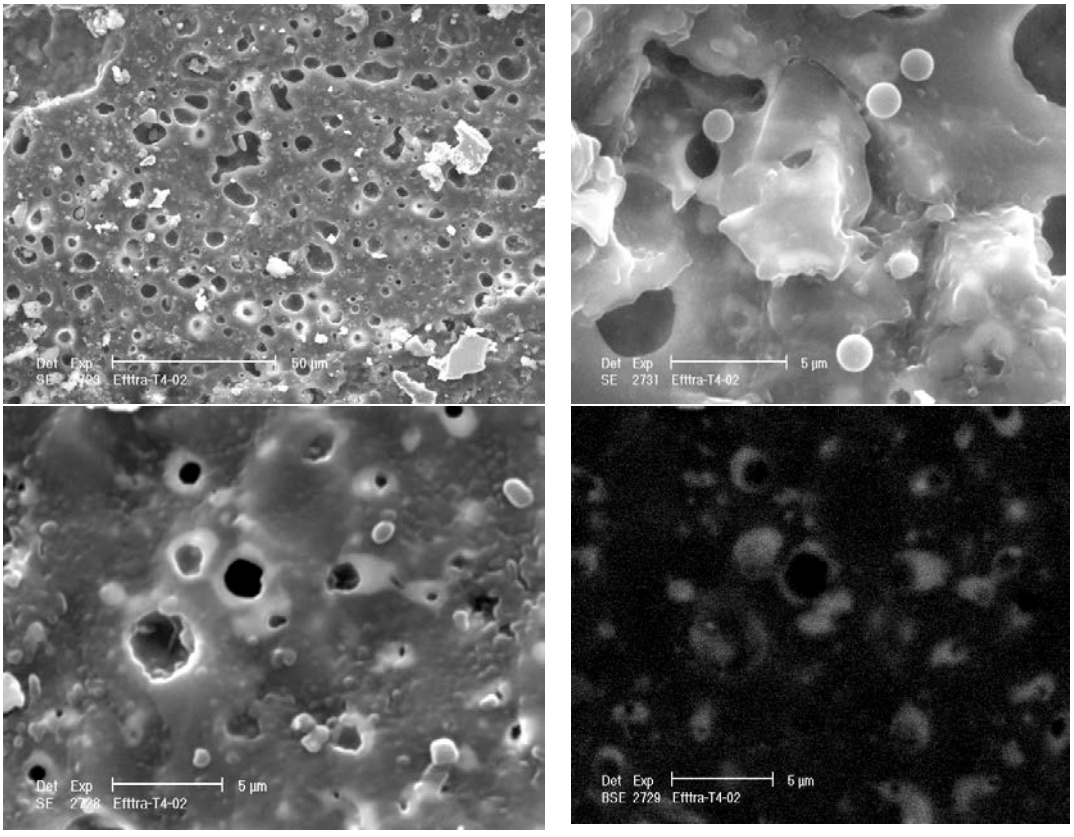

5.5.2 *ECRIX H PIE*

One of the ECRIX fuel pins (ECRIX H) has been removed from the Phénix reactor and subjected to non-destructive and destructive post-irradiation examination (PIE) at the hot cell facility at the Phénix reactor and LECA-STAR facility at the CEA's site at Cadarache. The first results have been reported in [1].

Non-destructive examinations

Visual inspection and eddy current testing of the ECRIX pin showed no abnormalities. Geometrical measurements reveal that there is no elongation of the pin, but a slight increase in diameter (6 µm) was detected in the zone of the 32 MgO-$AmO_{1.61}$ pellets. It is to be noted that this change in diameter is simply due to the thermal expansion of the cladding caused by the MgO-$AmO_{1.6}$ pellets, whose decay heat corresponds to about 5 Watts [1].

The ECRIX H fuel pin has also been examined by γ scanning [1] (see Figure 5.29). Thus, it was determined that the length of the column (MgO – $AmO_{1.61}$) increased by 5.5 µm, i.e. by 2.7%. This inspection also showed that the intensity at the bottom and top of the target column was 70 and 85% of the maximum value near the middle. No significant mobility of ^{137}Cs was noted, which would be expected, as the power (60-80 W/cm) was relatively low. Early design calculations [9] had predicted centre line temperatures of 1 300°C and pellet periphery temperatures of about 850°C.

Figure 5.29: γ scans of the ECRIX H pin

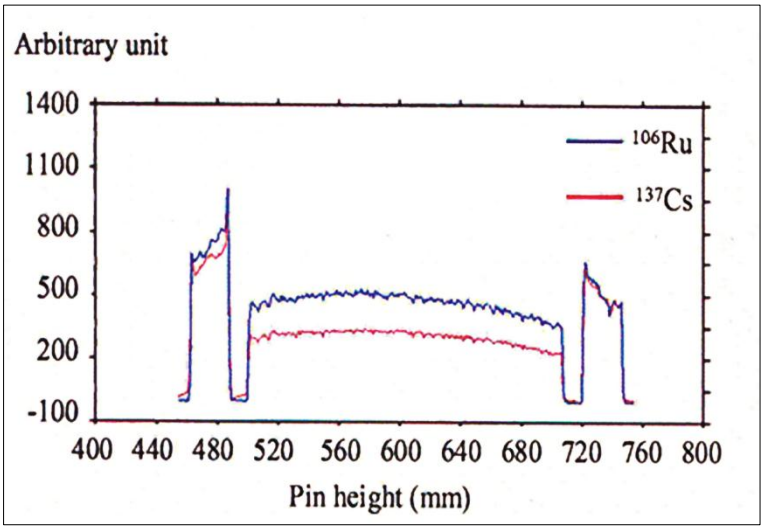

ECRIX H destructive examination

At the time of writing this review, destructive examination of the ECRIX H pin was on-going at the CEA's LECA-STAR facility, and detailed results are available in [1]. Table 5.16 shows the results of the gas analysis following puncturing of the pin.

Table 5.16: ECRIX-H gas analysis

Pin free volume (cm^3)	20.6 ± 1.6
Internal pressure prior to puncturing (bar)	2.6 ± 0.5
Volume of gas collected at 20°C, 1atm (cm^3)	53.4 ± 5.1
Volume of helium collected (cm^3)	51.71
Volume of xenon collected (cm^3)	1.56
Volume of krypton collected (cm^3)	0.13

Based on the neutronic calculations, the He release was about 23%, while 4% of the Xe and Kr inventories were released. One must note that He is released predominantly from the MgO-$AmO_{1.6}$ targets, while Xe and Kr have contributions from the enriched UO_2 pellets in the pins, and thus represent an average value for the two materials in the pin. It should be noted that the release ratio can only be truly validated when the burn-up is determined experimentally.

In a very intricate and delicate procedure, all the pellets, or fragments thereof were recovered from the pin individually. Many pellets were fragmented in large pieces, but two pellets (see Figure 5.30) were retrieved fully intact. Although occasional difficulty in recovering the targets was noted, it is clear that no fuel clad mechanical interaction (FCMI) had occurred. At BOL the radial gap was 200 µm.

Dimensional investigations revealed that the recovered pellets showed a height increase of 2.3%, which was not reflected in the γ scan of the column length variation. Their diameter increase was also about 2.3%, which would indicate an isotropic swelling of about 6.7% by volume. This is, in a similar domain, as observed in the MATINA 1A (8%) experiments on MgO-UO_2 fuel [4].

Hydrostatic density measurements of the MgO-$AmO_{1.6}$ ECRIX H pellet fragment also revealed a swelling of 5-6%, which was dependent on the position of the pellet in the fuel column.

Figure 5.30: ECRIX H: Irradiated MgO-$AmO_{1.6}$ pellet

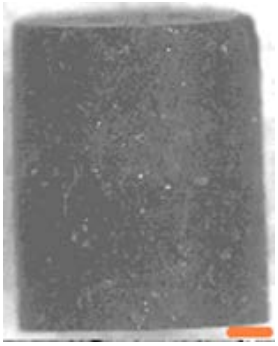

In a careful step, it was possible to assemble the fragments of pellets 14-18 and to perform an axial ceramographic analysis on this group (see Figure 5.31). Axial cracks are present in the centre and peripheral regions. They even propagate from one pellet to the next. Given that individual pellets showed a swelling of 2.3% axially, it is likely that fragments relocated in the pellet-cladding gap and by this means the individual pellet swelling was accommodated, without an overall column length increase, as found in the γ scans.

More detailed optical microscopy examination (see Figure 5.32) shows that the region previously occupied by the $AmO_{1.6}$ particles has become highly porous, and that to some extent fission product precipitates are found at the location of the parent $AmO_{1.6}$ particles.

Figure 5.31: ECRIX H fuel fragments, assembled axially, sectioned and polished

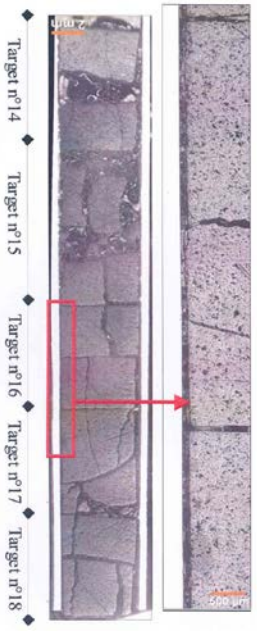

Figure 5.32: ECRIX H region corresponding to an ex $AmO_{1.6}$ particle

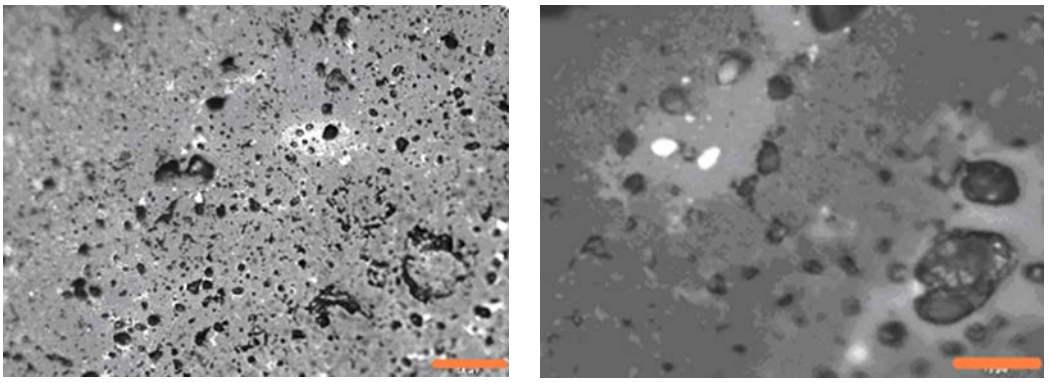

Bejaoui et al. [1] also reported that the ex AmO1.6 particles remain homogeneously distributed in the MgO matrix, and that some such actinide particles are linked by crack formation. Detailed porosity distribution, SEM and EPMA and dissolution tests have yet to be performed.

As the ECRIX H and EFTTRA T4 experiments are as yet the only IMF irradiation tests on which PIE has been performed, it is interesting to note some differences in their behaviour. In EFTTRA T4, the volumetric swelling (18 and 27% for 100 and 175 GWd/m^3) was far higher than the 6% noted in ECRIX H (210 GWd/m^3). Furthermore, ECRIX H exhibited a lower He release rate (23%) compared to EFTTRA T4 (48%) despite the larger production per volume in ECRIX H (5.84 vs. 4.56 mg/cm^3). In the EFTTRA T4 experiment, the temperature was lower (700°C) [11], which may have lead to an amorphisation of the magnesium aluminate spinel matrix, resulting in significant He bubble formation and concomitant swelling. The MgO matrix operated at a slightly higher temperature (800-900°C) in ECRIX H does not show bubble precipitation and yet He is retained in the lattice.

5.5.3 *CAMIX-COCHIX PIE*

PIE of these fuels is awaited.

5.5.4 *FUTURIX FTA PIE*

Currently, all FUTURIX FTA pins are located at the CEI laboratory at Phénix, awaiting unloading from their capsules.

5.5.5 *HELIOS PIE*

The PIE of the fuel pins has to be performed and will be achieved at CEA, NRG and JRC-ITU laboratories.

5.6 Thermomechanical modelling

5.6.1 *EFTTRA-T4*

No modelling of the EFTTRA-T4 experiment has been performed.

5.6.2 *ECRIX*

2-D axisymmetrical thermomechanical modelling of the ECRIX H irradiation using the CAST3M code has been performed at CEA [1]. The following characteristics of this simulation were included:

- 2-D axisymetrical thermomechanical mesh;

- homogeneous power distribution in the pellet;
- radial heat flow;
- external cladding temperature imposed as a fixed quantity;
- progressive thermal conductivity degradation using data from the MATINA1 test [4] and additional factors;
- variations in the gas gap conductivity.

The results are shown in Figure 5.32, for assumed R_{min} and R_{max} pellet radii and for a depression of the thermal conductivity of the fresh fuel by a factor of 0.8. These results indicate that the maximum pellet centre line and periphery temperatures were of the order of 885 and 776°C, respectively, which is significantly below the upper case conservative design values (see Garnier et al. [9]). Improved simulations will take into account thermal barriers generated by fragmentation and concomitant gas gaps.

Figure 5.33: Temperature variation at the core and surface of ECRIX H targets with minimum and maximum radii at the maximum flux plane as a function of the burn-up

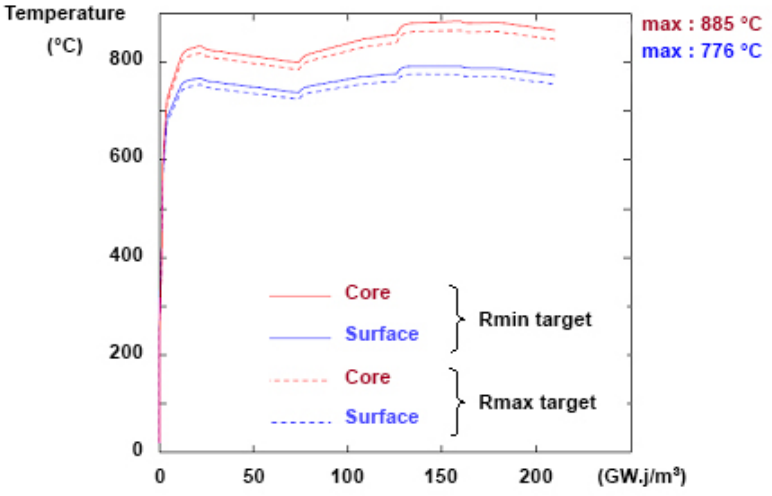

5.6.3 *CAMIX-COCHIX*

No modelling has been performed.

5.6.4 *FUTURIX FTA*

No modelling has been performed.

5.6.5 *HELIOS*

No modelling has been performed.

5.7 Safety behaviour

5.7.1 *Accident behaviour of EFTTRA-T4bis targets*

No in-pile transient test of the EFTTRA-T4 targets has been made, but a laboratory study on the behaviour of the irradiated material during thermal treatment has been made by Wiss et al. [21]. In this work, gas release was correlated to structural investigations. Samples were taken from the high porosity region of the fuel at $r/r_0 = 0.7$. The measurements were made after 4 years of storage, during which the helium content increased by about 50%. The

measured mass spectrometer signals are shown in Figure 5.34. The helium and xenon release data are shown as fractional release in Figure 5.35. Helium begins its release at 600 K, but only increases sharply at 1 550 K, being almost complete by 1 600 K. Up to this temperature, the Xe release is similar but only 35% of the inventory is released, with completion occurring at 2 200 K upon exhaustion of the sample (Plutonium (and Mg) sublimation also occurs rapidly at this temperature).

Figure 5.34: Mass spectrometer signals following heat up of an EFTTRA-T4 sample in a Knudsen cell

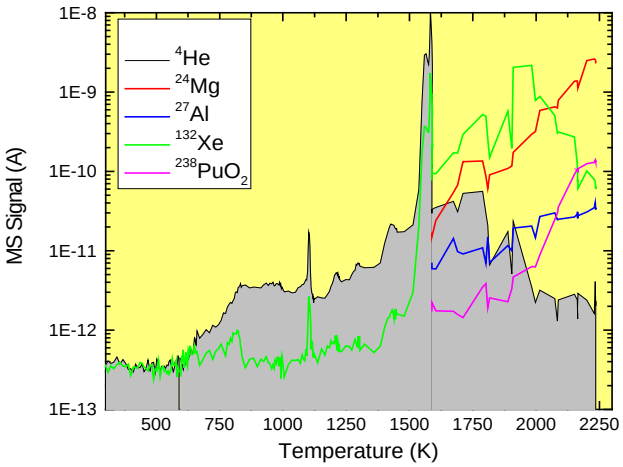

Figure 5.35: Fractional release of Xe and He from an EFTTRA-T4 sample

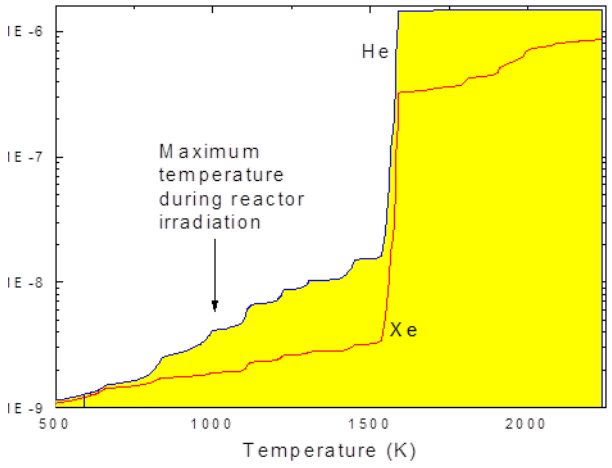

SEM analysis has also been performed following different temperatures (see Figure 5.36). No noteworthy change is observed following annealing up to 1 450 K. At 1 600 K (just above the sharp gas release), grains appear to have grown to about 1 µm, and seem to have been etched (possibly due to MgO vapourisation). The grain growth continues at 2 020 and 2 250 K, reaching 5-20 µm. Figure 5.37 summarises the gas behaviour in irradiated spinel.

Figure 5.36: EFTTRA T4 SEM micrographs taken at different annealing stages

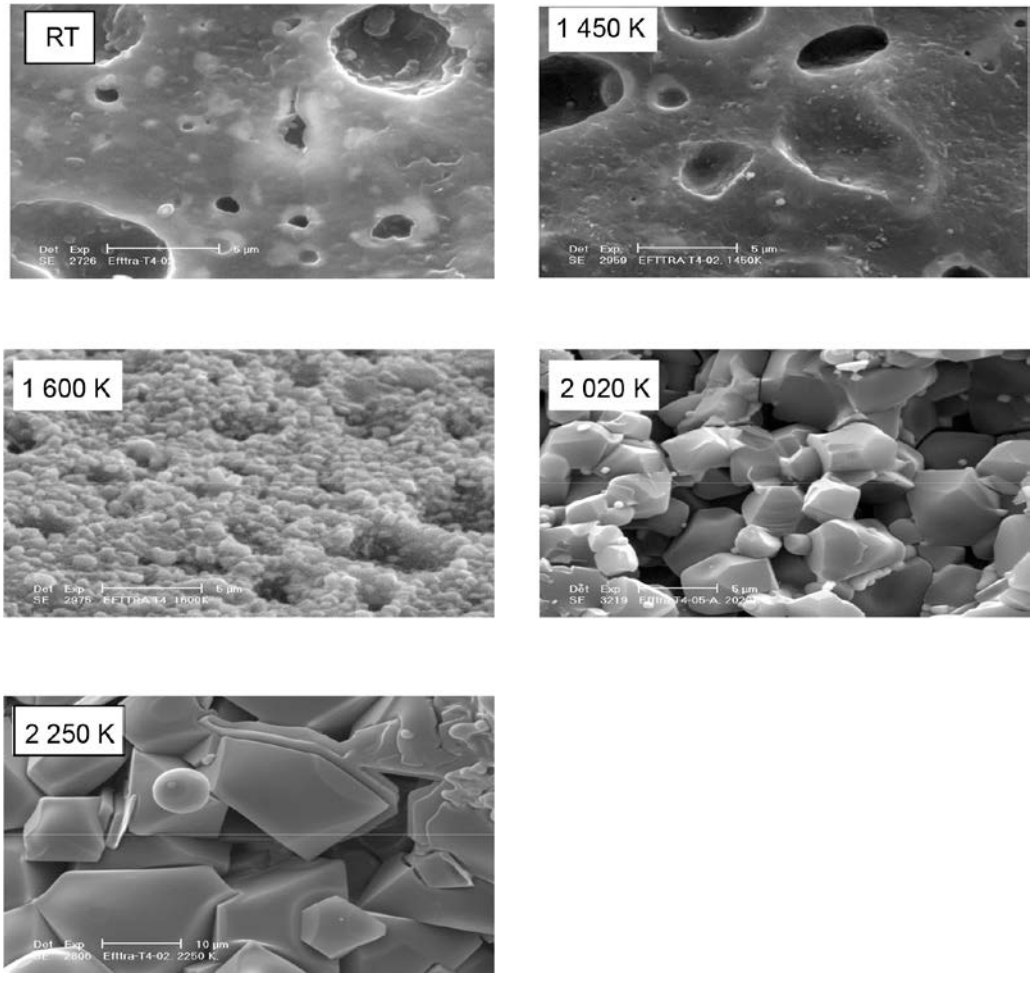

Figure 5.37: Schematic representation of the vapourisation and structural changes in irradiated EFTTRA-T4 fuel [19]

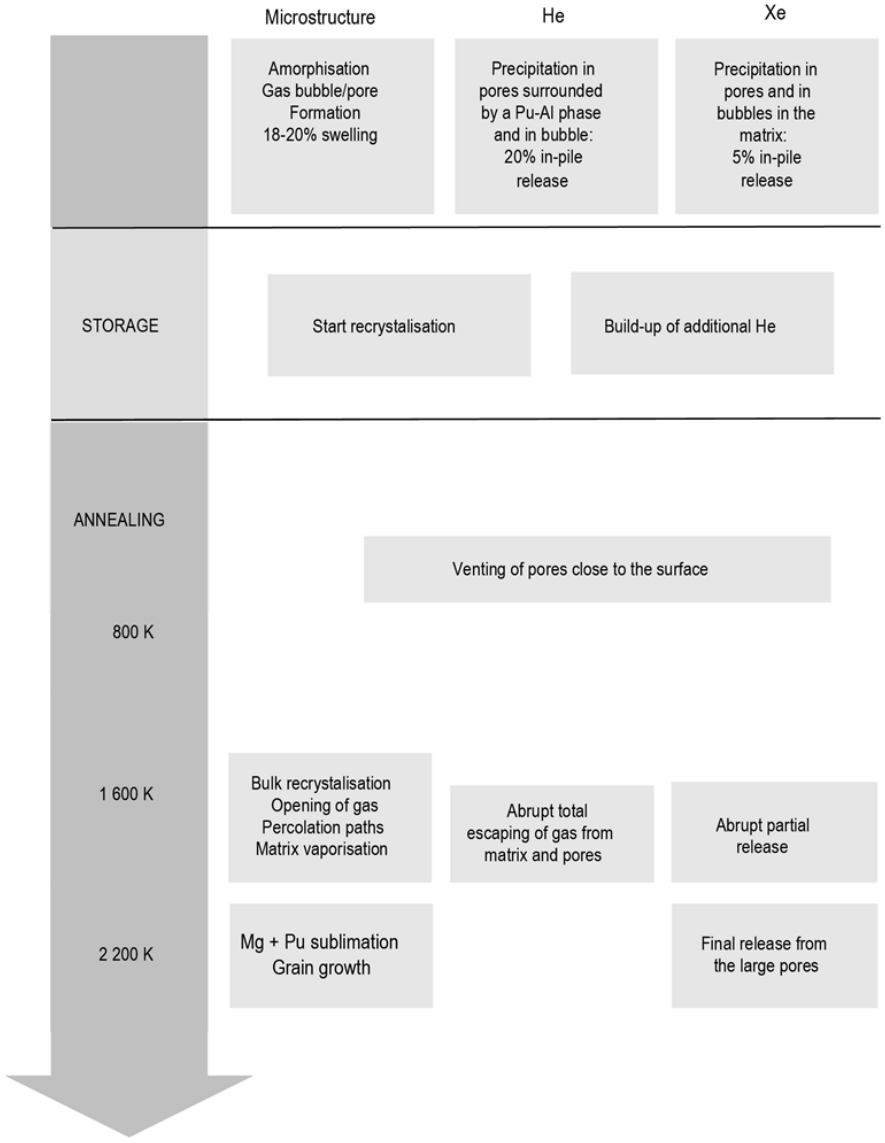

5.7.2 *ECRIX*

The behaviour of ECRIX fuels has been examined following irradiation, but vapourisation measurements on fresh MgO bearing fuels have indicated that MgO can vapourise in the presence of actinide oxide at relatively low temperatures.

5.7.3 *CAMIX-COCHIX*

No safety tests have been performed.

5.7.4 *FUTURIX FTA*

No in-pile transient safety tests have been performed, but vapourisation studies on the fresh fuel samples have been performed at JRC-ITU using a Knudsen cell (KC) mass spectrometry method. The vapourisation behaviour of FUTURIX CERMET and CERCER

fuels is shown in Figures 5.38, 5.39, 5.40, and 5.41. In the CERMET samples, discontinuities at about 2 500 K correspond to sample melting. Mo starts to vapourise above 2 300 K. In the case of the MgO CERCER, a significant vapourisation of MgO as Mg can be observed.

Recently, MgO-(Pu,Am)O_{2-x} pellets have been fabricated and their melting behaviour examined [14]. In contrast to the Knudsen cell experiments, where small samples are heated in vacuum, individual pellets were heated in Ar with small oxygen content. Following heating at 2 100°C, neither melting nor significant vapourisation of MgO were observed. Thermal treatment at 2 300°C provided evidence for sample melting due to a eutectic reaction. Furthermore, at 2 300°C evidence for Am loss from the (Pu,Am)O_{2-x} phase was noted.

Figure 5.38: Mass spectrometer measurements of CERMET FX5 samples

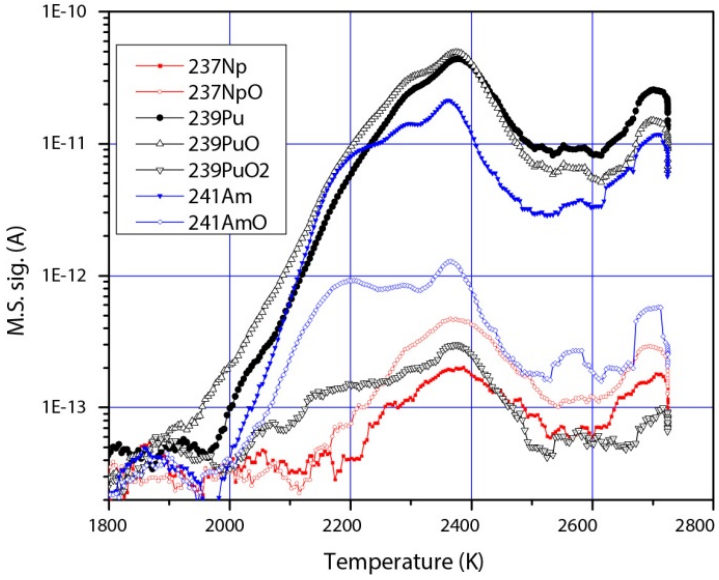

Figure 5.39: Mass spectrometer measurements of CERMET FX6 samples

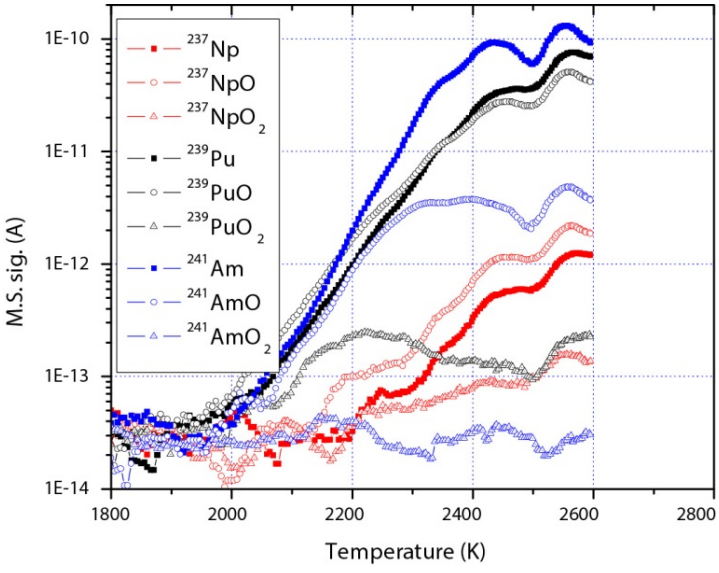

Figure 5.40: Mass spectrometer measurements of CERMET sample FX6

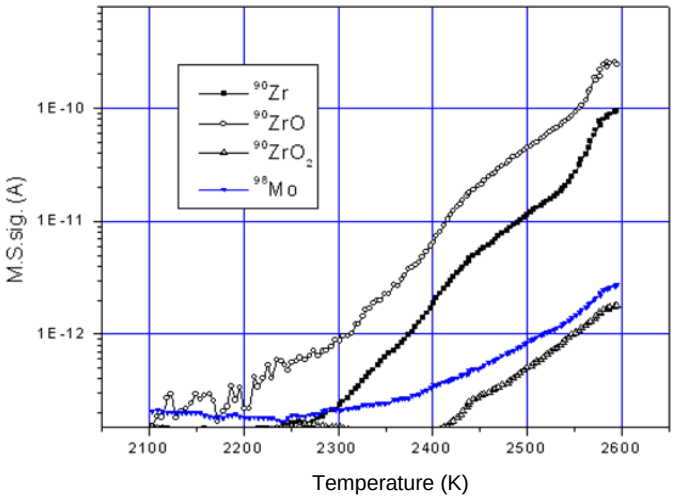

Figure 5.41: Mass spectrometer measurements of CERMET sample FX6

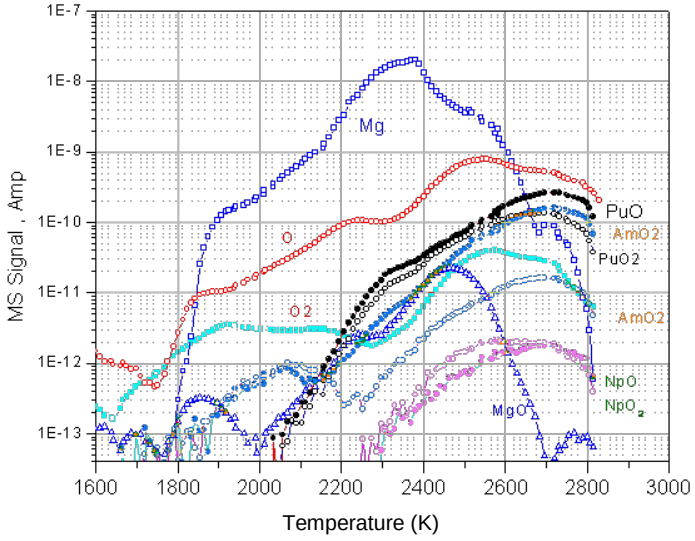

5.7.5 *HELIOS*

No safety related data are available.

5.8 Conclusions and technology readiness levels (TRLs)

5.8.1 *EFTTRA*

The EFTTRA-T4 and T4bis irradiation experiments marked an important milestone in the R&D of transmutation fuels. The main conclusions are:

- Fabrication using infiltration of green pellets is possible (but needs further development to control the distribution of the second phase).

- Helium management is a key issue in the performance of dedicated transmutation targets. Temperatures should be sufficiently high to encourage He release; an open porosity network would be beneficial.
- Large swelling due to helium must be avoided.
- The AIMI clad performed well under FCMI.
- Transmutation and fission rates of 99% and 50% were achieved.
- Both Pu and Mg evaporate at 1 700°C from the irradiated fuel in vacuum, which is detrimental to performance under a transient condition.
- Starting with the as fabricated material, full chemical compatibility is needed. The formation of new compounds ($AmAlO_3$) is not desirable in numerous phases during irradiation. This should be avoided in the future choice of matrices.

5.8.2 *ECRIX*

The ECRIX irradiation experiment has demonstrated that:

- powder metallurgical routes can be successfully deployed for the production of composite CERCER targets;
- MgO appears to have a good capacity to store helium during irradiation;
- pellet swelling up to 6% was observed;
- the AIMI clad performed well;
- transmutation and fission rates of 99% and 50% were achieved;
- MgO can exhibit unfavourable vapourisation behaviour.

5.8.3 *CAMIX-COCHIX*

Very few results are available. Fabrication showed that segregation of materials of different density may be an issue, when MgO-based CERCER pellets are deployed.

5.8.4 *FUTURIX*

Few results are available. The fabrication of CERMET pellets and CERCER pellets was demonstrated. Mo showed good vapourisation behaviour, while the onset of MgO release is rather low in temperature. No pin ruptures were observed during irradiation.

5.8.5 *HELIOS*

Fabrication routes using powder metallurgy and advanced liquid processing routes were developed and demonstrated. All fuel pins with associated thermocouple instrumentation behaved satisfactorily during irradiation.

5.9 Technology readiness levels (TRLs)

Figure 5.42 shows the TRL of the dispersion fuels. Tables 7.10 and 7.11 show the fabrication process maturity and irradiation maturity.

Figure 5.42: Irradiation and modelling maturity levels for dispersion fuels

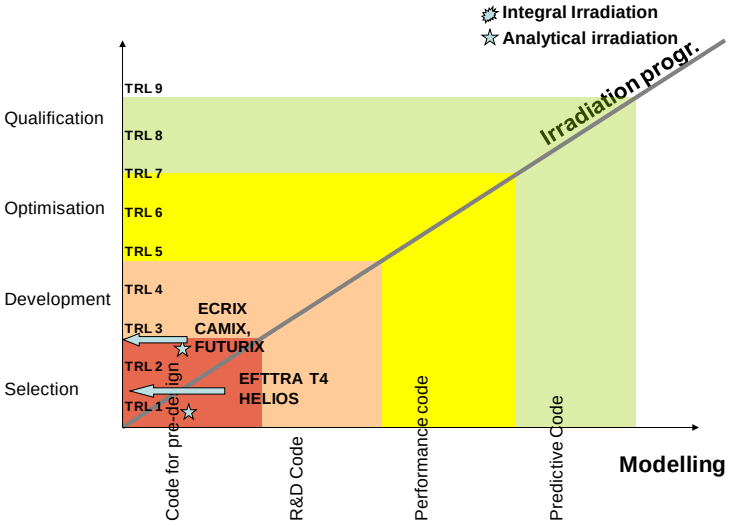

References

[1] Béjaoui, S., J. Lamontagne, J.M. Bonnerot, E. Brunon (2009), ECRIX-H Experiment: "First post-irradiation examinations and simulations", Global 2009, 6-11 September 2009, Paper 9357 Paris, France.

[2] Belin, R., P.J. Valenza, P.E. Raison, M. Tillard (2008), "Synthesis and rietveld structure refinement of americium pyrochlore $Am_2Zr_2O_7$", *J. Alloys Comp.*, 448. 321.

[3] Belin, R., P. M. Martin, P. J. Valenza, A.C. Scheinost (2009), "Experimental insight into the radiation resistance of zirconia-based americium", *Inorg. Chem.* 48. 5376.

[4] Bonnerot, J.M., D. Warin, M-P Ferroud-Plattet, L. Gosmain, J. Lamontagne (2007), "Progress on inert matrix fuels for minor actinide transmutation in fast reactor", Global 2007, 9-13 September 2007, Boise, Idaho, United States.

[5] Briesmeister, J.F. (Ed.) (1997), *MCNP, A General Monte Carlo Code for Neutron and Photon Transport*, versions 4A and 4B, Los Alamos National Laboratory, New Mexico, United States.

[6] Croixmarie, Y., E. Abonneau, A. Fernández, R.J.M. Konings, F. Desmoulière, L. Donnet (2003), "Fabrication of transmutation fuels and targets: The ECRIX and CAMIX-COCHIX experience", *J. Nucl. Mater.* 320. 11.

[7] Fontaine, B., J. Guidez, L. Martin, P. Chauchepart (2005), "Operation of the Phenix reactor and status of the irradiation experiments", Global 2005, 9-13 October 2005, Tsukuba, Japan.

[8] Forrest, R.A., J.Ch. Sublet (1995), "FISPACT 4 user manual", *EASY Documentation series UKAEA FUS* 287, UKAEA.

[9] Garnier, J.C., N. Schmidt, N. Chauvin, A. Ravenet, JM. Esceleine, C. Molin, F. Varaine, C. de Saint Jean, T. Philip, G. Vambenepe, G. Chaigne (1999), "The ECRIX experiments", Global 1999.

[10] Jorion, F., C. Maillard, J.C. Martin, L. Donnet, N. Drin (2007), "The FUTURIX-FTA experiment in Phenix: Status of oxide fuel fabrication", Global 2007, 9-13 September 2007, Boise, Idaho, United States.

[11] Klaassen, F.C., K. Bakker, R.P.C Schram, R. Klein Meulekamp, R. Conrad, J. Somers, R.J.M. Konings (2003), "Post-irradiation examination of irradiated americium oxide and uranium dioxide in magnesium aluminate spinel, *J. Nucl. Mater*. 319.108.

[12] Konings, R.J.M., R. Conrad, G. Dassel, B.J. Pijlgroms, J. Somers, E. Toscano (2000), "The EFTTRA-T4 experiment on americium transmutation", *J. Nuc. Mater.,* 282. 159.

[13] Martin, P.M., R. Belin, P. J. Valenza, A.C. Scheinost (2009), "EXAFS study of the structural phase transition in the americium zirconate pyrochlore", *J. Nucl. Mater*. 385. 126.

[14] Miwa, S., Y. Ishi, M. Osaka (2009), "Effect of oxygen partial pressure on the sintering behaviour of MgO based heterogeneous fuels containing $(Pu,Am)O_{2-x}$", *J. Nucl. Mater*. 389. 402.

[15] Richter, K., A. Fernandez, J. Somers (1997), "Infiltration of highly radioactive materials: A novel approach to the fabrication of targets for the transmutation and incineration of actinides", *J. Nucl. Mater*. 249.121.

[16] Ronchi, C., J.P. Ottaviani, C. Degueldre, R. Calabrese (2003), "Thermophysical properties of inert matrix fuels for actinide transmutation", *J. Nucl. Mater* 320. 54.

[17] Walter, M., J. Somers, A. Fernandez, D. Haas, K. Dardenne, M.A. Dennecke (2007), "Structural investigation on an aged americium transmutation fuel", *J. Nucl. Mater*., 362. 343.

[18] Warin, D. (2002), *Putting Transmutation Targets to the Test*, Clefs CEA Nb 46/2002.

[19] Wiss, T., J-P. Hiernaut, R. J. M. Konings, C. T. Walker, P. Damen, R.P.C. Schram, K. Bakker, F.C. Klaassen, R. Conrad (2002), "Structural characterization and He release behaviour in the EFTTRA T4 and T4bis irradiation", 26-27 September 2002, 2nd *ERMT,* ITU Karlsruhe, Germany.

[20] Wiss, T., R.J.M. Konings, C.T. Walker, H. Thiele (2003), "Microstructure characterisation of irradiated Am-containing $MgAl_2O_4$ (EFTTRA-T4)", *J. Nucl. Mater*. 320. 85.

[21] Wiss, T.A.G., P.M.G. Damen, J-P Hiernaut, C. Ronchi (2004), "Helium and xenon behaviour in irradiated Am-containing $MgAl_2O_4$(reactor experiment EFTTRA-T4)", *J. Nucl. Mater*. 334. 47.

6. Special mechanic fuel forms

6.1 Introduction

The production of minor actinide containing fuel is a major challenge, as it has to be performed remotely and maintenance work of mechanical devices becomes a major issue. Furthermore, it is necessary to control any potential dispersion of the fuel in the production area, such as dust from grinding procedures or any other volatile side product. Another aspect is the control of decay heat from elements like curium.

All these aspects make the conventional, well experienced and wide spread fuel pellet production an unfavourable process. This was already recognised in the early days of nuclear fuel development, therefore alternatives have been developed, from which two prominent particle fuels -vipac and sphere-pac- concepts arose (see Section 6.3). Despite all advantages in the production process, particle fuels represent a new fuel form, with new aspects in the fuel performance. Thermal conductivity, swelling, fission gas release and especially transient behaviour can be very different from the pellet fuel, showing some advantageous, but also some disadvantageous behaviour. One clear disadvantage is that particle fuels are not as well developed as pellet fuels.

6.2 Pellet fuels

Different approaches have been taken to simplify the pellet process, or to completely modify it. Some of these solutions suggest a fully aqueous production route up to the green pellet, without the need of a grinding step after sintering. An example of such an approach is the direct coagulation casting (DCC), [1]. A partial solution, where the powder mixing and milling can be omitted, represents a gelation process with an adjacent pellet pressing of microspheres [2], for an example of nitride fuel. The gelation process, described in Section 6.3.2, is the main production method for sphere-pac fuel. In the recent years, research has been focused on the simplification of the conventional pellet process for the production of fast reactor fuel. As this approach represents a major effort, the next section is devoted to this solution, shortly called, “simplified pellet process”.

6.2.1 Simplified pellet process

Figure 6.1 shows a flowchart of the conventional and the simplified pellet process, as in [3]. The suggested key technologies to reach the simplification are: the adjustment of mixing rate of PuO_2/UO_2 in the liquid state, the combination of de-nitration with granulation and the fabrication of a hollow-pellet with a lubricated die.

Apart from its simplicity, the distinctive characteristic of the simplified technology is its accuracy in adjustment of PuO_2/UO_2 ratio, since the mixing is carried out in the liquid state. Hence, complicated powder mixing processes needed in the conventional solid state mechanical mixing system can be avoided. In simulation experiments employing a mock-up system and typical liquids, a mixing accuracy of ±2.5% was attained. An overflow-type fixed-quantity service cylinder and an air lift separator supplying air free liquid into the service cylinder make this high precision possible. Laboratory experiments employing real fuel liquids (Pu/U=3/7) were also carried out. The powders were gained by de-nitrating the mixed solution with microwave heating, and a high Pu homogeneity was

reached (better than using the conventional method). Another distinctive characteristic of the simplified technology is the granulation done in the process of adjusting the U/Pu mixing rate. In this method, high speed agitation with rotating blades is efficiently employed, and no organic binder but rather water is sprayed, resulting in slippery particles. Thus, the flow ability of particles is improved (over 60 in Carr coefficient). The density of MOX hollow-pellets, which are filled with these particles and compacted by the usual press in a die, reach over 95% TD after sintering. Furthermore, hollow-pellet could be fabricated utilising the same MOX particles, and compressed using a lubricated die. These results demonstrated the feasibility of this simplified technology for MOX fuel production on the laboratory scale. Further details of these experiments are detailed in [4].

The simplicity of the process is a precondition for MA-bearing fuel, and additional aspects of the minor actinide inclusion are being considered. An important aspect is the decay heat during production which is addressed for the pellet production in [5].

Large scale development is planned, however, no irradiation programmes are reported and the technology lacks of experimental data. Therefore, it is difficult to assign a technical realisation level for the moment. However, the product is near to the conventional pellet fuel, and can certainly profit from its experience.

Figure 6.1: Flowchart of conventional and simplified pellet processes according to JAEA

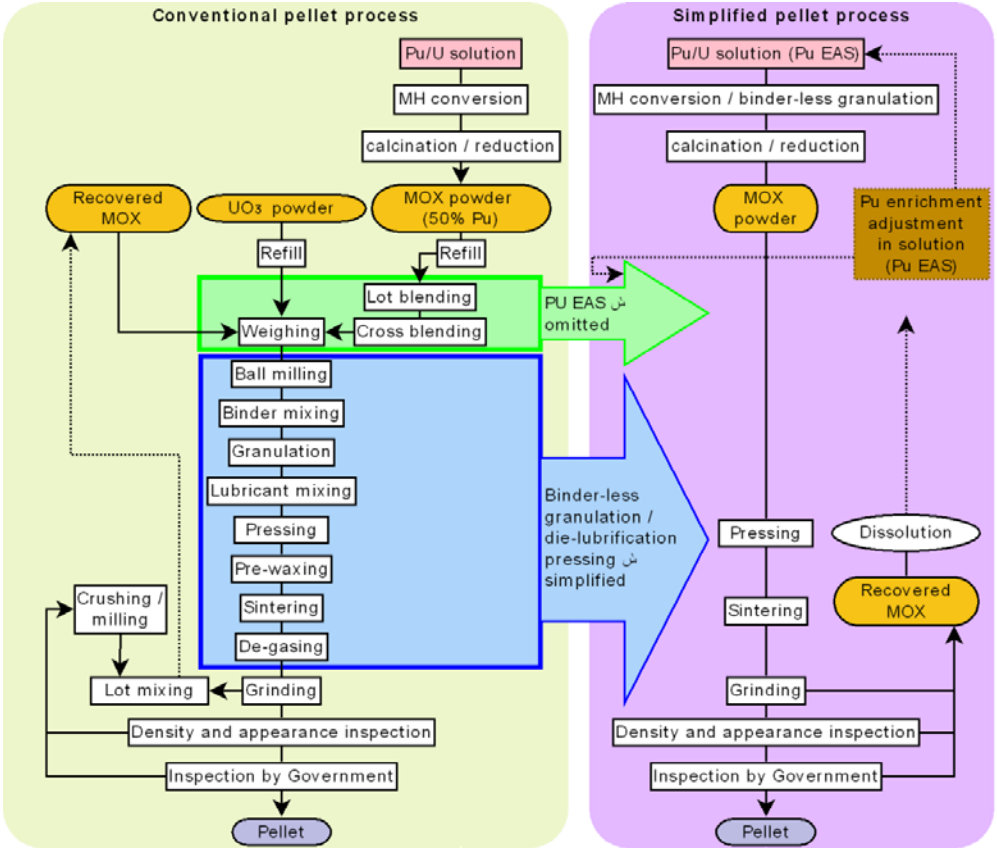

Reproduced (with modifications) from [3]. The key technology simplifying the processes are the Pu enrichment in solution (Pu EAS), the binder less granulation and the die-lubrification pressing.

6.3 Particle fuels

6.3.1 Introduction

Particle nuclear fuel is a simplified approach to load the combustible material into the rod. Classically, the fuel is pressed into cylindrical compacts, called pellets, which are stacked into the rod. In the case of particle fuel, microscopic pieces or the combustible material (in the μm to mm size range) are directly compacted into the cladding. In order to get acceptable high fuel densities, typically several particle size fractions are filled under vibration into the pin. There are two major types of particle fuel, i.e. vipac- and the sphere-pac. The motivation for both is the essentially simplified production process, which can be almost powder-less and omits the usage of important mechanical devices. This becomes especially advantageous, when the combustible material derives from reprocessing and contains minor actinides with their high radiotoxicity and a very high radioactivity, making remote operation in a heavily-shielded environment (hot cells) unavoidable. This aspect and other characteristics of particle fuel are explained below.

Features of particle fuel

The simple filling of particles into the fuel pin bears great advantages for fuels coming from reprocessing. Because of the high radioactivity and radiotoxicity, a remote operation is necessary, which makes it more difficult to conduct maintenance work of mechanical devices. In a conventional pellet process, the source powder is typically mixed, milled, pressed and grinded to the required dimension, which is all performed by mechanical devices with a potential wear and necessity for service. Each of these also produces very fine powders, dusts, which have to be handled. The powders cause problems of partially unpredictable nuclear material accumulation, which can cause criticality and activity (especially because of the minor actinides), and therefore also maintainability and human exposure concerns. In the case of particle fuel, at least, the pressing and final grinding steps are omitted. The advantages and disadvantages of particle fuel production are summarised below.

The production of particle fuels does not require press, nor grinder and massively reduces dust production. However, the filling of the pin is more difficult than in the pellet case as it involves sophisticated procedure with particle feeders and vibrator.

Besides the important production aspects, fuel performance remains the main criterion to determine whether a new fuel form is acceptable or not. The pellet type is the most common and experienced fuel form for power reactors world- and system-wide. It is the standard any other fuel form has to compete with.

The fuel pellets are designed in a rather dense way, where some porosity can potentially be designed to achieve some special properties. However, it is mostly a dense unit. In order to minimise fuel-cladding mechanical interaction due to thermal expansion and swelling, a gap is designed between the pellet and the cladding. In the case of the particle fuel, no gap can be designed, as the particles naturally touch their container, the cladding. A soft inner liner could be introduced to accommodate and distribute some of the particle bed pressure; but this is not necessary, as the particle beds are mechanically much softer than the solid pellets. At least, at the beginning of life, the particle bed can accommodate some material expansion, by elastic and also plastic deformation, as well as by sintering (diffusion related processes) between the individual particles. The initial touching points are so small that an upcoming bed pressure can easily be accommodated by these processes. Above a certain temperature, the sintering will cause a porous to dense structure after some time; the rim region (near cladding) will, however, retain its particle character because of the lower temperature (more or less pronounced depending on the system and the burn-up). The evenly distributed macroscopic vacancies throughout the particle bed (space between the spheres) can also help receive the additional material volume generated by swelling. The absence of a gap has advantages

for thermal conductivity; the heat transfer from the fuel surface to the cladding is much enhanced. Another characteristic of the particle fuel is the possibility to introduce during pin filling some special purpose particles for enhancement of the particle bed properties. Therefore, it is possible to adjust the oxygen potential, to increase the thermal conductivity, and potentially to introduce other property enhancements.

To summarise, the advantages of particle fuel for fuel performance aspects are:

- soft(er) mechanical behaviour of the initial fuel arrangement;
- better swelling behaviour;
- better heat transfer between the outer fuel surface and the cladding (no gap);
- option to introduce some special purpose particles.

However, the pellet fuel has a much higher internal thermal conductivity. The particle fuel presents many bottlenecks (small touching points between the particles) for the heat flow. Therefore, a higher fuel centre temperature has to be expected for the particle fuel. The partial sintering of the particle fuel can also cause a disadvantage in cases of accidents when an inner particle region has sintered to solid ring, and it comes to a reactor power excursion, because of the lower thermal conductivity of the outer particle like region. This inner ring would heat up more than the comparative region in a pellet. This would lead to a higher thermal expansion and therefore a higher mechanical load onto the cladding. Particle fuels also offer a comparably high specific surface and less diffusion path to the surface. Therefore, the fission gas release is higher than in the pellet case. Depending on the system and the cladding material, this can be a disadvantage.

The main disadvantages of particle fuel for fuel performance aspects are as follows:

- lower initial particle bed conductivity compared to pellet;
- potentially higher fuel cladding mechanical interaction in power excursions;
- higher fission gas release.

6.3.2 Types of particle fuel

The main difference between the two types, vipac and sphere-pac, are their origin and the particle shape. Vipac is commonly the compacted particles scraped from the electrode of a pyro-process (dry reprocessing) unit. The particle form is at random, typically an angular shape. Sphere-pac is the compaction of spherical particles deriving from a formation process of nitrate solutions from an aqueous reprocessing unit.

The choice on the type of fuel particle depends on the kind of reprocessing mode implemented in the fuel cycle, i.e. whether aqueous or dry reprocessing units are used. There are advantages and disadvantages for both concepts, but a cross-implementation of one concept would be incoherent (e.g. to use vipac after aqueous- or spehre-pac after dry-reprocessing).

Vipac

Vipac (or vibropac) is typically the compaction of angular particles (also called shards) coming from the electrode of dry reprocessing for usage in sodium-cooled fast reactors. It was originally developed at Hanford/Pacific Northwest Laboratory (United States), where other origins and usages were considered, e.g. fusing of nuclear material and the usage in LWR [6-8]. The Institute of Atomic Reactors, Dimitrovgrad (Russian Federation) is currently the main stakeholder of the vipac concept. It has developed a great expertise and conducted numerous irradiation programmes. The filling process with the compaction of the particles has been developed to a great extent by close collaboration with Rossendorf.

The main advantage of the vipac concept is that no particle forming process is necessary (direct extraction from electrode of dry reprocessing). In contrast, the main disadvantages are that the particles are a direct product of the deposition process on the electrode. In order to reach a favourable particle size distribution, a milling process is required, which produces some very fine fractions of dust. Therefore, a sieving process is needed.

Non fuel particles are often implemented as a metallic oxygen getter: these are uranium particles which are added to the fresh fuel that help control the oxygen potential and therefore to mitigate potential cladding corrosion.

This vipac concept has shown good performance in numerous irradiation programmes.

Sphere-pac

In general, sphere-pac particles are fabricated through the compaction of spherical particles coming from aqueous reprocessing for use in sodium-cooled fast reactors. Originally, this concept was developed at Oak Ridge National Laboratory in the United States. In some older literature, it is also sometimes called vipac, as it is also vibrated to reach a high compaction ratio. However, in this report vipac refers to the concept described in Section 6.3.1.

Compared to the vipac concept described above, in the sphere-pac concept the particles are not a natural product of reprocessing and a particle formation process has to be implemented.

The sphere-pac concept also presents a series of advantages and disadvantages:

- Advantages:
  - the wet route can be maintained up to the final particle formation, therefore the process is almost powerless;
  - no milling and sieving devices are necessary;
  - it is possible to evenly distribute a secondary/ternary phase into a primary/secondary phase;
  - numerous irradiation programmes have demonstrated the performance of the concept but proved to be less performant than the vipac concept.
- Disadvantages:
  - a rather sophisticated particle production process has to be implemented.

6.3.3 Fabrication

Particle fabrication

Two major production steps can be described for particle fuel fabrication: the particle production itself and the pin filling procedure as it appears to be very different from the one used in pellet fuel. These production steps are assumed to be either dry or aqueous reprocessing. The material can also come from fresh fuel stream (from U mine/enrichment, Th source or others). The early steps in the advanced process are variable and well-known and therefore, will not be mentioned here.

- Vipac

As described before, the original particles are a natural product of dry reprocessing; they are directly extracted from the electrode. The sophisticated particle production step comes afterwards in the right conditioning of this material. The particles have to be crushed/milled, cleaned and sieved into several size fractions, which have to be fed in parallel into the fuel pin (for a production flowchart see for example [30]). A mixing of

different source particles can be performed in order to adjust the fuel to the closed cycle requirements or to enhance its properties. An example for investigations towards super high burn-up, high Pu contents and the inclusion of minor actinides is given in [31].

- Sphere-pac

The source is a nitrate solution, which contains the fissile material. For the solidification, several methods have been developed over the years. Among them, water extraction process, external gemation or internal gelation will be described in this chapter.

All of them result in a more or less narrow size distribution of spherical particles in the ten micrometre to millimetre range. Smaller and larger sizes are not appropriate due to the dust classification on the lower side and the cladding dimension on the upper side. In the following sections, the different production methods are explained in detail. A special production method combining the latter two methods, the external and the internal gelation is described in [9] and is called "total gelation process of uranium (TGU)".

- Water extraction process

The water extraction process (also called ORNL process) was originally developed at the Oak Ridge National Laboratory (United States) [10]. It consists in the solidification of a specially prepared sol, a colloidal suspension of solid oxide particles composed of the wished fuel material. The production of the sol is, for instance, performed in a so-called "Concentrated Urania Sol Preparation" (CUSP) process [11] or a precipitation peptisation process for the preparation of plutonia and urania sols [12]. The preparation of different sols is described in [12].

In recent production programmes, this method did not seem to play an important role anymore. A clear advantage of the method is the lack of any organic solvents, and therefore the potential to produce products with fewer impurities.

After the sol fabrication, this process relies on the water extraction into organic alcohols. This process does not seem to be prone to a negative the influence from minor actinides.

- External gelation process

The external gelation process – also called SNAM-[14], KFA-[15] process, or the Gel Supported Precipitation (GSP) – is one of the most widely used methods to produce spherical nuclear fuel particles and had its main application in the production of fuel kernels of the TRISO fuel for high-temperature gas-cooled reactors (VHTR, HTR, HTGR).

A feed solution is prepared, based on uranyl nitrate in which an organic polymer such as a polyvinyl alcohol (PVA) and a modifier agent such as tetrahydrofurfuryl alcohol (THFA) are added. This feed solution is then dispersed into droplets through a vibrating nozzle (or multiple nozzles). The spherical droplets are formed in air from the effect of surface tension, before passing through an ammonia gas layer, hardening the bead surface into the final shape. The droplets are then collected in an aqueous concentrated ammonium hydroxide bath, where ammonia induces the precipitation of the uranyl nitrate in ammonium diuranate (ADU). The gelled droplets are aged for a suitable length of time to assure completion of the reaction. The excess ammonium nitrate produced during ADU precipitation is removed from the gelled droplets by washing in water or in a diluted ammonium hydroxide solution [16,17].

Depending on the exposure duration of the chemical components to the internally contained minor actinides, possible changes in chemistry are to be expected. Americium could for example cause important radiolysis, changing the pH value. Additionally Cm will heat the solution by its decay heat, which also represents an important change of the reaction condition. These factors have to be studied in detail, in order to realise a production of minor actinide containing fuel.

- Internal gelation process

The internal gelation process – also called the HMTA (HexaMethyleneTetraAmine) process – is an aqueous production method for ceramic spheres, where, due to a temperature-driven acidity shift, hydroxid precipitation is initiated leading to thixotrop solidification of mixed solution also called gelation. It was originally developed at KEMA in Arnhem, Netherlands by F.W. van der Brugghen [18] and J.B.W. Kanij [19]. The process is very similar to the external gelation, except, that all the chemical ingredients are contained in the feed solution, and only the temperature will initiate the gelation.

The precipitation of the internal gelation is driven by the acid (NO_3) catalysed decomposition of hexamethylenetetramine (HMTA) and hence formation of ammonia. This process is strongly temperature-sensitive, and can consequently be controlled by applying heat. If working with uranium solutions, urea needs to be added in order to prevent the formation of weaker complexes with HMTA, and therefore the preterm precipitation. For a detailed overview, the process description or the chemistry involved in the internal gelation process for uranium, uranium and plutonium, zirconium, and americium can be found in [20].

The main disadvantage of this approach is the use of silicon oil to heat up the droplets. It is very convenient, as the heating, the droplet reception and transportation media is the same. However, the use of silicon oil implies an additional cleaning step with organic solvents, and the silicon oil also potentially introduces impurities in the product. Furthermore, the silicon oil and the cleaning agents have to be recycled and disposed after some time. This generates the need for additional equipment, and increases the (liquid) waste volume. Therefore, there is an attempt to simplify the process by using other heat sources. One possibility is the heating by microwaves, which has already been implemented successfully [21-24]. There are also recent approaches to use microwaves [25-28], and there is an actual programme at Paul Scherrer Institute (PSI), where the process is being developed to be more reliable and applicable to laboratory scale fuel production [29].

For this process, the same minor actinide related concerns exist as for the external gelation process. These are a possible change in chemistry due to radiolysis, and an increase in temperature. In particular, the heating is critical here, as it triggers the gelation reaction. Solutions are an efficient cooling system, and instantaneous mixing before the gel is to be formed (before entering the nozzle). Such an instantaneous mixing process is for example presented in [32]. This approach might also resolve the change in chemistry and a possible degradation of chemical ingredients.

Pin fabrication

This section describes the procedure of producing a nuclear fuel pin from particle fuel. It is more complicated than for pellet fuel, as the particles have to be packed in a particle bed of reasonable high density and with a rather even density distribution. This requires both a good conditioning of the particle size distribution in several size fractions and the right feeding and vibration technique when filling into the cladding.

- Parallel filling

The filling process for a simulated vipac fuel (the origin of the particles is not an electrode but the crushing of pellets) is described in [33]. The corresponding description for the sphere-pac fuel is given in [34].

- Infiltration filling

The infiltration technique is the sequential filling of several (typically two) particle size fractions. The largest remaining size fraction always follows, as it allows the following smaller fraction to penetrate the network of spaces between the present spheres. After entering a new fraction, the existing bed is commonly fixed by an upper sieve like plug, to hinder a floating of a large fraction on a smaller one, but still allowing the infiltration of the smaller one. Practically, no more than two size classes are filled by this technique, as the size ratio between the classes should be around 10 (6.5 is the theoretical lower limit to penetrate a triangular pore), and with three size fractions a size ratio of 100 should be realised between the smallest and the large size fraction, which starts to be technically not attractive anymore (smallest fraction dust-like, largest fraction too large). To enhance an ideal packing arrangement, a vibration is applied during and/or after the infiltration.

Such a filling technique is for example described in [34], where a filling sequence with the corresponding vibration-accelerations and frequencies is reported.

6.3.4 Fresh fuel characterisation

The fresh fuel characterisation is very similar to that of the conventional pellet fuel. The main difference lies in the particle fuel specific shape characterisation of the single fragments as well as in their packing into the cladding. All other issues, as element analysis, hot spots, O/M ratio are more matrix dependent and not specific to the particle fuel.

For the final fuel density, the particle size distribution and the particle shape are of great importance. This is normally addressed by normal picture analysis, where representative probes of each size fraction are analysed. For a large production unit, an automated characterisation can be envisaged, where for example broken spheres are extracted on an inclined plane.

The fuel density and density distribution in the pin is crucial and has to be analysed with gamma scanning, but this is also a common procedure for pellet fuel.

6.3.5 Irradiation experiments

A collection of irradiation experiments is described in [16] and partially in [35] for some modelling aspects. For both the vipac and the sphere-pac concepts, there have been numerous production and irradiation programmes, however, only few were conducted with minor actinides containing fuel.

Vipac fuel

As mentioned earlier, the vipac concept originates from the United States, but was adopted by the Research Institute of Atomic Reactors (RIAR) in Dimitrovgrad/Russian Federation. RIAR together with Rossendorf (Germany) also established the concept as an adjacent production step to dry reprocessing. In addition to the two Russian programmes, a Danish and a Japanese-Swiss-Dutch programme were initiated. A list of experiments is described in [16,35], but a specific programme carried out at BOR 60 (Dimitrovgrad) on the transmutation of neptunium should be mentioned as it was performed with Np-containing fuel [37]. The fuel was composed of $(U,Np)O_2$ in stainless steel cladding (austenitic) for use in fast breeder reactor (FBR).

Np (5%) containing urania being produced by pyrochemical reprocessing and compacted into a steel cladding of the type ChS-68 was irradiated in the BOR-60 reactor to burn-ups of 13 and 20% h.a. The linear heating rates were in the range of 290-500 W/cm and the maximum cladding temperature was 680°C. A good fuel cladding compatibility was concluded from this test.

Sphere-pac fuel

The FUJI test was dedicated to the fabrication of MOX particle fuels with high Pu content (20%) and the study of their irradiation behaviour in the reactor. MOX and Np-MOX sphere-pac were irradiated at the High Flux Reactor (HFR) in Petten [39] [58-60].

Three fuel forms were produced and irradiated in order to compare their performance: MOX (with 20%Pu)-pellet, -vipac and -sphere-pac fuel, plus sphere-pac with additionally 5%Np. Start-up tests, restructuring tests and power to melt tests were performed. The start-up was conducted during 36 hours from 0 to full power, where the axial power profile was very pronounced, e.g. covered the range from 230 W/cm to 620 W/cm between mid of the two end slices. The restructuring tests had additionally holding times of 48 and 96 hours. In the power to melt experiment, after a holding time of 48 hours, the power was increased until central fuel melting could be observed in neutron radiographs. None of the pins failed in any of these tests. The power to melt was 600 W/cm and 730 W/cm PTM-LHR for sphere-pac and pellet fuel, respectively.

Figure 6.2: Comparison of ceramography photos according to the content of Np

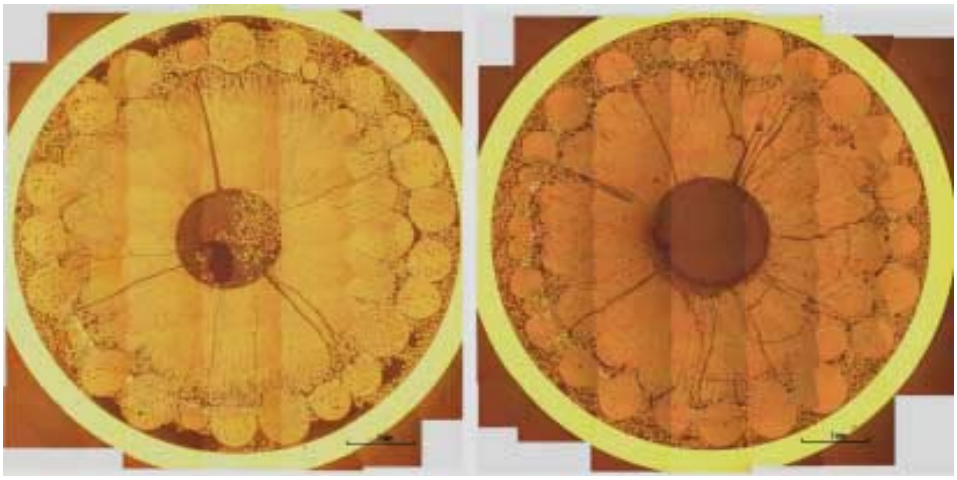

Reproduced from Figure 5.3-81 in [39], on the left side a MOX, and on the right a Np-MOX sample.

Figure 6.2 shows the comparison between two sphere-pac samples, on the left a MOX, and on the right a Np-MOX sample. The ceramography shows a slightly larger center hole for the Np-MOX, whereas the near cladding structure with its original spherical character has the same thickness in both cases. This suggests the same irradiation temperature near the cladding and a higher center temperature for the Np-MOX. Therefore the Np-MOX must have a lower thermal conductivity.

The steady power (after ramp) at the location of the Np ceramography in Figure 6.2 (right side) was 522 W/cm at 465°C (cladding temperature). The restructuring at steady power was performed for 48 hour.

It was concluded from these tests, that the influence from the Np onto the sphere-pac behaviour was minor and within the incertitude of the power distribution.

6.3.6 Comments on modelling

Particle fuel requires special modelling approaches, as the particle caused macrostructure importantly influences important properties, as for example the thermal conductivity, the fission gas release, the fuel cladding mechanical interaction and others. At PSI, special fuel performance codes have been developed for sphere-pac, i.e. SPACON and SPHERE. The first one concerns the conductivity evolution and temperature distribution

for the fresh fuel, and the latter one concerns sintering, thermal conductivity, fission gas and other properties throughout the fuel life. The models behind these codes are explained in [35].

6.3.7 Comments on safety

Fuel failure is significantly affected by the fuel cladding mechanical interaction and by the fuel cladding chemical interaction. Both have been extensively studied in the numerous irradiation experiments described in Section 6.3.5. The results considerably depend on the system. Generally, particle fuels behave softly compared to pellet fuels, exhibiting a less pronounced fuel cladding mechanical interaction. However, in a power excursion, an inner sintered ring could generate a high-mechanical load, as it reaches higher temperature in the pellet case due to the reduced thermal conductivity near cladding. Because of the potentially higher surface, the fission gas release is higher for particle fuels. For LWRs, with zircaloy claddings, this might lead to higher corrosion. For fast neutron systems, also being designed for 100% fission gas release, this seems to be an advantage.

The main issue related to fuel particle is its potential to dissolve and/or transfer into the coolant in the case of pin failure. This has been the subjects of several studies [1,62]. Modelling studies to calculate the necking of fuel particles and the corresponding adhesion forces which develop during reactor operation are described in [35]. An experimental approach, where an out-of-pile loss of spheres is addressed, simulating a UO_2 sphere-pac in the Phenix reactor is documented in [61]. Reference [62] describes different failure modes of a MOX sphere-pac fuel including the chemical interaction with sodium.

6.3.8 Technology readiness level

Particle fuels have been investigated since the early days of nuclear power. Numerous irradiation data can be found and large production facilities have already been implemented in the past.

As of today, fuel elements of vipac fuel can be produced by RIAR, therefore the technical realisation level is very high and could most probably be applied to a commercial mode of a fuel cycle with fast reactors. The technical knowledge is available, and scale-up should be feasible.

Many units of sphere-pac fuel have been prepared and fuel irradiation tests could easily be carried out. At PSI, in one of the latest silicon oil-based units MOX fuel could be produced in kg range per week (including the feed solution preparation and being limited by some safety limits for the concerned lab). Recycling the washing agents and silicon oil was in this case realised on a sophisticated level, thus optimising the resources. The new unit at PSI is realised with a microwave heater, and is more of an experimental nature for non Pu-bearing fuel. However, in a later stage, the unit will be transferred to the Pu laboratories.

References

[1] Streit, M., F. Ingold, M. A. Pouchon, L. J. Gauckler, J. -P. Ottaviani (2003), "Zirconium nitride as inert matrix for fast systems", *J. Nucl. Mater*. 319. 51.

[2] Ledergerber, G., F. Ingold, R.W. Stratton, H.-P. Alder, C. Prunier, D. Warin, M. Bauer, (1996), "Preparation of transuranium fuel and target materials for the transmutation of actinides by gel coconversion", *Nuclear Technol.*, 114 [2]194.

[3] JAEA (2008), "Toward innovative MOX fuel production by simplified process", *Research and Development of Advanced Nuclear System, R&D Review*, (http://jolisfukyu.tokai-sc.jaea.go.jp/fukyu/mirai-en/2008/1_10.html).

[4] Suzuki, M. et al. (2008), "Development of FR fuel cycle in Japan(3): Current state on unified technology of denitration conversion and granulation for simplified pellet fuel fabrication based on microwave heating", *Proceedings of 2008 International Congress on Advances in Nuclear Power Plants* (ICAPP 2008), Anaheim, CA, United States.

[5] Kawaguchi, K. et al. (2007), "Conceptual study of measures against heat generation for TRU fuel fabrication system", *Proceedings of International Conference on Advanced Nuclear Fuel Cycles and Systems* (Global 2007), Boise, United States.

[6] Hauth, J.J. (1959), "Vibration-compacted ceramic fuel elements", *HW-60346. Tech. rep., General Electric Co. Hanford Atomic Products Operation*, Richland, Wash., United States. Hauth, J. J., Anicetti, R. J., October 1959. Vibrational compaction of ceramic powders for nuclear fuel elements, HW-SA-1735. Technical report, United States Atomic Energy Commission.

[7] Hauth, J.J. (1967), "Vibrational compaction of nuclear fuels", Hausner, H. H. (Ed.), *Perspectives in Powder Metallurgy*. Vol. 2, Vibratory Compacting Principles and Methods, Plenum Press, New York, 253-276.

[8] Hauth, J.J. (1962), "Vibration-compacted ceramic fuels", *Nucleonics* 20 (9) 50.

[9] Fu, X., T. Liang, Y. Tang, Z. Xu, C. Tang (2004), "Preparation of UO_2 kernel for HTR-10 fuel element", *J. Nucl. Science and Technology,* 41 (9) 943.

[10] Wymer, R.G. (1968), "Laboratory and engineering studies of sol-gel processes at ORNL", *Proceedings of a Panel on "Sol-Gel Processes for Ceramic Nuclear Fuels"*, 131-172, IAEA, Vienna.

[11] McBride, J.P., K.H. McCorkle, W.L. Pattison, B.C. Finney (1971),"The cups process for preparing concentrated crystalline urania sols by solvent extraction", *Nucl.Technol.* 13. 148.

[12] McBride, J.P., K.H. McCorkel (1967), "Urania sol-gel processes", *Laboratory Studies of Sol-Gel Processes at the Oak Ridge National Laboratory*, Tennessee, United States. http://www.osti.gov/energycitations/product.biblio.jsp?osti_id=4197859.

[13] Bradley, R.A., J.A. Conlin, C.M. Cox, R.B. Fitts, B. Fleischer, P.A. Haas, F.J. Homan, A.Jostsons, J.Komatsu, W.J. Lackey, J.M. Leitnaker, T.B.Lindemer, E.L. Long, A.L. Lotts, E.J. Manthos, W.T. McDuffee, F.L. Miller, A.R. Olson, W.H. Pechin, J.D. Sease, R.L.Senn, J.O.Stiegler, T.N.Washburn, R.G. Wymer (1973), *Fast Breeder Reactor Oxide Fuels Development*, Final report, Technical report, Oak Ridge National Laboratory, Oak Ridge, Tennessee, United States.

[14] Brambilla, G., P. Gerontopouos, D. Neri (1970), "The SNAM process for the preparation of ceramic fuel microspheres", *Energia Nucleare*, 17 4. 217.

[15] Ganguly, C., H. Langen, E. Zimmer, E. R. Merz (1986), "Sol-gel microsphere pelletization process for fabrication of high density ThO_2-2% UO_2 fuel for advanced pressurized heavy water reactors", *Nucl. Technol.,* 73 1. 84.

[16] Pouchon, M.A., G. Ledergerber, F. Ingold, K. Bakker (2011), "Sphere-pac and vipac fuel", *Comprehensive Nuclear Materials*, ed. R. Konings, Yamanaka S., Elsevier.

[17] Charollais, F., S. Fonquernie, C.Perrais, M. Perez, O. Dugne, F.Cellier, G. Harbonnier, M.-P.Vitali, CEA, AREVA (2006), "R&D on HTR fuel fabrication and presentation of the CAPRI experimental manufacturing line", *Nuclear Engineering and Design* 236. 534.

[18] van der Brugghen, F.W., A. J. Noothout, M.E.A. Hermans, J.B.W. Kanji, O. Votocek (1970), "A U(VI)-process for microspheres production", *Symposium on Sol-Gel Pocesses and Reactor Fuel Cycles, Gatlinburg,* CONF-700502 253-263, Tennesee, United States.

[19] Kanij, J.B.W., A.J. Noothout, O. Votocek (1974), "The KEMA U(IV) process for production of UO_2 microspehere", *Sol-Gel Process for Fuel Fabrication*, IAEA-161, 185-195.

[20] Ledergerber, G. (1996), *Internal Gelation for Oxide and Nitride Particles*, JAERI-Review 96-009.

[21] Knotik, K., P.Leichter, E. Bonek (1981), "Herstellung von HTR-brennstoffkugeln durch mikrowellenhärtung von wässrigen metallsalz,-kunstharztröpfchen", *Atomenergie Kerntechnik*, 39. 191.

[22] Jungo, Ch., G. Ledergerber, "Verfahren und vorrichtung zur herstellung von mikrokugeln durch interne gelierung von mischfeedtropfen", European Patent EP 0 048 360 B1 (1982), *Process and apparatus for producing microspheres*, United States Patent 4,431,164 (1984) Japanese Patent 1, 548. 777.

[23] Ledergerber, G. (1982), "Improvements of the internal gelation process", *Trans. ANS*, 40. 55.

[24] Ledergerber, G. (1985), "Internal gelation using microwaves", *Advanced Fuel Technology and Performance,* IAEA-TECDOC (proceedings of An Advisory Group Meeting, 4-6 December 1984, 352, 165-174, Würenlingen, Switzerland.

[25] Yamagishi, S., A. Hasegawa, T. Ogawa (1994), *Development of Rapid Gelation Apparatus with Microwave Heating,* JAERI-Tech 94-010.

[26] Yamagishi, S., A. Hasegawa (1996), *Method and Apparatus for Producing Gel Particles*, United States Patent 5.581. 589.

[27] Yamagishi, S., (1998), "A new internal gelation process for fuel microsphere preparation without cooling initial solutions", *J. Nucl. Mat*. 254. 14.

[28] Rosin, A., A. Schmidt, T. Gerdes, J. Somers, M. Willert-Porada, C. Leonelli P. Veronesi (2005), "Microwave assisted internal gelation of droplets - A case study", *Proc. 10th International Conference on Microwave and High Frequency Heating,* 346-349, http://users.wpi.edu/~qwug/files/Rosin-Schmidt-et-al_2005.pdf.

[29] Pouchon, M.A., F. Ingold (2009), "Internal gelation at PSI: The past and the future", *Proc. Int. Congress on Advances in Nuclear Power Plants*, ICAPP2009, 10-14 May 2009, No. 9494, Shinjuku, Tokyo, Japan.

[30] Bychkov, A.V., S.K. Vavilov, O.V. Skiba, P.T. Porodnov, A.K. Paravin, G.P. Popkov (1997), "Pyroelectrochemical reprocessing of irradiated FBR Fuel III: Experiment of high burn-up fuel of the BOR-60 reactor", Global 1997*, Int. Conference on Future Nuclear Systems*, 5-10 October 1997, Vol. 2. 912-917, Yokohama, Japan.

[31] Bychkov, A.V., O.V. Skiba, P.T. Porodnov, M.V. Kormilitzin, L.G. Babikov (1995), "Cycle of an actinide burner reactor", *Int.Conf. on Evaluation of Emerging Nuclear Fuel Cycle Systems*, Global 1995, 11-14 September 1995, 516-523, Versailles, France.

[32] Yamagishi, S, (1998), "A new internal gelation process for fuel microsphere preparation without cooling initial solutions", *J. Nucl. Mater*., 254. 14.

[33] Shigetome, Y., S. Kono, Ch. Hellwig, P. Heimgartner (2003), "Vipac fuel fabrication for irradiation tests of the FUJI Project", Global 2003, 16-20 November 2003, New Orleans, Louisiana, United States.

[34] Hellwig, Ch., P. Heimgartner, Y. Tomita, S. Kono (2003), "Sphere-pac filling for irradiation tests of the FUJI Project", Global 2003, 1348-1353, New Orleans, Louisiana, United States.

[35] Pouchon, M.A., Ch. Hellwig, L.Å. Nordstrom (2011), "Modelling of sphere-pac and vipac fuel", *Comprehensive Nuclear Materials*", ed. R. Konings, S. Yamanaka, Elsevier.

[36] Knudsen, P., C. Bagger, N. Kjaer-Pedersen (1976), "Analysis of overpower performance of high-burnup pellet and vipac UO_2-Zr fuel pins", *Transactions of the American Nuclear Society*, 24. 172.

[37] Mayorshin, A.A., et al. (2002), "Experimental transmutation of neptunium in the BOR-60 reactor in the form of vibropac $UNpO_2$ fuel", *Seventh Information Exchange Meeting on Actinide and Fission Product Partitioning and Transmutation*, Session III: Progress in Fuels and Targets, 14-16 October 2002, Jeju, Republic of Korea.

[38] Gratchyov, A.F., et al. (2007), "Demonstration experiment of 3 BN-600 MOX vibropac FAs irradiation for the excess weapons plutonium disposal", *J. Nucl. Sc. Tech.* 44 (3) 504.

[39] Morihira, M., et al. (2005), *Final Report of the FUJI Project concerning the Research and Development of Advanced Sphere-pac Fuel among JNC, PSI and NRG*, JNC TY8400 2005-006. Technical report, Japan Nuclear Cycle Development Institute (JNC), Tokai-mura, Ibaraki, Japan.

[40] Beatty, R.L., R.E.Norman, K.J. Notz (1979), *Gel-sphere-pac Fuel for Thermal Reactors: Assessment of Fabrication Technology and Irradiation Performance*, ORNL-5469. Technical report, Oak Ridge National Laboratory, TN, United States.

[41] Kitts, F.G., R.B. Fitts, A.R. Olsen (1967), "Sol-gel urania-plutonia microsphere preparation and fabrication into fuel rods", pp. 195-210, *Int. Symp. Plutonium Fuels Technol.* Scottsdale Arizona, Nucl. Met. 13, ed. by K. E. Horton, R. E. Macherey, and R. J. Allio, American Institute of Mining, Metallurgical, and Petroleum Engineers, New York, United States.

[42] Olsen, A.R., C.M. Cox, R.B. Fitts (1969), "Low burnup irradiation tests of sphere-pac sol-gel $(U,Pu)O_2$ fuels", *Trans. ANS*, 12(2) 605-06.

[43] Fritz, R. (1970), *Die Entwicklung und Auslegung eines Prototyp Brennstofftestelements für einen Schwerwassermoderierten und Schwerwassergekühlten Thorium Brutreaktor mit Vibrationsverdichteten Brennstoffpartikeln*", Jül-654-RG. Technical report, Kernforschungsanlage, Jülich, Germany.

[44] Lahr, H.W.H., (1976), "Fabrication, properties, and irradiation behavior of U/Pu particle fuel for light water reactors", *Nucl. Technol.* 31. 183.

[45] Cervellati, A., G. Falcinelli, C. Lepscky, G. Cogliati, P. Guermani, G. Testa (1970), "Irradiation tests of sol-gel products", *Symposium on Sol-Gel Processes and Fuel Cycles*, 4-7 May 1970, CONF-700502, pp. 374-413, Gatlinburg, Tennessee, United States.

[46] van der Linde, A., J.H.N. Verheugen (1982), "Behaviour of $(U,Pu)O_2$ sphere-pac fuel with Pu in the large spheres only in low burn up tests under pressurised water reactor conditions", *Nuclear Technol.y*, 59. 70.

[47] van der Linde, A. (1989), *Sphere-pac versus Pellet UO_2 fuel in the Dodewaard BWR*, ECN report ECN-213. "Non-destructive post-irradiation examinations of sphere-pac and pellet UO_2 fuel rods irradiated in the Dodewaard BER", *Proc. EHPG Meeting on Fuel Performance Experiments and Analysis*, OECD Halden Project Report HPR-330/18, (1986), "Comparative testing of UO2 sphere-pac and pellet fuel in the Dodewaard BWR", *Proceedings of the European Nuclear Conference*, September 23-28, 1990, Lyon, France, ENC'90 (1990) pp. 1900-1903.

[48] van der Linde, A. (1987), *Microscopic Examinations of a Sphere-pac and Pellet UO_2 Fuel Rod Irradiated during 1530 days in the Dodewaard BWR*, Report ECN-199.

[49] van der Linde, A. (1990), Energiespectrum, page 165 (in Dutch).

[50] Smith, L., E.T. Aerne, B. Bürgisser, U. Flückiger, R. Hofer, F. Petrik (1979), *The Post-irradiation Examination of a Sphere-pac (UPu)C Fuel Pin Irradiated in the BR-2 Reactor*

(MFBS 7 experiment), EIR-Report Nr. 376, Eidg. Inst. Reaktorforschung, Würenlingen, Switzerland.

[51] Delbrassine, A., L. Smith (1980), "Pellet and sphere-pac (U,Pu)C fuel comparative irradiation tests", *Nucl. Technol*., 49. 129.

[52] Bischoff, K., L. Smith, R.W. Stratton (1980), *Performance of a Sphere-pac Mixed Carbide Fuel Pin Irradiated in the Dounreay Fast Reactor (DFR 527 /1 Experiment),* EIR-Report Nr. 415, Eidg. Inst. Reaktorforschung, Würenlinge, Switzerland.

[53] Stratton, R.W., G. Ledergerber, F. Ingold, T.W. Latimer, K.M. Chidester (1993), "Fuel fabrication processed, design and experimental conditions for the joint US-Swiss mixed-carbide test in FFTF (AC-3 test)", *J. Nucl. Mater.,* 204. 39-49.

[54] Mason, R.E., C.W. Hoth, R.W. Stratton, F. Botta (1992), "Irradiation and examination results of the AC-3 mixed-carbide test", *Trans. ANS, Soc.,* 66. 215.

[55] Bart, G., F.B. Botta, C.W. Hoth, G. Ledergerber, R.E. Mason, R.W.Stratton (2008), "AC-3-irradiation test of sphere-pac and pellet (U,Pu)C fuel in the United States fast flux test facility", *J. Nucl. Mater*. 376 (1) 47.

[56] Stratton, R.W., F. Botta, R. Hofer, G. Ledergerber, F. Ingold, C. Ott, J. Reindl, H.U. Zwicky (1991), "A comparative irradiation test of UO_2 sphere-pac and pellet fuel in the Gösgen PWR", *International Topical Meeting on LWR Fuel Performance*, 21-24 April 21-24 1991, pp. 174-183, Vol. 1. Avignon, France.

[57] Reindl, J., P. Schleuniger, R. Zumsteg, H.U. Zwicky (1992), *Zerstörungsfreie Nachbestrahlungsuntersuchungen an den Segmentierten Brennstäben,* 1104, 1105 und 1106, Zwischenbericht Nr. 2", Paul Scherrer Institut, Villigen, Switzerland.

[58] Pouchon, M.A., F. Ingold, Z. Kopajtic, Y. Tomita, S. Kono (2003), "Fabrication and characterization of mox microspheres for the FUJI Project", Global 2003, New Orleans, Louisiana, United States.

[59] Nordström, L.A., Ch. Hellwig, M. Nakamura, K. Bakker (2005), "PIE and modelling results for the FUJI irradiation test of sphere-pac MOX fuel", EHPG-Meeting, Lillehammer (NO), *OECD Halden Proceedings HPR-364*.

[60] Hellwig, Ch., K. Bakker, M. Nakamura, F. Ingold, L.Å. Nordström, Y. Kihara (2006), "FUJI: A comparative irradiation test with pellet, sphere-pac, and vipac fuels", *Nuclear Science and Engineering,* 153. 233.

[61] Botta, F. (1991), *Out of Piles Loss of Sphere Tests on UO_2-Sphere-pac Pins with Cladding Cracks*, TM-43-91-03. Technical report, Paul Scherrer Institut, PSI, Switzerland.

[62] Bottcher, J.H., (2000), "FBR MOX particle-fuel behavior in failure scenarios", *Proceedings of the 2000 Fall Meeting of the Atomic Energy Society of Japan*, 3. 808.

7. Summary and conclusions

This report summarises the technical issues and the state of the art associated with the development of innovative fuels targeted for use in advanced fuel cycles are summarised. The fuel types of interest for EGIF are those that contain minor actinides (MA) as opposed to standard fuels (i.e. uranium or uranium-plutonium fuels that are currently being used in the fuel cycle). The fuel types that are considered in detail are oxide, nitride, metallic and dispersion (CERCER and CERMET) fuels. Special mechanical forms (e.g. particle fuels, vibropac and sphere-pac fuels) are also considered. The summary of the state of the art for each fuel form includes the fabrication processes and irradiation performance of the fuels along with the available fundamental properties and characterisation activities. The state-of-the-art knowledge for each fuel type is also compared to a technology readiness level (TRL) scale defined in the appendix. The TRL is defined on a scale from 1 through 9, where 9 correspond to fully mature and largely commercialised technologies.

It is observed that for transuranic-bearing innovative fuels the fabrication processes used to date are limited to laboratory-scale studies (gram quantities of transuranics) for fabrication of small samples. Furthermore, stockpile materials (as opposed to feedstock from a prototypic separations process) are used for fabrication. Irradiation testing is limited to small samples or rodlets. Large-scale irradiation testing (few full-length rods or subassembly scale) has not been performed so far.

Table 7.1 summarises the maturity of fabrication processes and irradiation tests for the different kinds of fuels studied. The main conclusions are as follows:

- Oxides and metal transuranic-bearing fuels are the most mature ones, roughly corresponding to TRL 4-5 for oxide fuels and metal fuels (homogeneous transmutation) and TRL 3 for oxide fuels (heterogeneous version). Both are at an early stage of development.
- Some laboratory-scale data exist for the fabrication and characterisation of nitride fuels but successful irradiation testing to desired burn-ups is lacking. Large-scale fabrication of nitrides using a mature sintering process is also challenging because of AmN volatility. TRL for TRU-bearing nitride fuels is estimated around 3.
- The dispersion fuels (especially those with an inert matrix) are more recent. While successful fabrication processes at laboratory-scale have been demonstrated, the assessment of irradiation performance awaits the post-irradiation examination for the recent irradiation tests. The TRL level is judged to be between 3 and 4.
- There is currently a very limited set of studies with special fuel forms (vibro-pac and/or sphere-pac) that include transuranics (except for limited data with Np).

Table 7.1: Synthesis of TRL binning for fabrication process and irradiation performance maturity

	Fabrication	Irradiation
Metals	4 - 5	4 - 5
Oxides homogeneous	4 - 5	4 - 5
Oxides heterogeneous	4	4
Nitrides	3	3
Dispersion fuels	3 - 4	3 - 4

Homogeneous versus heterogeneous recycling options were evaluated with an input for the state of the art on innovative fuels [1]. The comparison is mostly based on available data for oxide fuels as the database for such a comparison for other fuels types is very limited or does not exist. The conclusions in [1] are summarised as follows:

The multi-criteria analysis performed shows no large discrepancies between the two modes of minor actinides transmutation. Both of them are feasible. Most of the criteria are equivalent. Some of them indicate some advantages versus drawbacks. The final choice will depend on the importance given by decision-makers to the different criteria. The conclusion of the above analyses is the following:

With homogeneous mode:

- fuel fabrication is easier but impacts all the fuel fabrication streams;
- fuel behaviour under irradiation is quite close to the typical standard one;
- a higher mass flux (number) of subassemblies with MA has to be managed within the fuel cycle compared to heterogeneous mode.

With heterogeneous mode:

- fuel fabrication is more complex but is concentrated in limited mass fluxes;
- fuel behaviour under irradiation is quite different as compared to the standard one due to a large production of curium and helium;
- there is no impact on main reactor core parameters but a higher thermal load of spent fuels (compared to the standard one) limits minor actinide content within targets and/or define new handling process at reactor stage;
- due to lower neutron fluxes, minor actinide inventories are higher compared to homogeneous mode;
- due to high neutron emission and power, the high MA content may impact several steps of the fuel cycle such as subassembly handling, washing, transport and intermediate storage.

7.1 Technology readiness levels (TRLs)

The TRLs for studied innovative fuels are described below.

7.1.1 TRL for metal fuels

Table 7.2: TRL binning for fabrication process maturity of metal fuels

	Bench-Scale (1g - 1 kg)	Laboratory-Scale (1 - 10 kg)	Engineering-Scale (10 - 100 kg)	Commercial-Scale (> 1 ton)
Representative Materials from Separations Process	TRL 4 - 5	TRL 6	TRL 7	TRL 8 - 9
Representative Materials from Stockpile	TRL 4	TRL 4 - 5		
Surrogate Materials	TRL 3			

Table 7.3: TRL binning for irradiation performance maturity of metal fuels

	Fundamental Property Measurements	Out-of-Pile Testing	In-Pile Testing with Intermediate conditions (< target burnup)	In-Pile Testing with Prototypic conditions (> traget burnup)	Transient Testing	Reactor Operations
Multiple Assemblies (Core Loads)						TRL 8 - 9
Bundle / Sub-assemblies				TRL 6 - 7	TRL* 7 - 8	TRL 8
Pins		TRL 4	TRL 5	TRL 6	TRL 6 - 7	
Samples & Rodlets	TRL 4	TRL 4	TRL 4	TRL 5	TRL 5 - 6	

7.1.2 TRL for oxide fuels

Table 7.4: TRL binning for fabrication process maturity of homogeneous oxide fuels

	Bench-Scale (1g - 1 kg)	Laboratory-Scale (1 - 10 kg)	Engineering-Scale (10 - 100 kg)	Commercial-Scale (> 1 ton)
Representative Materials from Separations Process	TRL 4 - 5	TRL 6	TRL 7	TRL 8 - 9
Representative Materials from Stockpile	TRL 4	TRL 4 - 5		
Surrogate Materials	TRL 3			

Table 7.5: TRL binning for irradiation performance maturity of homogeneous oxide fuels

	Fundamental Property Measurements	Out-of-Pile Testing	In-Pile Testing with Intermediate conditions (< target burnup)	In-Pile Testing with Prototypic conditions (> traget burnup)	Transient Testing	Reactor Operations
Multiple Assemblies (Core Loads)						TRL 8 - 9
Bundle / Sub-assemblies				TRL 6 - 7	TRL* 7 - 8	TRL 8
Pins		TRL 4	TRL 5	TRL 6	TRL 6 - 7	
Samples & Rodlets	TRL 4	TRL 4	TRL 4	TRL 5	TRL 5 - 6	

Table 7.6: TRL binning for fabrication process maturity of heterogeneous oxide fuels

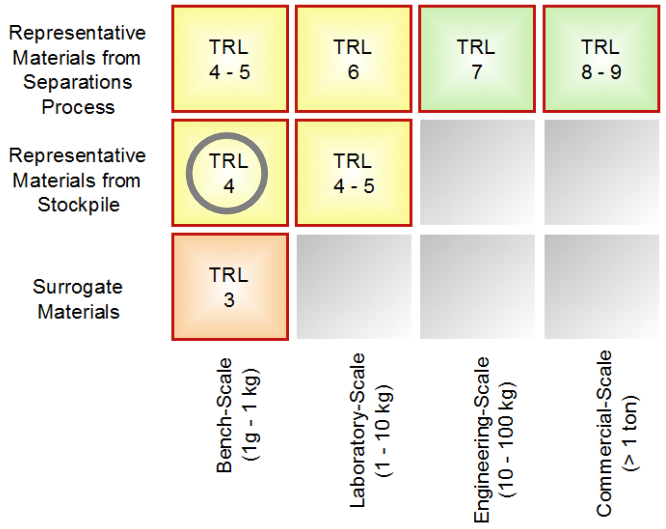

Table 7.7: TRL binning for irradiation performance maturity of heterogeneous oxide fuels

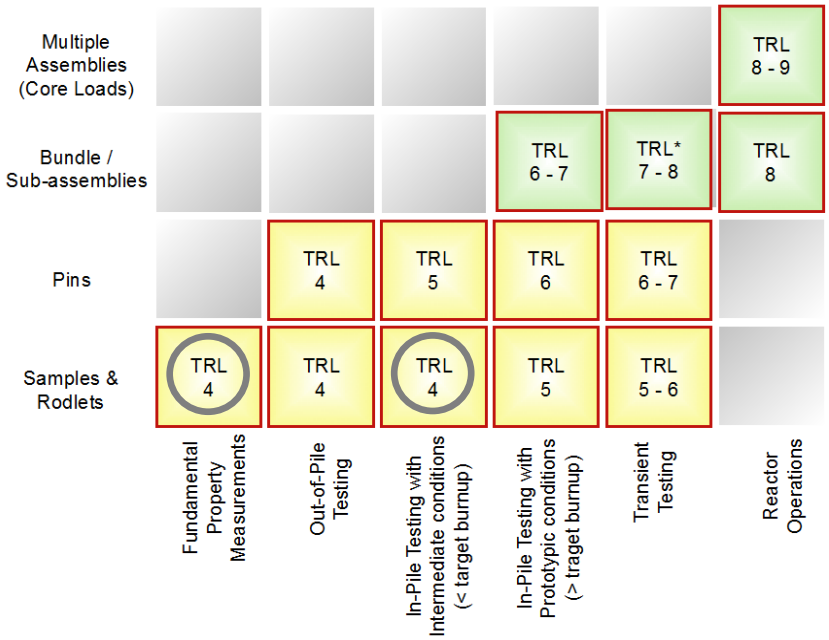

7.1.3 TRL for nitride fuels

Table 7.8: TRL binning for fabrication process maturity of nitride fuels

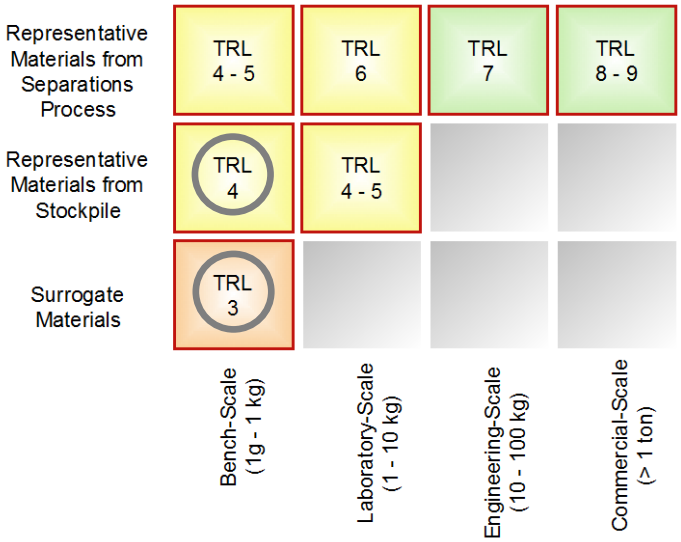

Table 7.9: TRL binning for irradiation performance maturity of nitride fuels

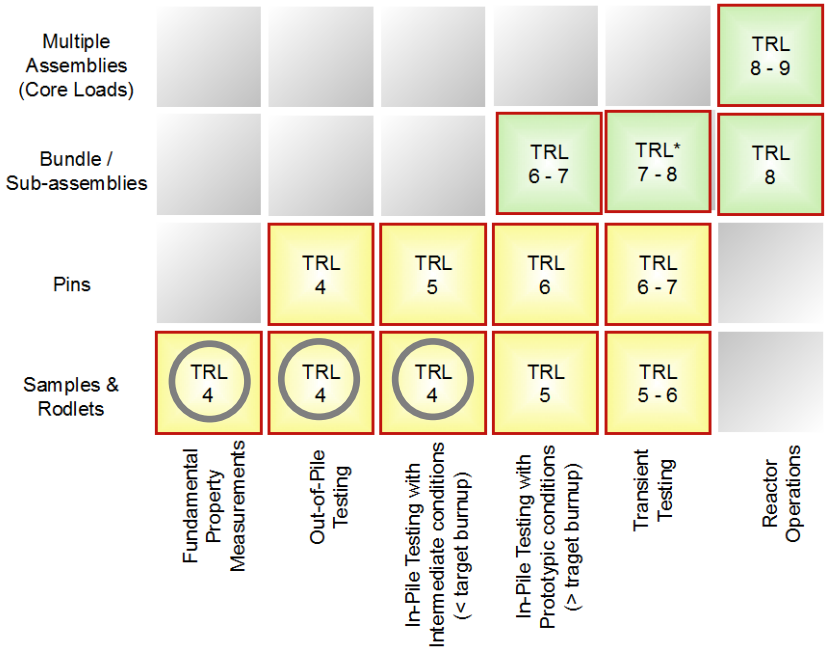

7.1.4 TRL for dispersion fuels

Table 7.10: TRL binning for fabrication process maturity of dispersion fuels

	Bench-Scale (1g - 1 kg)	Laboratory-Scale (1 - 10 kg)	Engineering-Scale (10 - 100 kg)	Commercial-Scale (> 1 ton)
Representative Materials from Separations Process	TRL 4 - 5	TRL 6	TRL 7	TRL 8 - 9
Representative Materials from Stockpile	TRL 4	TRL 4 - 5		
Surrogate Materials	TRL 3			

Table 7.11: TRL binning for irradiation performance maturity of dispersion fuels

	Fundamental Property Measurements	Out-of-Pile Testing	In-Pile Testing with Intermediate conditions (< target burnup)	In-Pile Testing with Prototypic conditions (> traget burnup)	Transient Testing	Reactor Operations
Multiple Assemblies (Core Loads)						TRL 8 - 9
Bundle / Sub-assemblies				TRL 6 - 7	TRL* 7 - 8	TRL 8
Pins		TRL 4	TRL 5	TRL 6	TRL 6 - 7	
Samples & Rodlets	TRL 4	TRL 4	TRL 4	TRL 5	TRL 5 - 6	

References

[1] OECD/NEA Report (2012), "Homogeneous versus Heterogeneous Recycle of Transuranics in Fast Reactors".

Appendix A: Definition of technology readiness levels (TRLs) for transmutation fuel development

A.1 Introduction

In order to provide a quantitative assessment for the maturity of a given system relative to its full-scale deployment, a technology readiness level (TRL) process is developed and used by the Department of Defense in the United States. Subsequently, NASA also successfully used the TRL process to develop and deploy new systems.

Transmutation fuel development is a critical part of the Advanced Fuel Cycle Initiative (AFCI) programme aimed at developing advanced technologies for closing the nuclear fuel cycle. Because the deployment of a new fuel form requires a lengthy and expensive research, development and demonstration programme, applying the TRL concept to the transmutation fuel development programme is very useful as a management and tracking tool.

In using TRL as an effective progress-tracking tool, the first step is to define quantitative definitions with specific criteria for different TRLs. The attributes to defining the quantitative definitions specifically for transmutation fuels are discussed in the following section.

A.2 TRL evaluation elements and attributes

There are two elements to assessing the maturity of a new fuel type in terms of readiness for deployment:

- Fabrication process maturity, which measures how well the fabrication process is understood and validated;
- Fuel performance maturity, which measures how well the in-pile performance of the fuel is understood and validated.

A TRL definition that provides a balance between these two elements is essential. It does not seem coherent to have a very mature fabrication process tested at very large-scales for fuels with large uncertainties in its performance. In contrast, collecting a lot of performance data through large-scale testing without a mature definition of the fabrication process is equally unbalanced. As shown in Figure 1, for each element, there are two attributes identified for assessing the TRL levels. Figure 1 also shows, for each attribute, the distinct bins against which the state-of-knowledge can be compared. The attributes and the bins summarised in Figure 1 are discussed in detail in the following subsection.

A.2.1 Fabrication process maturity

To gauge the maturity of the fabrication process, there are two important attributes that must be considered:

1. Quality of materials used for fabrication process development and testing.

This attribute is broken into three bins to gauge the TRL.

- Surrogate materials – These are typically non-radioactive or less-radioactive materials with properties similar to the actual actinides. The selection of a surrogate depends on the specific phenomenon of interest and the properties that are important to predict or duplicate the phenomenon as closely as possible without using actual actinide materials.
- Representative materials from stockpile – These are individually separated actinide elements that must be blended together for use in fuel fabrication experiments. Quite often the physical form of these materials is not prototypic of would be used as feedstock for fuel fabrication; thus, a non-prototypic conditioning step would be necessary. Also, the isotopic vectors for stockpile actinides are typically different than those obtained from the separation process using commercial spent nuclear fuel. Those differences must be accounted for in the fabrication testing as well.
- Representative materials from separations process – Ultimately, the fabrication process must be optimized using actinides recovered from the separation processes, co-precipitated through a prototypic process, and conditioned for use as feedstock. This phase of the development process requires a coordinated effort between the separations and fuel fabrication development activities.

Figure A.1: Summary of TRL evaluation elements, attributes and bins

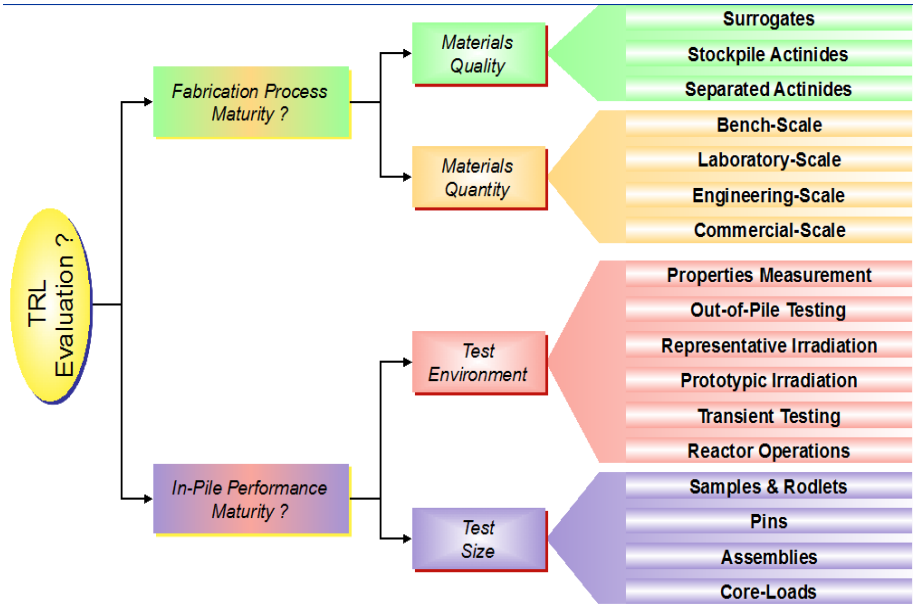

2. Quantity of materials used for fabrication process development and testing.

This parameter is broken into four categories to gauge the TRL. The quantity can be measured as batch size and/or throughput rate.

- Bench-scale fabrication – dealing with gram quantities up to 100 g batch sizes (multiple pellets/slugs per year).
- Laboratory-scale fabrication – dealing with kg quantity of batch-sizes with a equivalent throughput rate on the order of 10 kg TRU /year (multiple pins/year).
- Engineering-scale fabrication – dealing with 1 – 10 kg quantity batch-sizes with an equivalent throughput rate on the order of 100 kg TRU /year (a few assemblies/year).

- Commercial-scale fabrication – dealing with batch-sizes that are the same order of magnitude as the engineering-scale batch sizes but at a throughput rates on the order of tons of TRU/year (a few hundred assemblies per year – core loads).

A.2.2 Fuel performance maturity

To gauge the maturity of fuel performance, there are two important parameters that must be considered:

1. Test environment to determine performance parameters.

This parameter is broken into six categories to gauge the TRL.

- Fundamental property measurements – This category include measurements of basic mechanical, thermal and chemical properties of samples fabricated through a representative process and that conform to defined specifications.
- Out-of-pile testing – This category includes experiments conducted without using reactor/neutron irradiations but provide insight into the behaviour of fuel and cladding. Examples of such tests include diffusion-couple experiments, microstructure evolution tests, ion-beam irradiation tests, thermal segregation experiments.
- In-pile testing in representative spectrum – These are neutron irradiation experiments with fission where the spectrum and/or flux levels and/or thermal boundary conditions are not prototypic of fast reactors. Therefore, fuel design and enrichment levels may have to be adjusted to accommodate the non-prototypic nature of the irradiation environment. A good example is testing the fast reactor fuels using a thermal test reactor with or without partial filtering of thermal neutrons. Completion of the irradiation experiments implies that the associated post-irradiation examination (PIE) is performed.
- In-pile testing in prototypic spectrum – These irradiations are done typically in a fast reactor where flux, spectrum and thermal effects are very similar to the actual reactor conditions for which the fuel is being qualified. Completion of the irradiation experiments implies that the associated post-irradiation examination (PIE) is performed.
- Transient testing – This category includes transient tests to mimic fuel behaviour during design basis accidents. The failure threshold determination also is covered under this category. Full-size or partial size pins and small bundles both before and after irradiation can be used in these tests. Irradiated pins may be those tested in representative or prototypic spectrum (preferably with prototypic spectrum with prototypic dose on the cladding). Completion of the irradiation experiments implies that the associated post-irradiation examination (PIE) is performed. At assembly scale, transient testing is typically not performed. However, the lead test assemblies naturally go through operational transients while in the reactor.
- Reactor operations – At this level, large quantities of fuel (which is already licensed) are used in actual reactor operations. Post-irradiation examination of selected pins may be performed to verify performance.

2. Size of test campaigns to assess performance parameters.

This parameter is broken into four categories to gauge the TRL. In addition to size, the test geometry and the cladding used in the testing campaigns also are of importance for these categories.

- Samples and rodlets – These are samples (pellets, short slugs, etc…) testing in the form of rodlets (on the order of 10 cm fuel height). The testing may or may not

include prototypic cladding and prototypic clad-coolant interactions. These tests are typically designed to look at specific issues/phenomena.

- Pins – These tests are close to full-length pins with representative fuel heights and plenum volumes. Prototypic clad materials are typically used in these tests.
- Assemblies – These tests contain assemblies of prototypic design. Lead test assemblies as well as limited number of assemblies used for partial core conversion are included in this category. Prototypic clad and assembly materials are used in these tests. (For fast reactors assemblies are often referred to as sub-assemblies).
- Full-core assemblies – At this level, the irradiation is no longer a test programme but an operations programme where the statistical and long-term reliability related issues are quantified for the fuel type and design of interest.

A.3 TRL definitions

Full maturity requires long-term routine operations of commercial fabrication plant(s) supplying fuels to operating reactors. At this point, adequate statistical data are available for fuel fabrication and performance; and the system is optimised within the constraints of the performance envelope. This level of maturity is assigned a numerical score of 9 for the corresponding TRL.

At the other end of the spectrum, when a new concept is proposed and it is shown that the concept is viable based on first principles assessment, a numerical score of 1 is assigned for the corresponding TRL.

The intermediate steps are defined based on the logical progression of the research and development towards demonstration and deployment and the corresponding criteria are shown in Table 1. The criteria in Table 1 determine the completion of the corresponding TRL level.

Table A.1: TRL completion criteria

TRL	Criteria
9	Routine operations with licensed fuel established
8	Reactor full-core conversion to new licensed fuel completed
7	All qualification steps completed and fuel is licensed
6	Fuel safety basis established
5	Process parameters defined
4	Fuel design parameters and features defined
3	Success criteria and technical specifications are defined as a range
2	Technical options evaluated and parametric ranges are defined for design
1	Initial concept verified against first principles and evaluation criteria defined

The process of evaluating the TRL is based on binning the state-of-knowledge for each attribute.

Given the criteria, various activities required to achieve these goals are identified as a function of the technical elements, attributes and bins (discussed in Section 2). The resulting TRLs are shown in Tables 2 and 3, for the fabrication and performance elements, respectively.

Table A.2: TRL binning for fabrication process maturity

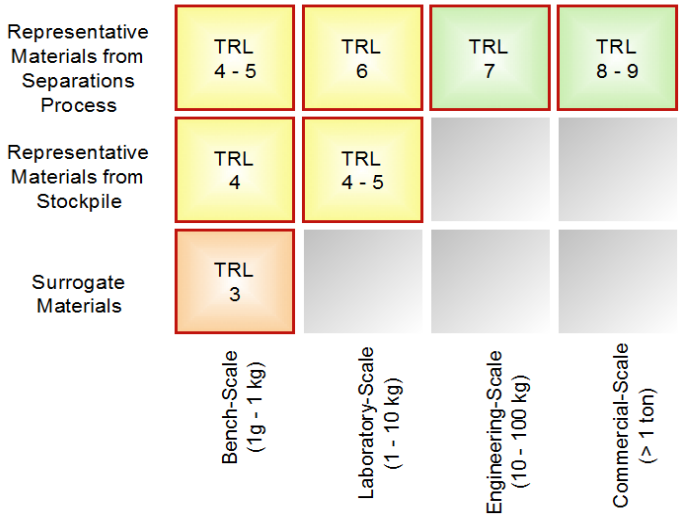

Table A.3: TRL binning for irradiation performance maturity

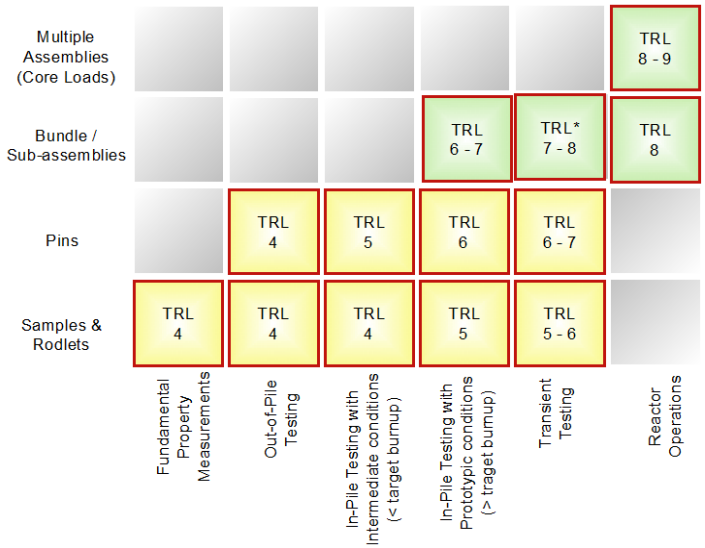

A.4 Summary and conclusions

Table 4 summarises the criteria and the activities needed to achieve the criteria for various TRL levels specific to transmutation fuel development. The definition of the TRL levels is based on a logical progression of the work while considering fabrication and performance testing activities in tandem. All the activities in a given level must be completed before advancing to the next level.

Also, as discussed in [1], another way of describing the fuel development process will be in 4 phases:

- Selection Phase: TRL 1 – 3
- Development Phase: TRL 3 – 5
- Optimisation Phase: TRL 5 – 7
- Qualification Phase: TRL 7 - 9

TRL concept is used as a programme management tool and is not meant as an absolute quantitative measure of maturity. There is naturally a level of subjectivity in defining and, also, in evaluating the TRLs. Nonetheless, with the granularity provided in the methodology outlined in this paper, the technical maturity evaluations will provide a semi-quantitative, relative measure for the transmutation fuel technology specifically and to any new fuel concept, in general.

Finally, it is important to recognise the difference between the TRL evaluations and technical risk. The TRL only provides a relative measure of where the technology maturity is compared to the end objective of large-scale deployment. A low TRL does not necessarily mean a high technical risk. Technical risks depend on many factors such as the complexity of the remaining work, the availability of the needed resources, schedule constraints, etc. and must be evaluated independently.

Table A.4: Summary of TRL definition for transmutation fuels

1	**Proof-of-Concept**	• A new concept is proposed and appears feasible based on similar systems/applications. • Technical options for the concept are identified and relevant literature data reviewed. • CRITERION: Initial development plan and evaluation criteria are developed.
2		• Technical options are ranked based on relevant available data (including data from similar fuel types) and evaluation criteria. • CRITERION: Performance range and fabrication process parametric ranges are defined based on analyses, relevant available data (including data from similar fuel types).
3		• Concepts are tested through bench-scale experiments and characterisation of fundamental properties. • Fabrication process tested at bench-scale using surrogates. • CRITERION: technical specifications are quantified as a range that satisfies the success criteria.
4	**Proof-of-Principle**	• Samples using stockpile materials are fabricated at bench-scale. • Limited bench-scale fabrication with separated materials and laboratory-scale fabrication with stockpile materials also are performed for process evaluation only. • Out-of-pile tests for important phenomena are conducted. • Fundamental properties (with uncertainties) are measured and compiled. • Irradiation testing of small-samples (rodlets) is performed in relevant environment. • CRITERION: Fuel design parameters and features are established. •
5		• Samples using stockpile materials and separated materials are fabricated at laboratory-scale using a representative process. • Irradiation testing of small-samples (rodlets) is performed in prototypic environment. • Irradiation testing of pins is performed in relevant environment. • Transient testing of fresh and irradiated samples and rodlets to establish failure mechanisms are performed. • Major models developed and tested; and performance code completed • CRITERION: Fabrication process parameters are defined

Table A.4: Summary of TRL definition for transmutation fuels *(Cont.)*

6		• Pins using separated materials are fabricated at laboratory-scale using a prototypic process. • Irradiation testing of pins is performed in prototypic environment. • Transient testing of fresh and irradiated pins and bundles are performed to establish DBA behaviour and failure thresholds. • Performance code verified and validated • CRITERION: Fuel design and process parameters and features are verified and fuel safety basis is established. LTA's are qualified for irradiation.
7	**Proof-of-Performance**	• Test assemblies using prototypic feedstock materials at engineering-scale are fabricated using prototypic fabrication process. • Assembly-scale irradiation testing at prototypic environment is performed (LTAs). Once LTAs are tested in a pilot reactor, operational transients are also covered. Transient testing of assemblies to DBA conditions and to failure is typically not necessary. • CRITERION: Fuel qualification process is completed and reactor safety basis is established for full-core operations. Fuel is licensed.
8		• A few core-loads of fuels are fabricated using a commercial-scale facility. At this TRL levels, occasional PIE of assemblies are still performed. • CRITERION: Reactors are operated using the new fuel for a few residence cycles.
9		• CRITERION: Multiple years of operational experience established for a commercial fabrication plant and routine operations of commercial reactors for multiple cycles.

List of contributors

France

N. Chauvin (CEA)

Japan

K. Minato (JAEA)
T. Ogata (CRIEPI)

Switzerland

M.A. Pouchon (PSI)

United States

K.O. Pasamehmetoglu (INL)
Y.J. Choi (INL, formerly at the OECD/NEA)

International organisations

S. Massara (OECD/NEA)
S. Cornet (OECD/NEA)
J. Sommers (ITU, EU)

Reviewers

J.R. Kennedy (INL)
K. McClellan (LANL)
C.B. Lee (CRIEPI)

Members of the Expert Group on Innovative Fuels

Canada

H.B. Hamilton (CNL, formerly AECL)

France

N. Chauvin (CEA)
F. Delage (CEA)
M. Salvatores (CEA)

Germany

F. Gabrielli (KIT)
W. Maschek (KIT)

Japan

K. Minato (JAEA)
T. Ogata (CRIEPI)
K. Tanaka (JAEA)

Republic of Korea

C.B. Lee (KAERI)

Switzerland

M.A. Pouchon (PSI)

United States

Y.J. Choi (INL, formerly at the OECD/NEA)
K.A. McCarthy (INL)
K.O. Pasamehmetoglu, (INL)
C. Stanek (LANL)

International Organisations

U. Basak (IAEA)
S. Cornet (OECD/NEA)
J. Somers (EU)

NEA PUBLICATIONS AND INFORMATION

The full **catalogue of publications** is available online at www.oecd-nea.org/pub.

In addition to basic information on the Agency and its work programme, the **NEA website** offers free downloads of hundreds of technical and policy-oriented reports.

An **NEA monthly electronic bulletin** is distributed free of charge to subscribers, providing updates of new results, events and publications. Sign up at www.oecd-nea.org/bulletin/.

Visit us on **Facebook** at www.facebook.com/OECDNuclearEnergyAgency or follow us on **Twitter** @OECD_NEA.

OECD/NEA PUBLISHING, 2 rue André-Pascal, 75775 PARIS CEDEX 16

State-of-the-art Report on Innovative Fuels for Advanced Nuclear Systems

Development of innovative fuels such as homogeneous and heterogeneous fuels, ADS fuels, and oxide, metal, nitride and carbide fuels is an important stage in the implementation process of advanced nuclear systems. Several national and international R&D programmes are investigating minor actinide-bearing fuels due to their ability to help reduce the radiotoxicity of spent fuel and therefore decrease the burden on geological repositories. Minor actinides can be converted into a suitable fuel form for irradiation in reactor systems where they are transmuted into fission products with a significantly shorter half-life.

This report compares recent studies of fuels containing minor actinides for use in advanced nuclear systems. The studies review different fuels for several types of advanced reactors by examining various technical issues associated with fabrication, characterisation, irradiation performance, design and safety criteria, as well as technical maturity.

OECD Nuclear Energy Agency
12, boulevard des Îles
92130 Issy-les-Moulineaux, France
Tel.: +33 (0)1 45 24 10 15
nea@oecd-nea.org www.oecd-nea.org

NEA No. 6895